Pioneering the development of CRISPR-guided photooxidation for guanine-to-cytosine (G→C) conversion in cellular DNA

Nicole Adrianna Frias

A THESIS SUBMITTED TO
THE FACULTY OF GRADUATE STUDIES
IN PARTIAL FULFILLMENT OF THE REQUIREMENTS
FOR THE DEGREE OF
MASTER OF SCIENCE

GRADUATE PROGRAM IN CHEMISTRY
YORK UNIVERSITY
TORONTO, ONTARIO

May 2025

Abstract

Adapted as an RNA-guided genome-editing system, CRISPR/Cas9 has served promising potential in the treatment of human genetic diseases. Specifically, enzymatic base editors can effectively catalyze single-nucleotide conversions in cellular DNA through the use of a catalytically-dead Cas9 and a deaminase. Current base editors primarily consist of cytosine and adenine base editors, which can create C→T and A→G conversions through deamination of the substrate, respectively. However, the use of enzyme-based approaches can give rise to exasperated levels of non-specific editing. New base editors are needed to expand the mutagenic repertoire of current base editing technologies, as well as reduce off-target effects associated with current editors. For this, the photooxidation of guanine was explored as a method of achieving precise G→C conversions in the cellular genome. The development of the first chemical base editor could therefore allow for the utmost spatiotemporal precision, potentially alleviating the off-target effects associated with enzymatic editors.

Dedication

To my grandmother, whose strength and resilience has inspired me in trying to focus on the positive in any situation.

To my Mom and Dad, for always supporting me in every step and challenge in my scientific career.

Acknowledgements

First and foremost, I would like to express my gratitude towards Prof. Ryan Hili and Prof. Brian Kim for providing me with the opportunity to work on research that balances my passion for chemical biology and my desire to contribute to gene-editing. When I first learned about CRISPR/Cas9 in my undergraduate courses, I was fascinated over its impact – I am eternally grateful for being part of the advancement of CRISPR technologies myself. This journey has offered many valuable (and hard) lessons that have fostered my personal and scientific growth, and I feel privileged to be in a secure academic environment where I am able to learn from experience. Although I have faced difficult challenges, I am thankful that I was able to overcome them with support from faculty and colleagues in the department. I cannot express enough appreciation for the support and mentorship that Prof. Hili provided me with since my undergraduate years. He has created an environment that has encouraged my intellectual growth and has greatly inspired my motivation in science.

I would like to express my appreciation for the members of my thesis and defence committee for their support as well: Prof. Mark Bayfield, Prof. Chris Caputo, and Prof. Vivian Saridakis.

My deepest gratitude also goes to Prof. Chris Caputo for his invaluable advice, mentorship, and encouragement over the years. His constant belief in my scientific abilities and incredible patience has made me feel so supported during my journey at York. I also want to thank Casey Lenart, and the rest of the Caputo lab, for encouraging me to be myself. Their influence made me a much more confident researcher heading into graduate school, and I will always be appreciative of the positive experience that they gave me.

Special appreciation for past and current members of the Kim and Hili labs, particularly my undergraduate mentee - Maha Munawar. I am so delighted that I was able to work with such a bright undergraduate student. Her perseverance and excitement were deeply motivating to me. Thank you for the friendships and discussions about science during my time here. Special thanks to Dr. Baktharaman Sivaraj for help on the synthesis and purification of a key compound for my

thesis - his expertise in synthetic chemistry has been truly valuable to the learning experience of my fellow lab-mates and I.
Also, thank you to Dr. Howard Hunter for always being so willing to provide guidance on NMR, as well as Dr. Maxime Rossato for assistance with mass spectrometry.

I also want to especially thank NSERC for providing support through an NSERC CGS-M scholarship and The Cancer Research Society for funding this project.

Lastly, but most importantly, my love and appreciation go towards my family: Mom, Dad, Michelle, and Daniel. They have stuck with me through thick and thin, genuinely listened to my challenges throughout this journey, and of course, celebrated the milestones. I wouldn't be where I am today without their support for anything I choose to do. I also deeply thank my grandparents, who have sacrificed a lot coming to Canada to build a better future for their kids and grandkids. I would not be able to do what I love if they had not immigrated here from a small island in Portugal.

Table of contents

List of figures

List of schemes

List of tables

List of abbreviations

CRISPR	Clustered Regularly Interspaced Palindromic Repeats
DNA	Deoxyribonucleic acid
RNA	Ribonucleic acid
PAM	Protospacer-adjacent motif
SpCas9	Cas9 from *Streptococcus pyogenes*
tracrRNA	Trans-encoded RNA
crRNA	CRISPR RNA
sgRNA	Single guide RNA
dsDNA	Double-stranded DNA
ssDNA	Single-stranded DNA
NUC	Nuclease lobe of Cas9
REC	Recognition lobe of Cas9
HNH	Histidine-Asparagine-Histidine
PI	PAM-interacting domain of Cas9
DSB	Double-stranded break
NHEJ	Non-homologous end-joining
HDR	Homology-directed repair
SCD	Sickle-cell disease
dCas9	Dead Cas9
Cas9n	Cas9 nickase
MMR	Mismatch repair
UGI	Uracil glycosylase inhibitor
ALL	Acute lymphoblastic leukemia
LDL-C	Low density lipoprotein – cholesterol
CBE	Cytosine base editor
ABE	Adenine base editor
BER	Base excision repair
ISC	Intersystem crossing
PET	Photoelectron transfer

τ_f	Lifetime of fluorescence
Φ_{ISC}	Quantum yield of ISC
NHE	Normal hydrogen electrode
Iz	Imidazolone
Oz	Oxazolone
8-oxoG	8-oxoguanine
Sp	Spiroiminodihydantoin
Gh	Guanidinohydantoin
SELEX	Systematic evolution of ligands by exponential enrichment
FACS	Fluorescence-activated cell sorting
DFHBI	3,5-difluoro-4-hydroxybenzylidene imidazolinone
DFHBI-IT	(Z)-5-(3,5-Difluoro-4-hydroxybenzylidene)-2-methyl-3-(2,2,2-trifluoroethyl)-3,5-dihydro-4H-imidazol-4-one
K_d	Dissociation constant
FAD	Flavin adenine dinucleotide
RB	Rose Bengal
RB-DFHBI	DFHBI-linked Rose Bengal
LC-MS/MS	Liquid chromatography with tandem mass spectrometry
mW	milliWatts
cm	centimetre
DMF	*N, N*-dimethylformamide
NaAc	Sodium acetate
Ac_2O	Acetic anhydride
EtOH	Ethanol
TFA	Trifluoroacetic acid
DCM	Dichloromethane
Et_2O	Diethyl ether
HATU	2-(7-Aza-1H-benzotriazole-1-yl)-1,1,3,3-tetramethyluronium hexafluorophosphate
DIPEA	Diisopropylethylamine
EDTA	Ethylenediaminetetraacetic acid

TEA	Triethylamine
HFIP	Hexafluoropropan-2-ol
NMR	Nuclear Magnetic Resonance
s	Singlet
d	Doublet
t	Triplet
m	Multiplet
J	J coupling constant
Ppm	Parts per million
Hz	Hertz

1 Introduction

1.1 The discovery and evolution of CRISPR/Cas9

Originally discovered in prokaryotic organisms in 1987, CRISPR/Cas9 was first found as an adaptive immune response towards invading viral pathogens.[1] The CRISPR locus is defined by 23-47 base-pair "repeats" that are regularly interspaced between unique targeting sequences called "spacers." Hence, the term "CRISPR" is derived from clustered regularly interspaced palindromic repeats.[2,3] The first stage of CRISPR biogenesis is called the adaptation (or acquisition) stage, which involves the incorporation of new spacers into the CRISPR locus from viral phage DNA (**Figure 1a**).[4] A set of *cas* genes is located ahead of the CRISPR locus, in which two Cas proteins are universally involved in all adaptive CRISPR/Cas systems: Cas1 and Cas2.[5] As they are the two proteins generally involved in the adaptation phase, they function together in the recognition and incorporation of invading species into the CRISPR genome. Mechanistically, upon Cas1-Cas2 complex formation *in vivo*, a pair of Cas1 dimers are directly involved with the recognition of a protospacer-adjacent motif (PAM) that is upstream of the target invading DNA.[6,7] Cas2 plays a role in determining the number of nucleotides to integrate into the genome, resulting in a defined 33-nucleotide spacer inserted ahead of the first repeat in the CRISPR locus (**Figure 1a**).[7] Using an adenine- and thymine-rich (A+T) leader sequence just upstream of the CRISPR locus, RNA transcription yields a CRISPR array containing spacers that target recently-encountered viral phage DNA.[8] Herein, the formation of effector complexes during the maturation stage of the immune response differs and can be broadly classified as types I, II, and III systems. As a Cas9-mediated process, the type II CRISPR system will therefore be our focus.

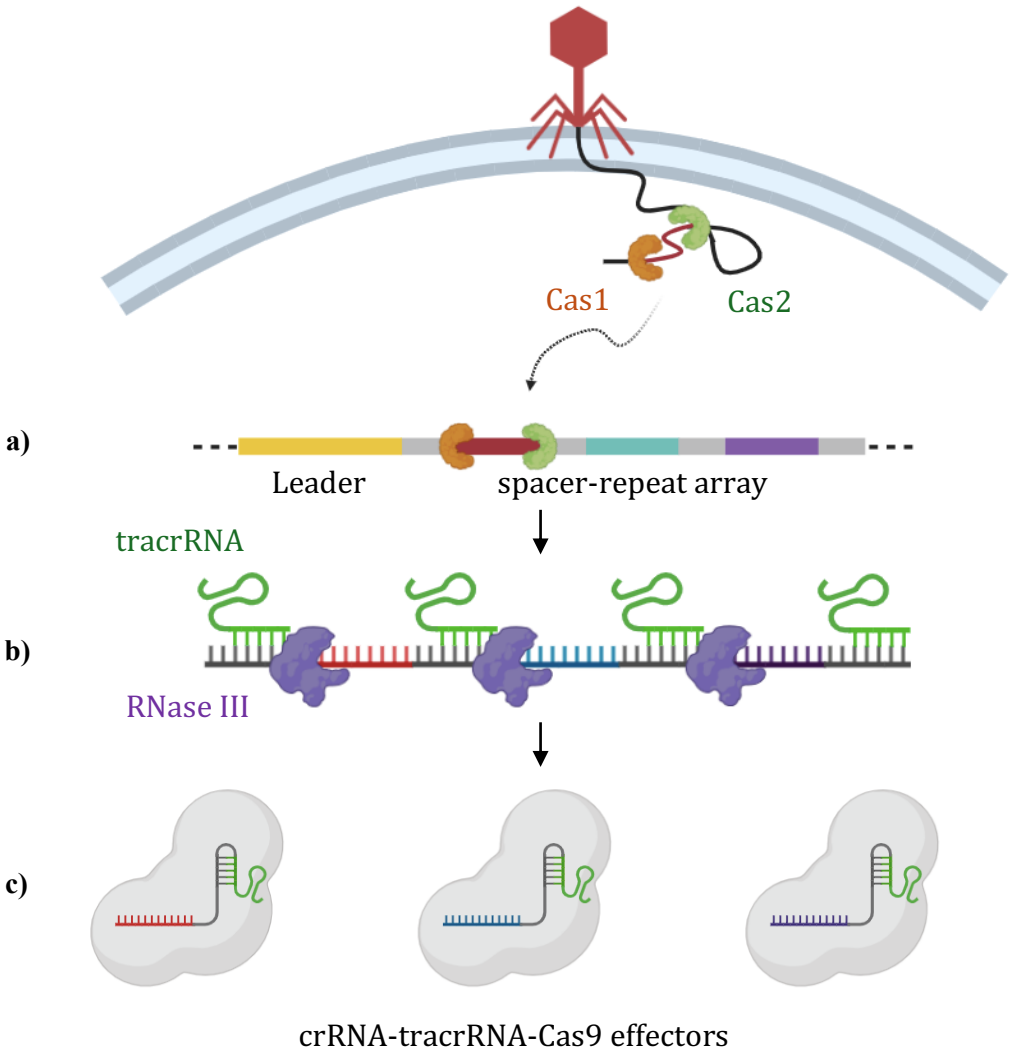

Figure 1. The three stages of CRISPR/Cas9 immunity in prokaryotes.
a) Acquisition stage: Upon injection, viral phage DNA is targeted by Cas1 and Cas2 homodimers, integrating a new spacer ahead of the first repeat in the CRISPR genome. **b)** RNA biogenesis: Following transcription of the CRISPR spacer-repeat array, the tracrRNA complimentary binds to the repeat region of the pre-crRNA transcript with the aid of Cas9 (not shown). Subsequent processing steps by RNase III and unknown enzymes result in crRNAs that are 39-42 nt in length. c) Effector complexes of crRNA, tracrRNA, and Cas9 available for target interference. Figure adapted from reference [10] (© 2011, Nature).

1.2 Type II-A CRISPR/Cas9 system

Following RNA transcription, targeting viral phage DNA involves the formation of effector complexes, which consist of a few distinct features for type II CRISPR systems. Among CRISPR systems, it was first found that the CRISPR RNA transcript is cleaved into approximately 60-nt crRNAs and the sequence at the 3' end was matched to the middle of the CRISPR repeat, meaning that the repeat sequence generally identifies as a cleavage site in CRISPR systems.[9]

Specifically, the processing of crRNAs was studied in *Streptococcus pyogenes,* deeming a type II-A system.[10] Charpentier *et al.*[10] identified a 171/89 base-pair trans-encoded RNA (tracrRNA) that is encoded upstream of the leader-spacer-repeat array, in which the tracrRNA is involved with processing of short crRNA effector complexes. The tracrRNA contains a 25-nt stretch that is said to complimentary base-pair to the repeat sequence of the pre-crRNA transcript with the aid of Cas9, allowing for the *in vivo* processing of crRNA. By providing an RNA duplex structure, the crRNA/tracrRNAs are co-processed through the cleavage of the repeat sequence by endogenous RNase III, resulting in a 2-nt overhang at the 3' end of the crRNA-tracrRNA complex.[2,10] This step results in 66 nt crRNAs that further undergo a secondary processing event involving cleavage within the spacer sequence, which results in trimming at the 5' end of the crRNA and yields 39-42 nt crRNAs (**Figure 1b**).[10] The individual short crRNAs now possess a spacer-derived sequence that is 20 nt long and a repeat-derived sequence that is 19-22 nt long, resulting in the formation of Cas9-crRNA-tracrRNA effector complexes now available for targeting viral RNAs (**Figure 1c**).

Effector complexes allow for target interference and ultimately provide immunity against viral pathogens without disrupting the host chromosome by distinguishing between viral and self DNA.[11] For target recognition and cleavage of target double-stranded DNA (dsDNA) to occur, there must be a complimentary match between the target DNA strand and spacer within the crRNA, which is induced by Watson-Crick-Franklin base-pairing.[2] This means that the dsDNA target contains a complimentary strand and non-complimentary strand, but complimentary base-pairing is not the only parameter to achieve target recognition. As previously mentioned briefly, the Cas9 protein must recognize a protospacer-adjacent motif (PAM) located at the 3' end of the spacer on the non-complimentary strand.[12,13] Specifically, *S. pyogenes* Cas9 searches for a PAM sequence of 5'-NGG prior to unwinding of the dsDNA and crRNA binding to the target strand.[14] Upon finding a complimentary match in the target genome using the crRNA sequence as a guide, Cas9 cuts both strands of the invading DNA, resulting in successful interference.[2] Thus, this CRISPR system provides bacteria with adaptive immunity, as it can target DNA that it has once encountered before.

1.3 A programmable RNA-guided DNA endonuclease for eukaryotic genome-editing

In 2012, bacterial CRISPR/Cas9 immunity was adapted as a dual RNA-guided genome editing technology by Jennifer Doudna and Emmanuelle Charpentier, who later won a Nobel prize in 2020 for their work.[14] Being adapted from the natural type II CRISPR system, it utilizes a dual RNA to guide Cas9 endonuclease to a target site in the genome: crRNA and tracrRNA. These two components are often fused into a single guide RNA (sgRNA) in genome-editing applications (**Figure 2**). RNA-guided SpCas9 nuclease identifies the 3-nucleotide PAM in the genome prior to unwinding of the dsDNA. Then, the sgRNA is used to find a complimentary match through complimentary base-pairing between the spacer and target region of the genome, resulting in the formation of an open R-loop structure (**Figure 2**).[14] Subsequently, this results in double-stranded cleavage at a specific region in the genome, which is not possible without the crRNA-tracrRNA-Cas9 tertiary complex.

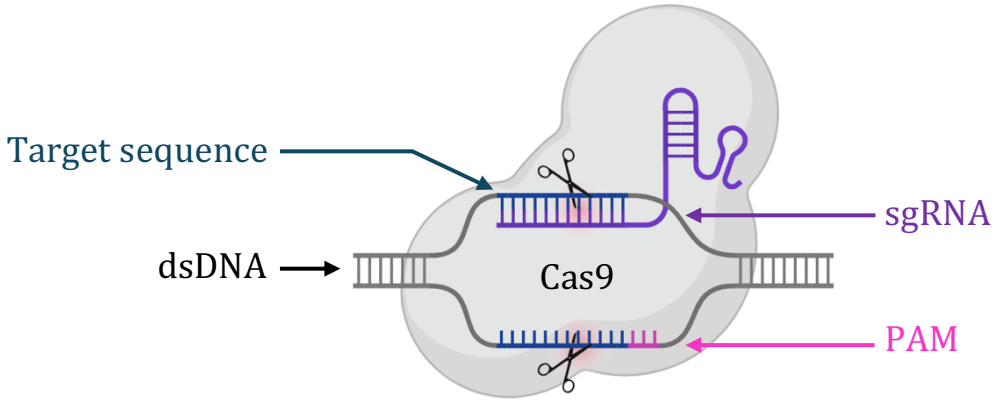

Figure 2. Dual RNA-guided target interference by Cas9 endonuclease.
Adapted by Doudna & Charpentier in 2012 as an RNA-guided gene-silencing system, a single guide RNA (sgRNA) guides Cas9 to a target region of the genome. Cas9 first searches for a protospacer-adjacent motif (PAM) on the non-complimentary strand prior to complimentary binding of the sgRNA to a target region of the genome. Upon finding a complimentary match, Cas9 makes a double-stranded cut 3 bp downstream from the PAM.

1.3.1 Structure and function of SpCas9 nuclease

The Cas9 nuclease consists of approximately 1368 amino acids and is divided into two lobes: the nuclease (NUC) lobe and the recognition (REC) lobe (**Figure 3a**).[15] Cas9 has two nuclease domains that are responsible for double-stranded DNA cleavage. The HNH domain, which is poorly ordered prior to sgRNA binding, is a two-stranded anti-parallel β-sheet surrounded by four α helices.[15] It is responsible for cleavage of the target strand of dsDNA substrates and has a conserved His840 residue that is required for nuclease activity, meaning that H840A mutations render the HNH nuclease inactive.[15,16] The RuvC domain, which is subdivided into RuvC I-III, forms the core of the nuclease domain with six β strands and four α helices surrounding them.[16] It is responsible for cleavage of the non-target strand during dsDNA cleavage, where D10A is often a mutation to render the RuvC nuclease domain inactive.[15] A positively-charged interface at the RuvC and PAM-interacting (PI) domains binds the 3' end of sgRNA and the PI is positioned to recognize the PAM on the non-target strand.

Furthermore, the recognition lobe consists of REC1 and REC2 with the latter being not as important for Cas9 binding and activity.[15] However, REC1 plays a vital role in the binding of Cas9 as it makes contact with the repeat (crRNA) and the anti-repeat (tracrRNA) region while the bridge helix intermolecularly interacts with the guide region as well.[15] Recognition of the crRNA and tracrRNA repeat/anti-repeat regions is essential for Cas9 binding to duplex DNA; otherwise, binding would be abolished.[15]

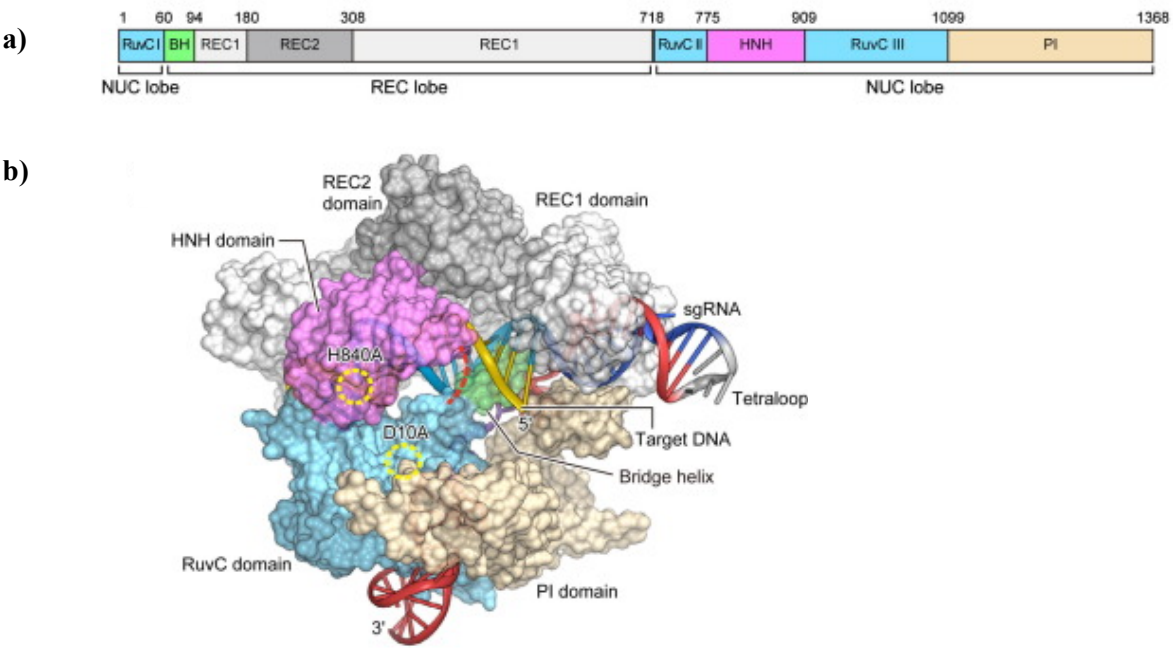

Figure 3. Structure of Cas9 from *Streptococcus pyogenes* (SpCas9).
a) SpCas9 consists of the NUC lobe (residues 1-59 and 718-1368) and REC lobe (residues 60-713), which are each subdivided into domains possessing their own unique functions. **b)** Surface representation of the sgRNA-Cas9 complex. The catalytic H840 and D10 residues in the HNH and RuvC domains, respectively, are indicated by yellow dashed circles. Figure from reference [15]. (© 2014, Cell).

1.3.2 Structure of the crRNA-tracrRNA

As mentioned previously, the tracrRNA is typically fused with the crRNA to produce the sgRNA used in CRISPR/Cas9 systems. Hence, the sgRNA forms a highly ordered RNA structure of approximately 118 nucleotides – 20 nucleotides for the crRNA and 98 nucleotides for the tracrRNA.[15,17] Within the 20 nt crRNA spacer, 10-12 of the nucleotides closest to the PAM encompass the "seed" region.[18,19] The seed region is particularly important for target specificity since off-target editing often arises from similarity with the seed region.[19] After the seed region and PAM, the repeat-anti-repeat region constitutes the upper stem loop of the tracrRNA, in which mutations in the upper stem loop have a dramatic impact on Cas9 function, as per the interactions with the REC lobe of Cas9.[15] There are three further stem loops (stem loops 1-3) for a total of four stem loops in the tracrRNA, while a 4-nucleotide linker separates stem loops 1 and 2 (**Figure 4**).[18] These stem loops act to reinforce the binding of Cas9 – stem loop 1 primarily interacts with the

REC lobe while stem loops 2-3 primarily interact with the NUC lobe.[15] Occasionally, the 3' stem loop is omitted in the design of sgRNA constructs in genome-editing.[18]

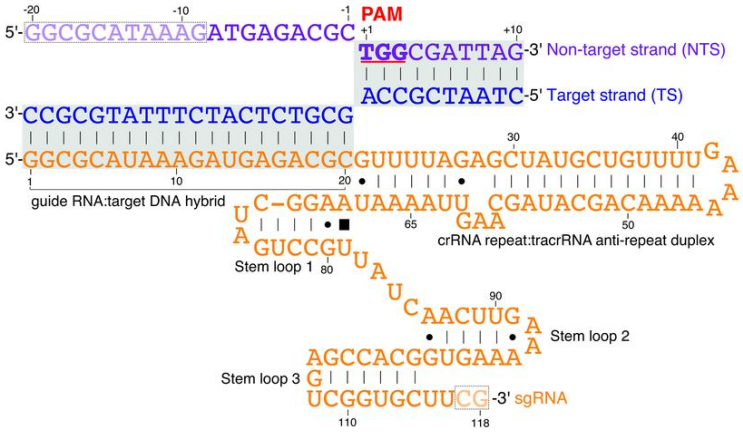

Figure 4. Schematic of the sgRNA scaffold.
The sgRNA consists of the 20 nt spacer element and 98 nt tracrRNA containing the anti-repeat region three additional stem loops. Dashes and dots represent canonical and non-canonical Watson-Crick-Franklin base-pairs, respectively. Bold squares represent π-stacking interactions. Figure from reference [17]. (© 2016, Science).

Although the tracrRNA is quite structured, there is such flexibility that allows researchers to utilize aptamer-fused Cas9 systems in applications such as transcriptional activation and repression.[20,21] Aptamers are single-stranded nucleic acid polymers that fold into unique secondary structures; and thus, they bind to molecular targets (*e.g.,* proteins).[22] Known RNA aptamers (*e.g.,* MS2, PP7)[20,21] have been fused into the sgRNA, allowing for the effective recruitment of their respective RNA-binding proteins (*e.g.,* MCP, PCP) to a target region of the genome with the guidance of Cas9. [20,21] Specifically, aptamers have typically been cloned as an extension of the upper stem loop of the tracrRNA, resulting in highly efficient fluorescence in Cas9-based fluorescent reporter systems (**Figure 5a**).[23,24] However, considering that the lower stem loops are not as required for Cas9 binding, aptamers have also been cloned into stem loop 2 with similar (or greater) efficiencies (**Figure 5b**).[20,23] Aptamers cloned at the 3' end of the sgRNA have shown high-fold changes of transcriptional control as well (**Figure 5c**).[21,23] Researchers have even gone to the extent of cloning multiple aptamers into the different stem loops for either dual labelling,[23] or enhancing the brightness in live cell imaging of low-copy gene sites.[25]

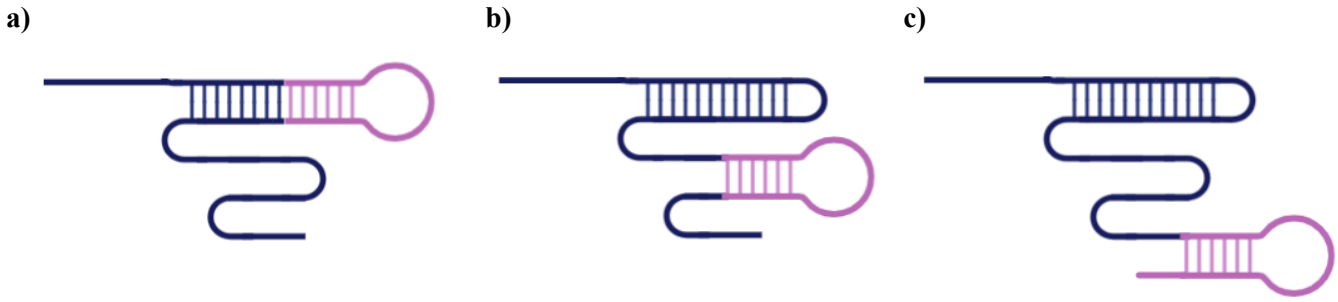

Figure 5. Examples of aptamer-fused sgRNA constructs.
a) RNA aptamer cloned as an extension of the repeat-anti-repeat duplex, b) RNA aptamer cloned into stem loop 2 of the tracrRNA component, and c) RNA aptamer cloned at the 3' end of the sgRNA.

1.3.3 Applicability of CRISPR/Cas9 gene-editing

Upon RNA-guided Cas9 binding to a target region of the genome, Cas9 creates a double-stranded break (DSB) approximately 3 nucleotides upstream of the PAM in a blunt-ended fashion.[14,26] The production of DSBs triggers one of two endogenous cellular repair pathways – one of which is called non-homologous end-joining (NHEJ). This pathway preferentially leads to the random insertion or deletion of nucleotides, termed indels, which can vary in length based on the number of nucleotides inserted/deleted.[27] Thus, CRISPR/Cas9 has been used to effectively "knock out" the function of specific genes through the NHEJ repair process.

For instance, it has shown great therapeutic potential in the treatment of sickle cell disease and β-thalassemia, as per the first FDA-approved CRISPR drug – Casgevy.[28,29] Normally, as the switch from γ-globin to β-globin occurs during adulthood, BCL11A acts as a suppressor towards fetal hemoglobin expression, consequently leading to the expression of β-globin instead of γ-globin.[29,30] However, sickle cell disease is caused by a defect in the β-globin gene, which does not allow for the normal production of hemoglobin, leading to sickled red blood cells. Through an NHEJ-mediated process, disrupting the function of the *BCL11A* enhancer region can lead to elevated levels of γ-globin, allowing for SCD patients to rely solely upon fetal hemoglobin instead.[29,30] This represents a very relevant example of how CRISPR/Cas9 and NHEJ-mediated repair can be used in effective treatments against human genetic disorders.

Further, NHEJ-mediated processes have also been effective in broad CRISPR screens for loss-of-function mutations, which help to uncover mechanisms of drug resistance and understand drug targets.[31,32] Nevertheless, many pathogenic point mutations can only be corrected through the precise replacement of a sequence in the genome. This can be achieved through the supply of a

donor dsDNA template, which is utilized in homology-directed repair (HDR) upon Cas9 cleavage. This pathway allows for the incorporation of a variety of edits in the resulting sequence (*e.g.,* single-nucleotide changes, gene insertions);[18] however, the efficiency of HDR-related genome editing is only approximately 0.1-5%.[33] HDR-related gene-editing is also limited to the G2 and S phases of the cell cycle, limiting its use in actively dividing cells.[34] Also considering the vast amount of off-target editing induced by slightly mismatched sgRNAs guiding Cas9 to incorrect regions of the genome,[35] it is key to develop more efficient and precise methods of genome engineering in order to maximize the applications in biomedical research.

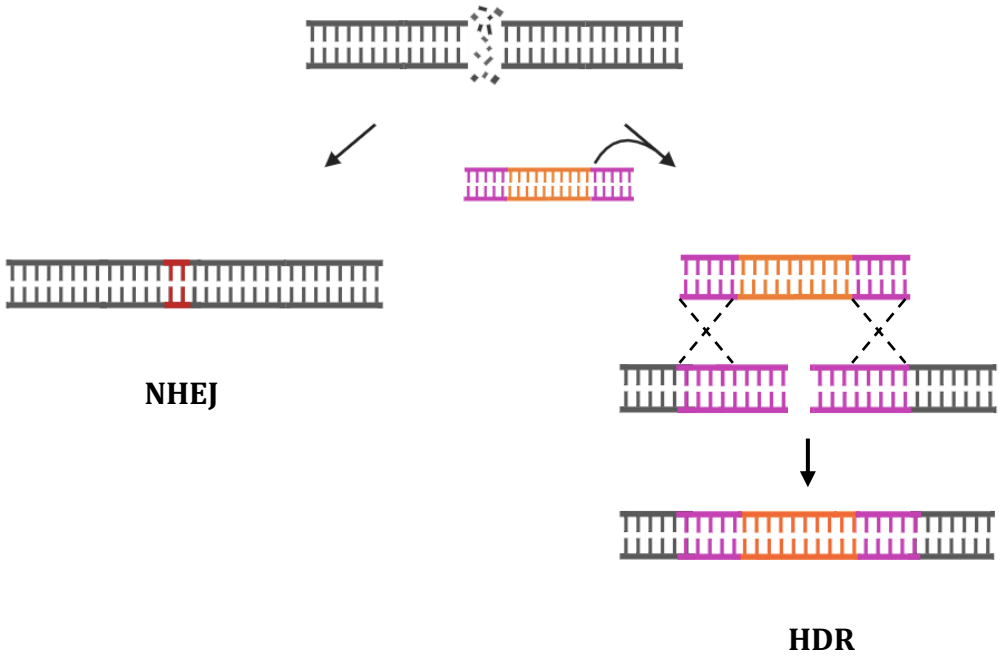

Figure 6. Two cellular repair pathways upon double-stranded DNA cleavage.
Non-homologous end-joining (NHEJ) results in random insertion/deletion of nucleotides (indels – red). Homology-directed repair (HDR) uses a donor dsDNA as a template for the incorporation of a unique edit into the genome. The homology arms are indicated in pink and the edited sequence is indicated in orange.

1.4 Base editing – a newly emerged approach to CRISPR gene editing

To overcome the challenges of HDR-based genome editing discussed thus far, the Liu group developed the concept of base editing.[33,36] It utilizes the fusion of a catalytically dead Cas9 (dCas9), as well as a deaminase, to induce precise single-nucleotide conversions in the genome. Upon RNA-guided binding of dCas9 to a target region of the genome, the deaminase (*e.g.,*

APOBEC1) converts, for instance, cytosine to uracil on the non-target strand (**Figure 7**).[33] Upon DNA replication and repair, adenine is expected to be incorporated opposite to uracil by Watson-Crick-Franklin base pairing, resulting in a permanent cytosine-to-thymine (C→T) conversion at the specific genomic site. However, improved base editors have been generated in order to reduce the chance of endogenous removal of the edited sequence. Rather than using dCas9 to target an area of the genome, they used a Cas9 nickase (D10A) capable of nicking the target DNA strand, triggering mismatch repair (MMR) in the replacement of the unedited sequence.[37] The addition of a bacterial uracil glycosylase inhibitor (UGI) also allowed for greater editing efficiencies by irreversibly inhibiting the removal of uracil from eukaryotic DNA during deamination.[38] The cytosine base editor was therefore the first demonstration of base editing, but adenine base editors have also been well-established as they are capable of adenine-to-guanine (A→G) mutations at targeted genomic sites.[36] Scientists used a variant of TadA, which is an RNA adenine deaminase from *E. coli*, in conjunction with dCas9 or Cas9 nickase.[36,39] As Cas9 is guided to a target region of the genome, the TadA* deaminase converts adenine to inosine (A→I) through deamination, which ultimately is read as guanine by polymerases during replication.

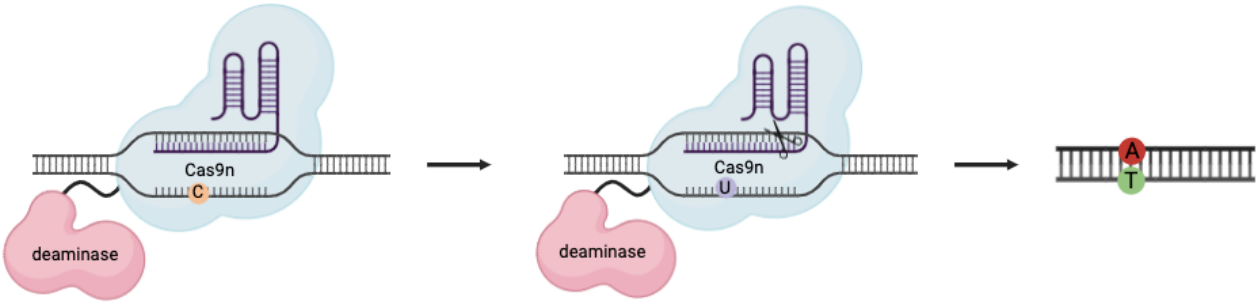

Figure 7. Depiction of a cytosine base editor.
Cas9 nickase (Cas9n) finds a target region of the genome based on a complimentary match with the sgRNA sequence. Subsequently, the deaminase (APOBEC1) converts cytosine to uracil (C→U) on the non-target strand and Cas9n cuts only the target strand. Upon replication and repair, the C:G base pair is converted to a T:A base pair.

1.4.1 Therapeutic applications of base editing

Numerous *in vivo* studies have already shown the therapeutic potential of cytosine and adenine base editors, including in clinical trials. For example, base editing was used to engineer T-cells to be less susceptible to T-cell fratricide and graft-host disease prior to the addition of

CAR7 receptor-encoding DNA.[40] These CAR7-expressing T-cells were then able to target T-cells of acute lymphoblastic leukemia (ALL) through CD7 recognition, effectively achieving antileukemic responses after 28 days post-administration. Moreover, adenine base editing has proven to be very effective at knocking down both alleles of the *PCSK9* gene by causing aberrant splicing, which resulted in lower levels of low density lipoprotein cholesterol (LDL-C).[41] Verve Therapeutics has adapted this technology into a gene therapy for treating individuals with heterozygous familial hypercholesterolemia and it has made progress in clinical trials, displaying significantly reduced levels of LDL-C in human patients.[41,42] It should be noted that although base editing has shown applications in clinical trials, it is not without adverse effects that need to be accounted for.[40–42]

1.4.2 Current methods and limitations of base editing

To date, cytosine and adenine base editors have been broadly explored for therapeutic potential in clinical studies,[40,41] mediating C→T and A→G transitions in resolving single-nucleotide polymorphisms. The opposite T→C and G→A transitions can also be achieved through the careful identification of the target and non-target strand as well; however, it requires the precise location of a PAM three nucleotides from the cleavage site.[26] Variants of SpCas9 have been engineered to reduce the restrictions on the PAM sequence, such as SpG (NGN) and near-PAMless SpRY, which have been applied to base editors.[43] Despite efforts in abolishing the stringent PAM parameters, SpRY still shows a preference towards NRN (R = A or G) PAM motifs, meaning that guanine and thymine base editors would expand the toolbox necessary for optimizing high editing efficiencies at intended genomic sites.

Out of 33,739 known human genetic variants associated with disease, 58% of them are caused by point mutations.[44–46] Although current CBEs and ABEs can reverse many of these pathogenic point mutations, the current scope of base editors limits the types of mutations that can be corrected for. New base editors are therefore required to directly create precise single-nucleotide conversions to reverse other known single-nucleotide polymorphisms. No deaminase-based guanine or thymine editors currently exist, but new approaches to base editing have taken effect in order to expand the chemical toolbox. For instance, researchers have recently developed

thymine and cytosine base editors capable of T-to-S (S = G or C) and C-to-G conversions, respectively, through structure-informed rational mutagenesis of uracil DNA glycosylase.[47] It relies on the pathway of abasic site production for direct thymine and cytosine editing. A direct guanine base editor has also been generated by engineering a variant of *N*-methylpurine DNA glycosylase, which allowed for G-to-Y (Y = C or T) conversions.[48] However, these glycosylase-centered editors have significant levels of unwanted conversions, including the substantial incorporation of adenine into the abasic site, in which this brings issues with product purity and specificity. Further, the use of abasic sites ultimately results in high levels of indel formation due to the repair mechanisms by BER enzymes such as AP lyase.[47–49] Thus, new approaches to base editing are needed to induce precise nucleotide changes with less formation of by-products.

A major drawback of current base editors is derived from the fact that they are currently all enzyme-based approaches.[33,36,47,48] Aside from the off-target effects associated with Cas9 binding itself, off-target deamination can arise during DNA replication or RNA transcription, as they expose various single-stranded regions in the genome. Hence, elevated mutation rates can arise due to the cellular overexpression of deaminases expressed from DNA vectors, which has shown to have deleterious effects observed in cancer.[50,51] Furthermore, product purity from C-to-U base editing has been significantly improved with the addition of a uracil glycosylase inhibitor, albeit with increased C-to-U mutation rates elsewhere in the genome.[33,52] Along with off-target editing at a completely separate region of the genome, bystander editing can also occur within the sgRNA-binding site.[45] Although the greatest editing efficiencies occur within the 5-bp editing window, editing can still occur within the R-loop of single-stranded DNA (termed “bystander editing.”)[33,36,45] The requirement for a narrower editing window will only increase with the growing field of achieving PAM-less SpCas9 nucleases.[43]

1.5 Photooxidation of guanine

1.5.1 Type I and type II photosensitizers

Once exposed to light of the appropriate wavelength, a ground state (S_0) photosensitizer typically converts to the first singlet excited state (S_1) upon excitation, which can then relax to the ground state by a radiative (fluorescence) or a non-radiative pathway.[53] Another pathway involves intersystem crossing (ISC), which involves a spin-forbidden process that converts a singlet state photosensitizer to a triplet state photosensitizer. The ability of a photosensitizer to catalyze photoelectron transfer (PET) in the singlet state is largely dependent on the lifetime of fluorescence (τ_f). A photosensitizer with a τ_f of less than 1 nanosecond generally does not undergo PET in the singlet excited state; and therefore, the energy is dissipated in other pathways such as ISC.[53] ISC would result in the triplet-state photosensitizer, which is able to undergo further catalysis through PET. A greater quantum yield of the triplet state (ϕ_{ISC}) generally increases the chance of the triplet-state photosensitizer undergoing PET during catalytic processes.[53]

1.5.2 Photooxidation of guanine by type I photosensitizers

As the most readily oxidizable nucleobase in DNA, guanosine is known to undergo electrooxidation at approximately 1.03 V versus NHE.[54,55] It can oxidize *via* one of two pathways – type I or type II photooxidation – which ultimately result in different product outcomes due to different mechanistic details.[56] *Via* type I photooxidation, guanine undergoes one-electron oxidation to form a guanine radical cation, which then proceeds through one of two oxidative pathways largely dependent on the nucleic acid environment (**Scheme 1**).[57] In single-stranded and double-stranded DNA, the guanine radical cation becomes deprotonated to form a neutral radical. As the photosensitizer transfers an electron to oxygen during catalytic turnover to form superoxide anion (O_2^-), O_2^- reacts with the guanine radical at the C^5 position.[53,58] Subsequent steps eventually yield the imidazolone (Iz) product; or alternatively, oxazolone (Oz) is formed.[57] In a secondary pathway, the guanine radical cation may also directly encounter nucleophilic addition of water, yielding 8-oxoguanine (8-oxoG). 8-oxoG is highly susceptible to further oxidation, resulting in

further oxidized products: spiroiminodihydantoin (Sp) and guanidinohydantoin (Gh).[56] Since type I photooxidation results from the direct oxidation of guanine, a type I photosensitizer will require an excited reduction potential that is higher than the oxidation potential of guanine in DNA.[53] For example, riboflavin is a type I photosensitizer largely characterized by a flavin moiety. It has a reduction potential of +1.50 V in the excited triplet state, which means it should allow for the oxidation of guanine.[54,55,59]

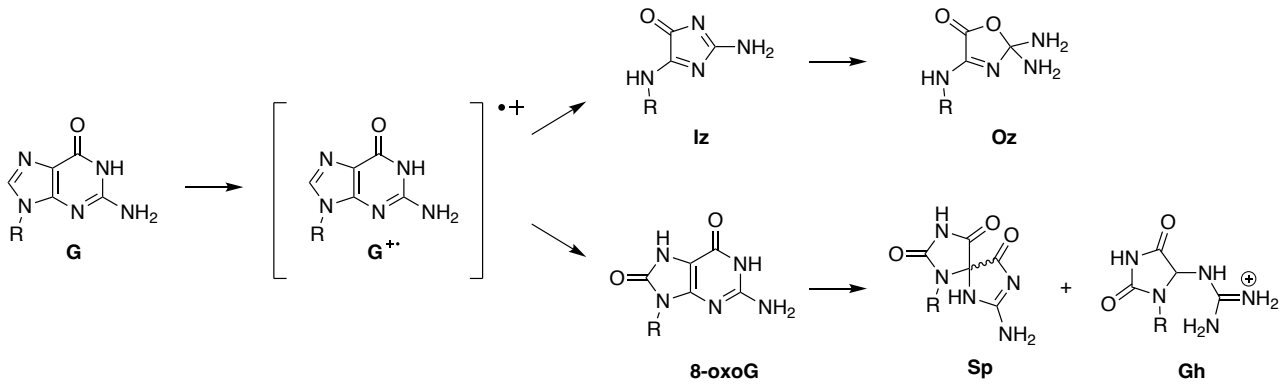

Scheme 1. Photooxidation of guanine by type I photosensitizers.
One-electron oxidation of guanine yields a radical cation that can further react with oxygen species in one of two pathways. It can yield imidazolone (Iz) and/or oxazolone (Oz). Or, it can yield 8-oxoguanine (8-oxoG) – which can then further oxidize into spiroiminodihydantoin (Sp) and guanidinohydantoin (Gh).

1.5.3 Photooxidation of guanine by type II photosensitizers

Type II photooxidation of guanine proceeds through a less direct approach, as it does not involve the direct abstraction of an electron from the nucleobase. Rather, upon excitation of a type II photosensitizer, it converts to the triplet excited state and reacts with ground state triplet oxygen ($^3O_2$) to produce singlet oxygen ($^1O_2$).[56] Singlet oxygen is an electrophile that reacts with nucleophilic substrates (*e.g.,* guanine) in cycloadditions, yielding 8-oxoguanine that can further react with $^1O_2$ to produce Sp and Gh (**Scheme 2**).[60] Type II photosensitizers do not produce Iz upon photooxidation of guanine, as their primary pathway is through the generation of $^1O_2$.[56] Specifically, having a very short τ_f of 0.5 ns, Rose Bengal undergoes fast ISC conversion to the triplet excited state – and so $^1O_2$ can therefore be produced (**Figure 8b**).[53]

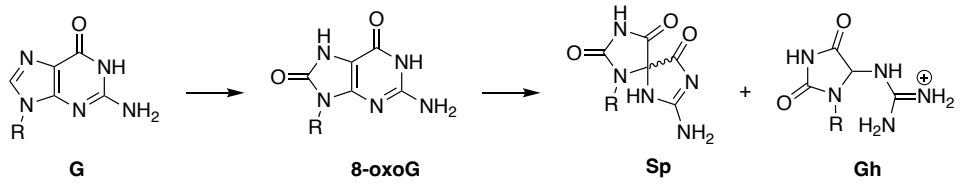

Scheme 2. Photooxidation of guanine by type II photosensitizers.
Upon photoexcitation of a type II photosensitizer, singlet oxygen ($^1O_2$) is produced. Reactive $^1O_2$ species can generate oxidized products from guanine; namely, 8-oxoguanine (8-oxoG) that further undergoes oxidation into spiroiminodihydantoin (Sp) and guanidinohydantoin (Gh).

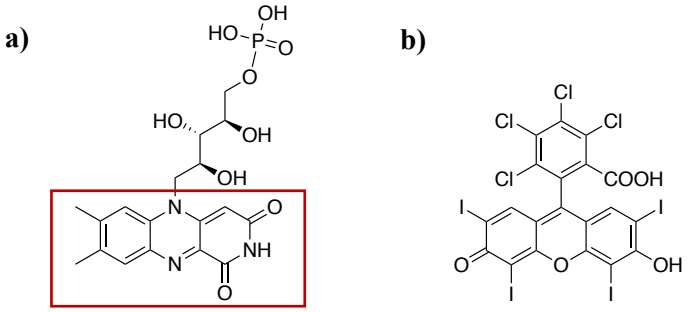

Figure 8. Chemical structures of photosensitizers.
Chemical structure of **a)** Riboflavin and **b)** Rose Bengal. The redox-active moiety of riboflavin is indicated by the red rectangle.

1.6 RNA aptamers

1.6.1 Broccoli RNA Aptamer

The broccoli aptamer has been evolved using a combination of systematic evolution of ligands by exponential enrichment (SELEX) and fluorescence-activated cell sorting (FACS) to sort high-affinity aptamers against a small molecule ligand.[61] Functioning similarly to the previously evolved spinach aptamer, the broccoli aptamer specifically binds to (*Z*)-4-(3,5-difluoro-4-hydroxybenzylidene)-1,2-dimethyl-1*H*-imidazol-5(4*H*)-one (DFHBI) – in which fluorescence is activated upon binding. Compared to the spinach aptamer, the broccoli aptamer is small and does not require a tRNA scaffold *in vitro* and *in vivo*, making it more useful for applications in cellular imaging.[62,63] The structure of the spinach and broccoli aptamers is defined by a G-quadruplex region that is responsible for DFHBI binding (**Figure 9a**).[63] These aptamers generally possess two helical domains separated by an internal loop; in which, the internal loop contains the G-

quadruplexes. DNA mimics of the broccoli aptamer have been evolved as well – for instance, the 53 nt Lettuce aptamer was evolved using SELEX, highlighting that ssDNA sequences can fold into complex architectures just as RNA aptamers do (**Figure 9b**).[64] Through further structure-guided optimization, the P1 stem was omitted while P2 was shortened and point mutations were produced to induce greater fluorescence. This yielded the 37 nt aptamer – Bibb Lettuce.

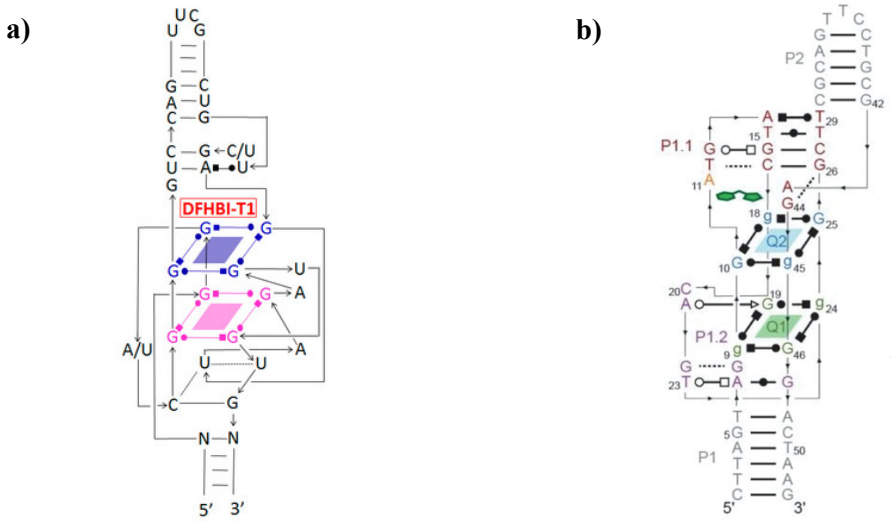

Figure 9. Two-dimensional structures of aptamers.
Shown is the a) broccoli RNA aptamer and b) Lettuce DNA aptamer with DFHBI bound above the G-quadruplex region. Arrows and Leontis-Westhof symbols represent connectivity and base-pairing, respectively. (a) is from reference [63] (© 2021, Molecules) and (b) is from reference [64] (© 2023, Nature).

DFHBI is a small molecule fluorophore that mimics the properties of GFP upon binding to the broccoli aptamer with a K_d of approximately 337 nM.[61] It can be modified at the N^3 position without disrupting the binding of DFHBI to the broccoli aptamer (**Figure 10a**).[61,65] Conjointly, photosensitizers such as Rose Bengal and riboflavin have also shown that they can be chemically modified without abolishing their photophysical properties. Specifically, carboxyester derivatives of Rose Bengal have shown to remain active while riboflavin can also be modified via the chemical replacement of the ribitol group (**Figure 10b and 10c, respectively**).[66,67] Thus, chemical conjugation of these photosensitizers to DFHBI can allow for these photosensitizers to be used with the broccoli aptamer.

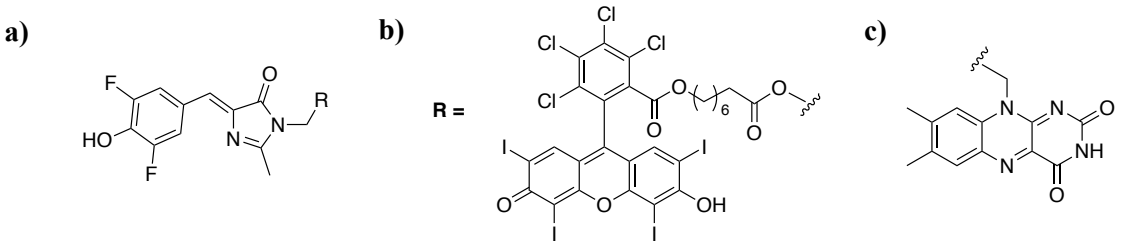

Figure 10. Chemical structures of DFHBI-linked photosensitizers.
Chemical structure of **a)** DFHBI, **b)** Rose Bengal conjugate, and **c)** riboflavin conjugate.

1.6.2 X2B2 aptamer

The X2B2 aptamer was evolved to specifically bind to the oxidized form of riboflavin, or flavin-containing molecules such as flavin adenine dinucleotide (FAD), which this specificity for oxidized forms of co-factors is not normally accounted for.[68] A mutant form of X2B2 that contains a C14U point mutation displayed the highest affinity to flavin molecules, possessing a K_d of approximately 243 nM, and is the same number of nucleotides as the broccoli aptamer. The structure encompasses a binding pocket for binding to the isoalloxazine ring of riboflavin/FAD, which contains four base triples that have deemed to be required for binding: U30:A10•A9, C29:G11•C23, A12:U28•A22, and U14•G13•G27 (**Figure 11**).[68] Thus, the X2B2-C14U aptamer can be used to preferentially bind the oxidized form of riboflavin with minor effect on the change in reduction potential, possibly allowing for the effective recruitment of riboflavin to a localized area of the genome for photooxidation of guanine.

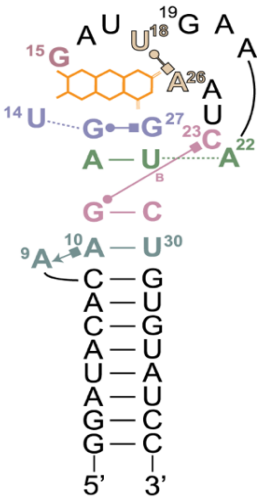

Figure 11. Two-dimensional structure of the X2B2-C14U aptamer.
The isoalloxazine ring (orange) is bound to the binding region. Leontis-Westhof symbols represent base-pairing involved. Base triples are shown: U30:A10•A9 (cyan), C29:G11•C23 (pink), A12:U28•A22 (green), and U14•G13•G27 (purple). From reference [67] (© 2022, Nature Chemical Biology).

1.7 CRISPR-guided photooxidation of guanine in cells

Through the utility of a type I or type II photosensitizer, the photoinduced oxidation of guanine can be leveraged in the development of a novel guanine base editor.[56] By fusing single-stranded RNA aptamers into the sgRNA construct, RNA-guided dCas9 can be used to recruit a photosensitizer to a target region of the genome.[23,24] Proceeding either through the direct or indirect recruitment of a photosensitizer, the aim is to create a high concentration of photosensitizer to a localized region of the genome, so that site-specific oxidation towards guanine is achieved.

The primary approach is to use the broccoli aptamer to bind and recruit DFHBI-linked photosensitizers (*i.e.,* Rose Bengal) to a target genomic site. Using an sgRNA construct with the broccoli aptamer cloned into the tracrRNA region,[24,61] dCas9 will search for a complimentary match within the genome prior to the indirect recruitment of the photosensitizer. Upon exposure to a specific wavelength of light, the photosensitizer will "switch on" and likely oxidize nearby guanines in the double-stranded region of the dCas9-bound complex. Oxidized bases in the form of Sp and Gh are known to individually base-pair with G during replication, yielding guanine-to-cytosine (G→C) mutations upon repair and replication.[69] Thus, an RNA-guided dCas9 system could ultimately achieve precise G→C conversions at specific sites in the cellular genome.

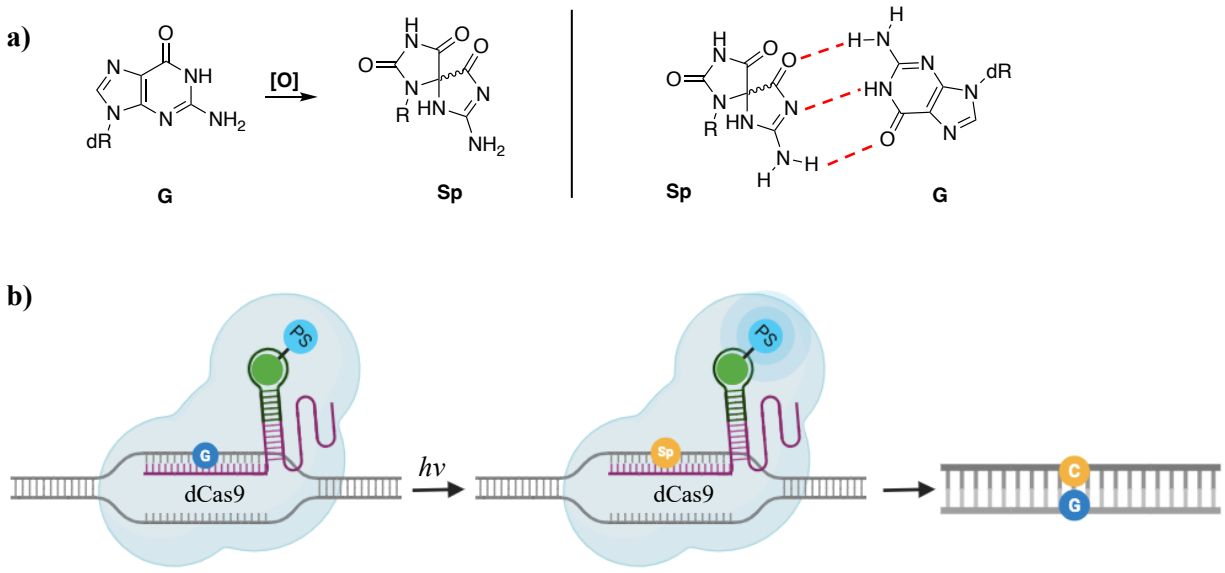

Figure 12. CRISPR-guided photooxidation using the broccoli-DFHBI RNA-binding pair.
a) Photooxidation of guanine by type II photosensitizers primarily yields spiroiminodihydantoin (Sp), which is known to be read as cytosine by polymerases. b) Catalytically-dead Cas9 (dCas9) is guided by the sgRNA-broccoli scaffold to a target genomic site. Upon excitation of the photosensitizer with visible light, photooxidation of guanine yields guanine-to-cytosine (G→C) conversion after DNA replication and repair.

An alternative approach to CRISPR-guided photooxidation of guanine is to use an aptamer that has been evolved to directly bind a photosensitizer – in this case, the X2B2-C14U aptamer.[68] Using an sgRNA construct with the X2B2-C14U aptamer cloned into the tracrRNA region,[23,24,68] the dCas9 system can directly recruit riboflavin to a localized region of the genome for targeted photooxidation. Upon exposure to light of an appropriate wavelength, riboflavin may initiate direct oxidation of guanine in its excited triplet state.[53] If so, oxidized products, such as Iz and Oz, also are known to base-pair with guanine, yielding G→C conversions upon DNA replication and repair.[69] Thus, the X2B2 aptamer is proposed to be able to effectively bind and recruit riboflavin, consequently leading to CRISPR-guided photoinduced G→C conversions at particular genomic sites in cellular DNA.

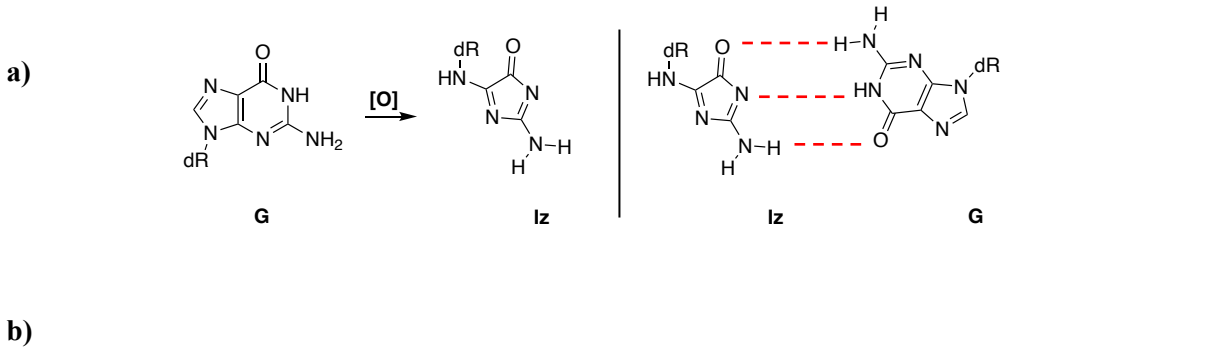

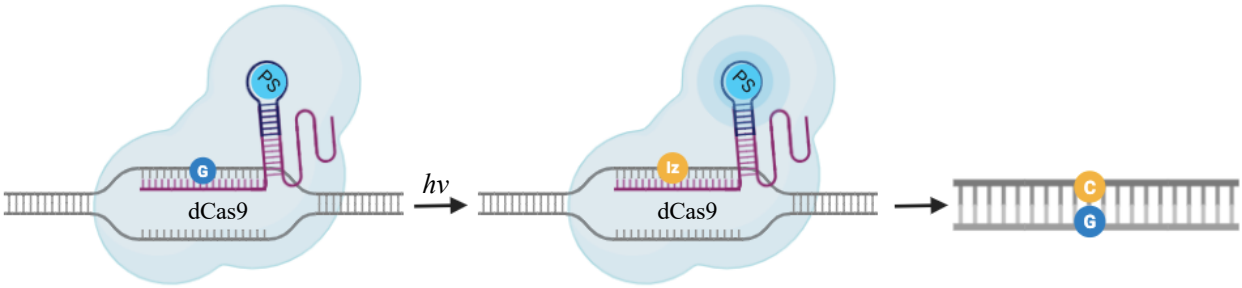

Figure 13. CRISPR-guided photooxidation using the X2B2-riboflavin RNA-binding pair.
a) Photooxidation of guanine by type I photosensitizers primarily yields imidazolone (Iz), which is known to be read as cytosine by polymerases. b) Catalytically-dead Cas9 (dCas9) is guided by the sgRNA-X2B2 scaffold to a target genomic site. Upon excitation of the photosensitizer with visible light, photooxidation of guanine yields guanine-to-cytosine (G→C) conversion after DNA replication and repair.

2 Results and Discussion

2.1 *In vitro* screening of photosensitizers

To identify a photosensitizer to be used in CRISPR-guided photooxidation, the initial step was to determine which photosensitizers can intermolecularly oxidize guanine in a single-stranded DNA sequence. As such, five photosensitizers were screened for their ability to oxidize guanine: Rose Bengal, fluorescein, methylene blue, rhodamine B, and riboflavin (**Figure 14a**). Upon initial exposure of white light for 1 hour, Rose Bengal and riboflavin were the two photosensitizers where oxidation of guanine had been observed by LC-MS/MS analysis. Subsequent experiments were done with a more specific wavelength of light used, such as 550 nm for rhodamine B,[53] which also did not allow for the photoinduced oxidation of guanine. While rhodamine B has a very similar excited reduction potential in the triplet state as per Rose Bengal, it has a substantially lower ϕ_{ISC} – 0.12 compared to 0.77 for Rose Bengal.[53] This means that it does not readily convert to the triplet state photosensitizer; and consequently, singlet oxygen cannot be produced in high enough concentrations for type II photooxidation of guanine. Meanwhile, the quantum yield of triplet conversion for Rose Bengal is substantially greater; so, although its reduction potential in the triplet state is quite similar, it is still able to produce singlet oxygen. Furthermore, riboflavin had shown to be extremely reactive with initial exposure to white light for an hour, as the ssDNA starting material had not been detected by LC-MS/MS (**Supplementary Figure 1**). This can be attributed to the fact that riboflavin has a very high excited reduction potential of 1.50 V (SCE) in the triplet state,[59] which is far above the average oxidation potential of guanine in DNA.[55] Hence, it was most likely that nearly all of the starting single-stranded DNA sequence was degraded; and thus, less harsh conditions were then explored for riboflavin-catalyzed photooxidation.

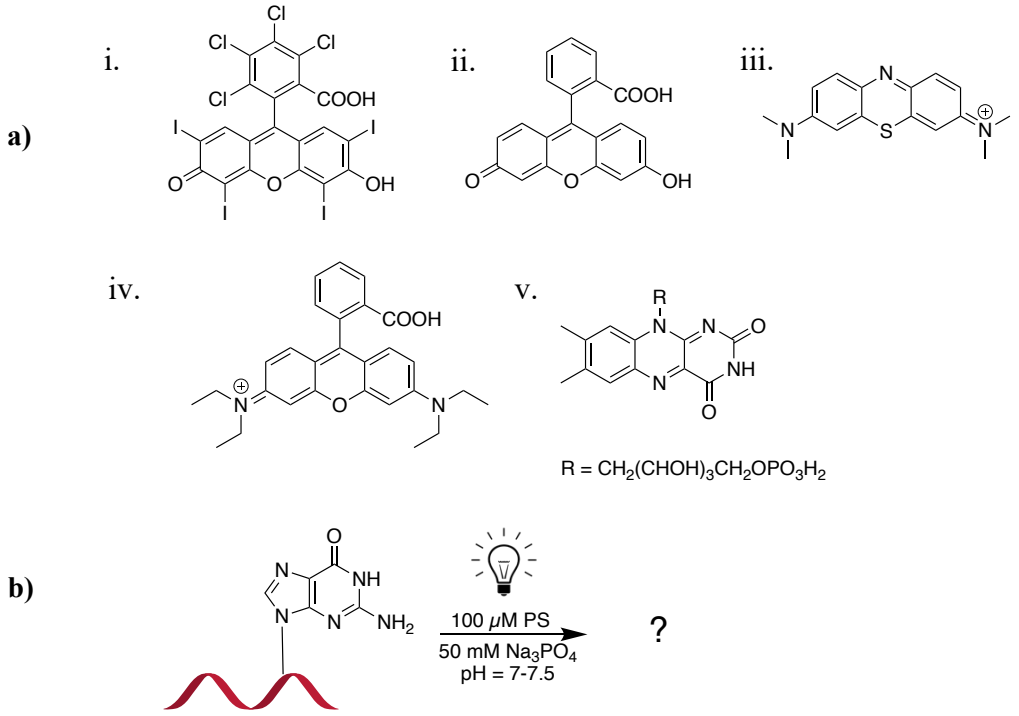

Figure 14. *In vitro* screening of photosensitizers.
a) Photosensitizers that were screened for oxidative activity were i. Rose Bengal, ii. Fluorescein, iii. Methylene blue, iv. Rhodamine B, and v. Riboflavin. b) Conditions for testing the photooxidative activity of guanine in a ssDNA sequence with one guanine. PS = photosensitizer.

2.1.1 Photooxidation of guanine by Rose Bengal

Initial findings proposed that there had been photooxidation of a guanine-containing DNA sequence with Rose Bengal, although no oxidation was observed using the other xanthine-based dyes (*e.g.,* fluorescein, rhodamine B). Investigating this finding in further detail, a time-course study was done to determine how much oxidation increases over time. Using the salt form of Rose Bengal with a high intensity of light (14.3 mW/cm^2) of wavelength 550 nm, no oxidation products were observed after 10 minutes for two of three trials. However, exciting Rose Bengal for 20 minutes was sufficient in producing spiroiminodihydantoin (Sp) as the major product besides starting material – conducive to +32 amu compared to the mass of starting material (m/z 6013). Since no imidazolone (Iz) appeared to be produced, it is presumed that Rose Bengal catalyzes guanine oxidation through type II photooxidation, requiring the triplet state photosensitizer to generate singlet oxygen.[53] After 30 minutes of light exposure, the percentage of Sp was shown to increase to an average of 13% (**Figure 15**). Although this is seemingly low yield, it is evidently

selective towards guanine over the other three types of nucleobases (A, C, T) in the 20 nt sequence, presumably due to the fact that guanine is the most susceptible to oxidation.[54,55] The intermediate oxidation product, 8-oxoguanine (8-oxoG), was not detected by the mass spectrometer, as there were no adducts corresponding to + 16 amu – corresponding to the addition of oxygen. This was expected *in vitro* as 8-oxoG is highly susceptible to further oxidation and there are no biological enzymes (*e.g.,* polymerases) to repair G→8-oxoG formation.[56,69] The production of Sp was accompanied by a slow decline of relative starting material in the reaction, giving evidence that 14.3 mW/cm^2 of green light does not have substantial photodegradation of DNA (**Figure 16**).[70] However, the oxidation of guanine by Rose Bengal with high-intensity light appears to give Sp/Gh product formation that is quite variable, as shown by the large error bars in figure 14. Therefore, further exploration of the optimal light intensity needs to be done prior to cellular studies.

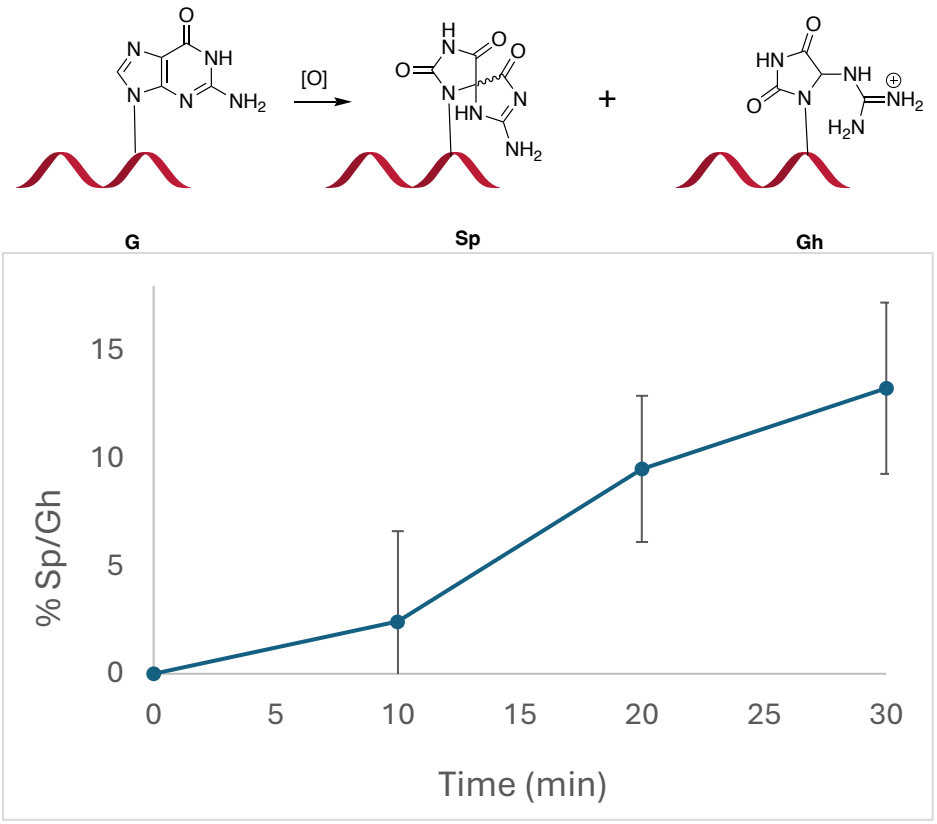

Figure 15. Production of Sp/Gh upon excitation of Rose Bengal with exposure to high intensity light. In a reaction mixture containing a ssDNA-1G sequence, Rose Bengal was excited with visible light of 550 nm at an intensity of 14.3 mW/cm^2 for timepoints of 0, 10, 20, and 30 min. The production of spiroiminodihydantoin (Sp) and guanidihydantoin (Gh) was monitored and assessed by LC-MS/MS. n = 3 trials. Error bars were generated using the standard deviation (SD) of 3 trials.

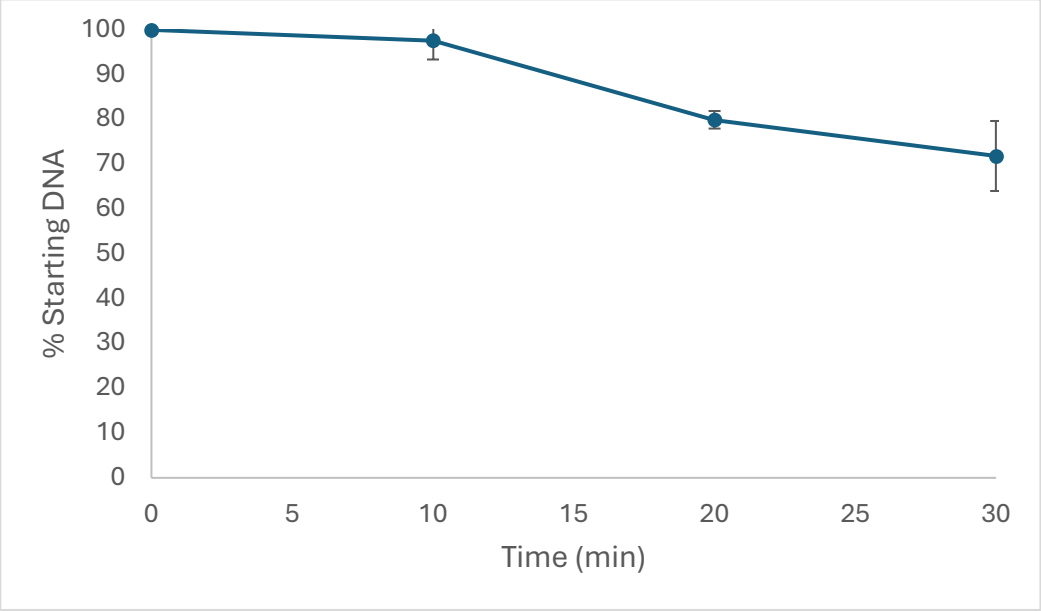

Figure 16. Percentage of starting DNA upon excitation of Rose Bengal with exposure to high intensity light.
In a reaction mixture containing a ssDNA-1G sequence, Rose Bengal was excited with visible light of 550 nm at an intensity of 14.3 mW/cm^2 for timepoints of 0, 10, 20, and 30 min. The remaining starting material (ssDNA-1G and Na adduct) was monitored and assessed by LC-MS/MS. n = 3 trials. Error bars were generated using the standard deviation (SD) of 3 trials.

The effect of lowering the intensity of green light was then observed for the Rose Bengal-catalyzed photooxidation of guanine. With a light intensity of 6.37 mW/cm^2, the relative yield of Sp and Gh was approximately 24% after only 10 minutes of exposure to green light, as indicated by m/z signals of + 32 and +7, respectively (**Figure 17 and Supplementary Data 7**). It is also worth noting a by-product proposed as a result of the reaction conditions: a mass loss of 133 amu, which indicates depurination of the guanine base. After 20 minutes of exposure to light, Sp was the primary product in the reaction mixture – signifying a preference for the $^1O_2$-mediated oxidation of guanine over other nucleobases and oxidation products (**Supplementary Data 8**). Nevertheless, the yield of Sp does not greatly increase past approximately 25% after supplying more than 20 minutes of green light to the Rose Bengal-catalyzed reaction, as it reaches a maximum possible yield (**Figure 17** – blue). This is likely due to a photobleaching effect in which reactive oxygen species (*e.g.,* $^1O_2$, O_2^-) are produced in the mixture; and in turn, they react with the Rose Bengal during its photodegradation.[71,72] As a light intensity of 6.37 mW/cm^2 appears to provide a greater yield of G→Sp formation (~25%) in a shorter timeframe compared to 14.3 mW/cm^2 (~13%), the use of high-intensity light likely caused dramatically enhanced

photodegradation as well.[72] In further evidence of the limited activity of Rose Bengal with high intensity light, 30 minutes of exposure to 14.3 mW/cm^2 light yielded a reaction mixture that primarily consists of starting material, along with minor adducts (**Figure 17 & Supplementary Data 5**). Meanwhile, 30 minutes of exposure to 6.37 mW/cm^2 light yielded a reaction mixture primarily consisting of Sp (+32 amu), signifying that Rose Bengal had been less photobleached using the light of lower intensity.

Expectedly, lowering the intensity of green light to 2.29 mW/cm^2 displayed a decreased rate of Sp/Gh formation, as only about 8.69% Sp was formed in 10 minutes (**Figure 17** - orange **and Supplementary Data 11**). Although, this rose to about 20% upon irradiation for a constant 30 minutes with minimal photoinduced DNA damage, especially considering the starting material had remained as the primary component of the reaction mixture (**Figures 17 and 18**). As seen by figure 16, the formation of Sp had not reached a maximum yield after 30 minutes of exposure to green light of 2.29 mW/cm^2 intensity. Hence, although photobleaching of Rose Bengal is minimized, lower light intensities are not very efficient for catalyzing photooxidation of guanine in cells. Short bursts of energy are typically used in cellular systems that involve the induction of oxidative stress,[73,74] so maximal G→Sp conversion needs to be achieved in a short timeframe. This ultimately means that 10-20 minute pulses of light should be viable for CRISPR-guided photooxidation of guanine in mammalian cells. A light intensity of 6.37 mW/cm^2 has therefore shown to maximize G→Sp formation *in vitro* within 10-20 minutes while minimizing photobleaching of Rose Bengal dye, allowing these conditions to be ideal for CRISPR-guided photooxidation.

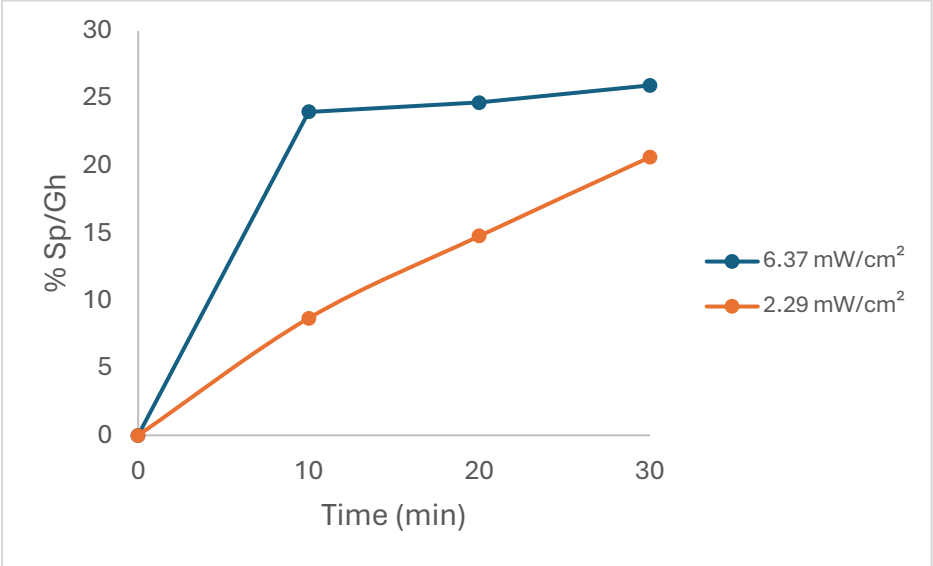

Figure 17. Production of Sp/Gh upon excitation of Rose Bengal with exposure to light of lower intensities. In a reaction mixture containing a ssDNA-1G sequence, Rose Bengal was excited with visible light of 550 nm at an intensity of 6.37 and 2.29 mW/cm^2 for timepoints of 0, 10, 20, and 30 min. The production of spiroiminodihydantoin (Sp) and guanidinohydantoin (Gh) was monitored and assessed by LC-MS/MS.

With lower intensities of green light used to excite Rose Bengal, the relative amount of starting material drastically decreased over the 30-minute period (**Figure 18**). It is indicative of the rapid consumption of starting ssDNA as the number of oxidized products had increased; whereas, the use of high-intensity light did not result in a rapid decrease in relative starting material primarily due to the photobleaching (**Figure 16**).[71,72] At 10 minutes of exposure to 6.37 mW/cm^2 light, approximately 61% of the reaction mixture was starting material – displaying that short pulses of light at 6.37 mW/cm^2 will not evidently destroy the DNA by reactive oxygen species (**Figure 18** - blue). The starting material starts to be significantly degraded past 20 minutes, likely due to an uncontrolled amount of $^1O_2$ in the reaction mixture.[56,58] In contrast, using a light intensity of 2.29 mW/cm^2 expectedly did not degrade the starting material as quickly since approximately 83% of the mixture contains starting material after 10 minutes (**Figure 18** – orange). However, the formation of Sp/Gh does not occur nearly as fast as with an intensity of 6.37 mW/cm^2.

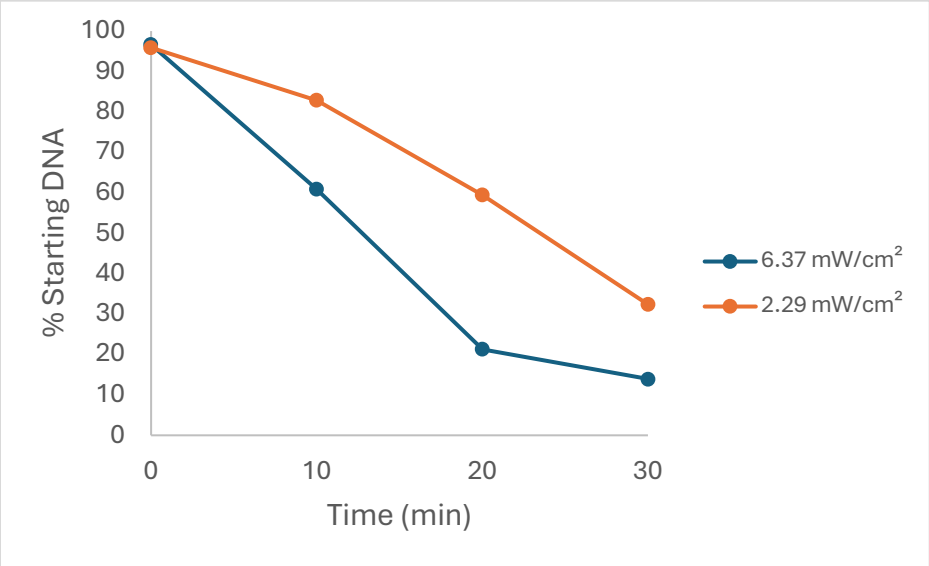

Figure 18. Percentage of starting DNA upon excitation of Rose Bengal with exposure to light of lower intensities.
In a reaction mixture containing a ssDNA-1G sequence, Rose Bengal was excited with visible light of 550 nm at an intensity of 6.37 and 2.29 mW/cm^2 for timepoints of 0, 10, 20, and 30 min. The remaining starting material (ssDNA-1G and Na adduct) was monitored and assessed by LC-MS/MS.

Following the optimization of Rose Bengal-catalyzed photooxidation of guanine, 10 minutes of exposure to green light with an intensity of 6.37 mW/cm^2 should be used in achieving precise G→C conversion in cellular DNA (**Table 1**). These parameters ultimately allow for maximal G to Sp/Gh conversion within a short timeframe of light exposure in order to minimize cellular phototoxicity – also evident by the incomplete consumption of starting material. However, cellular DNA repair enzymes may remove the edit from the genome, which would result in a lower yield of G→C conversion *in cellulo*.[49] Repeated cellular treatment with green light should therefore be done to maximize G→C conversion at cellular genomic sites. For this, the *in vitro* activity of Rose Bengal upon multiple exposures to green light was tested by pre-exposing Rose Bengal to light prior to the addition of ssDNA (**Figure S2**). Given the evidence of dye photodegradation when high-intensity light was used, it was determined that replenishment of Rose Bengal is needed upon multiple light treatments. To further determine the frequency of dye replenishment in cells, a further look into these studies should be done using light of lower intensity (*i.e.,* 6.37 mW/cm^2).

Table 1. Optimization of Rose Bengal-catalyzed photooxidation of guanine.
The photooxidation of guanine by Rose Bengal was optimized in terms of the intensity/distance and time of exposure to blue light. Optimized parameters are shown in the scheme below. Deviation from the optimized parameters are listed, along with the amount (%) of starting material and Sp/Gh in the reaction mixture. RB = Rose Bengal. G = guanine. S. M. = starting material. Sp/Gh = Spiroiminodihydantoin/guanidinohydantoin.

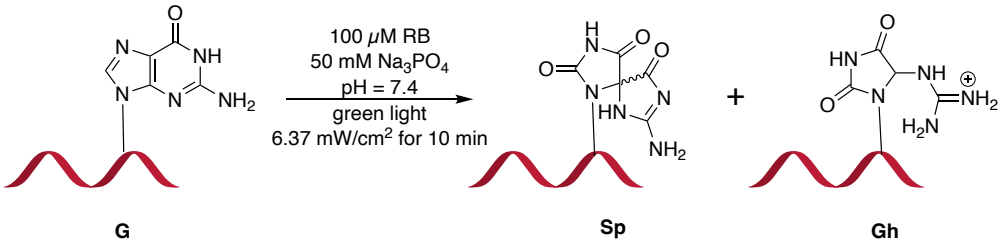

Entry	Deviation from optimized conditions	S. M. (%)	Sp/Gh (%)
1	14.3 mW/cm^2 for 10 min	100.0	0.0
2	14.3 mW/cm^2 for 20 min	80.0	9.5
3	14.3 mW/cm^2 for 30 min	71.8	13.2
4	Optimized	69.9	24.0
5	20 min of light exposure	21.3	24.7
6	30 min of light exposure	26.0	14.0
7	2.29 mW/cm^2 for 10 min	8.7	82.9
8	2.29 mW/cm^2 for 20 min	14.8	59.4
9	2.29 mW/cm^2 for 30 min	20.6	32.4

2.1.2 Photooxidation of guanine by riboflavin

Upon finding that riboflavin had most likely completely oxidized the ssDNA during the initial screening of photosensitizers, it was deemed crucial to finetune the selectivity towards the oxidation of guanine. Given the high excited reduction potential of riboflavin in the triplet state,[59] short times of exposure to blue light were first explored to minimize unwanted DNA photodamage. With a light intensity of 26.3 mW/cm^2, the Iz product was observed at approximately 15.8% after only two minutes of exposure to blue light, given by a mass adduct of -39 amu (**Figure S1a**). Given the fact that riboflavin-catalyzed photooxidation had given Iz as the major product, riboflavin allows for the type I photooxidation of guanine in DNA.[58] Beyond 5 minutes of light exposure at this intensity, Iz cannot be properly detected by LC-MS/MS. In fact, the starting material could no longer be detected, signifying the complete photodegradation of DNA possibly due to high levels of $O_2^{\bullet-}$ generated (**Figure S1b**).[58]

The intensity of light was then explored by modifying the distance from the blue light source. Upon initial studies, it was found that the selectivity towards guanine was dramatically

enhanced by increasing the distance to 30 and 50 cm (from 11 cm) upon exposure for 2-5 minutes (**Figure S1**). A time-course study was then tested in determining the maximum amount of time that photooxidation can occur. Here, it was determined that 5 minutes of exposure to light of 3.54 mW/cm^2 achieved maximal editing yield of Iz/Gh of approximately 26.7% +/- 4.5% (**Figure 19** - blue). The Iz and Oz products can be defined as mass losses of -39 and -21 amu, respectively. Iz was detected by mass spectrometry as a -39 adduct; however, the Oz product may have become protonated. Hence, it has been detected as -20 or -19 amu due to the presence of an extra proton or two. Nevertheless, it appears that an exposure time greater than 5 minutes for 3.54 mW/cm^2 is detrimental to the yield of Iz/Oz, as the product yield starts to generally decline (**Figure 19** - blue). Coincidingly, the starting material also cannot be detected upon exposure to 3.54 mW/cm^2 blue light for greater than 5 minutes (**Figure 20** - blue).

Upon lowering the intensity of blue light to 1.27 mW/cm^2, the production of Iz/Oz was detected after 5 minutes, increasing from 5.4% to 25.2% between 5 and 15 minutes of exposure (**Figure 19** – orange). This coincided with an almost linear decrease in starting material until there was a ~8.8% abundance of starting DNA remaining after 30 minutes of light. On average, the yield of Iz/Oz increased with respect to time, especially since an average of 35.7% Iz/Oz had been detected by LC-MS/MS after 30 minutes (**Figure 19** - orange). However, these long times of exposure to blue light gave rise to drastic variability – indicated by the large standard deviation acquired compared to when there were only 2-15 minutes of light exposure (**Figure 19** – orange). This therefore means that reproducibility is an issue with longer times of exposure to blue light; consequently, short exposure times are suitable for accounting for the extreme activity of riboflavin in photoredox catalysis.

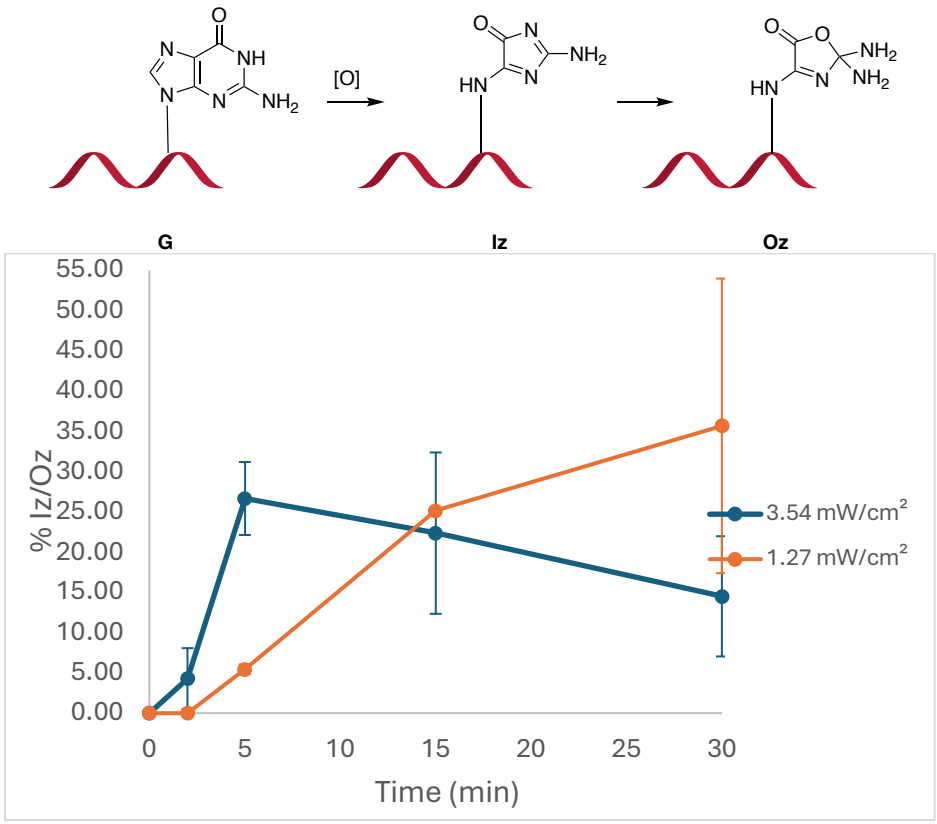

Figure 19. Production of Iz/Oz upon excitation of riboflavin with exposure to light of variable intensities. In a reaction mixture containing a ssDNA-1G sequence, riboflavin was excited with blue light at an intensity of 1.27 and 3.54 mW/cm^2 for timepoints of 0, 2, 5, 15, and 30 min. The production of imidazolone (Iz) and oxazolone (Oz) was monitored and assessed by LC-MS/MS. n = 2-3 trials. Error bars were generated using the standard deviation (SD) of 2-3 trials.

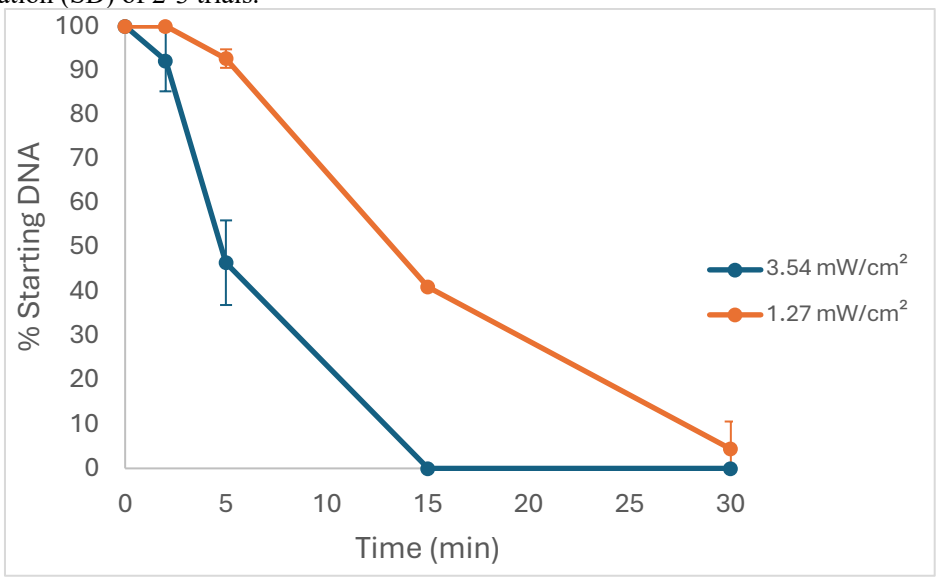

Figure 20. Percentage of starting DNA upon excitation of riboflavin with exposure to light of variable intensities.

In a reaction mixture containing a ssDNA-1G sequence, riboflavin was excited with blue light at an intensity of 1.27 and 3.54 mW/cm^2 for timepoints of 0, 2, 5, 15, and 30 min. The remaining starting material (ssDNA-1G and Na adduct) was monitored and assessed by LC-MS/MS. n = 2-3 trials.

Following the *in vitro* optimization of riboflavin-catalyzed photooxidation of guanine, 5 minutes of exposure to blue light with an intensity of 3.54 mW/cm^2 should be used in achieving maximal G→C conversion in cellular DNA. Since riboflavin allows for direct oxidation of guanine by type I photooxidation,[58,59] it may provide a more narrow base editing window than Rose Bengal. Proceeding through $^1O_2$ production,[53,58] Rose Bengal will likely create a high concentration of $^1O_2$ near a specific genomic site during CRISPR-guided photooxidation while it diffuses out. This would likely cause a broad editing window and may consequently lead to different applications than riboflavin. The use of blue light of low intensity and minimal exposure times will likely mean for minimal cellular phototoxicity upon the treatment of cells.[70] Allowing for selective G→Iz/Oz conversion of approximately 26.7% upon one light treatment, riboflavin could allow for precise G→C conversion when guided by dCas9 at cellular genomic sites. Nevertheless, multiple light treatments should be used in order to combat the DNA repair pathways, which will naturally lower the editing yield *in cellulo*.

Table 2. Optimization of riboflavin-catalyzed photooxidation of guanine.
The photooxidation of guanine by riboflavin was optimized in terms of the intensity/distance and time of exposure to blue light. Optimized parameters are shown in the scheme below. Deviation from the optimized parameters are listed, along with the amount (%) of starting material and Iz/Oz in the reaction mixture. RF = riboflavin. G = guanine. S. M. = starting material. Iz/Oz = Imidazolone/oxazolone. n. d. = not detected.

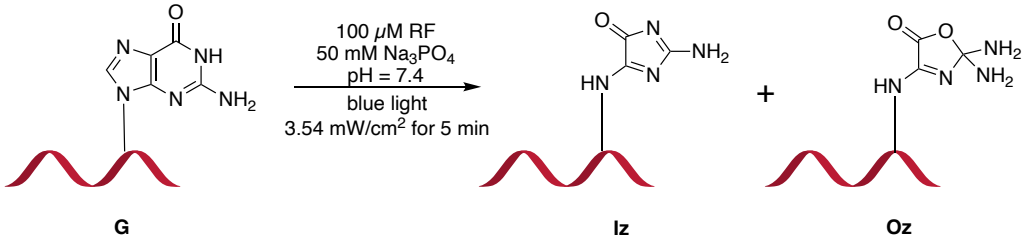

Entry	Deviation from optimized conditions	S. M. (%)	Iz/Oz (%)
1	26.5 mW/cm^2 for 2 min	19.5	15.8
2	26.5 mW/cm^2 for 5 min	0	n. d.
3	2 min of light exposure	92.10	4.3
4	Optimized	46.5	26.7
5	15 min of light exposure	0	22.4
6	30 min of light exposure	0	14.5
7	1.27 mW/cm^2 for 2 min	100	0
8	1.27 mW/cm^2 for 5 min	92.6	5.5
9	1.27 mW/cm^2 for 15 min	41	25.2
10	1.27 mW/cm^2 for 30 min	4.4	35.7

2.2 Synthesis of DFHBI-linked photosensitizers

Since the screening identified two key photosensitizers (Rose Bengal and riboflavin) that were able to oxidize guanine in a DNA sequence, it was crucial to determine a method for recruitment of the photosensitizer to a localized area of the genome. As DFHBI can be chemically modified at the N^3 position, it can be used in conjunction with the broccoli aptamer to indirectly bind and recruit the photosensitizer to a target region of the genome.[61,65] As Cas9 uses the sgRNA-broccoli scaffold to find a target genomic site, the DFHBI-linked photosensitizer can bind to the broccoli aptamer, resulting in it being proximal to the genomic site for targeted oxidation.

As a fluorescein-based dye, the active form of Rose Bengal (RB) contains a carboxyl group required for activity, which naturally interconverts between the active and inactive (lactone) form (**Scheme 3a**).[53] This carboxyl handle can be effectively used for chemical modification of the photosensitizer through amide coupling chemistry; however, direct amide coupling unfortunately abolishes the fluorescence of Rose Bengal (**Scheme 3b**).[75] The oxygen atom from the OH group

is therefore highly important for preserving the photocatalytic abilities of the dye. Luckily, the ester form of Rose Bengal remains active and these RB conjugates have consistently been used for photodynamic therapy – in fact, they have been shown to enhance photodynamic activity compared to the dye itself (**Scheme 3c**).[76–78]

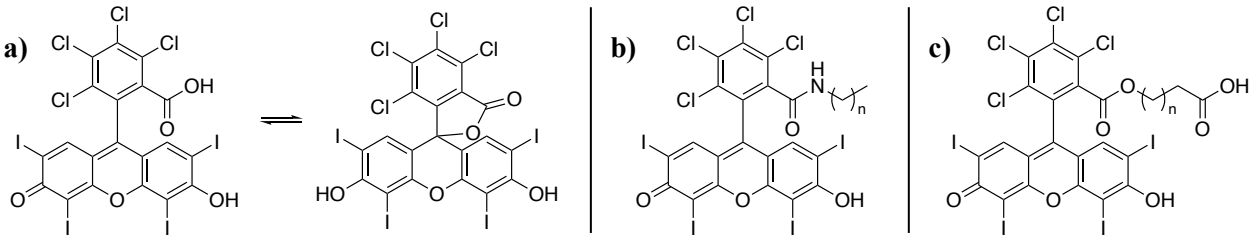

Scheme 3. Rose Bengal and derivatives.
a) Rose Bengal interconverts between its carboxyl (active) and lactone (inactive) form. b) Amide and c) ester form of Rose Bengal. b) and c) are from (75) © 2011 J. Contr. Rel. and (78) © 2007 *Bioconjugate Chem*.

An 8-carbon linker was used to generate a carboxyester form of Rose Bengal, which had been reported in the literature to still maintain fluorescence upon excitation with 530 nm.[67] As shown below, Rose Bengal can undergo an SN2 reaction with a brominated 8-carbon linker to yield the product. Rose Bengal theoretically contains two nucleophilic sites – 1) the hydroxyl group at the C^6 position and 2) the carboxyl group at the $C^{2'}$ position.[67] However, only the $C^{2'}$ carboxyl group is actually accessible for nucleophilic attack, allowing for the isolation of the product to be made easy. To avoid distillation of *N, N*-dimethylformamide (DMF), centrifugation was used to isolate the pure product and wash away starting material – affording the pure compound by ^{1}H NMR spectroscopy. The product is now suitable for coupling to DFHBI via an amine handle without largely compromising the activity of Rose Bengal.

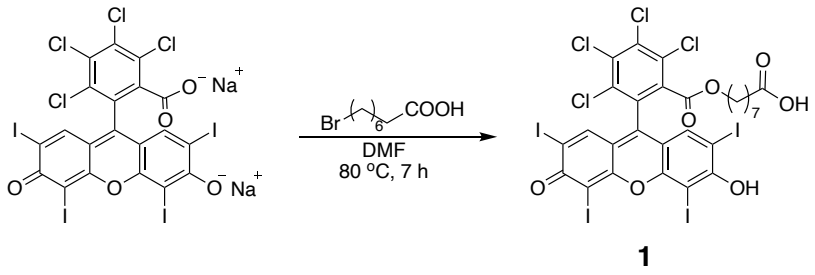

Scheme 4. Synthesis of carboxyester form of Rose Bengal.

To eventually chemically attach photosensitizers to the broccoli-binding small molecule, chemical synthesis of DFHBI was achieved through a series of steps. The first step involved a

base-assisted aldol condensation between *N*-acetylglycine and 3,5-difluoro-4-hydroxylbenzaldehyde in which acetate ion (Ac^-) is used to deprotonate the most acidic position of *N*-acetylglycine (**Scheme 5**).[65] The newly-formed anion then adds to the electrophilic aldehydic carbon prior to subsequent H^+ exchange and dehydration. Following ring closure and dehydration, formation of the oxazolone ring affords the precursor to DFHBI – ahead of the formation of the imidazolone ring (**Scheme 6**). Upon cooling, the product was isolated by filtration – affording a yield of 56% for a bright yellow crystalline solid in high purity.

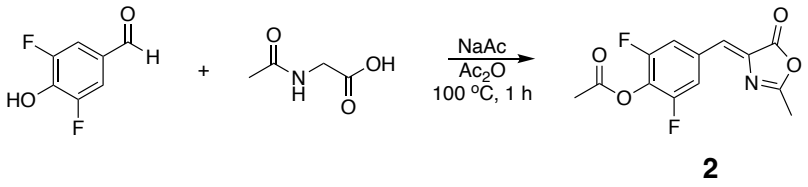

2

Scheme 5. Synthesis of (Z)-2,6-difluoro-4-((2-methyl-5-oxooxazol-4(5H)-ylidene)methyl)phenyl acetate.

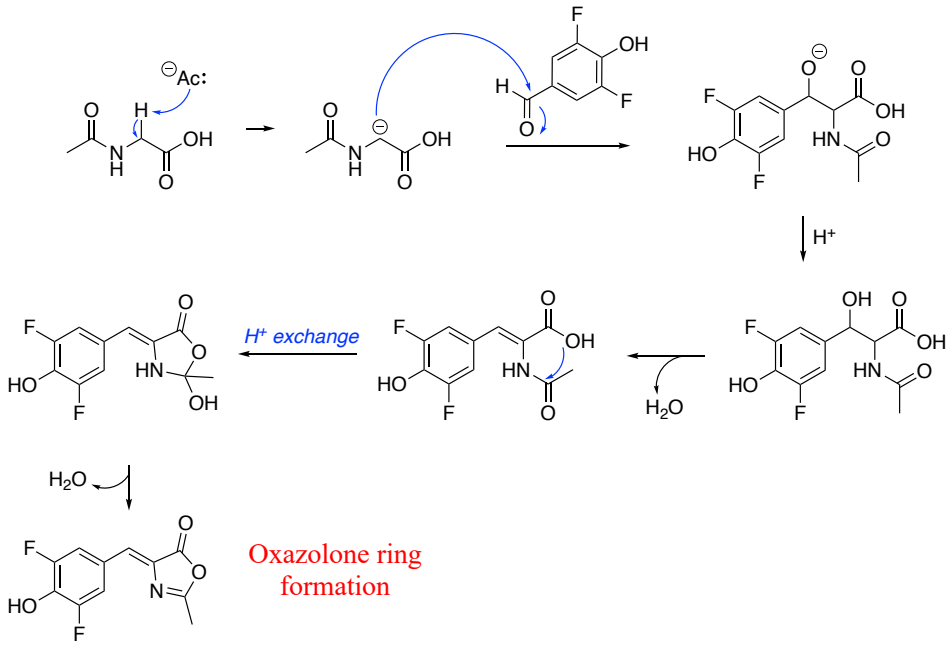

Scheme 6. Mechanistic details of base-assisted aldol condensation and ring closure in the synthesis of the oxazolone ring of the DFHBI precursor.

The next step of DFHBI synthesis worked towards the replacement of the oxazolone ring with imidazolone, which proceeded through another base-assisted reaction (**Scheme 7**). A ring-opening mechanism was facilitated through a nucleophilic attack of the carbonyl carbon by the boc-substituted hexyldiamine linker; then, subsequent ring closure and dehydration yielded the imidazolone ring. Boc protection is required to provide selectivity in nucleophilic attack by the

amine towards the activated ester (**Scheme 8**). Modifications were made to the original protocol in terms of reaction setup and purification.[65] It was found that this synthetic step is extremely moisture-sensitive; and so, care was taken to ensure that the reaction has been under the presence of argon for the duration. In addition, materials and glassware were dried prior to their use – including the potassium carbonate salt that was used for activation of the starting material. The brick red filtrate (containing the product) was concentrated prior to protonation of the phenolate using a buffered solution of sodium acetate, allowing it to be isolated and purified by flash chromatography. Purification yielded a pure orange compound in approximately 53% yield.

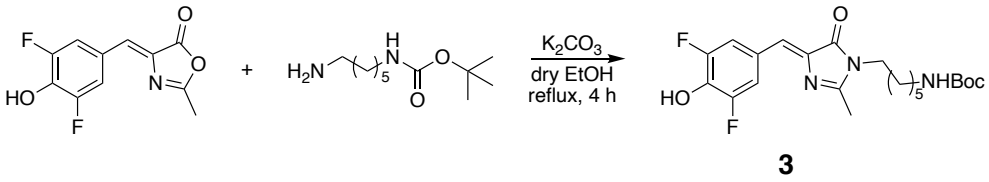

3

Scheme 7. Synthesis of (Z)-3-(6-aminohexyl)-5-(3,5-difluoro-4-hydroxybenzylidene)-2-methyl-3,5-dihydro-4H-imidazol-4-one.

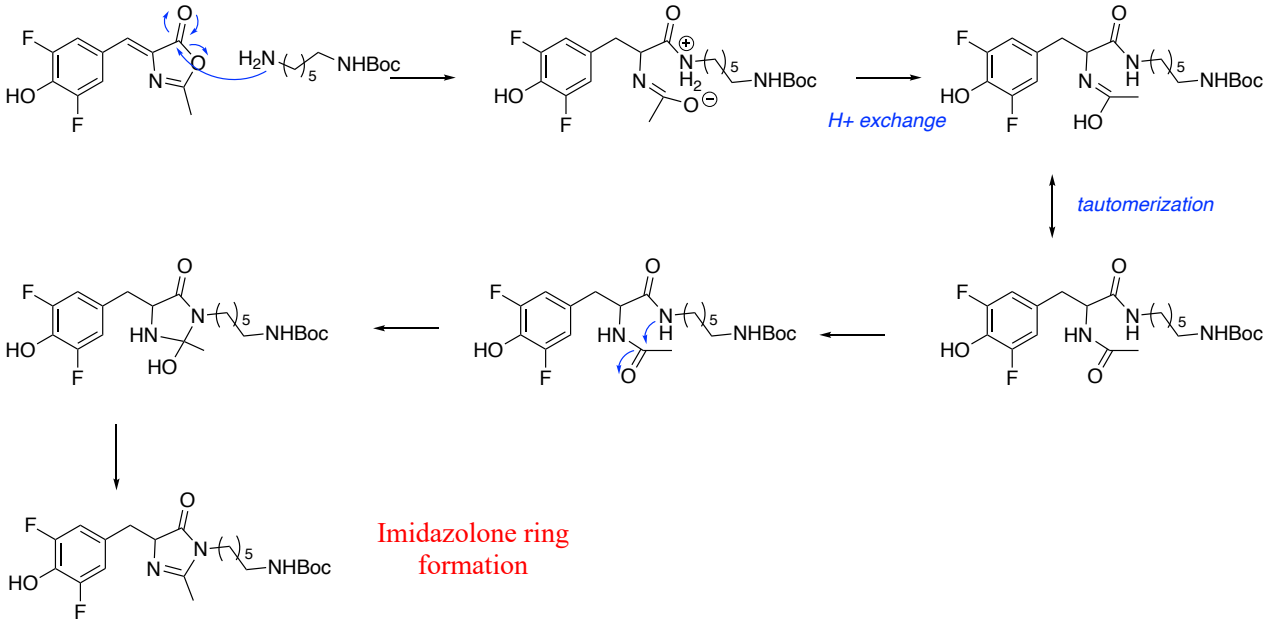

Scheme 8. Mechanistic details of base-assisted ring opening and ring closure to afford the imidazolone ring of DFHBI.

DFHBI conjugates have possessed alkyl extensions at the N^3 position with no disruption to the binding to the broccoli aptamer, including the commonly used DFHBI-IT molecule that is often used for efficient fluorescent imaging.[61,65] Further, as mentioned previously, it is also known that

the carboxyester form of Rose Bengal has been reported to be active as well.[67] Using the amine and carboxyl handles of the DFHBI and Rose Bengal conjugates, peptide coupling can be performed to chemically link these two components together, supposedly without disrupting either the binding to broccoli or the photocatalytic activity of Rose Bengal.

To ultimately proceed with the last step towards the synthesis of DFHBI-linked photosensitizers, a deprotection step is required to remove the boc protecting group from the DFHBI-linked amine (**Scheme 9**). For this, trifluoroacetic acid was used to remove the boc protecting group. As the deprotection goes to completion, the resulting TFA adduct was directly used in the final step towards the synthesis of RB-DFHBI.

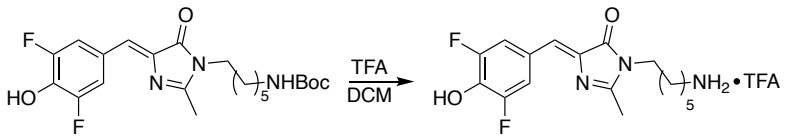

4

Scheme 9. Boc-deprotection of aminohexyl conjugate of DFHBI.

The final step for the synthesis of DFHBI-linked Rose Bengal involved the amide coupling between amine-linked DFHBI and Rose Bengal carboxyester, which can be done using HATU/DIPEA coupling reagents (**Scheme 10**). Amide coupling effectively avoided adverse side reactions since there is only one carboxylic acid functional group in Rose Bengal to be coupled to the deprotected amine of DFHBI. Upon deprotonation of the carboxylic acid handle on Rose Bengal, the formation of the activated ester allows for subsequent peptide coupling upon the addition of the amine-linked DFHBI substrate. Upon work-up and purification by silica gel chromatography, a HATU impurity remained. This was washed off through trituration, affording a dark purple solid. The remainder of the purple colour was a strong indicator that the fluorescent properties of Rose Bengal had not been compromised upon coupling to DFHBI, as direct amide coupling to Rose Bengal has afforded a white crystalline solid in previous reports.[75]

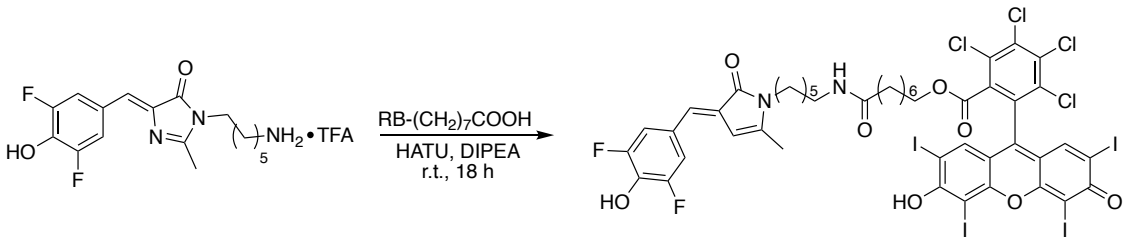

5

Scheme 10. Amide coupling of DFHBI and Rose Bengal conjugates.

Given the vast number of protons in compound **5**, the most valuable method of characterization to confirm the product was mass spectrometry. The exact mass of the compound should be approximately 1432.75, which was detected as an M+H peak (m/z 1433.75) by mass. Since chlorine has an abundance of 3:1 for ^{35}Cl and ^{37}Cl, respectively, the presence of four chlorine atoms drives the pattern of isotopic abundance. Consistent with the isotopic abundance of chlorine, the M+2 peak shows the most intense peak intensity while the M+8 peak is essentially negligible, considering it would only have an abundance of 0.39%.

Since riboflavin has also been identified as a key candidate to conduct CRISPR-guided photooxidation, the chemical synthesis of a DFHBI conjugate of riboflavin is currently in progress. For this, an aldehyde version of riboflavin can be used for reductive amination with the amine-linked DFHBI compound (**3**), which has been done before in producing conjugates of the flavin moiety.[66] Although these conjugates have been shown to remain active in generating reactive oxygen species during photodynamic therapy, it has been observed that photolytic cleavage results in the degradation into lumichrome upon 20 minutes of exposure to blue light.[66] However, as seen earlier in this chapter, 5 minutes of exposure to blue light is deemed quite efficient at catalyzing oxidation of guanine in DNA. Also, photolytic cleavage into inactive lumichrome could reduce the chances of off-target editing during CRISPR-guided photooxidation *in cellulo*.

Contributions:

Dr. Sivaraj developed the synthetic and purification protocol for compounds (**3**) to (**5**), as well as carried out the chemical synthesis and characterization.

2.3 Photophysical characterization of RB-DFHBI

2.3.1 Photooxidative activity of RB-heptylCOOH

Although Rose Bengal-peptide conjugates have shown success in applications of photodynamic therapy, the activity of fully-synthesized RB-DFHBI needs to be examined to ensure that the photoredox properties have not been compromised.[67,76,77,79] First, Rose Bengal carboxyester was tested for photooxidative activity against a guanine-containing ssDNA sequence in the same molar concentration as the previous *in vitro* experiments (**Figures 21 and 22**). It was found that the formation of Sp/Gh had increased over time – from 8.6% after 15 minutes of light exposure to approximately 12% after 30 minutes (**Figure 21**). After 30 minutes of exposure, the yield of Sp/Gh compared to the yield of using Rose Bengal salt – with only a 12.6% difference. The carboxyester form of Rose Bengal therefore closely resembles the activity of Rose Bengal itself; meaning, photosensitizer activity is clearly not quenched by the formation of the ester linkage. It was suspected that the ester formation could lock Rose Bengal into its active form,[53] enhancing photocatalytic activity against guanine in DNA – but this was not the case. Given the fact that Sp/Gh is not formed as quickly as with light of lower intensities (*i.e.,* 25% with 6.37 mW/cm^2 in 10 min), it appears that the carboxyheptylester form of Rose Bengal is also subject to photodegradation upon exposure to highly illuminative sources.[71] Nevertheless, longer exposure times can still drastically increase the yield, provided by the fact 35.4% Sp/Gh was produced after 60 minutes of exposure to green light. Along with this, a gradual decrease in relative starting ssDNA material was observed upon excitation of the Rose Bengal ester – further evidence of the oxidative activity of Rose Bengal being preserved (**Figure 22**). Therefore, the ester linkage does not evidently quench the activity of Rose Bengal, which had been the major concern for conjugating photosensitizers to the broccoli-binding DFHBI molecule.

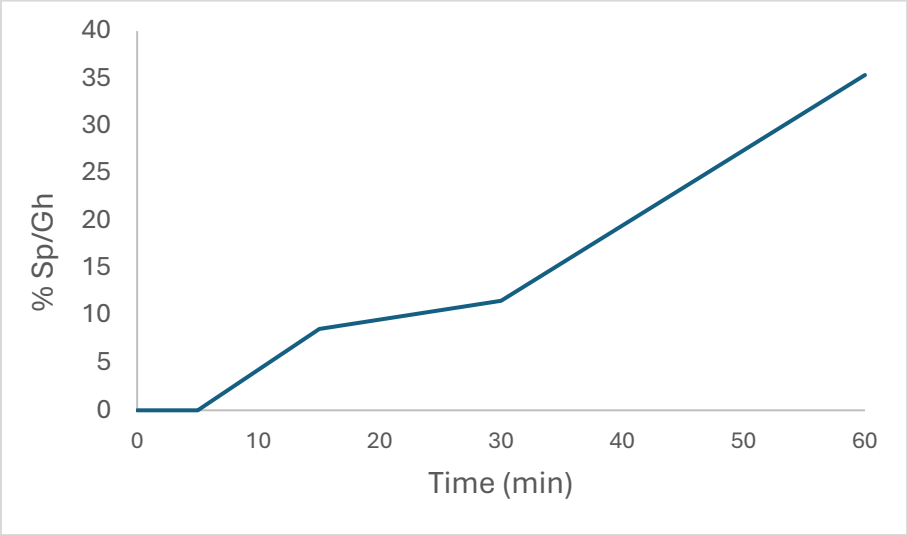

Figure 21. Production of Sp/Gh upon photoexcitation of RBheptylCOOH with exposure to high intensity light.
In a reaction mixture containing a ssDNA-1G-2 sequence, RB carboxyheptyl ester was excited with green light at an intensity of 14.3 mW/cm^2 for timepoints of 0, 2, 5, 15, 30, and 60 min. The production of spiroiminodihydantoin (Sp) and guanidinohydantoin (Gh) was monitored and assessed by LC-MS/MS.

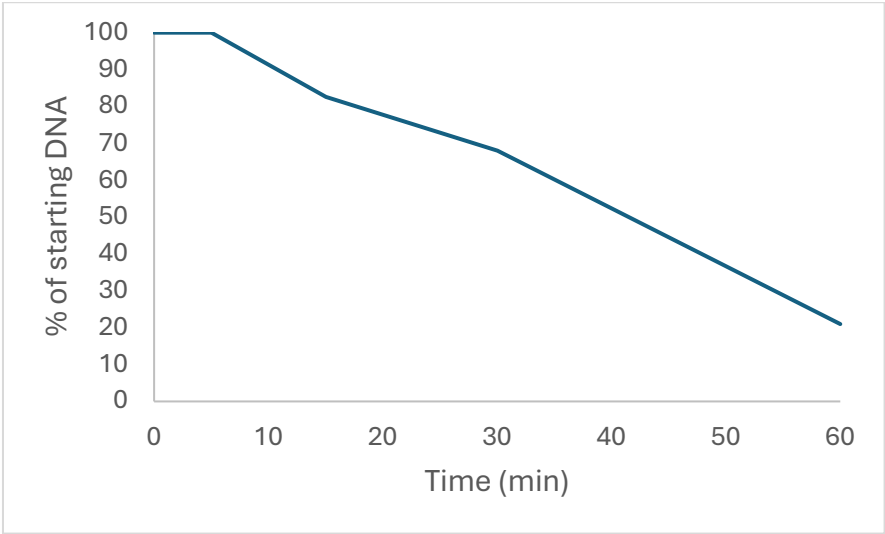

Figure 22. Percentage of starting DNA upon excitation of RBheptylCOOH with exposure to high intensity light.
In a reaction mixture containing a ssDNA-1G-2 sequence, RB carboxyheptyl ester was excited with green light at an intensity of 14.3 mW/cm^2 for timepoints of 0, 2, 5, 15, and 30 min. The remaining starting material (ssDNA-1G-2 and Na adduct) was monitored and assessed by LC-MS/MS.

2.3.2 Photophysical characterization of RB derivatives

Since RB-heptylCOOH previously produced oxidation upon irradiation with green light of high intensity, the RB-DFHBI molecule was expected to also be photoactive – as DFHBI and Rose Bengal are separated by a chemical linker. Thus, the intermolecular photooxidation of guanine was tested by irradiating RB-DFHBI with green light of high, medium, and low intensities. However, no oxidation of the ssDNA starting material was observed. This had caused some unexpected speculation over the photophysical properties of the synthesized RB-DFHBI. To observe whether there had been a shift in excitation wavelength of Rose Bengal when conjugated to DFHBI, the absorbance can be measured over a range of wavelengths. The wavelength of maximum absorbance (λ_{max}) then corresponds to the excitation wavelength for fluorescence of Rose Bengal (or conjugates).[77] Rose Bengal was first used to determine the minimum concentration that is needed to measure the excitation wavelength of the newly synthesized compound – RB-DFHBI. From measuring the absorbance of Rose Bengal for a range of concentrations (125 nM to 100 µM), 5 µM was sufficient for obtaining ideal signal by the plate reader. It gave a λ_{max} of 550 nm with a shoulder at approximately 510-520 nm, in accordance with the reported value (**Figure 23** – blue).[77] The absorbance spectrum for RB-heptylCOOH displayed a slightly red-shifted λ_{max} of 560 nm, signifying that the electron-donation from the ester linkage has some impact on the photophysical nature of Rose Bengal (**Figure 23** – green). Although, the ability of Rose Bengal to catalyze photooxidation of guanine appeared uncompromised with the addition of the linker (**Figure 21 and 22**). As seen by the absorption spectrum, RB-heptylCOOH has an absorbance of 0.515 at 550 nm of green light – slightly greater than the absorbance given by Rose Bengal at this excitation wavelength. This may be explained by the fact that the carboxyheptyl ester form of the photosensitizer locked in the active form, as it has previously been shown to increase absorbance/fluorescence.[67] This is due to the fact that increased conjugation typically causes a bathochromic shift and an increase in absorbance, as RB-heptylCOOH would no longer convert to the less conjugated lactone form of Rose Bengal.[80] Also, 550 nm is just off the λ_{max}, which could also further explain the reason why photooxidative activity is preserved with the addition of the chemical linker.

Interestingly, conjugation of DFHBI to the Rose Bengal carboxyester caused an even further bathochromic shift of approximately 20 nm compared to the ester form (**Figure 23** – red).

The λ_{max} of RB-DFHBI is therefore equal to 580 nm and it displays greater absorbance than both Rose Bengal and Rose Bengal carboxyester. This observance likely correlates to a reduced HOMO-LUMO gap ($\pi \rightarrow \pi^*$ transition), despite the fact that the conjugated systems of DFHBI and Rose Bengal are separated in RB-DFHBI.[81]

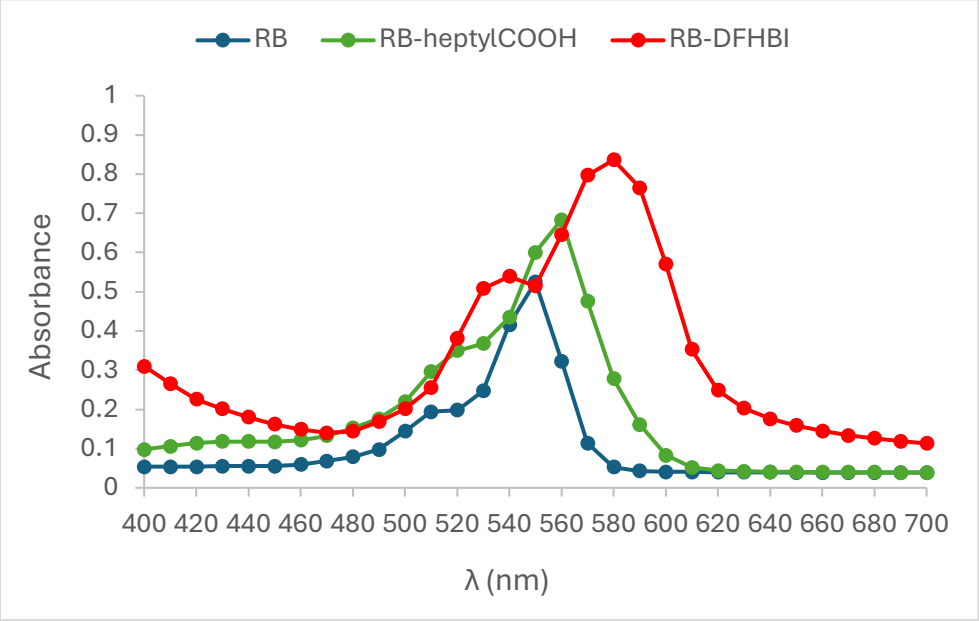

Figure 23. Absorbance spectra of RB derivatives.
Using 50 µM of each RB derivative, the optical density (OD) was measured for a wavelength range of 400 to 700 nm. The excitation wavelength is given by the wavelength of which there is maximum absorbance (λ_{max}). RB = Rose Bengal salt. RB-heptylCOOH = Rose Bengal carboxyheptyl ester. RB-DFHBI = DFHBI-linked Rose Bengal.

The bathochromic shift to 580 nm for RB-DFHBI means that irradiation of the molecule with yellow light, rather than green light, would theoretically allow for optimal photooxidation of guanine. Consequently, the photooxidation of guanine was tested using a broad-spectrum sunlamp in exciting RB-DFHBI to the triplet excited state. Even at a distance of 5 cm, which is closer than the distance used for the initial screening of photosensitizers, there was no oxidation observed over a 30-minute timeframe. Supposedly, this could be due to one of two reasons. First, the excitation wavelength of 580 nm provides photons of lower energy, which may not be sufficient for the DFHBI-linked photosensitizer to undergo a $\pi \rightarrow \pi^*$ transition during excitation.[81] However, it seemed unlikely that there would be no evidence of oxidation while using a broad spectrum source and long exposure times to excite the photosensitizing molecule. It seemed particularly unlikely since the HOMO-LUMO energy gap is expected to decrease in size with a more red-shifted excitation wavelength. The other reason may be that there is a self-quenching mechanism involved

between DFHBI and Rose Bengal that does not allow for energy transfer to produce $^1O_2$ from $^3O_2$, which was further investigated.

2.3.3 Intermolecular quenching of RB-DFHBI

To determine whether DFHBI affects the photooxidative activity of xanthine-based dyes, Rose Bengal-catalyzed photooxidation of guanine was tested in the presence and absence of DFHBI-IT (**Figure S3**). Accordingly, it was found that the presence of DFHBI did not abolish the activity of Rose Bengal, as selective oxidation towards guanine was observed through the detection of Sp/Gh formation by LC-MS/MS analysis. This also correlated with a normal reduction in starting material upon $^1O_2$ production, since 30 minutes of exposure to green light resulted in 15.0 and 21.2% starting material in the presence and absence of DFHBI, respectively. Supporting this finding, DFHBI is not reported to absorb light beyond 500 nm[82] – meaning that the energy from 550 nm light should not excite DFHBI itself. Thus, an intermolecular quenching mechanism between DFHBI and Rose Bengal is not occurring in this case, leaving intramolecular quenching as a possible explanation for the lack of RB-DFHBI's ability to photooxidize guanosine – to be investigated.

2.3.4 Intramolecular quenching of RB-DFHBI

Fluorescence of Rose Bengal occurs through the $S_1 \rightarrow S_0$ transition after initially being excited to the high-energy S_1 state by an appropriate wavelength of light.[53] Initial experiments aimed to monitor fluorescence of Rose Bengal by exciting at the λ_{max}, but it fell short of being able to observe significant fluorescence. Luckily, although Rose Bengal has a short lifetime of fluorescence of 0.5 ns, fluorescence can effectively be monitored by exciting off of a shoulder maximum of the absorbance spectrum (**Figure 23**).[83] Thus, Rose Bengal was excited using 518 nm of light while emission was captured within the range of 540-700 nm. However, the addition of a chemical linker to form RB carboxyester caused a red shift of this shoulder maximum by nearly 20 nm. The RB carboxyester was consequently excited with 535 nm of light, while emission range was set to 555-700 nm to accommodate for this change. Since the wavelength at the shoulder

maximum did not quite change with conjugation to DFHBI, RB-DFHBI was also excited with 535-540 nm with the same emission range captured (**Figure 23**). Both RB and RB carboxyester displayed high levels of fluorescence that were relatively equal to each other, which had been consistent with the literature representation (**Figure 24** – blue and green).[83] However, upon excitation of RB-DFHBI, fluorescence was dramatically reduced, as the fluorescence at 590 nm is not much above the baseline (**Figure 24** - red). It has been previously reported that photosensitizers can be conjugated to quenchers via a chemical linker separating the two. For example, pyropheophorbide-α had been conjugated to several quenchers, such as blackhole quencher 3, which has shown greater than 95% reduction in both fluorescence and $^1O_2$ generation.[84] The reduction in fluorescence caused by quenching is consistent with the dramatic reduction of fluorescence obtained for the synthesized RB-DFHBI. The putative quenching mechanism occurs through a process of energy transfer to the quencher, even with the presence of a lysine linker – like the carbon linker used to synthesize RB-DFHBI. Therefore, a similar quenching mechanism may be involved with DFHBI acting as a quencher to Rose Bengal upon excitation of the RB-DFHBI conjugate.

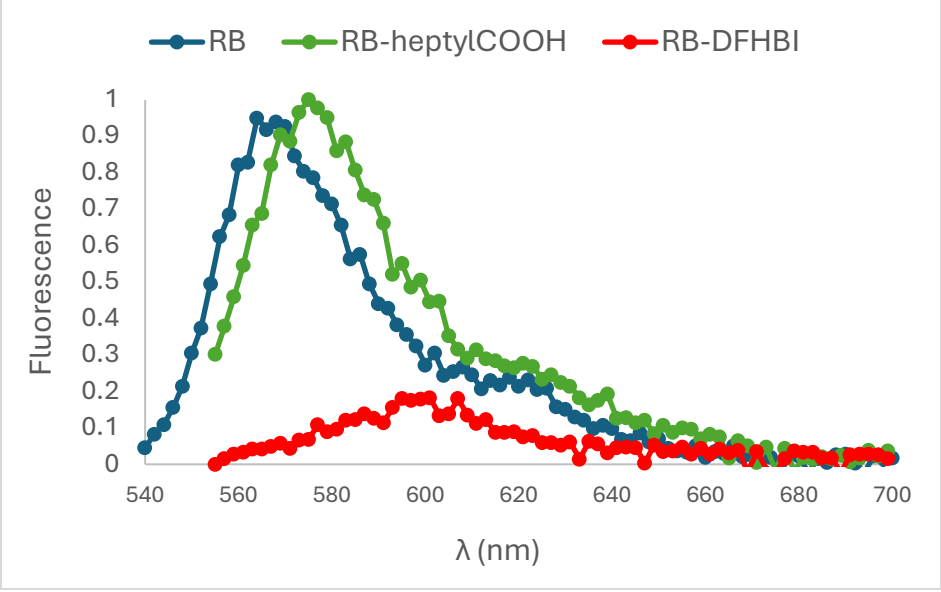

Figure 24. Fluorescence emission spectra for RB, RB-heptylCOOH, and RB-DFHBI.
RB was excited with 518 nm of light and emission was obtained from 540-570 nm. RB-heptylCOOH and RB-DFHBI were excited with 535 nm of light and emission was obtained from 555-570 nm. Data points were taken in 2 nm increments.

To propose what is likely occurring on the atomic level in further detail, a photoinduced electron transfer (PET) process at the intramolecular scale may be occurring. Upon excitation of the "acceptor" by irradiation with light, the "donor" donates an electron back to the acceptor orbital via a HOMO (donor) → LUMO (or SOMO acceptor) transition (**Figure 25**).[53,85] This then yields free ions of A^- and D^+, which may undergo back-electron transfer (BET) to revert back to the ground-state reactants.[53] In the case of RB-DFHBI, the DFHBI-linked segment of the molecule may be acting as a donor while Rose Bengal acts as the acceptor. Upon excitation of an electron from the Rose Bengal moiety via the $\pi \rightarrow \pi^*$ transition,[81] an electron from the DFHBI-linked segment may then participate in electron transfer to the newly-formed SOMO. This would consequently require that the HOMO contribution is greater for the donor (*i.e.,* DFHBI) than the acceptor (Rose Bengal); otherwise, PET would not occur. With PET occurring intramolecularly, the typical $S_1 \rightarrow S_0$ transition responsible for fluorescence of Rose Bengal would not occur, which could evidently explain the loss of fluorescence of RB-DFHBI upon excitation with the appropriate wavelength (**Figure 24**).

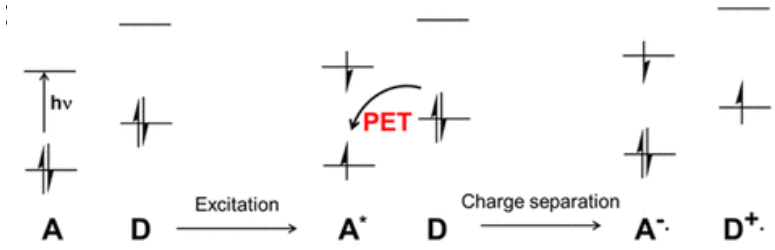

Figure 25. Intramolecular Photoinduced Electron Transfer (PET) of donor-acceptor systems.
Upon excitation of an electron within the acceptor (A), the donor participates in a PET process via a HOMO to SOMO transition. Ion pairs A^- and D^+ are the resulting products. Adapted from reference [85] (© 2016, *Acc. Chem. Res.*).

2.3.5 Aptamer-induced $^1O_2$ production by RB-DFHBI

Following the finding that the fluorescence of Rose Bengal is quenched by the chemical linkage to DFHBI, it was hypothesized that binding of RB-DFHBI to the broccoli aptamer could occupy the DFHBI moiety and restore the activity of Rose Bengal. To test this hypothesis, a DNA mimic of the broccoli aptamer – Bibb Lettuce[64] – was used to observe whether there is a change

in fluorescence upon binding of DFHBI-linked Rose Bengal to the aptamer. As it contains the antiparallel G-quadruplex region required for binding of the fluorophore, the Lettuce aptamer can bind to DFHBI (or conjugates such as DFHBI-IT) in the presence of divalent metal cations – just as broccoli does.[61,64,86] Binding of DFHBI itself was first tested to ensure that Bibb Lettuce properly folds into the proper secondary and tertiary structure upon renaturation of the DNA, as well as to ensure that the buffer and concentrations are ideal to obtain sufficient signal. Since DFHBI only fluoresces upon binding to broccoli and broccoli mimics, fluorescence was monitored (**Figure S4**). Indeed, there was a 19-fold increase in fluorescence of DFHBI with addition of the Bibb Lettuce aptamer compared to the control containing no aptamer (**Figure S4**). This provides evidence that the Bibb Lettuce properly folds into its proper structure upon renaturation; and consequently, these conditions were used to test for whether RB-DFHBI restores fluorescence upon binding to the aptamer.

Addition of the Lettuce aptamer in excess of RB-DFHBI displayed relatively the same level of fluorescence as RB-DFHBI alone, which is considerably lower than the fluorescence obtained for both RB and RB carboxyester (**Figure 26**). From this experiment, the fluorescence of the photosensitizer is not restored upon selective binding of RB-DFHBI to broccoli-type aptamers – in this case, the Lettuce aptamer. However, the loss of fluorescence does not negate the possibility of RB-DFHBI producing $^1O_2$ upon binding, especially considering the fact that Rose Bengal alone has a quantum yield of $^1O_2$ conversion that is far greater than the quantum yield of fluorescence.[53] Hence, if the Rose Bengal moiety readily converts to the triplet-state photosensitizer to catalyze $^3O_2 \rightarrow {}^1O_2$ conversion, then type II photooxidation of guanine could still be a viable route for developing a guanine base editor with enhanced spatiotemporal precision.[58] As such, a method of detecting either $^1O_2$ production or direct oxidation of guanine is required to observed whether this may be the case.

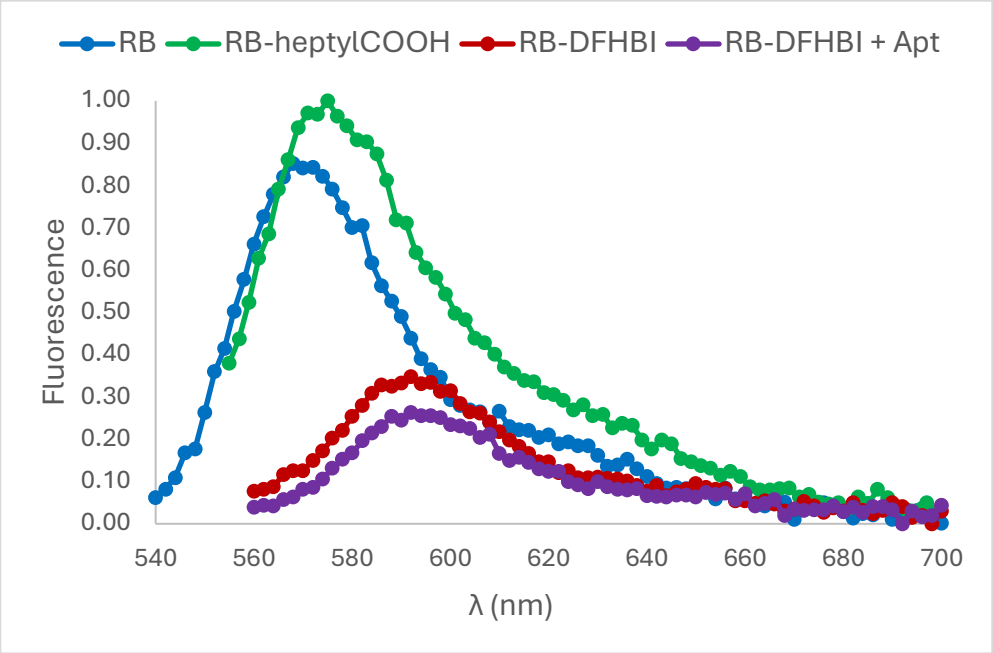

Figure 26. Fluorescence of RB-DFHBI upon addition of Lettuce aptamer.
In Tris buffer, 5 µM small molecule (RB, RB-heptylCOOH, RB-DFHBI) was excited with the appropriate wavelength of light (518, 535, 540 nm). Fluorescence of RB-DFHBI was also observed after the addition of 20 µM bibb lettuce DNA and excitation with 540 nm light.

To determine whether RB-DFHBI can catalyze $^3O_2 \rightarrow {}^1O_2$ conversion and subsequent photooxidation of guanine upon binding to the Lettuce aptamer, a reaction mixture containing an approximately 1:1 ratio[64] of aptamer to RB-DFHBI was exposed to white light for an hour (**Scheme 11**). As the starting material normally elutes at approximately 2.4 minutes, the photooxidation of guanines within the Lettuce aptamer was determined by LC-MS/MS analysis (**Supplementary Data 27**). It was of immediate notice that 1-2 new peaks had shown in the LC-MS/MS chromatograph, which were located at approximately 2.7-2.8 min (**Supplementary Data 28**). Upon analysis of these new peaks, it was found that it correlated with many oxidized products centered around the mass of the Lettuce aptamer (m/z 11617). Since there are 20 guanines in the Bibb Lettuce aptamer, it was expected that there would have been a lot of oxidized products that are difficult to decipher. However, the major product of the photoredox reaction was observed as m/z 11657 – which is proposed to be a combination of Sp (+32) and Gh (+7) in the Lettuce sequence (**Supplementary Data 29**). Oxidation was therefore observed in approximately 27.6% ± 4.5% with reference to starting material (**Figure 27**). This was in vast contrast to the minimal oxidation produced from replacing Lettuce with a scrambled DNA sequence of Lettuce, as seen by 8.3% ± 0.06% oxidation (**Figure 27**). Although, oxidation of the scrambled sequence did not

result in any known masses pertaining to oxidized guanine (*e.g.,* m/z 11657), so this may be attributed to DNA photodamage from long timeframes of exposure to intense light. The error associated with oxidative damage of the scrambled sequence is very low, so this base level of oxidation may also be due to the sensitivity of the assay and/or nonspecific photodamage of DNA. However, an increase in sample size may be required to show statistical significance of the change in oxidation between Lettuce and the scrambled Lettuce sequence, as only two replicates were performed (**Figure 27**). Moreover, increasing the amount of RB-DFHBI to 100 µM (5-fold) did not elicit greater oxidation, meaning that a 1:1 molar ratio of aptamer to RB-DFHBI likely is sufficient for maximal oxidation (**Figure S5**). Since the major products likely only consist of 2-3 oxidized guanines, it is very likely that there is a minimal chemical space where $^1O_2$ can diffuse out from the location of RB-DFHBI, allowing for precise targeting of genomic sites in CRISPR-guided photooxidation.

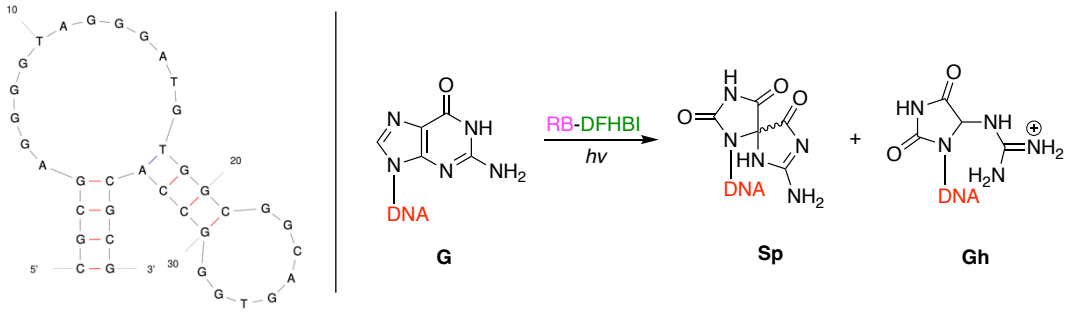

Scheme 11. Photooxidation of guanine via binding of RB-DFHBI to a broccoli mimic.
The Bibb Lettuce aptamer contains 20 guanines (G) that can potentially be oxidized to spiroiminodihydantoin (Sp) and guanidinohydantoin (Gh) upon excitation of RB-DFHBI with a broad range sunlamp.

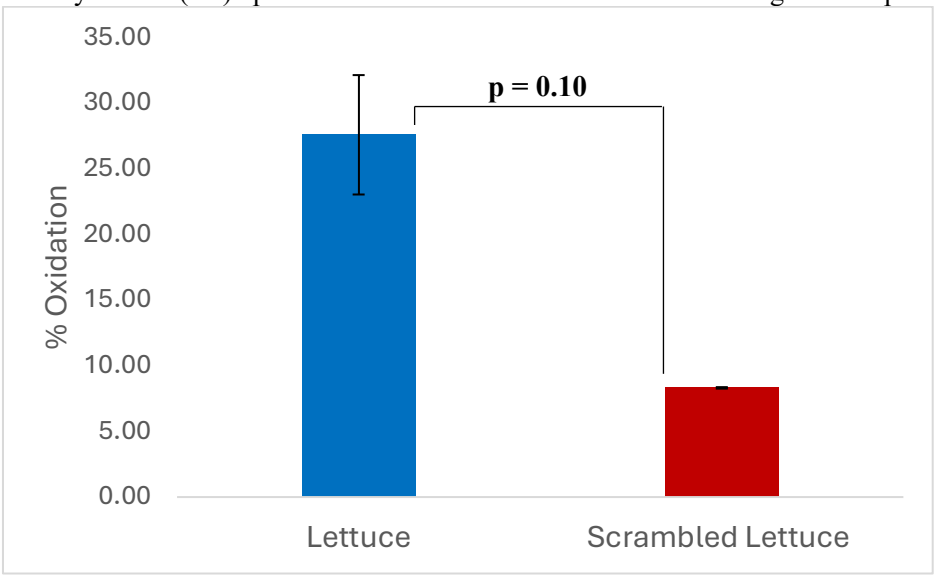

Figure 27. Photooxidation of Lettuce upon binding of RB-DFHBI.

A reaction mixture containing a 1:1 molar ratio of Lettuce DNA aptamer and RB-DFHBI was exposed to white light for 1 hour. The amount of oxidation (%) was determined by integrating the peaks corresponding to starting material (Lettuce) and oxidized products. % Oxidation = (Area of oxidized product peaks)/(Area of starting material peak)*100. Error bars represent the standard deviation (SD) of n = 2 trials.

From these initial studies using RB-DFHBI to oxidize the aptamer, it can be inferred that selective binding to the broccoli aptamer (or mimics) poses a "turn on" mechanism that allows for photooxidation by RB-DFHBI. Although substitutions to the phenyl ring are not directly conjugated to the photosensitizing xanthine ring, these substitutions can dramatically affect the fluorescence lifetime and quantum yield of fluorescein-based dyes (such as Rose Bengal).[87] Through electron-donating properties at the *ortho* position of the phenyl ring, the addition of the amine-linked DFHBI likely enhances PET, leading to more prominent deactivation of the S_1 state.[85,87] The photophysical properties, including redox potential, of photosensitizing molecules can be altered by the binding to their respective aptamers.[68] Thus, the binding of the Lettuce aptamer to DFHBI may change the electron-donating properties of DFHBI, leading to a change in the one-electron reduction potential of the donor in intramolecular PET. This would essentially mean that PET of the S_1 state is less feasible when RB-DFHBI is bound to the DNA aptamer; consequently, the S_1 state can be converted to the T_1 state during ISC to undergo $^1O_2$ production. Moreover, the ability to observe fluorescence decreases as quantum yield decreases – so if minimal PET occurs when RB-DFHBI is bound to the aptamer, it could abolish any visible fluorescence considering the quantum yield of Rose Bengal itself is only 0.09.[53,87] This would explain why fluorescence was not restored upon binding of RB-DFHBI (**Figure 26**). However, the quantum yield of triplet conversion is far greater than the quantum yield of fluorescence for Rose Bengal due to the heavy atom effect.[88] Meaning, the effect of the triplet-state photosensitizer is still observable even with minimal PET occurring when RB-DFHBI is bound to DNA.

2.4 Aptamer placement in the sgRNA scaffold

Prior to optimization of CRISPR-guided photooxidation in mammalian cells, the optimal placement of the aptamer within the sgRNA scaffold needs to be determined. This was examined by analyzing the percentage of indels formed by Cas9-induced double-stranded cleavage of genomic DNA, as target site cleavage acts as an indicator of Cas9 properly binding to the sgRNA

scaffold for target recognition.[14,26,27] The tolerance of aptamers at the 5' end of the sgRNA scaffold was first tested upon cloning of the riboflavin-binding X2B2 C14U aptamer to the 5' end. Unfortunately, this aptamer-sgRNA scaffold dramatically reduced the efficiency of Cas9 towards dsDNA cleavage. It resulted in a 3-fold reduction in Cas9-mediated indel formation for the *HEK3* genomic site – from 31.0 to 9.9% (**Figure 28**). This aptamer placement also had a dramatic effect on Cas9-mediated cleavage at the *HEK2* site, effectively abolishing any activity (**Figure 28**). It is said that aptamers appended to the 5' end of the sgRNA can inhibit threading of the sgRNA, creating only a partial R-loop complex that renders the HNH and RuvC domains in an inactive conformation.[89] The addition of just two unpaired nucleotides (*e.g.,* GG) at the 5' end are also not well-tolerated for Cas9 dsDNA cleavage.[89] Although 5' appendage clearly inhibits dsDNA cleavage, this strategy may be used if only binding of Cas9 is required for application. However, the development of efficient CRISPR base editors requires the use of a Cas9 nickase, ultimately requiring the HNH and RuvC nuclease domains in a proper R-loop conformation.[33,36]

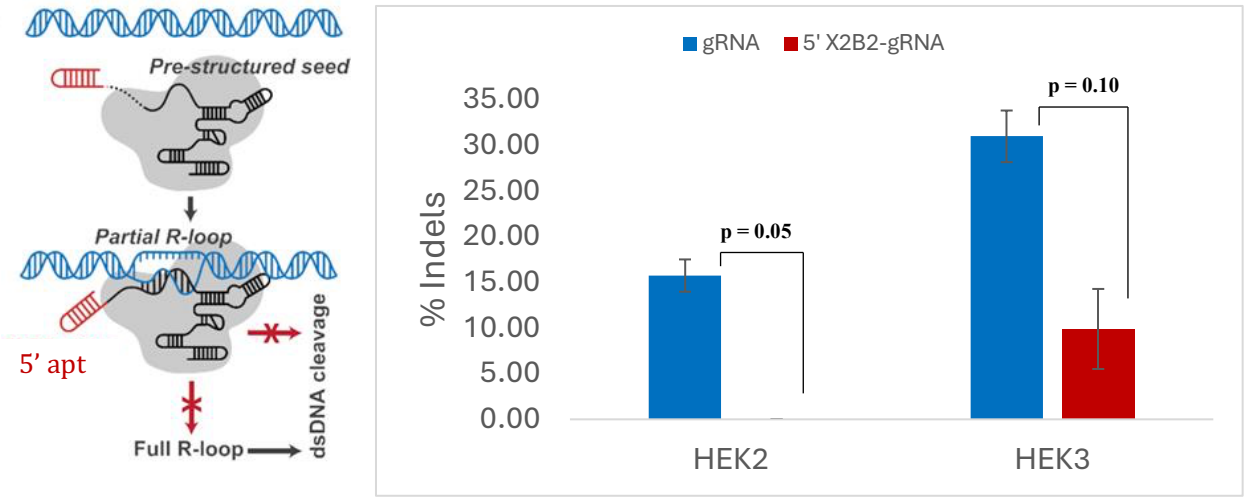

Figure 28. Cas9 cleavage efficiency with aptamer at the 5' end of sgRNA.
The X2B2 aptamer (5' apt) was cloned at the 5' end of the sgRNA scaffold and assessed for Cas9 binding and dsDNA cleavage at two target genomic sites in mammalian cells. Error bars represent the standard deviation of n = 2 trials. Figure adapted from (89) © 2020 *Nucleic Acids Research*.

As aptamers cloned into the upper stem loop of the sgRNA generally allow for full R-loop formation,[89] it was proposed that this placement would lead to proper Cas9 binding and function. In fact, the upper stem loop of the tracrRNA is in direct proximity to neighbouring duplex DNA (**Figure 29**). This supposedly allows for direct photooxidation of guanine at guanine bases in the nearby duplex DNA upon binding of the photosensitizer to the aptamer, making the upper stem

loop a prime candidate for aptamer placement. Upon testing the efficiency of Cas9-induced cleavage, there was an indel rate of approximately 23.4% with the sgRNA-broccoli scaffold and 23.9% with normal sgRNA for the *HEK3* site (**Figure 30**). This showed that proper sgRNA-Cas9 complex formation had led to complete R-loop formation, allowing for subsequent cleavage of dsDNA at the target site.[89] Targeting the EMX1 site with a similar sgRNA-broccoli construct also allowed for very similar efficiencies of Cas9-induced double-stranded cleavage – 17.2% ± 1.7% compared to 14.1% ± 1.2% for normal gRNA (**Figure 30**). Therefore, the indel efficiencies are relatively equal between normal sgRNA and the broccoli-fused sgRNA, signaling the fact that broccoli does not disrupt Cas9 from binding properly to the tracrRNA region[15]

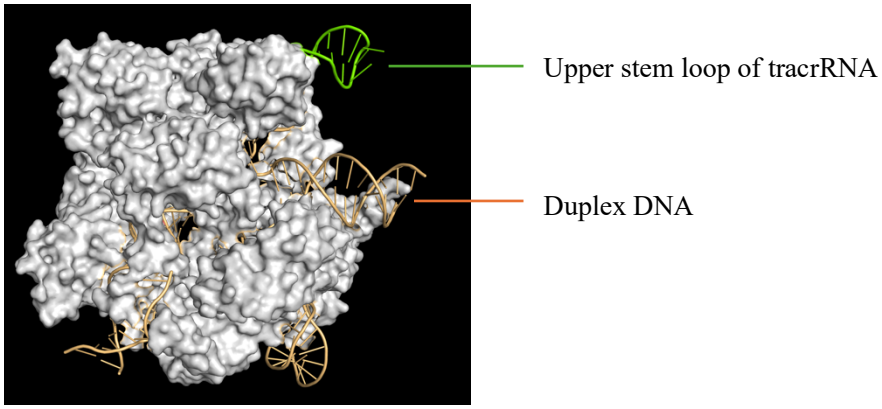

Figure 29. Structure of Cas9 complexed with guide RNA.
The upper stem loop in the 3' tracrRNA (green) shows the location where the aptamer can bind the photosensitizer for site-directed photooxidation in duplex DNA (orange).

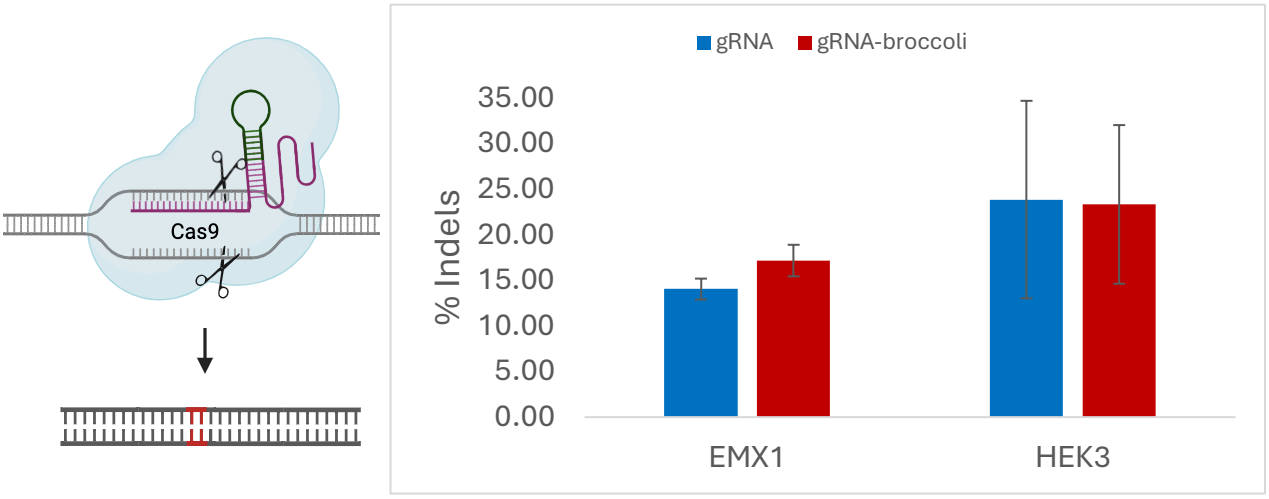

Figure 30. Cas9 cleavage efficiency with aptamer in the upper stem loop of sgRNA.
The broccoli aptamer (green) was cloned within the upper stem loop of the sgRNA scaffold and assessed for Cas9 binding and dsDNA cleavage at two target genomic sites in mammalian cells. On the left, indels are represented in red/ Error bars represent the standard deviation of n = 3 trials.

As it was expected to give similar editing efficiencies due to being the same size as the broccoli aptamer, the riboflavin-binding X2B2 aptamer[68] was also cloned into the same upper stem loop of the sgRNA scaffold. However, Cas9-induced cleavage had unfortunately dramatically decreased when guided by an sgRNA-X2B2 scaffold. The frequency of indel formation decreased from approximately 16.5% ± 3.9% for normal gRNA to 6.20% ± 1.8% for sgRNA-X2B2 while targeting the *HEK3* site – which has consistently been efficient at editing genomic DNA otherwise (**Figure S6**). Moreover, Cas9 editing efficiency was completely knocked down for the *FANCF-A* site, showing 0% indels. This means that the X2B2 aptamer likely does not allow for the proper binding of Cas9 to the sgRNA scaffold, disabling the ability to induce full R-loop formation and concerted cleavage by the Cas9 nuclease domains.[89]

3 Conclusions and Future Work

Two key photosensitizers – riboflavin and Rose Bengal – have been identified as candidates to catalyze photooxidation of guanine at targeted genomic sites using RNA-guided Cas9 protein. Proceeding through two different oxidative pathways, riboflavin and Rose Bengal provide different profiles of reactivity.[58] Riboflavin was shown to act as a type I photosensitizer in catalyzing G→Iz/Oz conversion through the direct one-electron oxidation of guanine; meanwhile, Rose Bengal was observed to catalyze G→Sp/Gh conversion through the production of $^1O_2$ during type II photooxidation.[54,58] These mutagenic profiles both ultimately lead to G→C conversion in cellular DNA,[69] but the photophysical differences in the photosensitizers lead to different reactivities. Having a high excited reduction potential in the triplet state,[59] riboflavin can catalyze selective G→Iz/Oz conversion within 5 minutes of exposure to 3.54 mW/cm^2 blue light. On the contrary, a slightly higher intensity of green light with longer exposure time is optimal for Rose Bengal-catalyzed photooxidation of guanine: 6.37 mW/cm^2 for 10 minutes.

As the broccoli aptamer was cloned into the upper stem loop of the sgRNA scaffold and verified to not affect Cas9 binding, it can be used to indirectly recruit the photosensitizer to a Cas9-targeted genomic site. DFHBI, which is the small molecule that binds to broccoli,[61] was therefore chemically-conjugated to a carboxyester form of Rose Bengal – yielding RB-DFHBI. Photophysical characterization of RB-DFHBI led to the discovery that an intramolecular photoinduced electron transfer (PET)[85,87] process quenches the S_1 state of the photosensitizer; and therefore, the ability of the photosensitizer to catalyze $^1O_2$ through the T_1 state. However, addition of a broccoli mimic (*i.e.,* Lettuce)[64] "turns on" the activity of Rose Bengal, creating an aptamer-inducible system for precise G→C conversion in cells.

As the photooxidative activity of RB-DFHBI is restored when bound by a broccoli-type aptamer, this "turn on" feature could create the utmost spatiotemporal precision. As Cas9 is guided by the broccoli-fused sgRNA to a target genomic site, the activity of RB-DFHBI should only be active once it is bound to the broccoli scaffold and the cells are exposed to green light. This could be the development of the first chemical base editor, which could deem a substantial decrease in off-target editing.

In the near future, further characterization of the aptamer-induced activity of RB-DFHBI is required prior to cellular studies. This "turn on" activity should first be tested using the broccoli

RNA aptamer itself, which would need to be transcribed *in vitro* prior to oxidation studies. Although mass spectrometry was good indicator of photooxidative activity, sequencing can be performed in order to determine the effect of proximity on guanine photooxidation. Further, a more specific wavelength of light (*e.g.,* 570 nm) should be used to excite RB-DFHBI, as it can lower cellular phototoxicity.[70] Then, the optimal intensity and time required to induce sufficient photooxidation using RB-DFHBI need to be determined, which would then be translated to cellular CRISPR-guided photooxidation of guanine.

Upon the application of RB-DFHBI to catalyze precise photooxidation of guanine in cells in the future, the location of guanine photooxidation and the editing window will need to be extensively studied. The time of exposure and intensity of light may need to be slightly modified, but repeated exposures to light will need to be done to maximize G→C conversion and combat DNA repair pathways.[37] After determining which DNA strand will be targeted by guanine oxidation, the specific Cas9 nickase can be chosen to induce replacement of the unedited DNA sequence.

Ultimately, once the guanine chemical base editor is developed in cells, on- and off-target analysis will be extensively studied to study both the precision and efficacy of the novel gene-editing system. Afterwards, the applicability of CRISPR-guided photooxidation of guanine will be studied in a number of different cell lines.

As riboflavin also provides a means of achieving precise and selective photooxidation of guanine using RNA-guided Cas9, the chemical conjugation to DFHBI will be done through the use of an aldehydic form of riboflavin (**Scheme 12**). From here, the same characterization of the photophysical properties and activity will be determined for DFHBI-conjugated riboflavin prior to the application in a cell line. By catalyzing type I photooxidation of guanine upon binding to the broccoli in the RNA-guided Cas9 system, DFHBI-linked riboflavin could allow for further precise oxidation in a narrower editing window within a shorter timeframe of exposure to blue light, minimizing cellular phototoxicity.

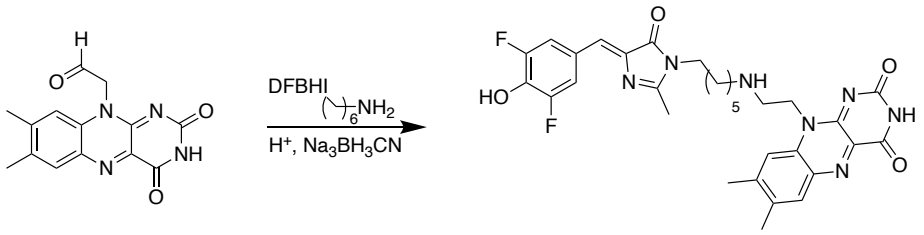

Scheme 12. Chemical conjugation of DFHBI to riboflavin photosensitizer via reductive amination.

Unfortunately, the X2B2 aptamer failed to allow for efficient Cas9 binding and function when it was cloned at the 5' end, as well as within the upper stem loop, of the sgRNA scaffold. However, placement of aptamers at the far 3' end of the sgRNA scaffold has effectively been done and may allow for the effective recruitment of riboflavin to a Cas9-targeted genomic site.[21,23] Thus, an immediate future outlook would be to clone the X2B2 aptamer at the 3' end of the sgRNA, followed by testing of the efficiency for Cas9-induced double-stranded cleavage to determine whether it affects the Cas9-sgRNA R-loop formation (**Scheme 13**). With a more direct approach to recruitment of a photosensitizer (*i.e.,* riboflavin), it could prevent the use of strenuous chemical synthesis and purification, which would increase the applicability of the chemical base editor towards the study of biological disease.

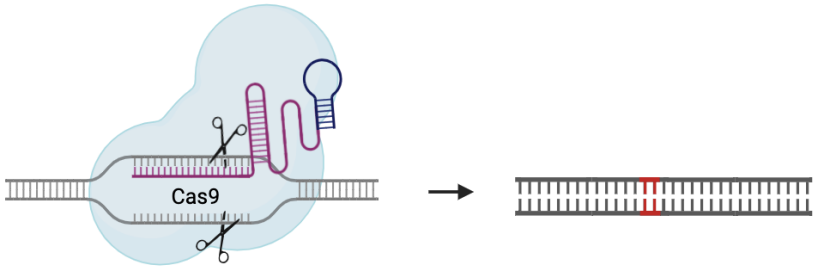

Scheme 13. Measuring efficiency of Cas9-induced DNA cleavage with X2B2 at the 3' end of the sgRNA. Cas9 uses the sgRNA-X2B2 scaffold to locate a target genomic site in cellular DNA prior to concerted double-stranded cleavage 3 nucleotides from the protospacer-adjacent motif (PAM). The efficiency of Cas9-induced cleavage is determined by the percentage of indels (red) formed during cellular DNA repair.

Through the indirect or direct recruitment of a photosensitizer by an aptamer-fused RNA-guided Cas9 system, the development of a chemical guanine base editor holds promising potential in expanding the scope of current base editors.[33,36,47,48] Employing the use of both an aptamer-inducible and photoinducible chemical system could alleviate the off-target editing associated with enzymatic base editors, as well as increase product purity. Following pioneering the development of CRISPR-guided photooxidation of guanine, it will give rise to the first guanine base editor capable of achieving precise G→C conversion at target sites in genomic DNA.

4 Materials and methods

4.1 In vitro photooxidation of DNA conditions

4.1.1 DNA sequences

ssDNA-1G-1: 5’ CCTCACTACCTCATGAAAAA
ssDNA-1G-2: 5’ CCTCACTACCTCATAGAAAA
ssDNA-1G-3: 5’ CCTCACTACCTCATAAGAAA
ssDNA-1G-7: 5’ ATCTCACCTACGCCTAAAAA

4.1.2 Intermolecular photooxidation of guanine in ssDNA

To a PCR tube, 48 µL of Milli-Q water and 50 µL of sodium phosphate buffer (100 mM, pH = 7.4) were added. Subsequently, 1 µL of 2 mM ssDNA-1G and 1µL of ~ 10 mM photosensitizer (in water or DMSO) were added to the reaction mixture. The reaction was exposed to either white light or visible light of an appropriate wavelength at a specific intensity for a duration of time. Subsequently, 20 µL of the reaction mixture was transferred to a microcentrifuge tube for ethanol precipitation. To the 20 µL volume, 2 µL of 5 M NaCl and 55 µL of ice-cold ethanol were added. It was centrifuged at 12,000 x g for 30 min at 4 ^{o}C. Samples were dried under vacuum prior to resuspension in 20 µL of water. For analysis, 10 µL of the sample was injected to LC-MS/MS in negative ion mode.

4.1.3 Riboflavin-catalyzed photooxidation of guanine in ssDNA

To a PCR tube, 48 µL of Milli-Q water and 50 µL of sodium phosphate buffer (100 mM, pH = 7.4) were added. Subsequently, 1 µL of 2 mM ssDNA-1G and 1 µL of ~ 10 mM riboflavin (in DMSO) were added to the reaction mixture. The reaction was exposed to blue light with an intensity of 26.3 mW/cm^2, 3.54 mW/cm^2, or 1.27 mW/cm^2 for timepoints of 0, 2, 5, 15, and 30

minutes. Subsequently, 20 µL of the reaction mixture was transferred to a microcentrifuge tube for ethanol precipitation. To the 20 µL volume, 2 µL of 5 M NaCl and 55 µL of ice-cold ethanol were added. It was centrifuged at 12 000 x g for 30 min at 4 ºC. Samples were dried under vacuum prior to resuspension in 20 µL of water. For analysis, 10 µL of the sample was injected to LC-MS/MS in negative ion mode.

4.1.4 Rose Bengal-catalyzed photooxidation of guanine in ssDNA

To a PCR tube, 48 µL of Milli-Q water and 50 µL of sodium phosphate buffer (100 mM, pH = 7.1) were added. Subsequently, 1 µL of 2 mM ssDNA-1G and 1 µL of ~ 10 mM Rose Bengal (in water) were added to the reaction mixture. The reaction was exposed to green light (550 nm) with an intensity of 14.3 mW/cm^2, 6.37 mW/cm^2, or 2.29 mW/cm^2 for timepoints of 0, 10, 20, and 30 minutes. Subsequently, 20 µL of the reaction mixture was transferred to a microcentrifuge tube for ethanol precipitation. To the 20 µL volume, 2 µL of 5 M NaCl and 55 µL of ice-cold ethanol were added. It was centrifuged at 12,000 x g for 30 min at 4 ºC. Samples were dried under vacuum prior to resuspension in 20 µL of water. For analysis, 10 µL of the sample was injected to LC-MS/MS in negative ion mode.

4.1.5 Intramolecular photooxidation of Lettuce DNA aptamer

To a PCR tube, 48 µL of Milli-Q water and 50 µL of 2X Tris buffer (20 mM Tris-HCl pH 7.5, 150 mM KCl, 20 mM $MgCl_2$) were added. Subsequently, 1 µL of 2 mM Lettuce DNA (or scrambled Lettuce DNA) and 0.22 µL of ~ 10 mM RB-DFHBI (in DMSO) were added to the reaction mixture. Alternatively, 1 µL of 10 mM RB-DFHBI (in DMSO) was added. The reaction mixture was exposed to white light for 1 hour. To the 100 µL volume, 10 µL of 5 M NaCl and 275 µL of ice-cold ethanol were added. It was centrifuged at 12,000 x g for 30 min at 4 ºC. Samples were dried under vacuum prior to resuspension in 20 µL of water. For analysis, 10 µL of the sample was injected to LC-MS/MS in negative ion mode.

4.16 LC-MS/MS analysis conditions

LCMS analyses were performed using Agilent Infinity Lab LC/MSD system.

Samples were diluted in water prior to injection into the LC-ESI-MS/MS in negative ionization mode. Chromatographic conditions consisted of a solvent gradient, starting at 10% A and 90% B at 0 minutes. From 0 to 4 minutes, the concentration of A increases to 90%. Afterwards, it ramps down to 10% A between 4 to 5 minutes and stays constant for 1 minute. Flow rate: 0.5 mL/min. Column: HALO 400 A, ES-C18, 3.4 uM, 2.1 x 30 mm. ESI^- ionization mode.

Solvent A: 10 µM EDTA, 0.038% TEA pH 7, 0.75% HFIP in 90:10 MeOH:Milli-Q.

Solvent B: 10 µM EDTA, 0.38% TEA pH 7, 0.75% HFIP in Milli-Q. Flow rate: 0.5 mL/min.

4.2 Chemical synthesis of RB-DFHBI

4.2.1 Synthesis of Rose Bengal carboxyheptyl ester (1):

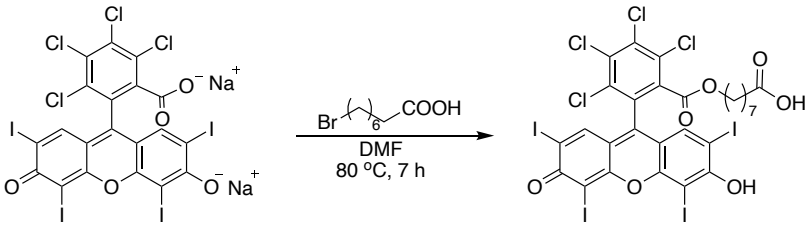

1

In a round-bottom flask, Rose Bengal salt (100 mg, 0.1 mmol) and 8-bromooctanoic acid were dissolved in *N,N*-dimethylformamide (1 mL). This solution was magnetically stirred and heated for 7 h at 80 °C. Upon work-up, 30 mL of diethyl ether was added and the mixture was centrifuged at 4 °C for 5 minutes, affording a pellet. The pellet was washed with diethyl ether (5 mL) prior to another centrifugation. Distilled water (20 mL and 5 mL) was used to remove the excess starting material and inorganic species. The pellet was finally washed with diethyl ether (5 mL) again prior to the last centrifugation. ^{1}H NMR {400 MHz, DMSO-d_6} δ 11.9 (br.s, COOH), 8.17 (br.s, ArOH),

7.48 (s, ArH, 2H), 3.93 (t, J = 6.3 Hz, 2H), 2.18 (t, J = 7.8 Hz, 2H), 1.43 (m, J = 7.5 Hz, 2H), 1.03-1.08 (m, J = 7.7 Hz, 6H), 0.89 (m, J = 7.3 Hz, 2H). ^{1}H NMR matched the literature.

4.2.2 Synthesis of (*Z*)-2,6-difluoro-4-((2-methyl-5-oxooxazol-4(5*H*)-ylidene)methyl)phenyl acetate (2):

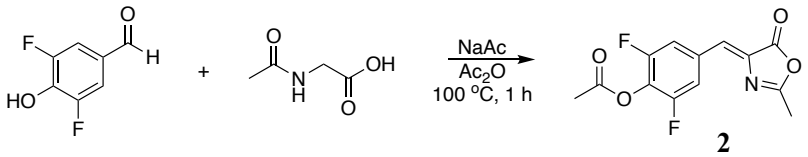

2

N-acetylglycine (753 mg, 6.44 mmol), anhydrous sodium acetate (529 mg, 6.44 mmol), and 4-hydroxy-3,5-difluorobenzaldehyde (1.018 g, 6.44 mmol) were added to a round-bottom flask with acetic anhydride (3 mL). The reaction was stirred at 100 °C for 1 h. After cooling the reaction to room temperature, cold ethanol (30 mL) was added while stirring and the reaction was left stirring overnight at 4 °C. The resulting crystalline solid was filtered and washed with a small amount of cold ethanol, hot water, and hexanes. 56% yield. ^{1}H NMR {400 MHz, $CDCl_3$} δ 7.78 (d, J = 8.5 Hz, 2H), 6.98 (s, 1H), 2.45 (s, 3H), 2.42 (s, 3H). ^{1}H NMR matched the literature.

4.2.3 Synthesis of *tert*-butyl (*Z*)-(6-(4-(3,5-difluoro-4-hydroxybenzylidene)-2-methyl-5-oxo-4,5-dihydro-1*H*-imidazol-1-yl)hexyl)carbamate (3):

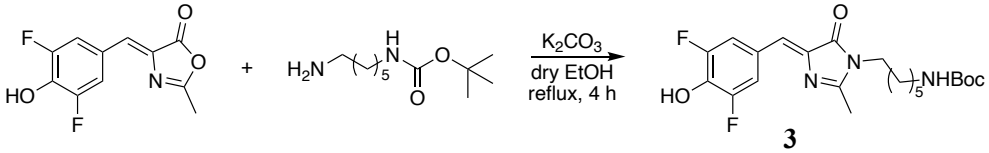

3

In a round-bottom flask under an inert atmosphere, compound **2** (500 mg, 1.76 mmol) and potassium carbonate (608 mg, 4.4 mmol) were dissolved in anhydrous ethanol (8 mL) prior to the addition of *N*-boc-1,6-hexadiamine (840 mg, 3.87 mmol). The reaction mixture was heated to reflux for 4 h. The brick red filtrate was concentrated and redissolved in a 1:1 mixture of ethyl acetate and 500 mM sodium acetate (pH 3). The organic layer was dried over magnesium sulfate prior to removal of the solvent by rotary evaporation. The compound was purified by column chromatography using 6:4 ethyl acetate/hexanes. 53% yield. 1H NMR {400 MHz, $CDCl_3$} δ 7.76-7.78 (m, 2H), 6.91 (s, 1H), 4.57 (br.s, 1H), 3.60 (t, J = 7.4 Hz, 1H), 3.12 (q, J = 6.3 Hz, 2H), 2.40 (s, 3H), 1.64 (m, 3H), 1.46 (s, 11H), 1.37 (m, 4H). ^{1}H NMR matched the literature.

4.2.4 Synthesis of DFHBI conjugate of Rose Bengal (5):

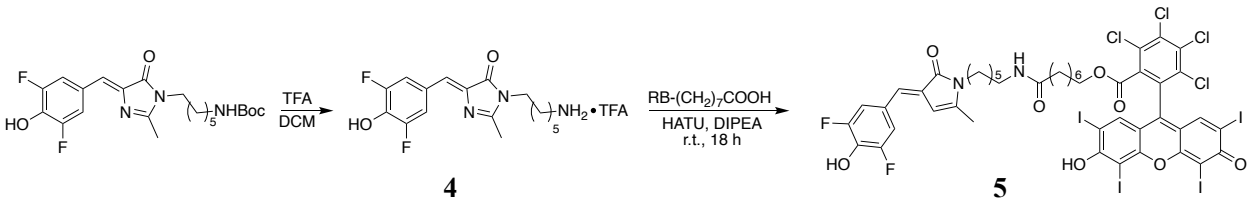

4 **5**

In a round-bottom flask, compound **3** (140 mg, 0.32 mmol) was dissolved in dichloromethane (5 mL) prior to the addition of trifluoroacetic acid (1 mL, 1.489 g/mL, 13.1 mmol). The reaction mixture was concentrated and used in the next step without purification. Compound **4** (23 mg, 0.054 mmol) and compound **1** (30 mg, 0.027 mmol) were dissolved in DMF (1 mL). HATU (20.52 mg, 0.054 mmol) was then added, followed by DIPEA (18 µL, 0.742 g/mL, 0.108 mmol). The reaction was left to stir at room temperature for 18 h. The reaction mixture was diluted with 40 mL of water prior to extraction with ethyl acetate (3 x 40 mL). The organic layer was dried over $MgSO_4$ and concentrated under reduced pressure. The product was isolated via column chromatography using 20% MeOH/DCM prior to trituration with Et_2O/DCM. 63% yield. ^{1}H NMR {400 MHz, DMSO-d_6}: δ 10.94 (br.s, 1H), 10.06 (br.s, 1H), 8.32 (s, 1H), 7.98 (m, 1H), 7.69 (m, 1H), 7.62, (m, 1H), 6.90 (s, 1H), 3.91 (t, 2H), 3.01 (q, 2H), 2.42 (m, 1H), 2.38 (s, 1H), 1.66 (m, 1H), 1.52-1.56 (m, 1H), 1.47 (d, 1H), 1.39 (m, 4H), 1.24 (m, 6H), 1.16 (m, 1H), 1.05 (m, 6H), 0.87 (m, 3H). ^{13}C{^{1}H} NMR {400 MHz, DMSO-d_6}: δ 172.4, 157.1, 137.1, 79.6, 76.8, 38.8, 36.0, 29.5, 28.9, 28.1, 26.4, 25.9, 25.5, 15.9.

4.3 Measuring absorbance and fluorescence of RB and RB derivatives

4.3.1 Measuring absorbance of RB and RB derivatives

To a 96-well transparent plate, 5 µL of 100 µM RB, RB carboxyester, or RB-DFHBI was added in 95 µL of 10 mM Tris-HCl (pH 7.5, 75 mM KCl, 10 mM $MgCl_2$) buffer. Absorption spectra were acquired in the range of 400 to 700 nm with data points obtained in 10 nm increments. Absorbance measurements were taken using a BioTek Synergy H1 microplate reader.

4.3.2 Measuring fluorescence of RB and RB derivatives

To a 96-well black plate, 5 µL of 100 µM RB, RB carboxyester, or RB-DFHBI was added in 95 µL of 10 mM Tris-HCl (pH 7.5, 75 mM KCl, 10 mM $MgCl_2$) buffer. If aptamer was needed in the mixture, 1 µL of 2 mM Bibb Lettuce was added. Fluorescence spectra were acquired with the following excitation wavelengths (λ_{exc}) and ranges of emission (λ_{em}). Emission was observed in 2 nm increments. Fluorescence measurements were taken using a BioTek Synergy H1 microplate reader.

Table S1. Excitation (λ_{exc}) and emission wavlengths (λ_{em}) used for fluorescence spectra.
RB = Rose Bengal salt. RB carboxyester = carboxyheptyl ester form of Rose Bengal. RB-DFHBI: DFHBI-linked Rose Bengal.

Small Molecule	λ_{exc} (nm)	λ_{em} (nm)
RB	518	Start: 540 End: 700
RB carboxyester	535	Start: 555 End: 700
RB-DFHBI	535 or 540	Start: 555 or 560 End: 560-700

4.4 Assessing the aptamer stability within the sgRNA scaffold

4.4.1 Cell lines

The human embryonic kidney cell line expressed with SV40 T antigen (HEK293T) was cultured in DMEM supplemented with 10% FBS, 1% GlutaMax, and 1% P/S (Penicillin/Streptomycin). The cells were incubated at 37 °C and 5% CO_2.

4.4.2 Plasmids

Original plasmids were purchased from Addgene but sequence modifications were confirmed by Sanger sequencing prior to experimental usage. Plasmids purchased for mammalian transfection were SpRY with BPNLS-3xFLAG-P2A-EGFP and SpCas9 gRNA backbone (BPK1520) BsmBI. Custom plasmids were purchased for testing X2B2 and broccoli in the upper stem loop of the

sgRNA. Plasmids were isolated using GB-Clean™ Plasmid Miniprep Kit (HiPure Mini system) and guidelines were followed according to the manufacturer.

4.4.3 DNA sequences for spacers

EMX1	5’ CACCGAGTCCGAGCAGAAGAAGAA 5’ AAACTTCTTCTTCTGCTCGGACTC
FANCF-A	5’ CACCGGAATCCCTTCTGCAGCACC 5’ AAACGGTGCTGCAGAAGGGATTCC
HEK2	5’ CACCGAACACAAAGCATAGACTGC 5’ AAACGCAGTCTATGCTTTGTGTTC
HEK3	5’ CACCGGCCCAGACTGAGCACGTGA 5’ AAACTCACGTGCTCAGTCTGGGCC

4.4.4 DNA primers for genomic site amplification

EMX1	5’ CAGCTCAGCCTGAGTGTTGA 5’ CTCGTGGGTTTGTGGTTGC
FANCF-A	5’ CATTGCAGAGAGGCGTATCA 5’ CATGCCGACCAAAGCGCCG
HEK2	5’ CCAGCCCCATCTGTCAAACT 5’ TGAATGGATTCCTTGGAAACAATGA
HEK3	5’ ATGTGGGCTGCCTAGAAAGG 5’ CCCAGCCAAACTTGTCAACC

4.4.5 Molecular cloning of X2B2 at the 5’ end of sgRNA

For a total reaction volume of 25 µL, the following were added to a PCR tube: 16.55 µL of Milli-Q water, 5 µL of 5X Q5 Reaction buffer, 0.5 µL of 10 mM dNTPs, 1.25 µL of each 10 µM primer, approximately 10 ng template DNA, and 0.25 µL of 2 kU/mL Q5 polymerase. The reaction was placed on the thermocycler with the following protocol: 98 °C for 30 seconds, 98 °C for 10

seconds, 60 °C for 20 seconds, 72 °C for 3 minutes, repeat steps 2-4 for 32 cycles, then 72 °C for 2 min. Subsequently, blunt-end ligation was performed as follows: 5 µL Milli-Q water, 1 µL of 10X T4 Ligase buffer, 1 µL of linearized PCR product, and 3 µL of KLD mix were added to a PCR tube. The reaction mixture was incubated at room temperature for 1 h prior to transformation of *E. coli* DH5α cells. Sanger sequencing confirmed the correct sequence.
KLD mix: a 1:1:1 mixture of T4 polynucleotide kinase, Dpn I, T4 DNA ligase (400 kU/mL).

4.4.6 Molecular cloning of sgRNA plasmids

The insert was prepared by annealing a mixture of 1:1 ratio of the forward and reverse compliment oligonucleotides, then subsequently diluting 1:25 for use in molecular cloning. To a PCR tube was added: 2 µL of 10X T4 Ligase buffer, 100 ng template plasmid DNA, 1 µL of 1:25 diluted insert, 1 µL of 10 kU/mL BsmB1, 2 µL of 400 kU/µL T4 ligase, and water up to a volume of 20 µL. The reaction was placed on the thermocycler with the following protocol: 37 °C for 5 minutes, 16 °C for 10 minutes, repeat steps 1-2 for 10 cycles, 37 °C for 15 minutes, 80 °C for 5 minutes. The reaction mixture was then used to transform *E. coli* DH5α cells. Sanger sequencing confirmed the correct sequence.

4.4.7 DNA Transfection

Approximately 18-24 hours prior to transfection, cells were seeded into a 96-well plate (with DMEM) to reach a confluency of 70-80% at the time of transfection. Approximately 100 ng of Cas9 plasmid and 50 ng of each guide RNA plasmid were diluted to 5 µL. Subsequently, 5 µL of 12% Lipofectamine in optimum was added to the mixture and it was then incubated for 10 minutes at room temperature. After incubation, HEK293T cells were transfected with 10 µL of the mixture (containing DNA and Lipofectamine). The cells were then incubated for 3 days at 37 °C. The media were aspirated out prior to the addition of 75 µL of lysis buffer (10 mM Tris-HCl, pH 7.5, 0.05% SDS, 25 µg/mL proteinase K) to each well. The plate was incubated for 1 h at 37 °C and then the lysate was transferred to PCR tubes for incubation at 80 °C for 30 min to deactivate proteinase K. Experiments were carried out in duplicate.

4.4.8 Amplification of endogenous genomic sites

Genomic DNA was isolated using the E.Z.N.A.® Genomic DNA Isolation Kits, Omega Bio-Tek Kit and the resulting concentrations were quantified by Nanodrop. To a reaction mixture was added: 12.5 µL of GB-AMP 2X PCR Mix, 1.25 µL of 10 µM forward primer, 1.25 µL of 10 µM reverse primer, 50 ng genomic DNA, and water filled to a 25 µL reaction volume. Samples were purified using the GB-Clean™ Gel-PCR 2in1 HiPure DNA Kit prior to Sanger sequencing.

Supplementary Information

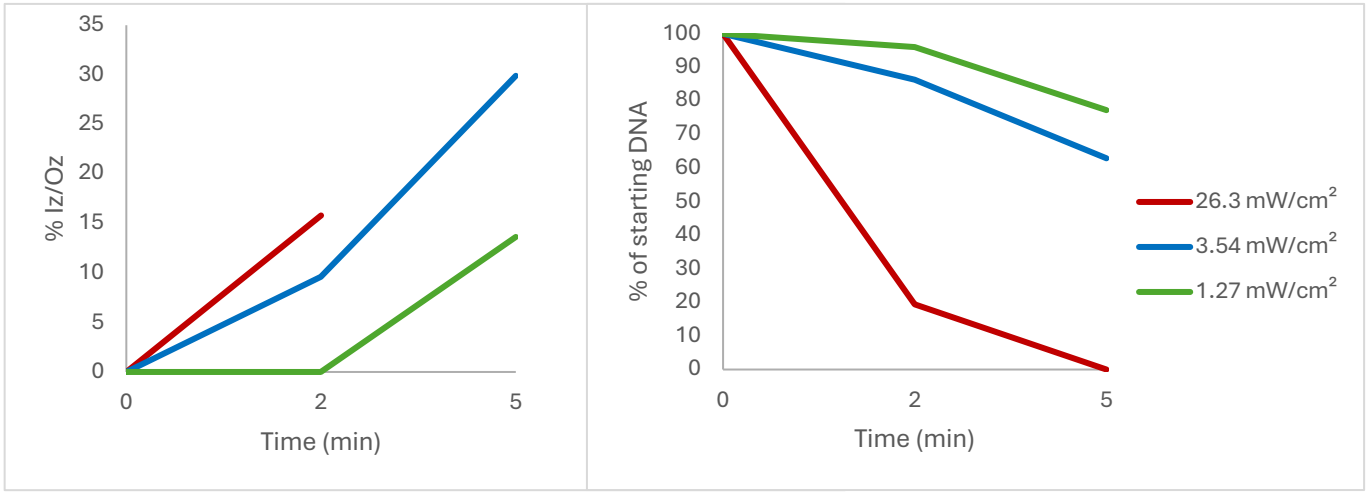

Supplementary Figure 31. Initial optimization of riboflavin-catalyzed oxidation of guanine in DNA. In the presence of 20 µM ssDNA-1G-2, 100 µM riboflavin was exposed to blue light with an intensity of 26.3 mW/cm^2, 3.54 mW/cm^2, or 1.27 mW/cm^2 for 0, 2, and 5 minutes.

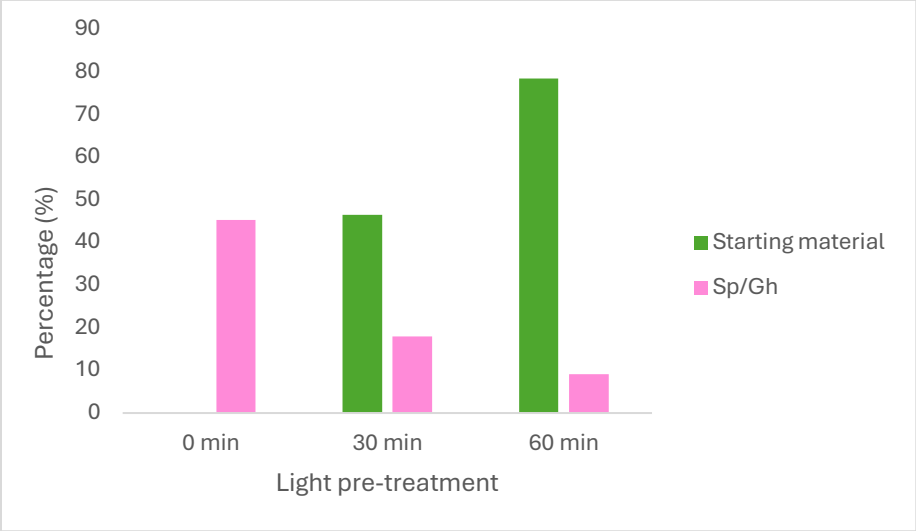

Supplementary Figure 32. Pre-exposure of Rose Bengal to light prior to guanine oxidation. Rose Bengal salt was pre-exposed to green light with an intensity of 14.3 mW/cm^2 for 0, 30, and 60 minutes. 20 µM ssDNA-1G-7 was then added upon exposure to 30 minutes of green light with the same intensity.

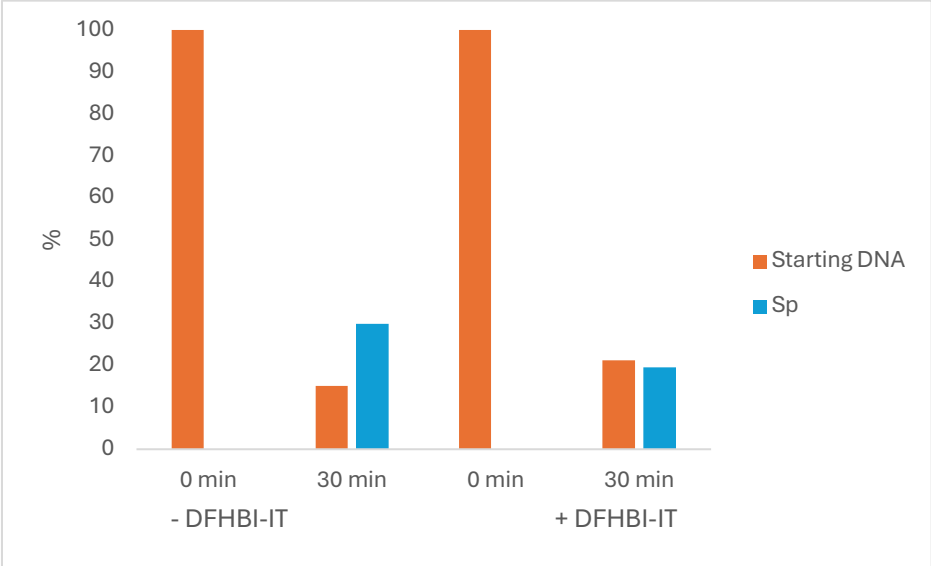

Supplementary Figure 33. Photooxidation of guanine by Rose Bengal in the presence of DFHBI-IT.
The $^1O_2$-mediated intermolecular photooxidation of a ssDNA-1G-1 sequence was observed in the presence and/or absence of DFHBI-IT. Green light (550 nm) with an intensity of 6.37 mW/cm^2 was used to excite Rose Bengal salt for 0 and 30 minutes with/without DFHBI-IT present in the reaction mixture.

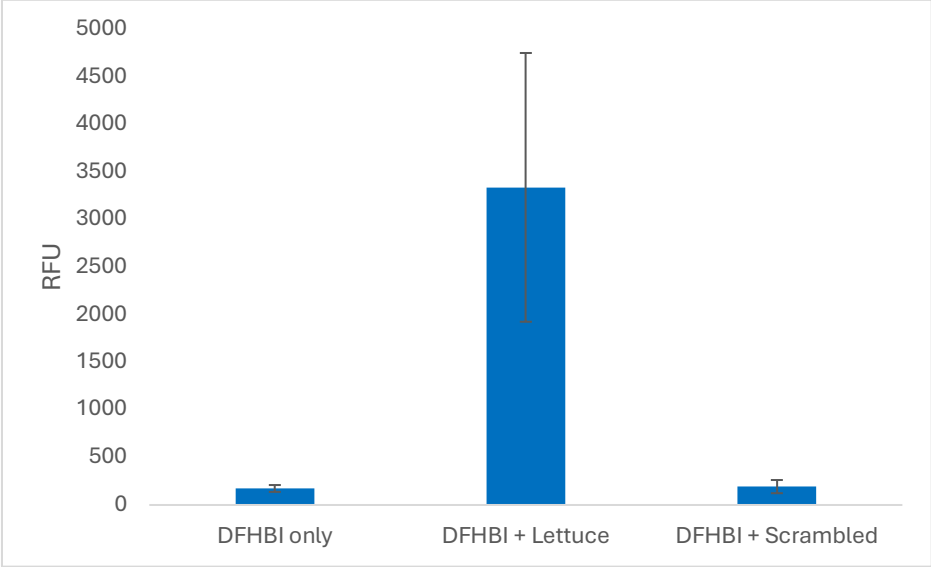

Supplementary Figure 34. Fluorescence upon binding of DFHBI to Lettuce.
In Tris buffer, 5 µM DFHBI-IT was excited with light of 482 nm in the presence/absence of 20 µM Bibb Lettuce DNA aptamer and 20 µM scrambled Bibb Lettuce DNA sequence. DFHBI was excited by light of 482 nm. Emission was captured at a wavelength of 505 nm.

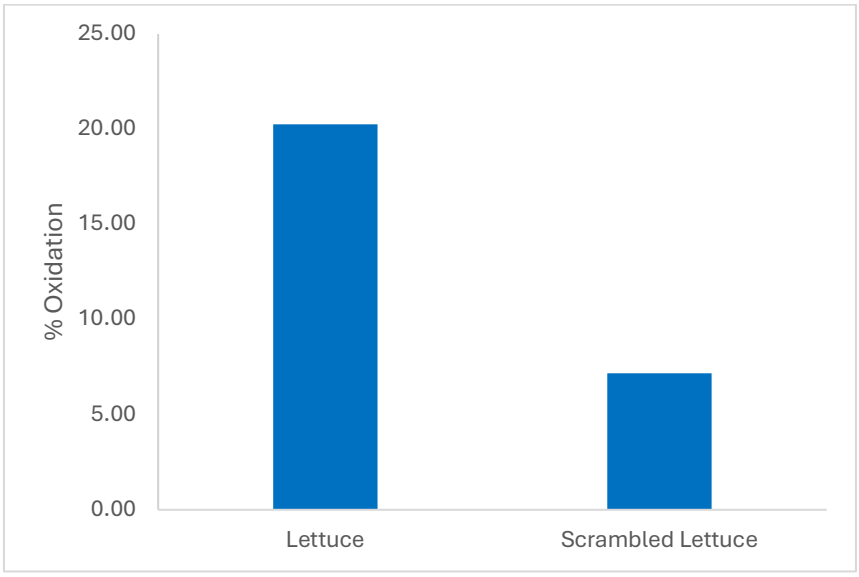

Supplementary Figure 35. Photooxidation of Lettuce using 5-fold greater RB-DFHBI.
A reaction mixture of 20 µM aptamer/non-aptamer DNA and 100 µM RB-DFHBI in tris buffer was exposed to white light for 1 hour. Photooxidation of the Lettuce aptamer was compared against a control of a scrambled sequence of Lettuce.

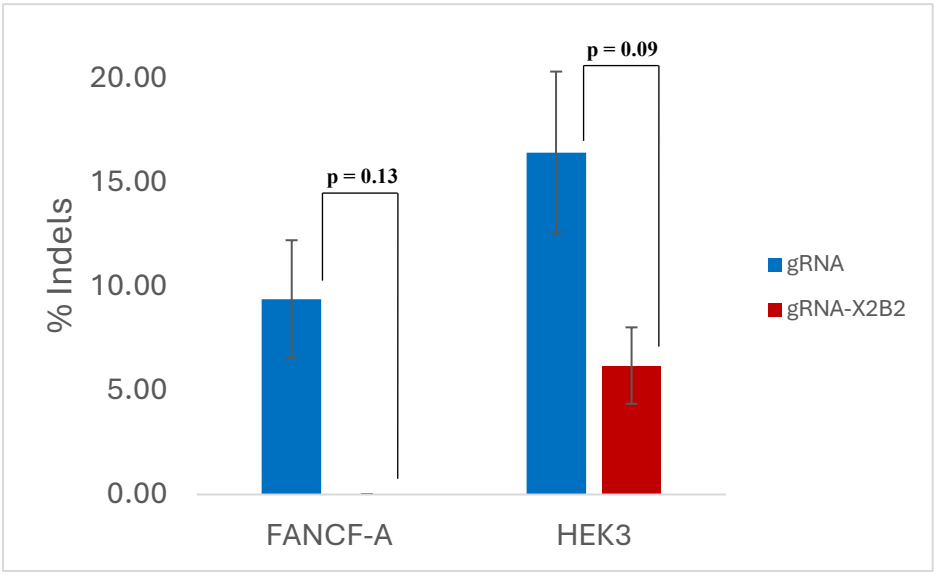

Supplementary Figure 36. Cas9 cleavage efficiency with X2B2 cloned into the sgRNA scaffold.
X2B2 was cloned within the upper stem loop of the sgRNA for subsequent analysis of its stability with the Cas9 protein. Percentage of indels (%) was used to measure the efficiency of Cas9 dsDNA cleavage.

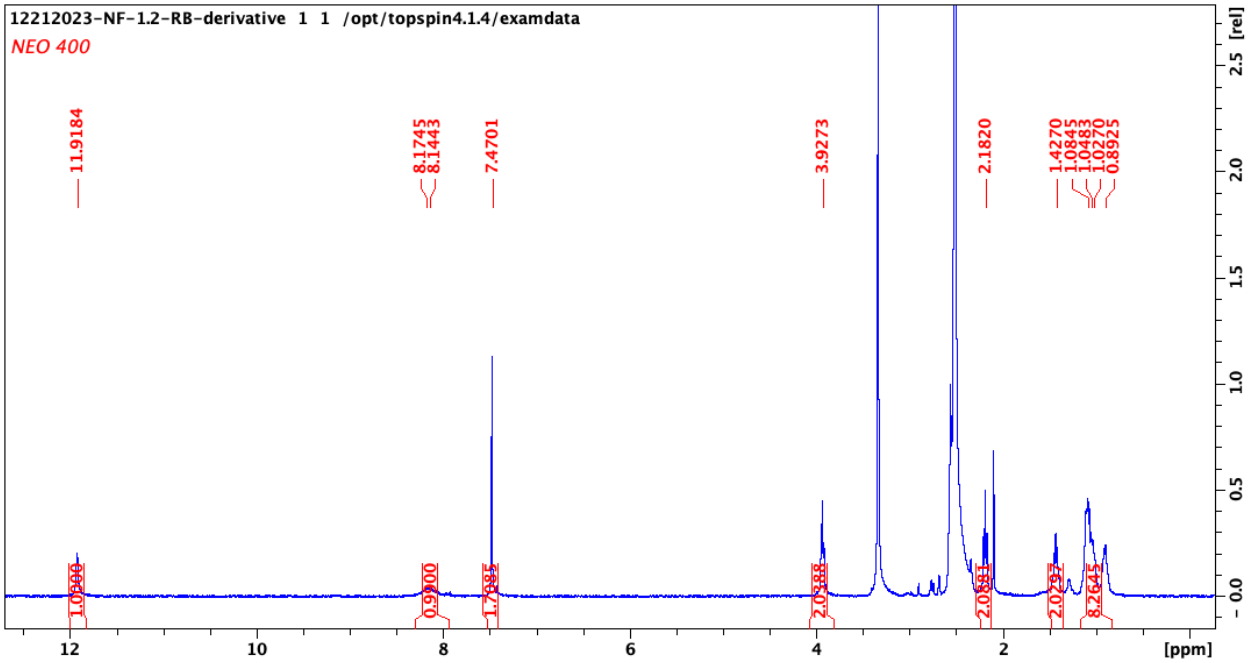

^{1}H NMR spectrum of Rose Bengal carboxyheptyl ester (**1**)

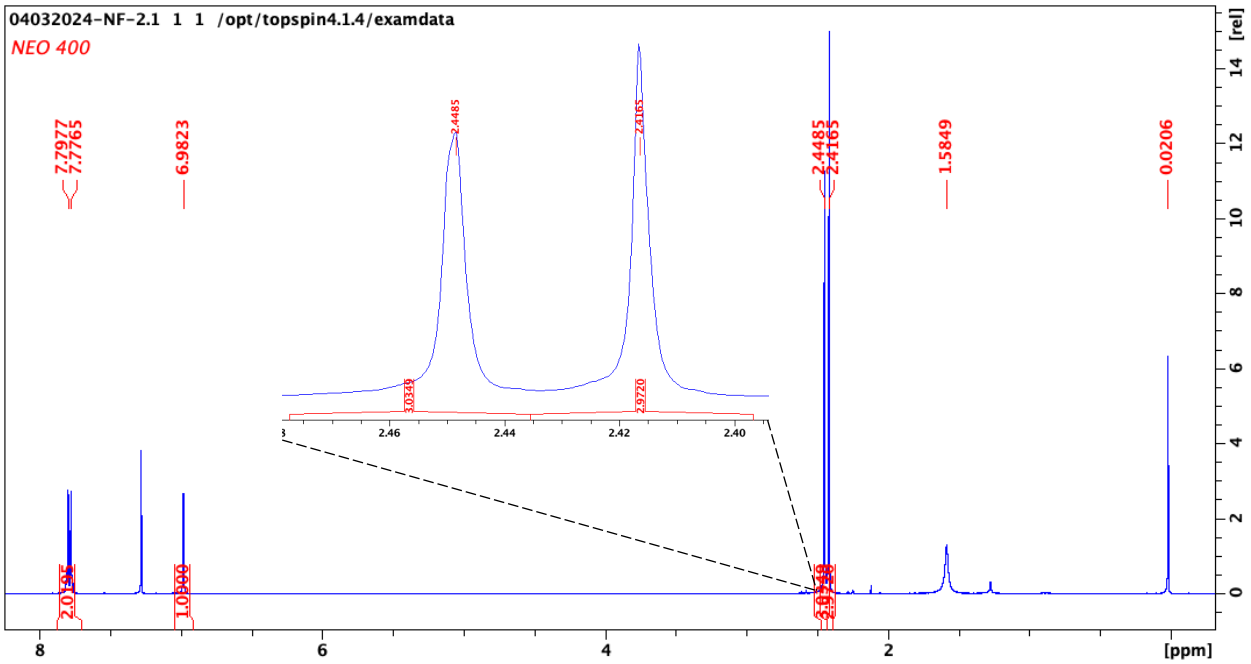

^{1}H NMR spectrum of (*Z*)-2,6-difluoro-4-((2-methyl-5-oxooxazol-4(5*H*)-ylidene)methyl)phenyl acetate (**2**)

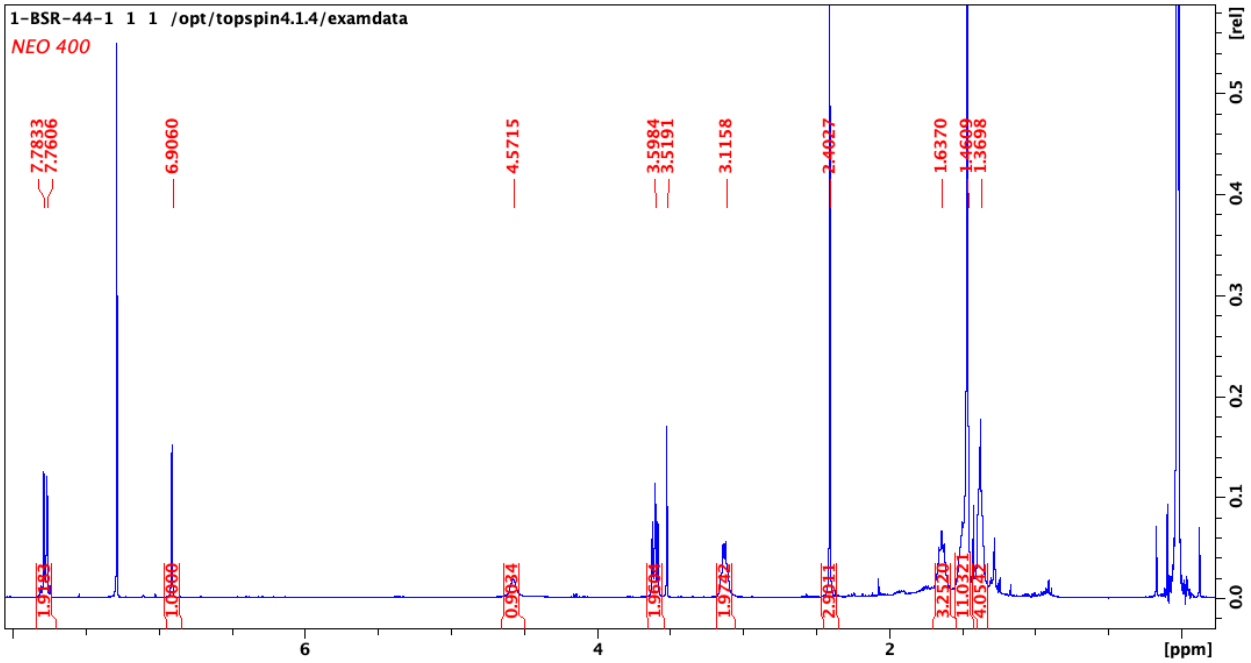

^{1}H NMR spectrum of *tert*-butyl (*Z*)-(6-(4-(3,5-difluoro-4-hydroxybenzylidene)-2-methyl-5-oxo-4,5-dihydro-1*H*-imidazol-1-yl)hexyl)carbamate (**3**)

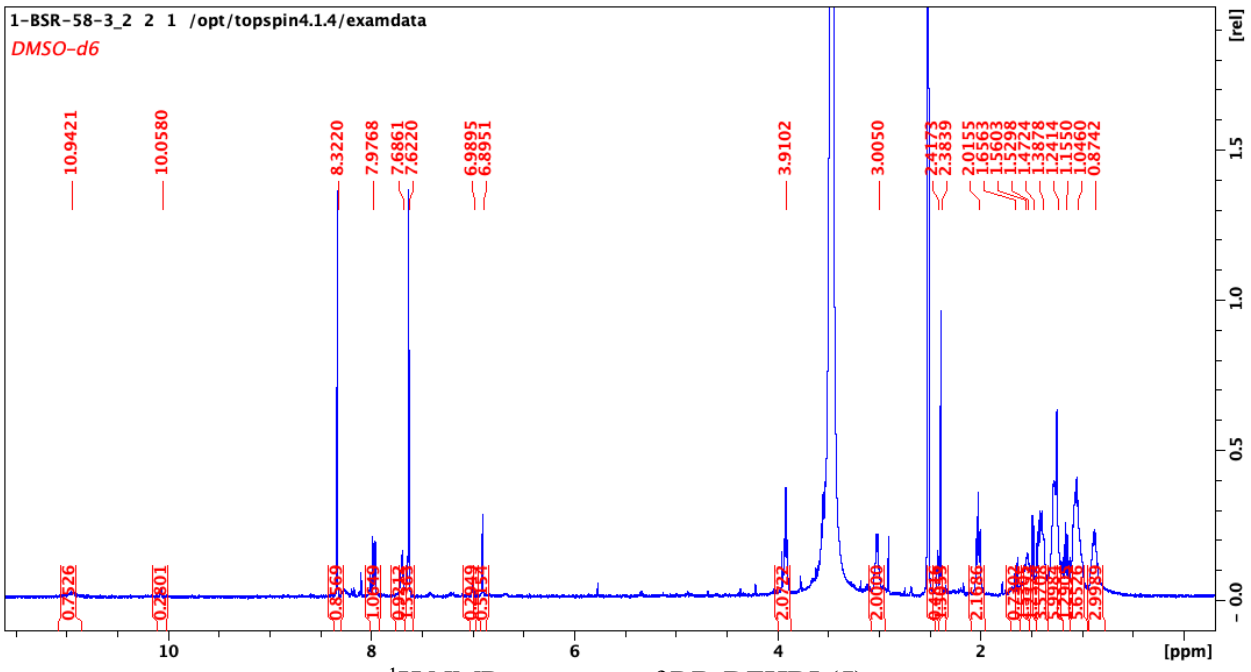

^{1}H NMR spectrum of RB-DFHBI (**5**)

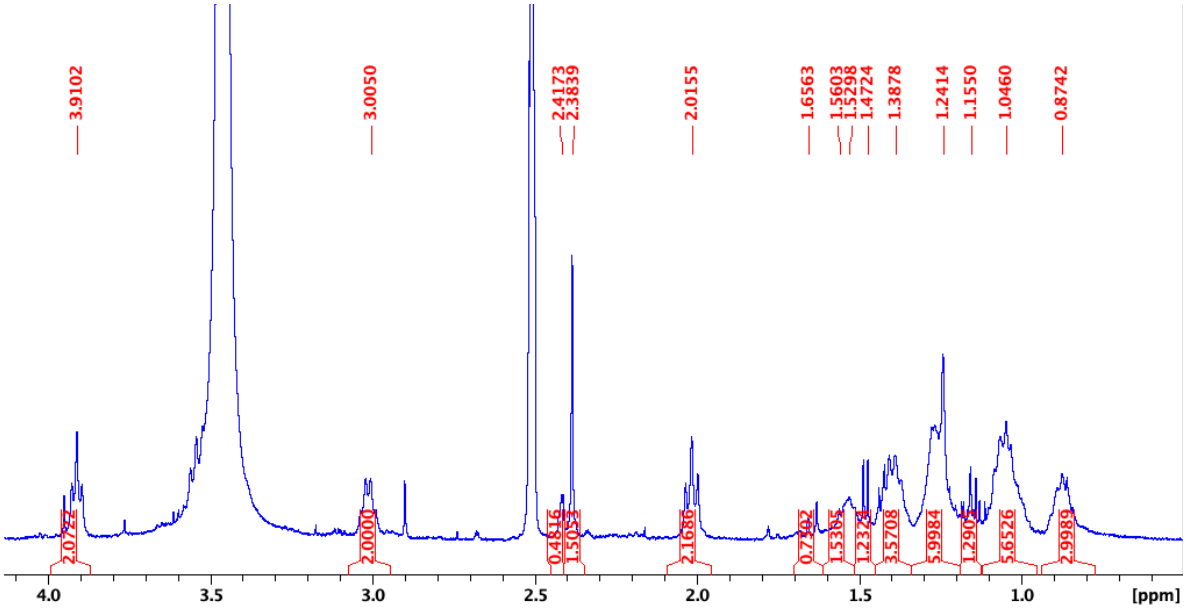

View of the 0-4.0 ppm region for the ^{1}H NMR of RB-DFHBI (**5**)

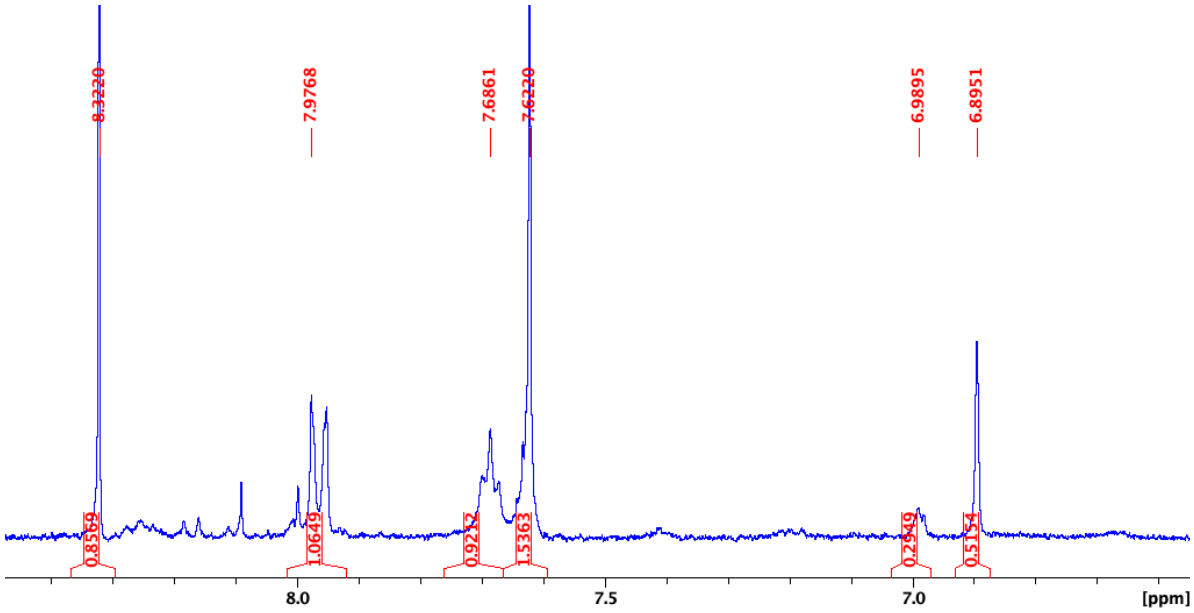

View of 6.6-8.4 ppm region for the ^{1}H NMR of RB-DFHBI (**5**)

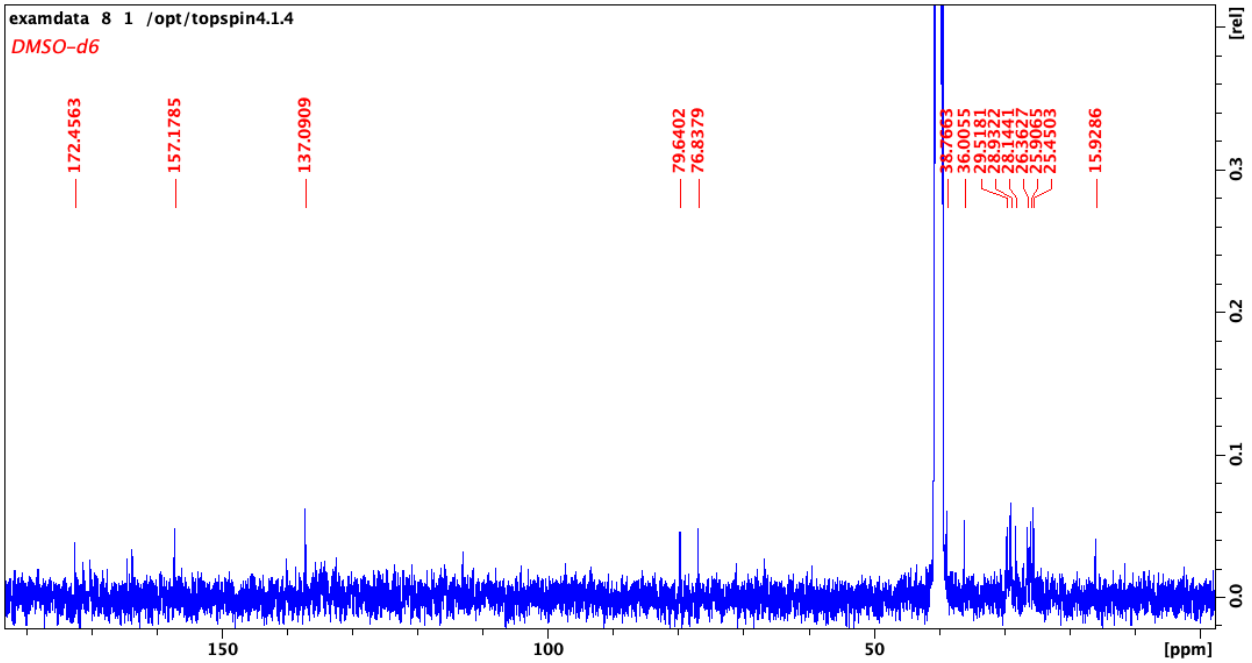

^{13}C NMR NMR spectrum of RB-DFHBI (**5**)

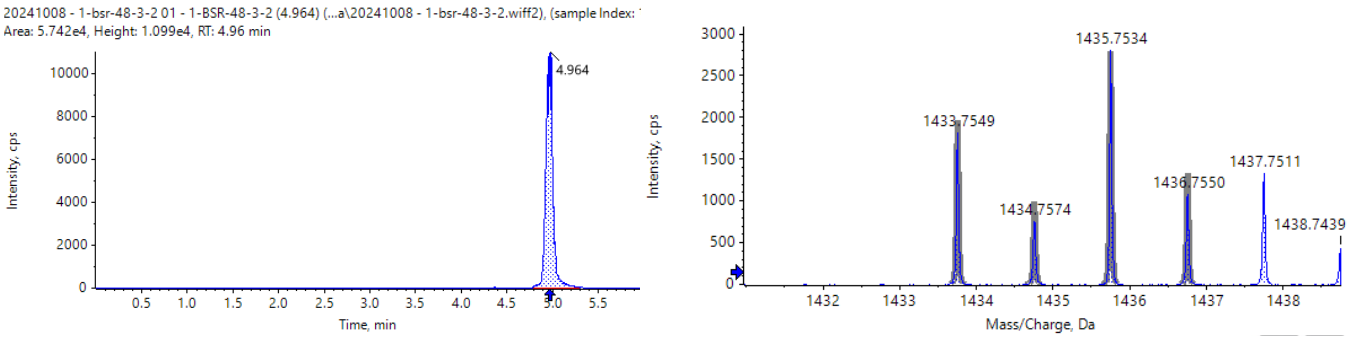

Mass data for RB-DFHBI (**5**)

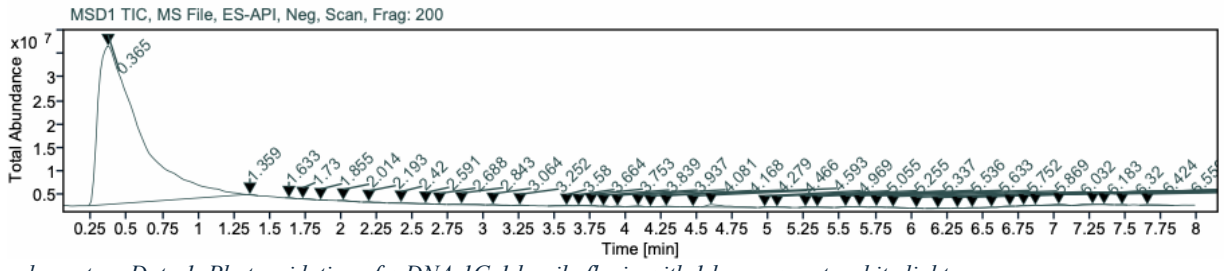

Supplementary Data 1. Photooxidation of ssDNA-1G-1 by riboflavin with 1 h exposure to white light.

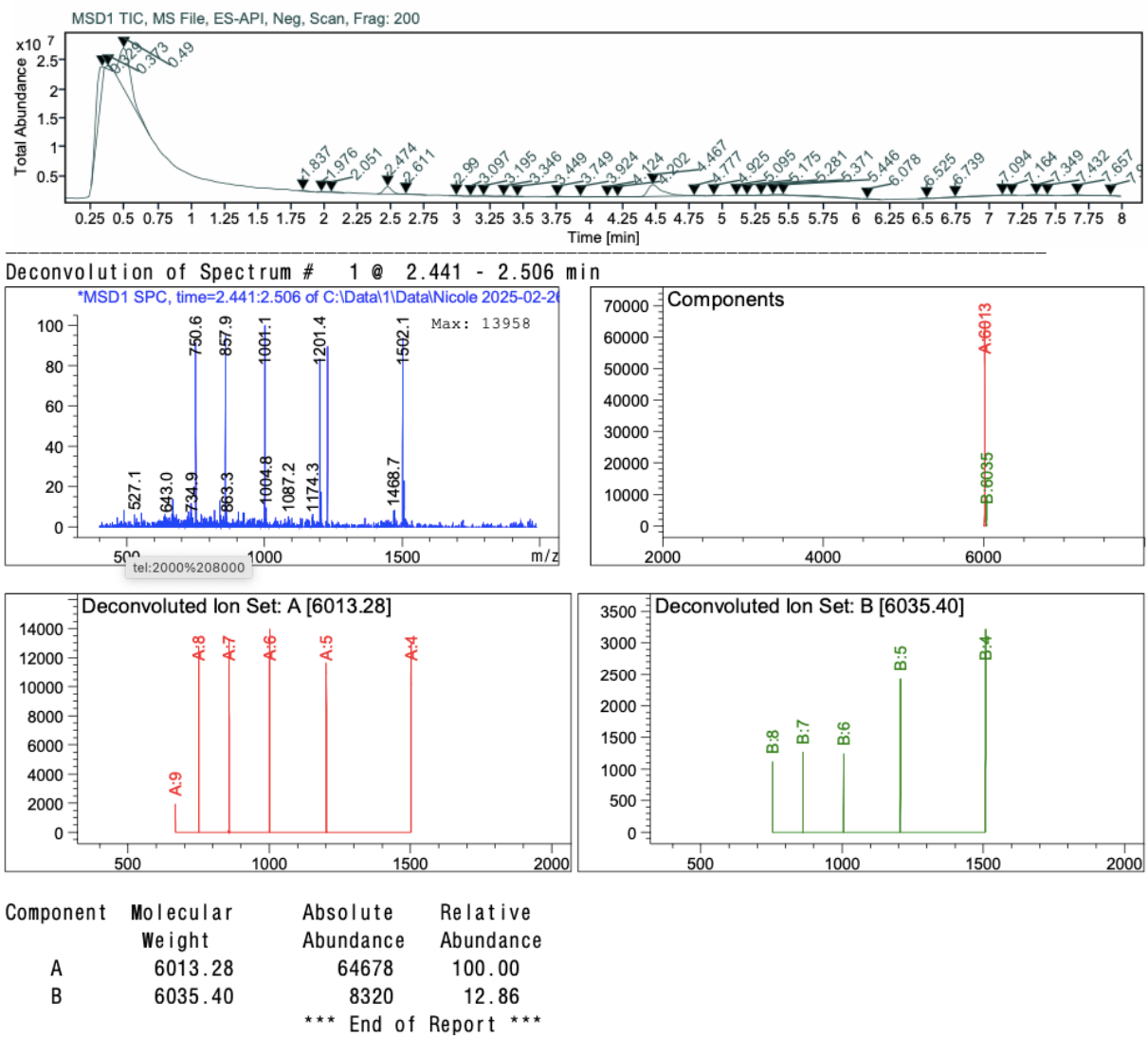

Component	Molecular Weight	Absolute Abundance	Relative Abundance
A	6013.28	64678	100.00
B	6035.40	8320	12.86

*** End of Report ***

Supplementary Data 2. Photooxidation of ssDNA-1G-1 by Rose Bengal with no exposure to light.

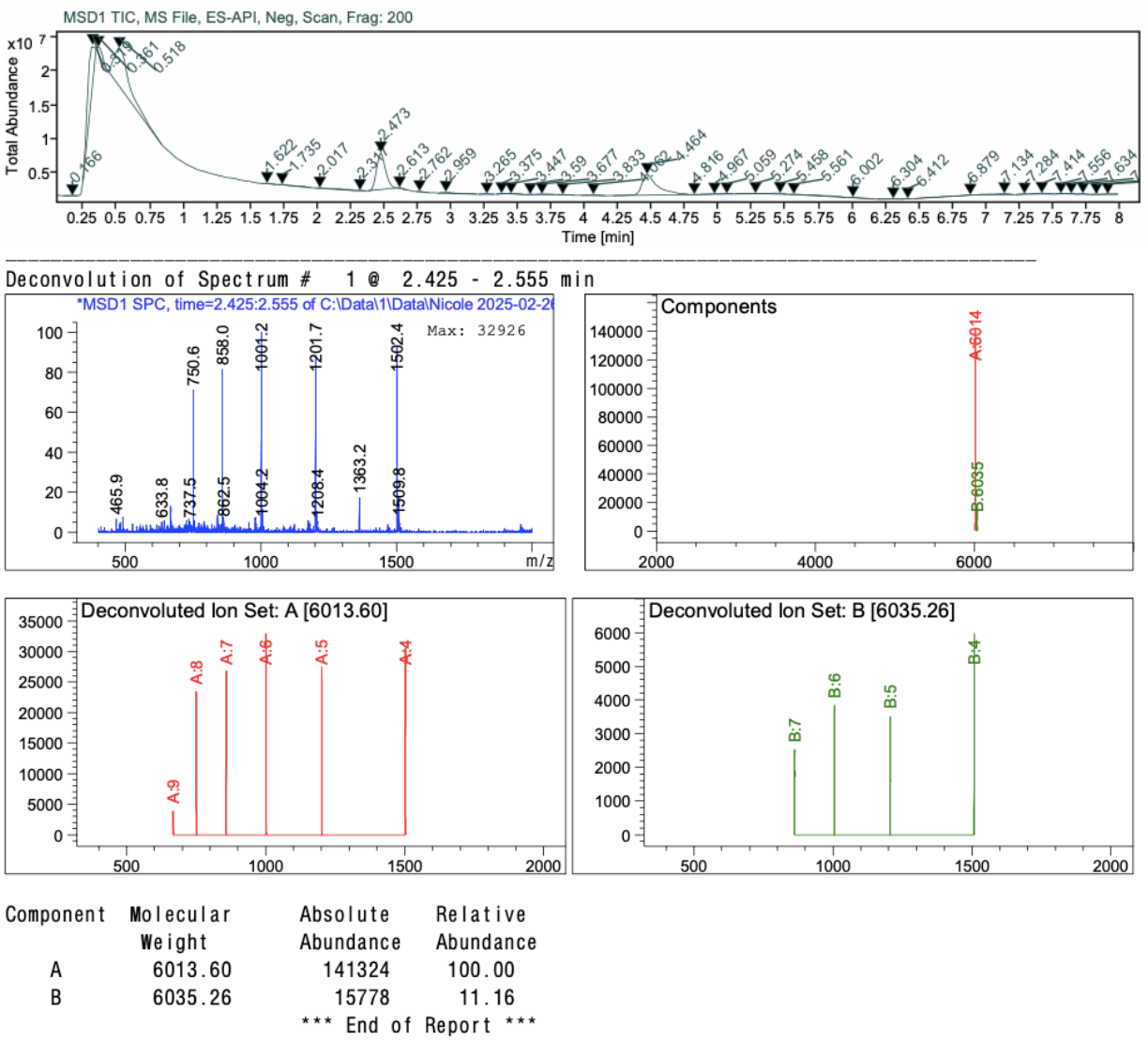

Component	Molecular Weight	Absolute Abundance	Relative Abundance
A	6013.60	141324	100.00
B	6035.26	15778	11.16

*** End of Report ***

Supplementary Data 3. Photooxidation of ssDNA-1G-1 by Rose Bengal with 10 minutes of exposure to high-intensity light of 550 nm.

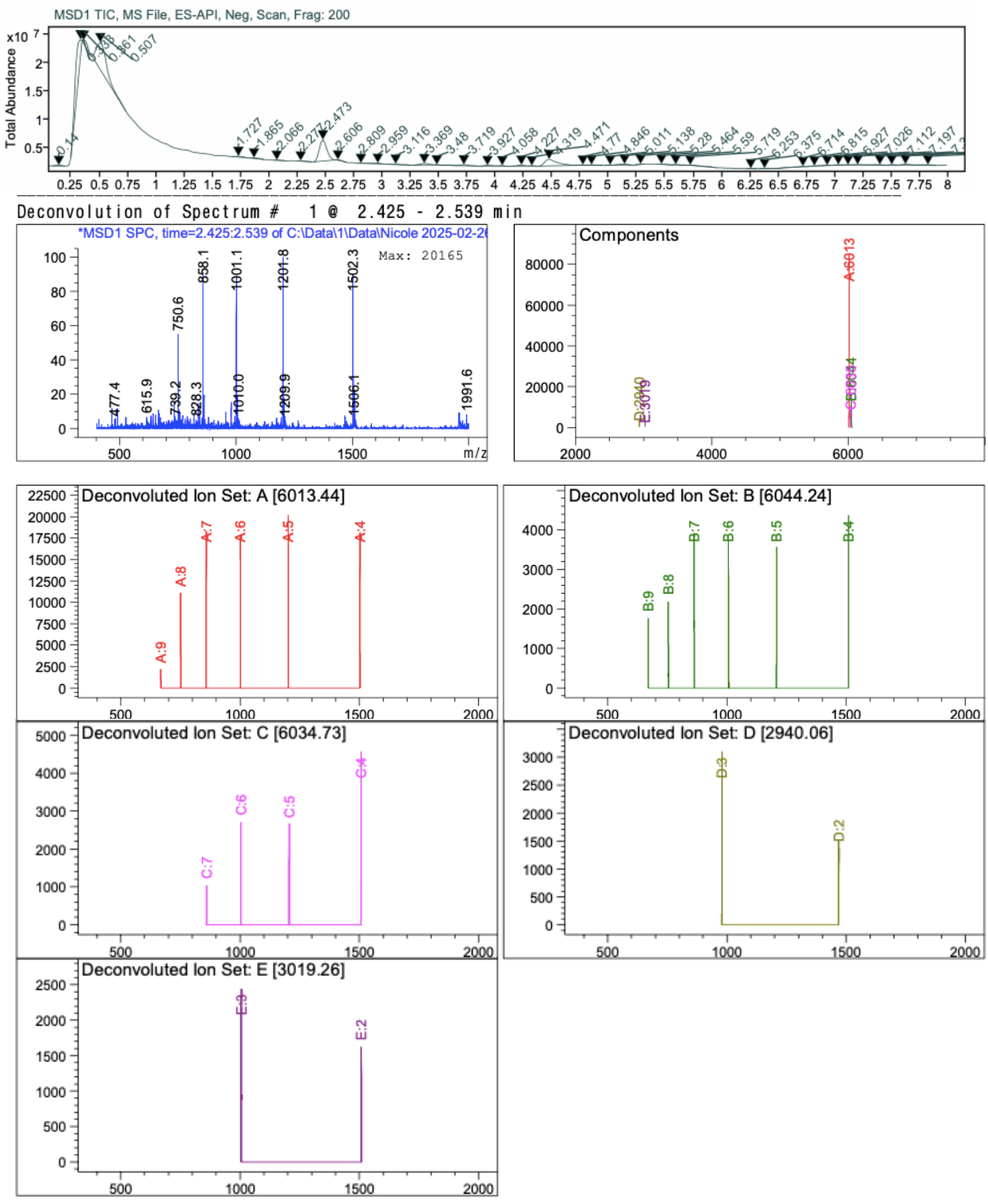

Component	Molecular Weight	Absolute Abundance	Relative Abundance
A	6013.44	84802	100.00
B	6044.24	15518	18.30
C	6034.73	10420	12.29
D	2940.06	3709	4.37
E	3019.26	2573	3.03

*** End of Report ***

Supplementary Data 4. Photooxidation of ssDNA-1G-1 by Rose Bengal with 20 minutes of exposure to high-intensity light of 550 nm.

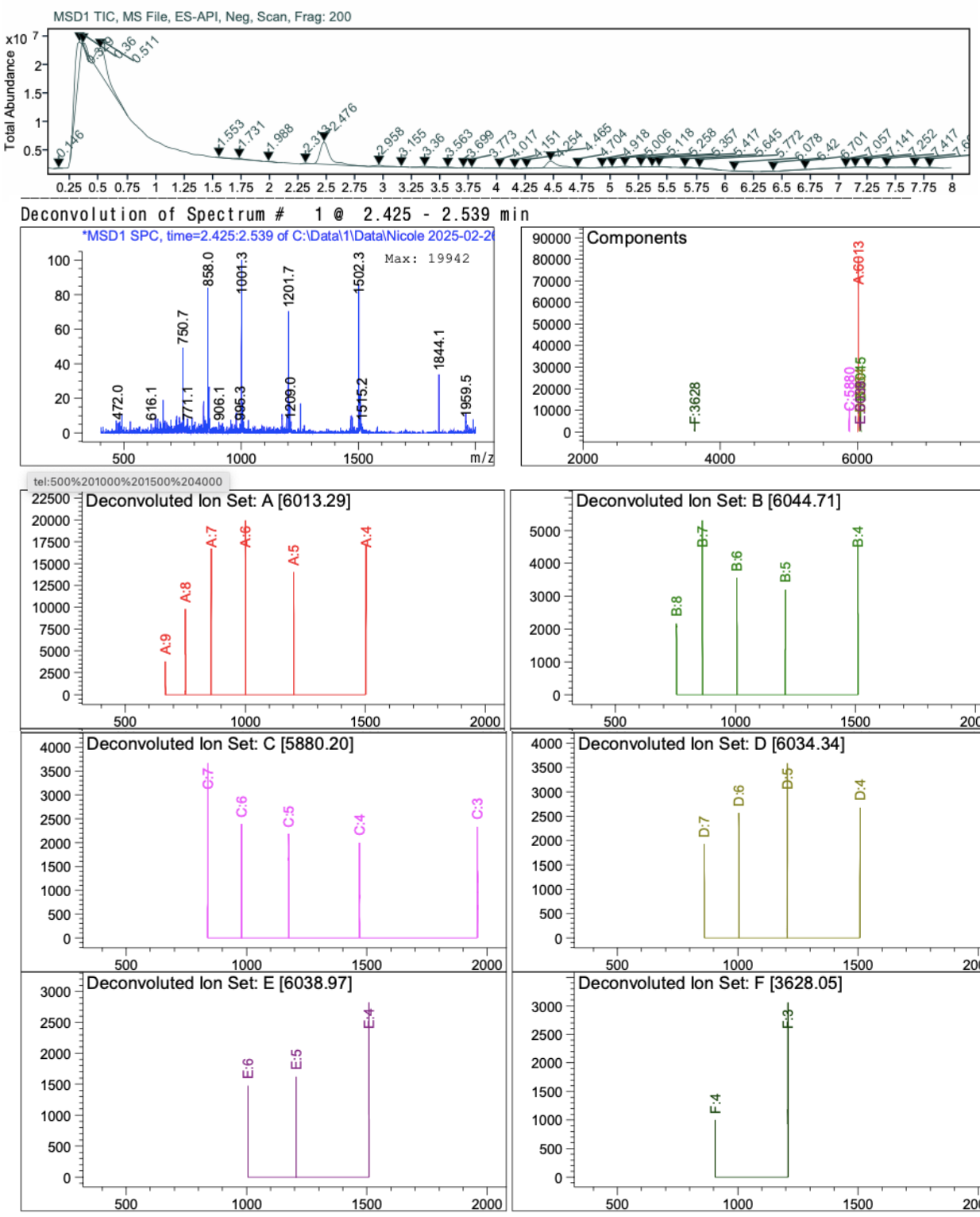

Component	Molecular Weight	Absolute Abundance	Relative Abundance
A	6013.29	80741	100.00
B	6044.71	16851	20.87
C	5880.20	11414	14.14
D	6034.34	10533	13.05
E	6038.97	5511	6.83
F	3628.05	4028	4.99

Supplementary Data 5. Photooxidation of ssDNA-1G-1 by Rose Bengal with 20 minutes of exposure to high-intensity light of 550 nm.

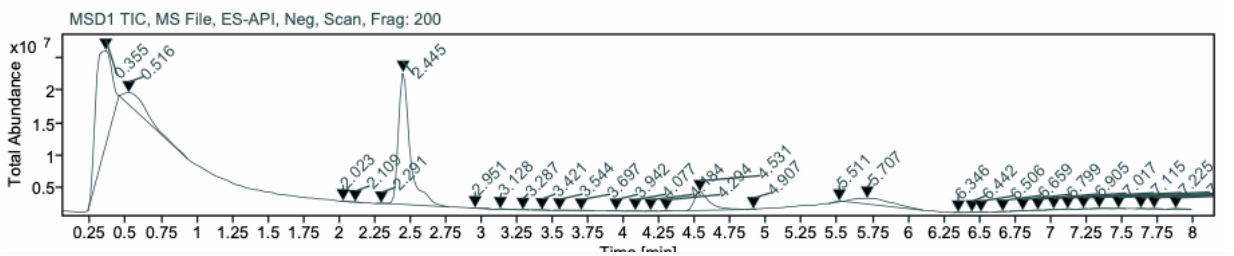

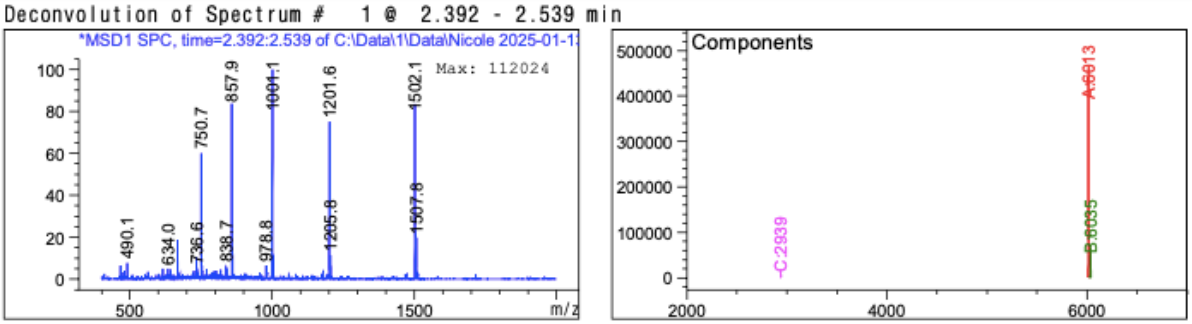

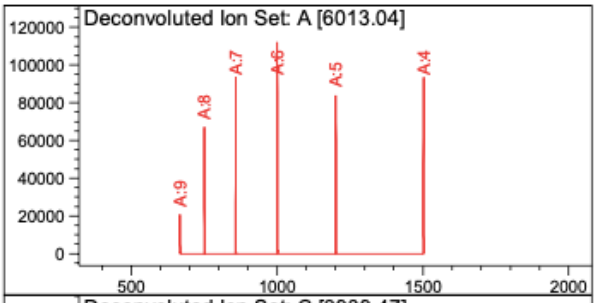

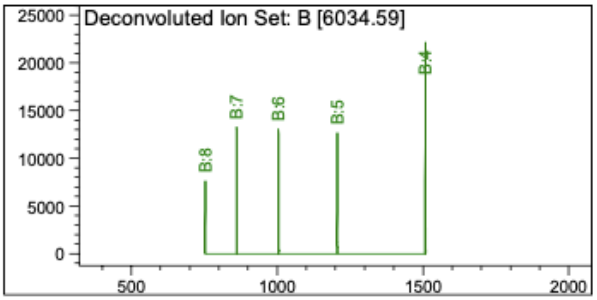

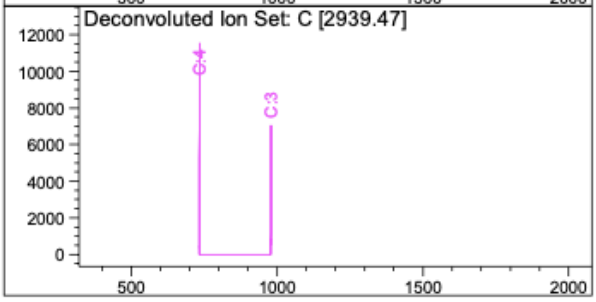

Component	Molecular Weight	Absolute Abundance	Relative Abundance
A	6013.04	465036	100.00
B	6034.59	65071	13.99
C	2939.47	18534	3.99

*** End of Report ***

Supplementary Data 6. Photooxidation of ssDNA-1G-1 by Rose Bengal with no exposure to light.

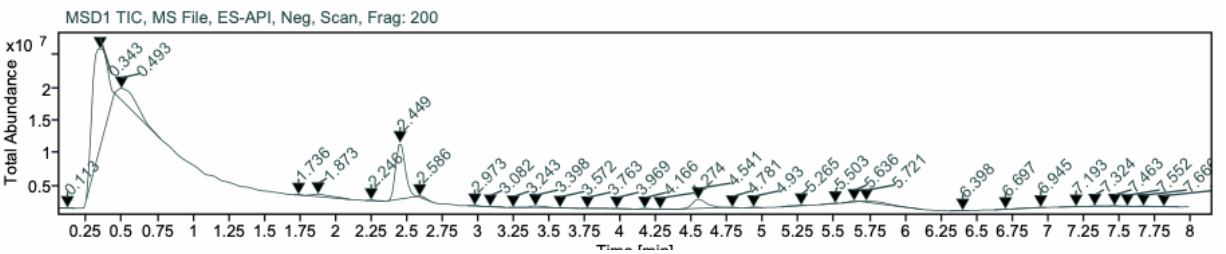

Deconvolution of Spectrum # 1 @ 2.392 - 2.620 min

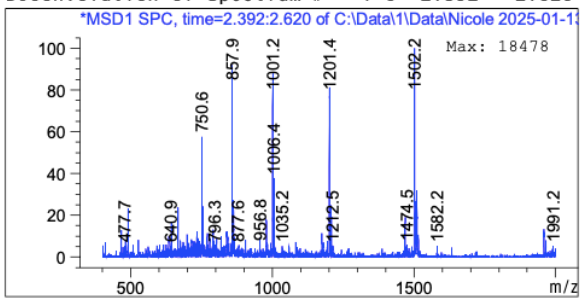

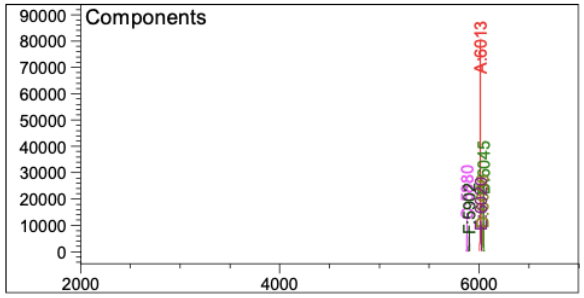

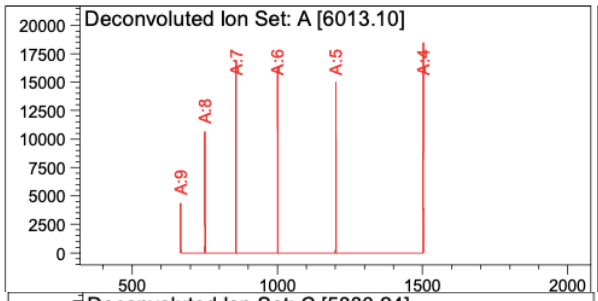

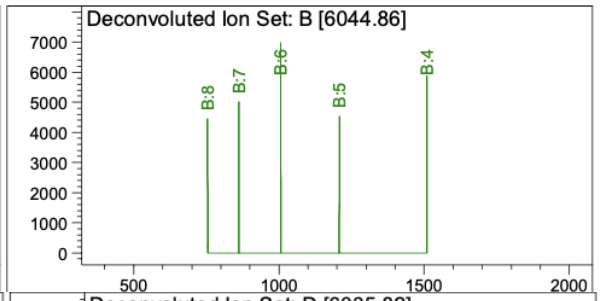

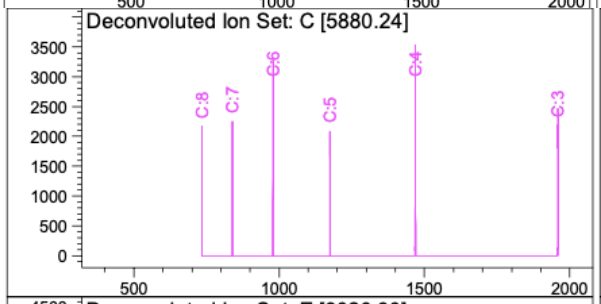

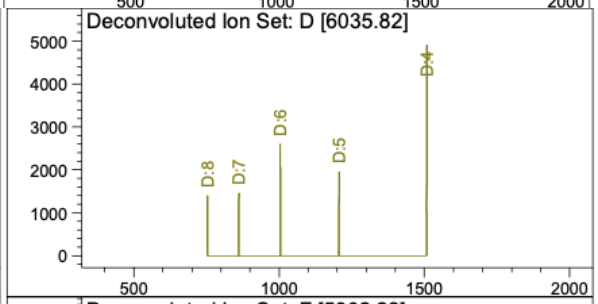

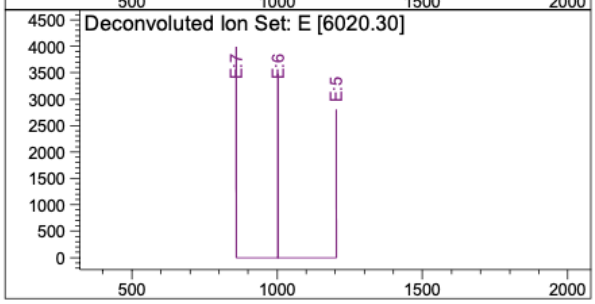

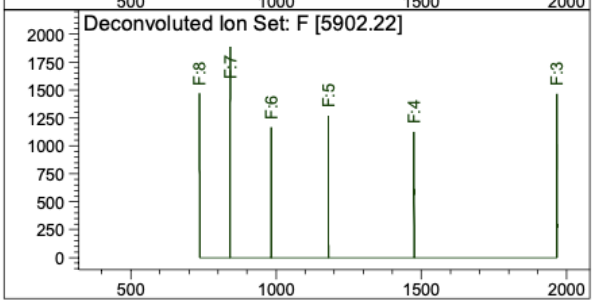

Component	Molecular Weight	Absolute Abundance	Relative Abundance
A	6013.10	79912	100.00
B	6044.86	25990	32.52
C	5880.24	14763	18.47
D	6035.82	10785	13.50
E	6020.30	9777	12.23
F	5902.22	7729	9.67

*** End of Report ***

Supplementary Data 7. Photooxidation of ssDNA-1G-1 by Rose Bengal with 10 minutes of exposure to 550 nm light with an intensity of 6.37 mW/cm².

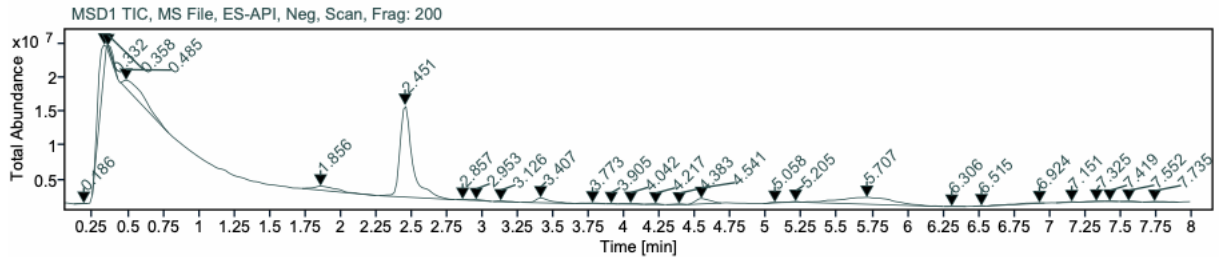

Deconvolution of Spectrum # 1 @ 2.392 - 2.620 min

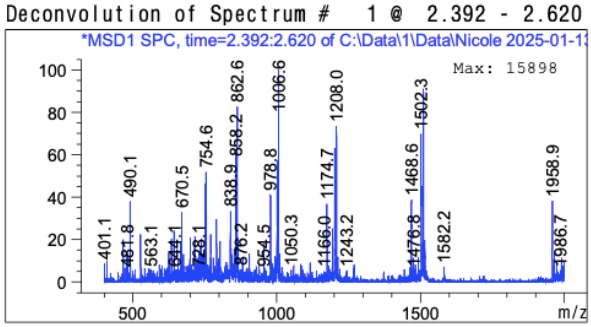

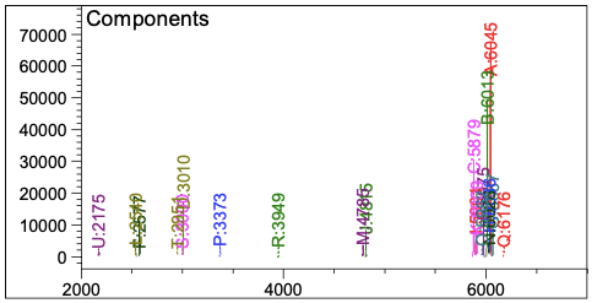

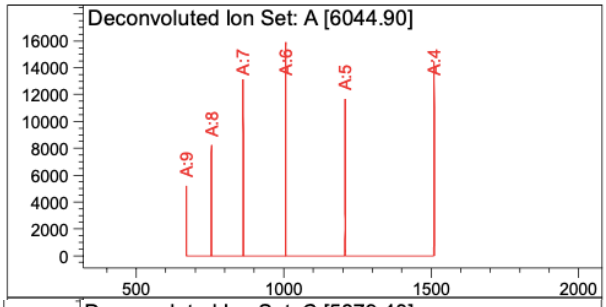

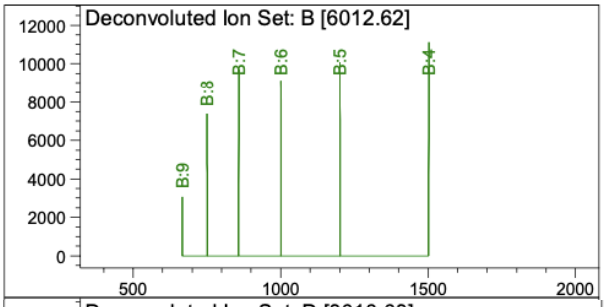

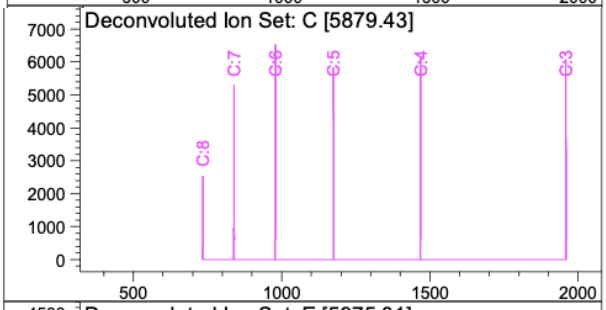

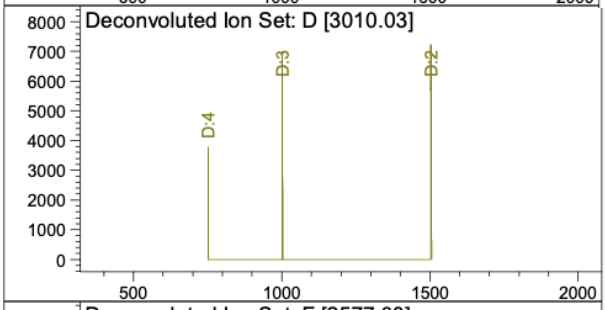

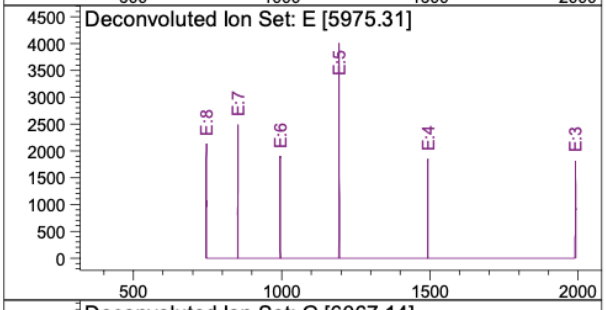

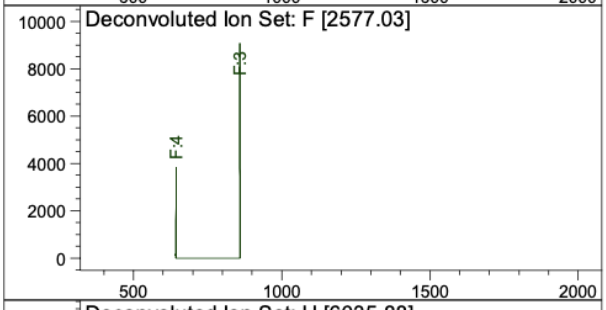

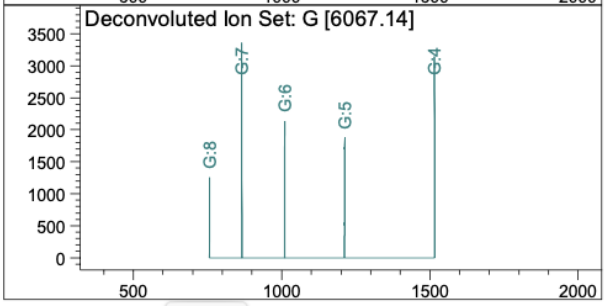

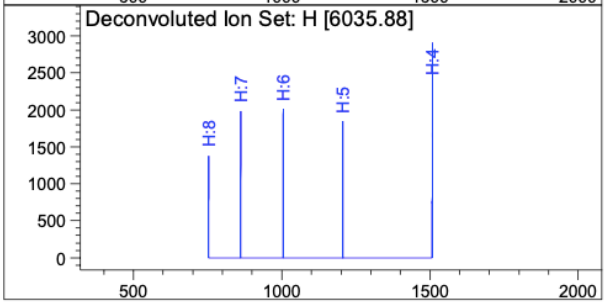

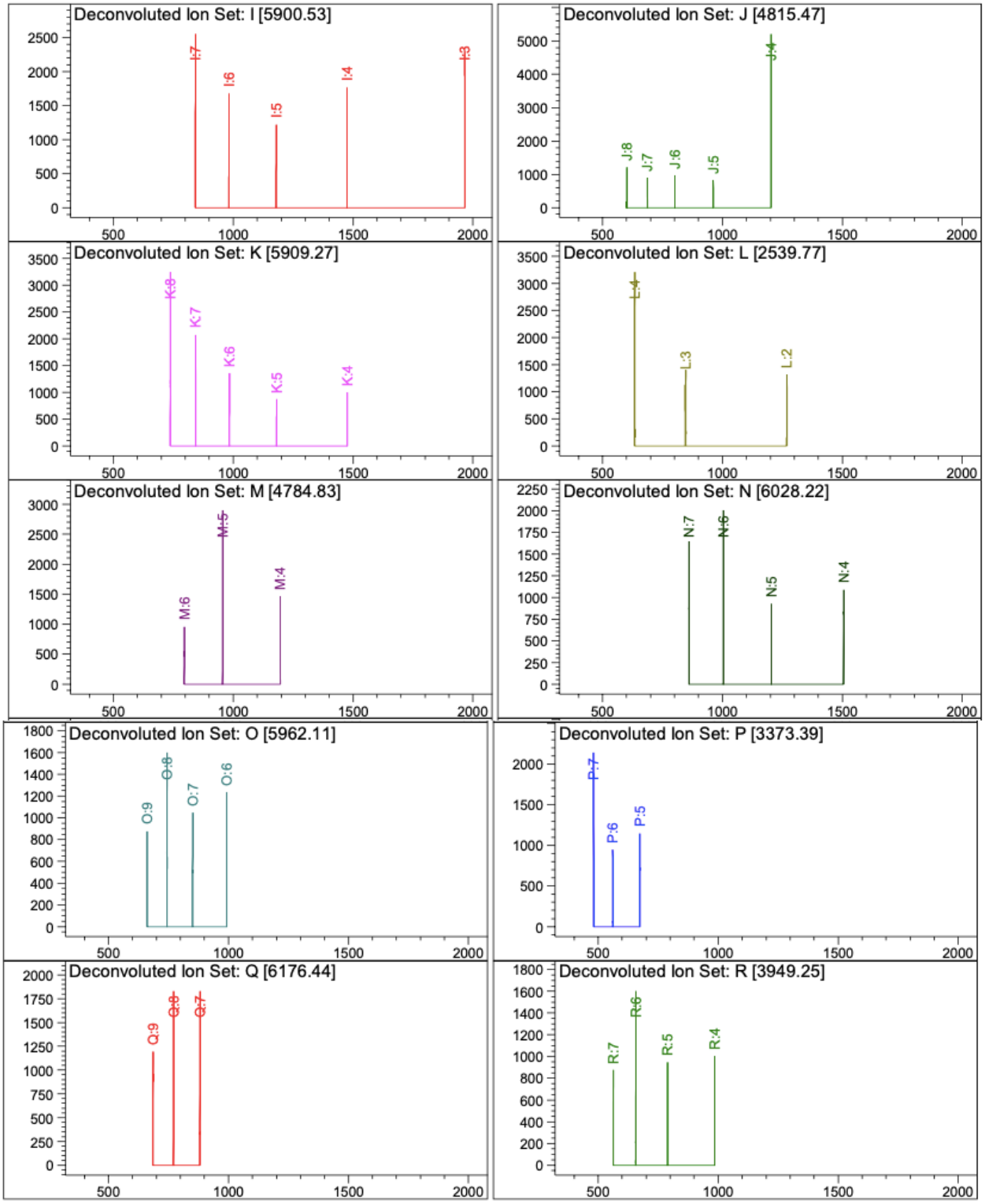
Deconvoluted Ion Set: I [5900.53]
I:7
I:6
I:5
I:4
I:3
Deconvoluted Ion Set: J [4815.47]
J:8
J:7
J:6
J:5
J:4
Deconvoluted Ion Set: K [5909.27]
K:8
K:7
K:6
K:5
K:4
Deconvoluted Ion Set: L [2539.77]
L:4
L:3
L:2
Deconvoluted Ion Set: M [4784.83]
M:6
M:5
M:4
Deconvoluted Ion Set: N [6028.22]
N:7
N:6
N:5
N:4
Deconvoluted Ion Set: O [5962.11]
O:9
O:8
O:7
O:6
Deconvoluted Ion Set: P [3373.39]
P:7
P:6
P:5
Deconvoluted Ion Set: Q [6176.44]
Q:9
Q:8
Q:7
Deconvoluted Ion Set: R [3949.25]
R:7
R:6
R:5
R:4

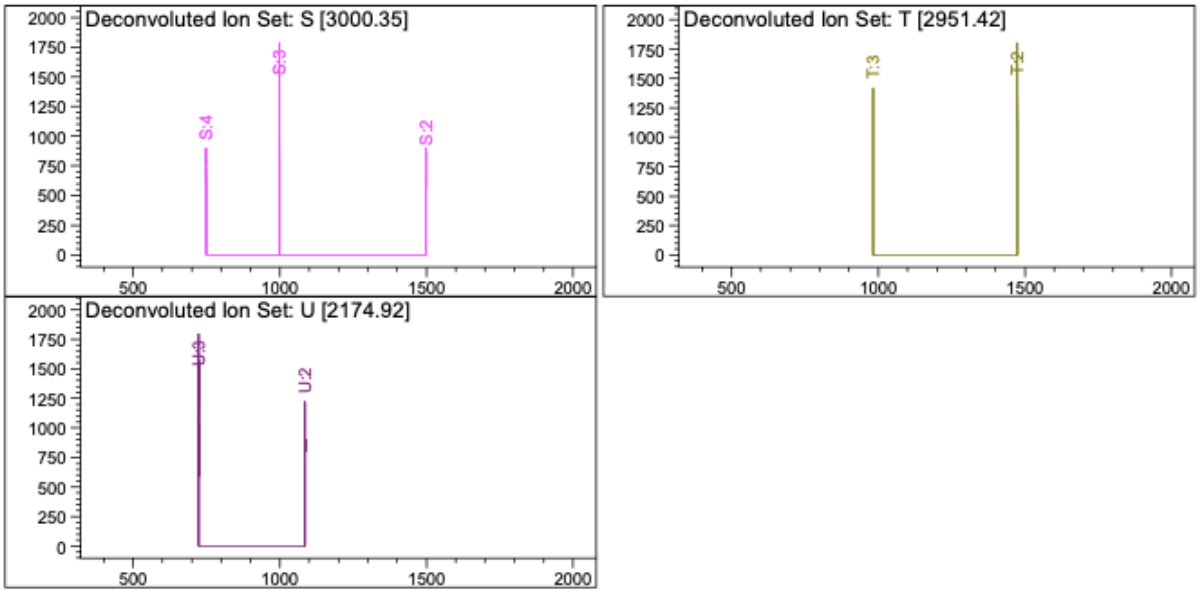

Component	Molecular Weight	Absolute Abundance	Relative Abundance
A	6044.90	67245	100.00
B	6012.62	49065	72.96
C	5879.43	30467	45.31
D	3010.03	17470	25.98
E	5975.31	13270	19.73
F	2577.03	11488	17.08
G	6067.14	10309	15.33
H	6035.88	8790	13.07
I	5900.53	8414	12.51
J	4815.47	8407	12.50
K	5909.27	8225	12.23
L	2539.77	5593	8.32
M	4784.83	4397	6.54
N	6028.22	4359	6.48
O	5962.11	4230	6.29
P	3373.39	4051	6.02
Q	6176.44	3530	5.25
R	3949.25	3468	5.16
S	3000.35	3265	4.86
T	2951.42	3228	4.80
U	2174.92	2968	4.41

Supplementary Data 8. Photooxidation of ssDNA-1G-1 by Rose Bengal with 20 minutes of exposure to 550 nm light with an intensity of 6.37 mW/cm^2.

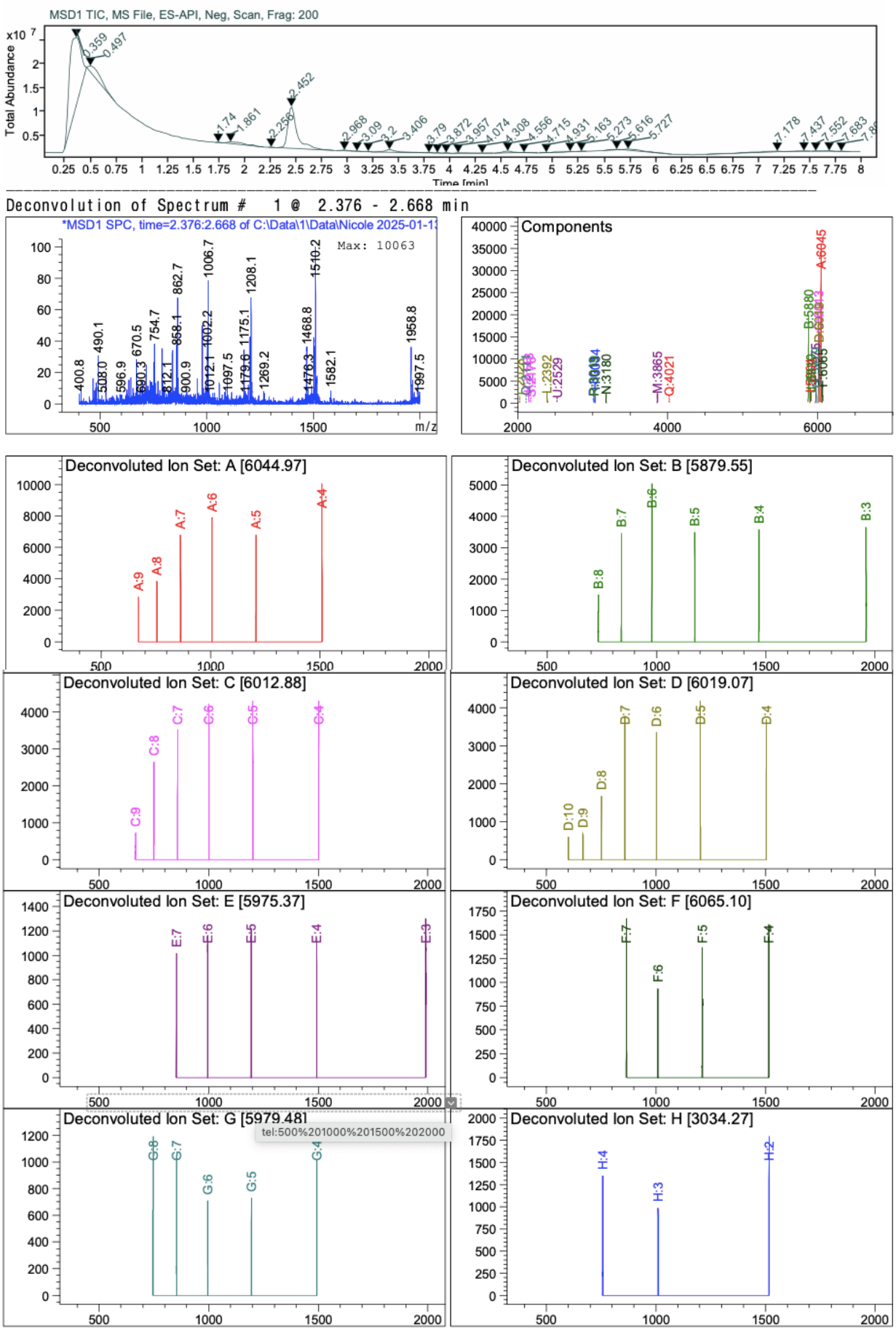
MSD1 TIC, MS File, ES-API, Neg, Scan, Frag: 200
Total Abundance
Time [min]
Deconvolution of Spectrum # 1 @ 2.376 - 2.668 min
*MSD1 SPC, time=2.376:2.668 of C:\Data\1\Data\Nicole 2025-01-1
Max: 10063
m/z
Components
Deconvoluted Ion Set: A [6044.97]
Deconvoluted Ion Set: B [5879.55]
Deconvoluted Ion Set: C [6012.88]
Deconvoluted Ion Set: D [6019.07]
Deconvoluted Ion Set: E [5975.37]
Deconvoluted Ion Set: F [6065.10]
Deconvoluted Ion Set: G [5979.48]
Deconvoluted Ion Set: H [3034.27]

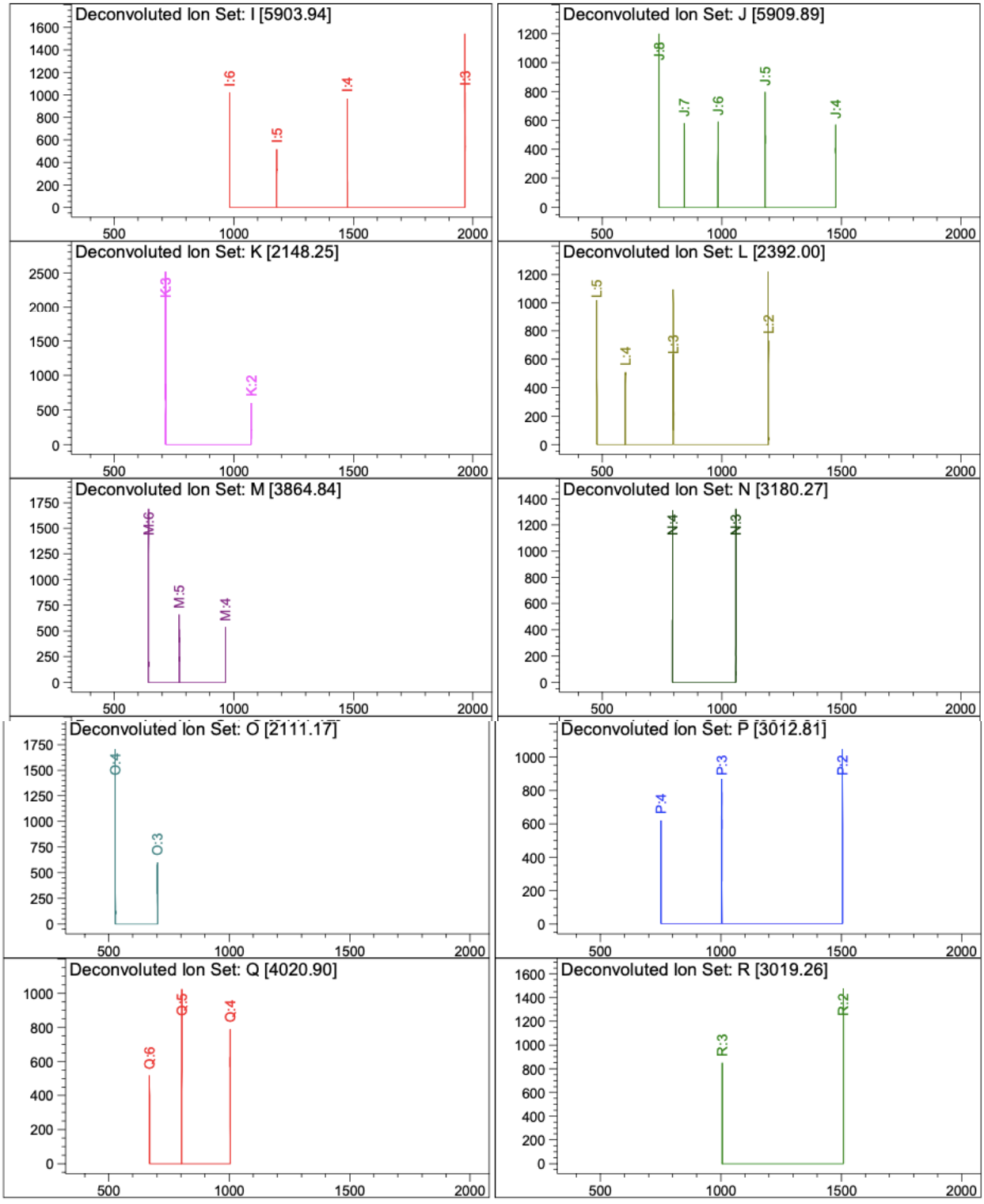
Deconvoluted Ion Set: I [5903.94]
I:6
I:5
I:4
I:3
Deconvoluted Ion Set: J [5909.89]
J:8
J:7
J:6
J:5
J:4
Deconvoluted Ion Set: K [2148.25]
K:3
K:2
Deconvoluted Ion Set: L [2392.00]
L:5
L:4
L:3
L:2
Deconvoluted Ion Set: M [3864.84]
M:6
M:5
M:4
Deconvoluted Ion Set: N [3180.27]
N:4
N:3
Deconvoluted Ion Set: O [2111.17]
O:4
O:3
Deconvoluted Ion Set: P [3012.81]
P:4
P:3
P:2
Deconvoluted Ion Set: Q [4020.90]
Q:6
Q:5
Q:4
Deconvoluted Ion Set: R [3019.26]
R:3
R:2

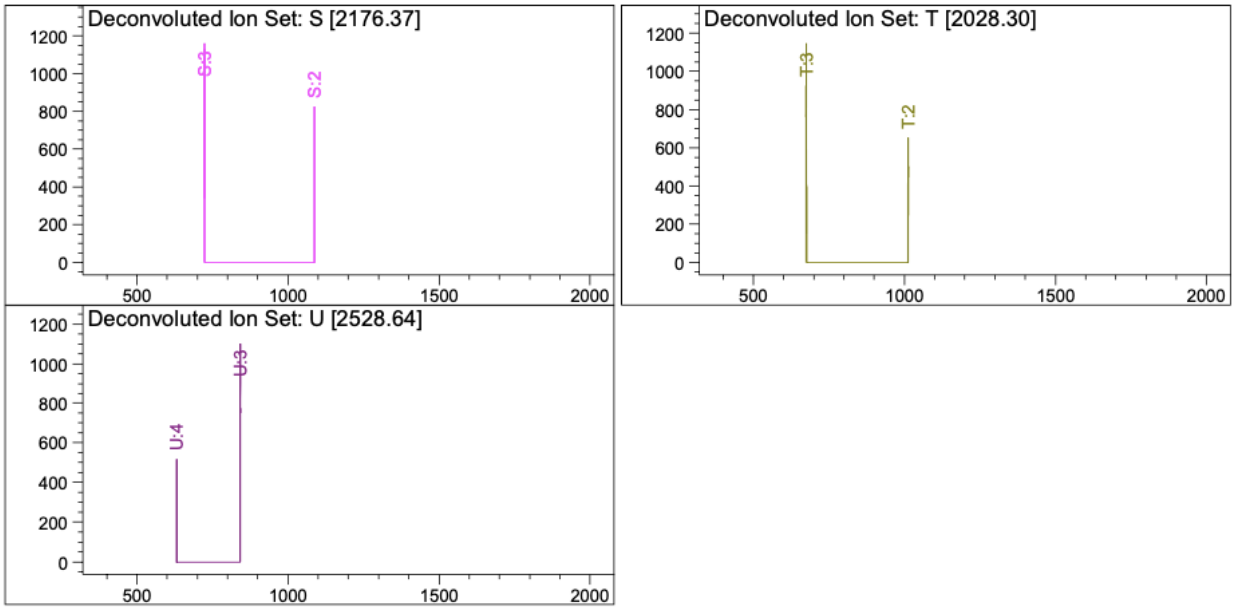

Component	Molecular Weight	Absolute Abundance	Relative Abundance
A	6044.97	35862	100.00
B	5879.55	19756	55.09
C	6012.88	19272	53.74
D	6019.07	16108	44.92
E	5975.37	5442	15.17
F	6065.10	4182	11.66
G	5979.48	3964	11.05
H	3034.27	3683	10.27
I	5903.94	3498	9.75
J	5909.89	2974	8.29
K	2148.25	2792	7.79
L	2392.00	2622	7.31
M	3864.84	2612	7.28
N	3180.27	2489	6.94
O	2111.17	2125	5.93
P	3012.81	2013	5.61
Q	4020.90	1974	5.50
R	3019.26	1904	5.31
S	2176.37	1758	4.90
T	2028.30	1619	4.51
U	2528.64	1454	4.05

*** End of Report ***

Supplementary Data 9. Photooxidation of ssDNA-1G-1 by Rose Bengal with 30 minutes of exposure to 550 nm light with an intensity of 6.37 mW/cm^2.

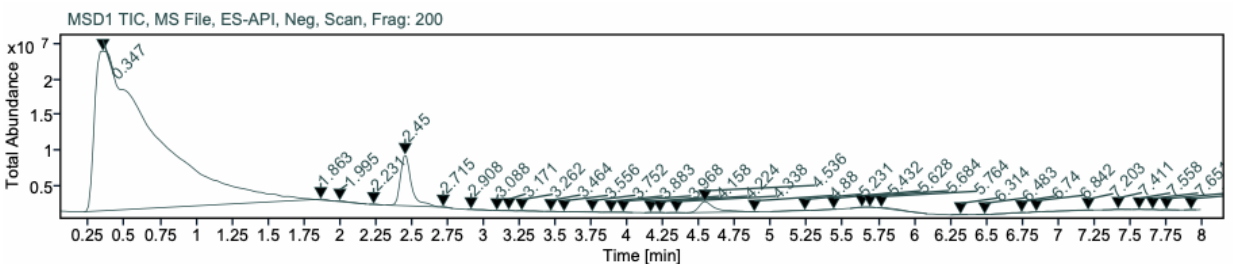

Deconvolution of Spectrum # 1 @ 2.392 - 2.571 min

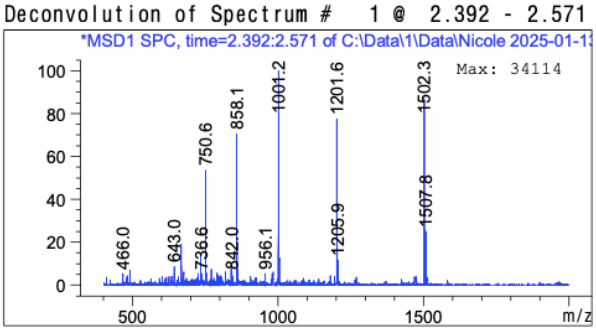

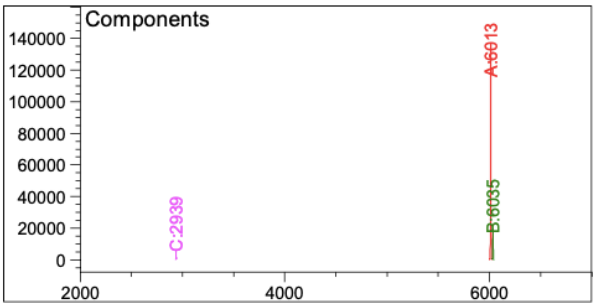

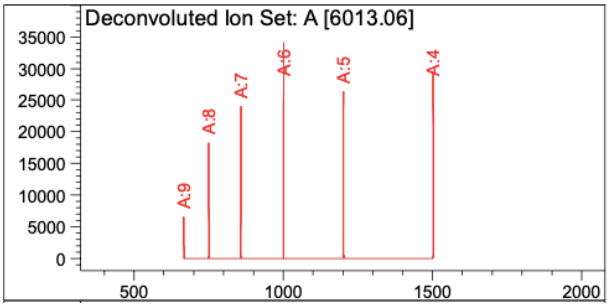

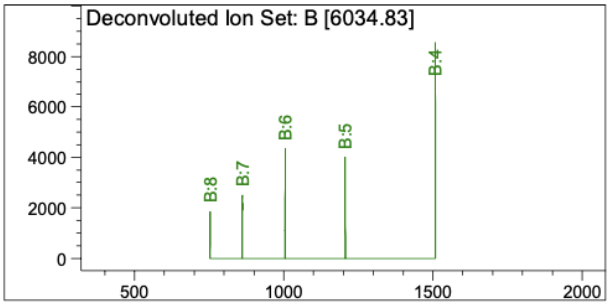

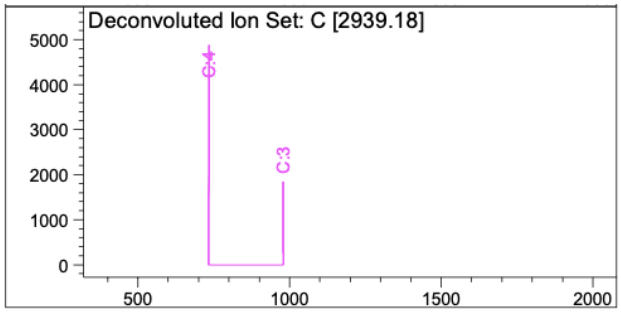

Component	Molecular Weight	Absolute Abundance	Relative Abundance
A	6013.06	136686	100.00
B	6034.83	20134	14.73
C	2939.18	6719	4.92

*** End of Report ***

Supplementary Data 10. Photooxidation of ssDNA-1G-1 by Rose Bengal with no exposure to 550 nm light with an intensity of 2.29 mW/cm^2.

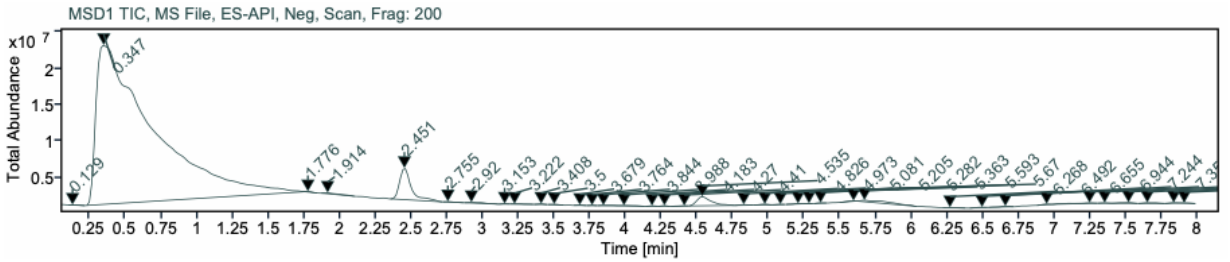

Deconvolution of Spectrum # 1 @ 2.376 - 2.620 min

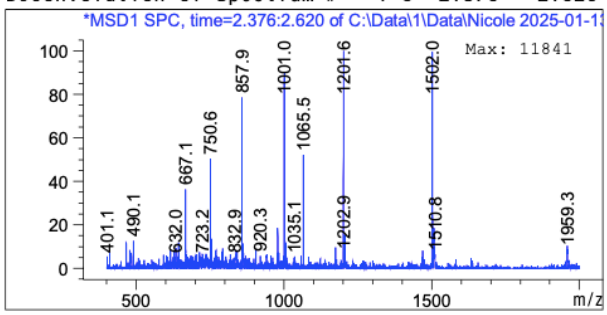

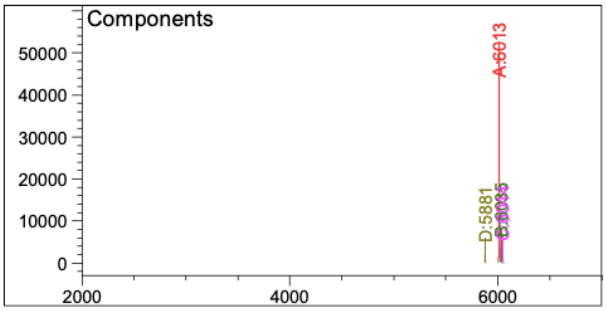

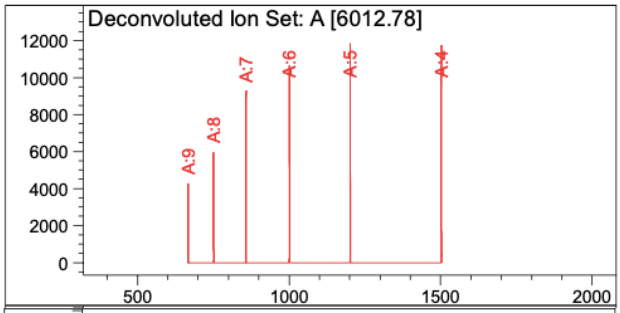

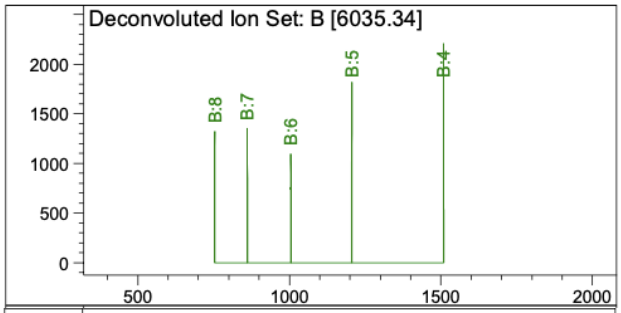

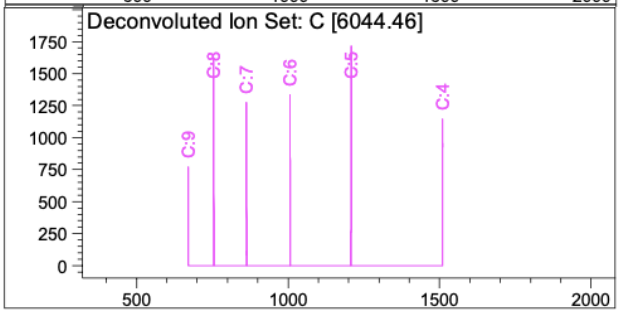

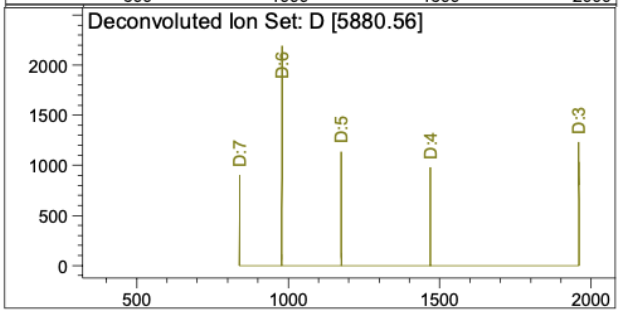

Component	Molecular Weight	Absolute Abundance	Relative Abundance
A	6012.78	52155	100.00
B	6035.34	7211	13.83
C	6044.46	6225	11.94
D	5880.56	6033	11.57

*** End of Report ***

Supplementary Data 11. Photooxidation of ssDNA-1G-1 by Rose Bengal with 10 min of exposure to 550 nm light with an intensity of 2.29 mW/cm^2.

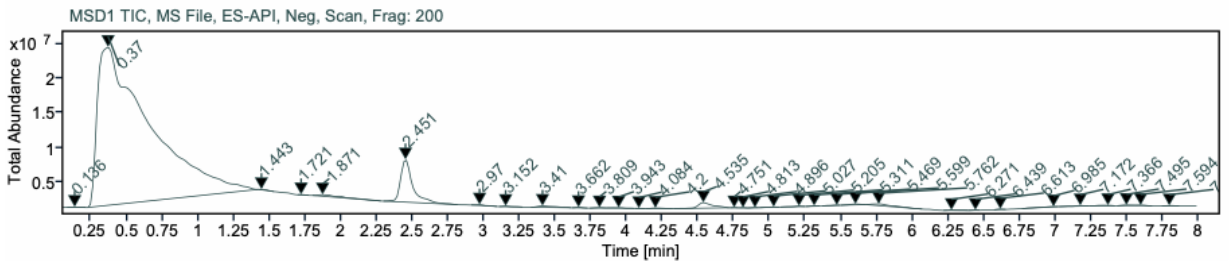

Deconvolution of Spectrum # 1 @ 2.376 - 2.620 min

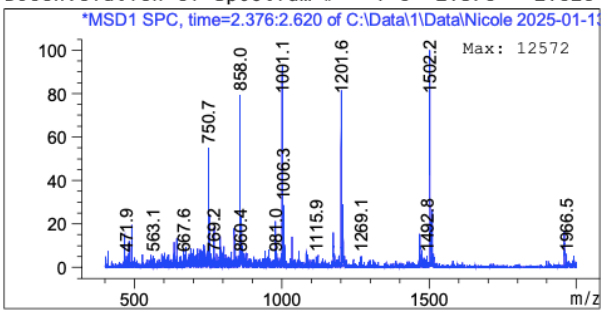

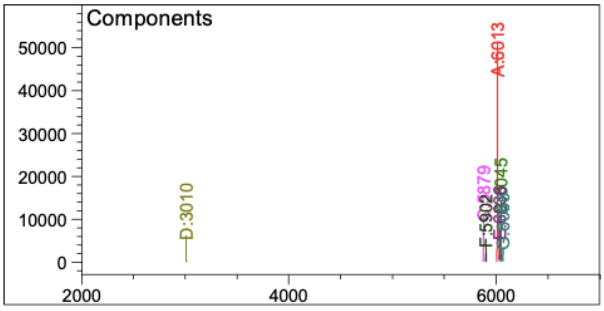

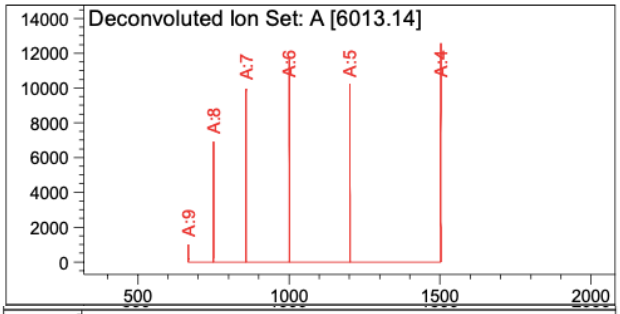

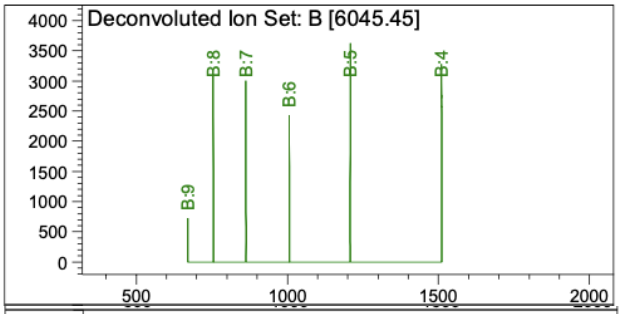

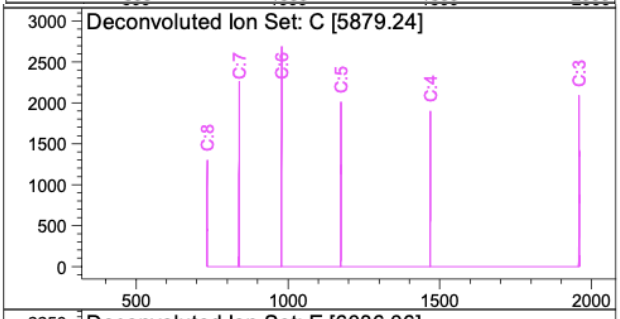

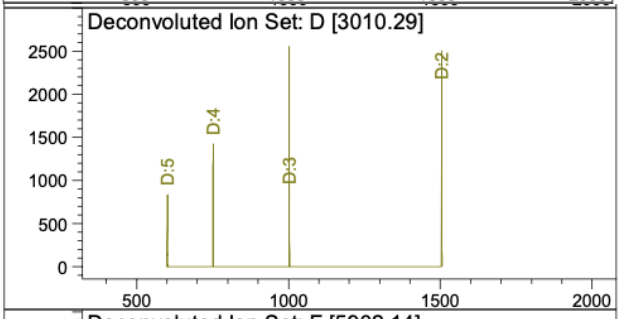

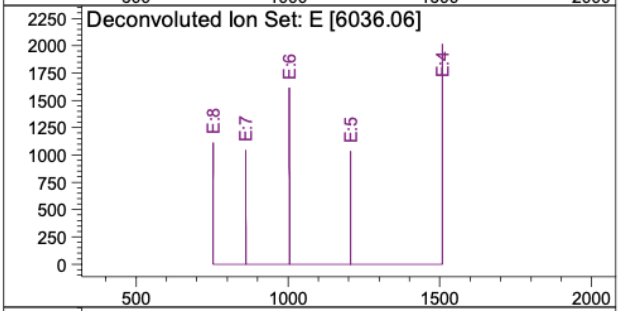

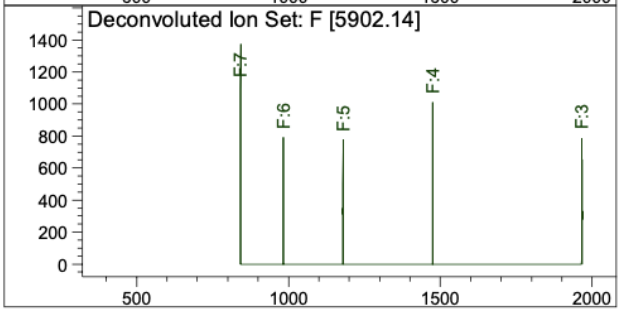

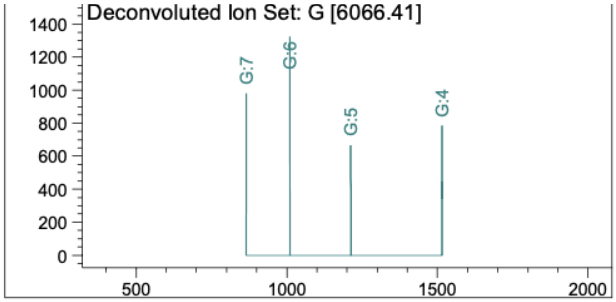

Component	Molecular Weight	Absolute Abundance	Relative Abundance
A	6013.14	51025	100.00
B	6045.45	14190	27.81
C	5879.24	11064	21.68
D	3010.29	6240	12.23
E	6036.06	6006	11.77
F	5902.14	4072	7.98
G	6066.41	3362	6.59

*** End of Report ***

Supplementary Data 12. Photooxidation of ssDNA-1G-1 by Rose Bengal with 20 min of exposure to 550 nm light with an intensity of 2.29 mW/cm^2.

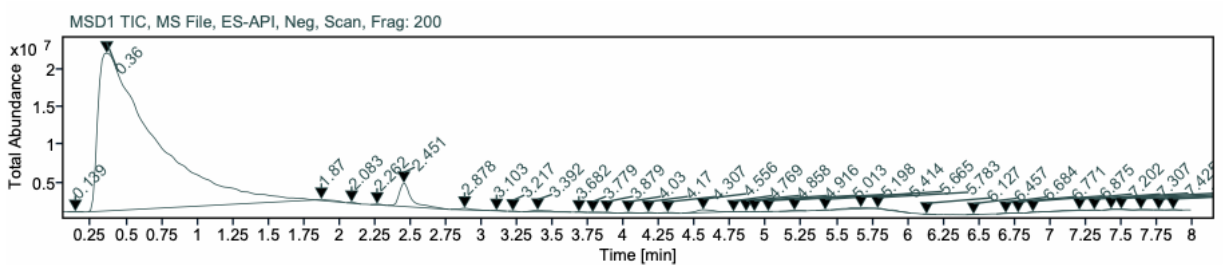

Deconvolution of Spectrum # 1 @ 2.392 - 2.620 min

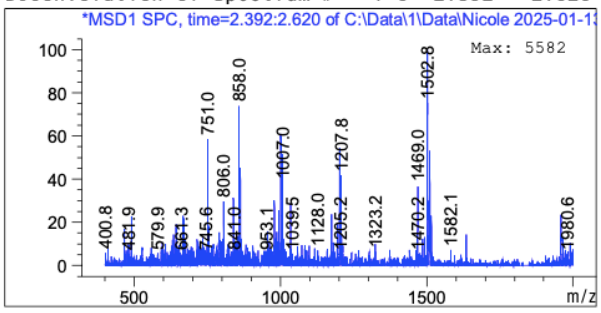

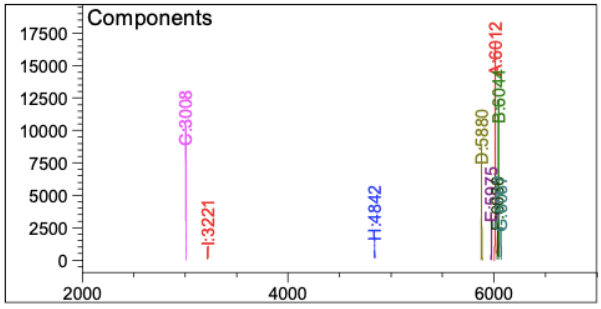

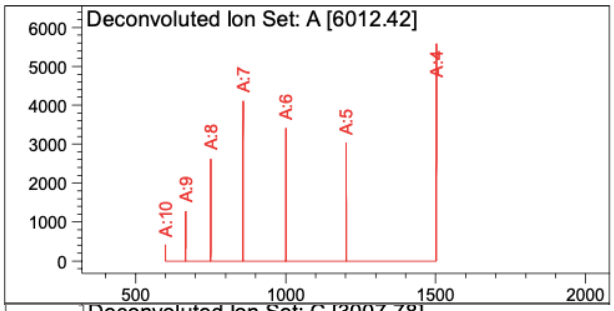

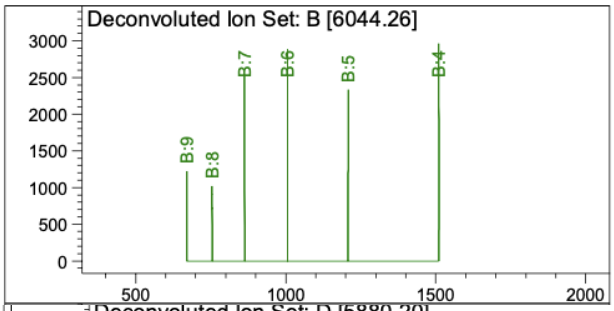

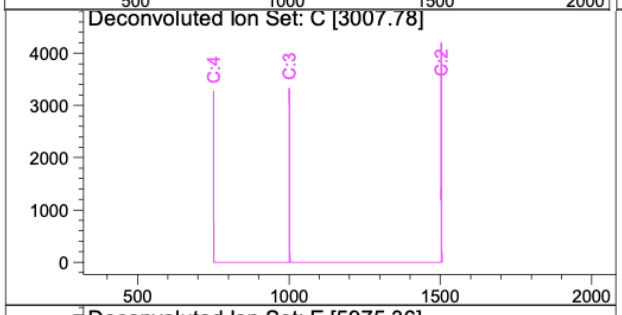

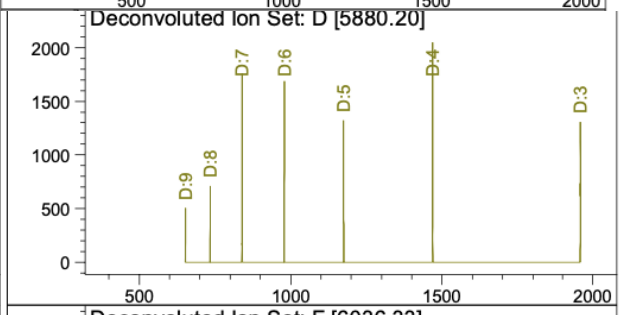

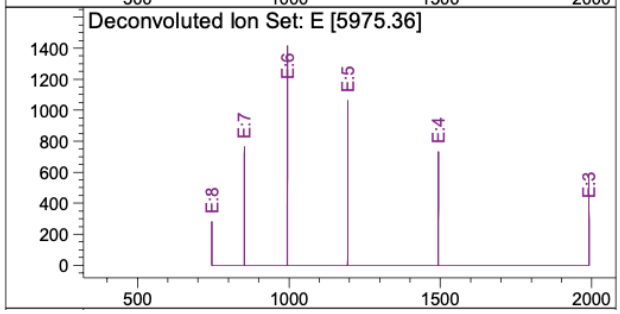

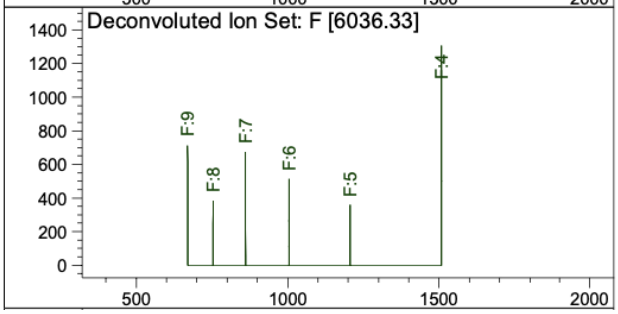

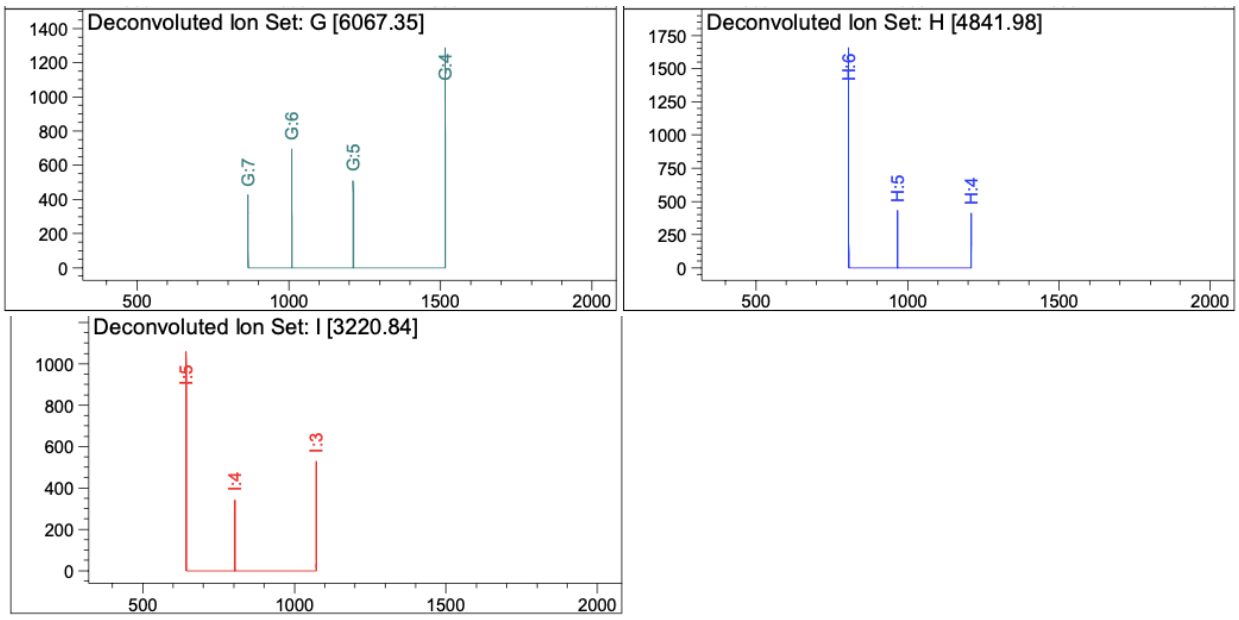

Component	Molecular Weight	Absolute Abundance	Relative Abundance
A	6012.42	16779	100.00
B	6044.26	12442	74.15
C	3007.78	10404	62.01
D	5880.20	8727	52.01
E	5975.36	3528	21.03
F	6036.33	2741	16.34
G	6067.35	2573	15.33
H	4841.98	1809	10.78
I	3220.84	1278	7.62

*** End of Report ***

Supplementary Data 13. Photooxidation of ssDNA-1G-1 by Rose Bengal with 30 min of exposure to 550 nm light with an intensity of 2.29 mW/cm^2.

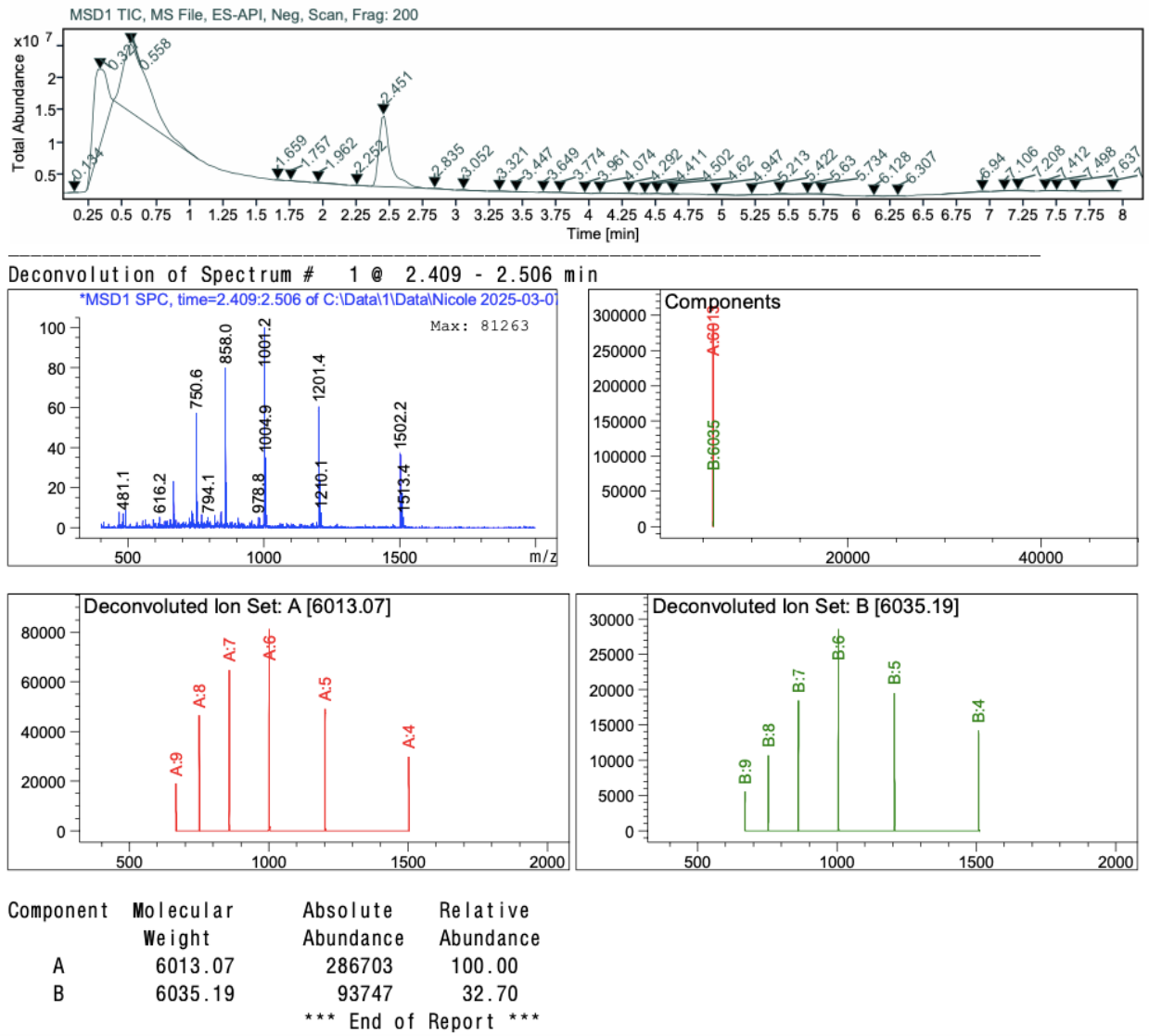

Component	Molecular Weight	Absolute Abundance	Relative Abundance
A	6013.07	286703	100.00
B	6035.19	93747	32.70

*** End of Report ***

Supplementary Data 14. Photooxidation of ssDNA-1G-3 by riboflavin with 0 min of exposure to blue light with an intensity of 3.54 mW/cm^2.

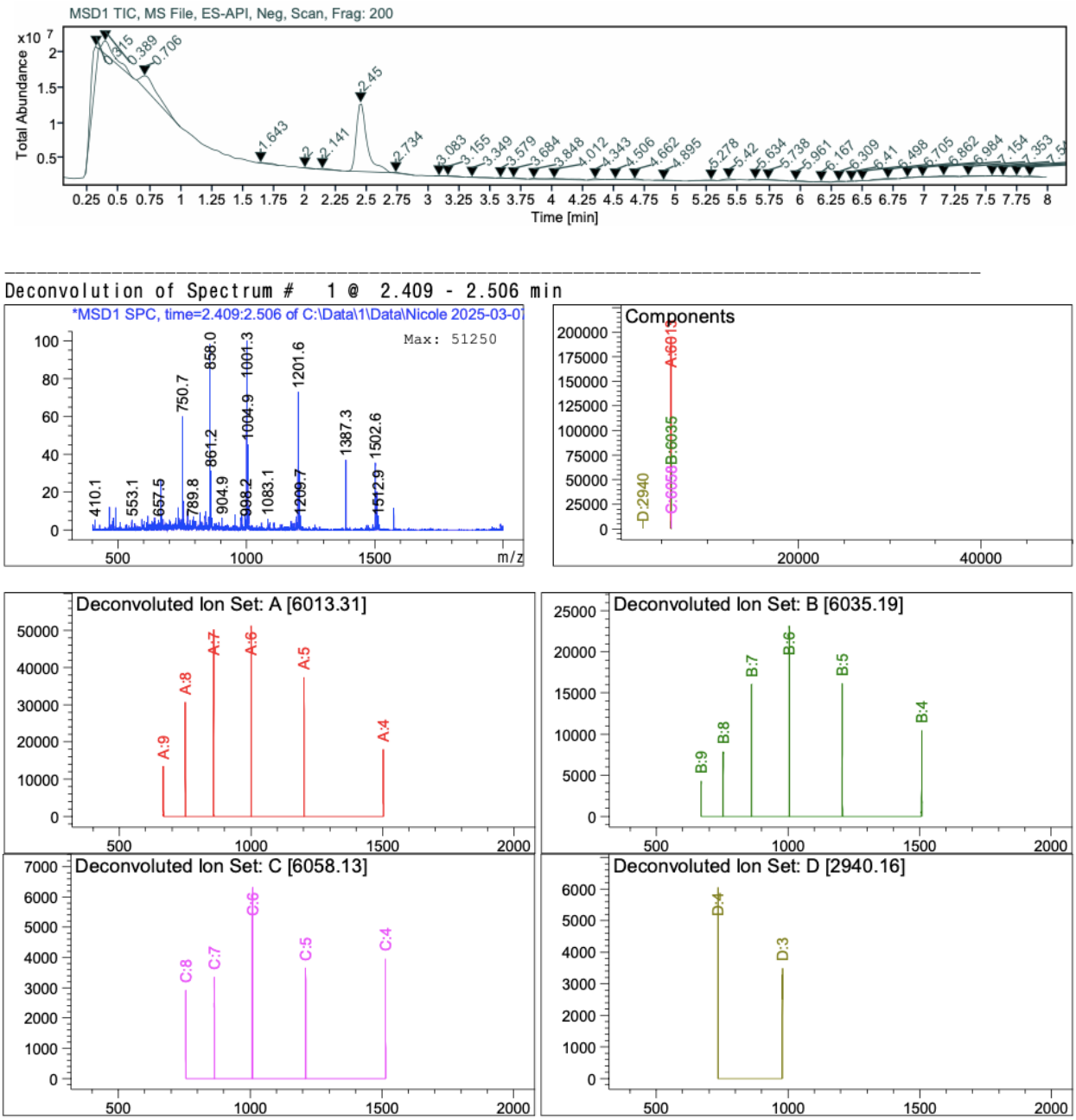

Component	Molecular Weight	Absolute Abundance	Relative Abundance
A	6013.31	193896	100.00
B	6035.19	77260	39.85
C	6058.13	18337	9.46
D	2940.16	9218	4.75

*** End of Report ***

Supplementary Data 15. Photooxidation of ssDNA-1G-3 by riboflavin with 2 min of exposure to blue light with an intensity of 3.54 mW/cm^2.

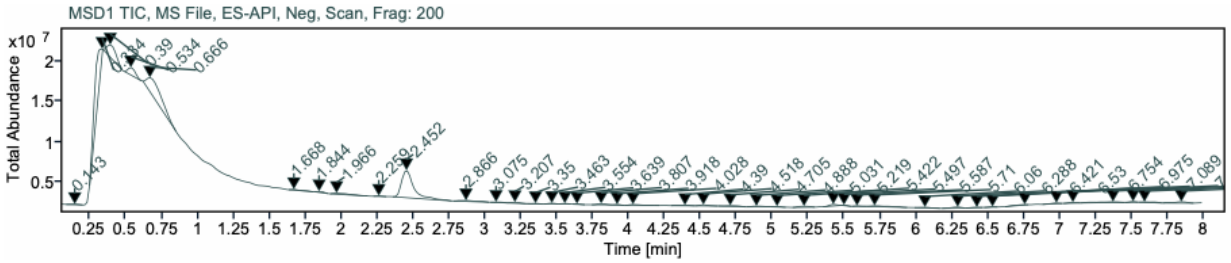

Deconvolution of Spectrum # 1 @ 2.393 - 2.523 min

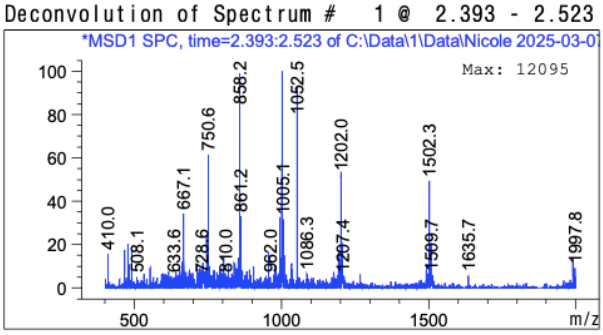

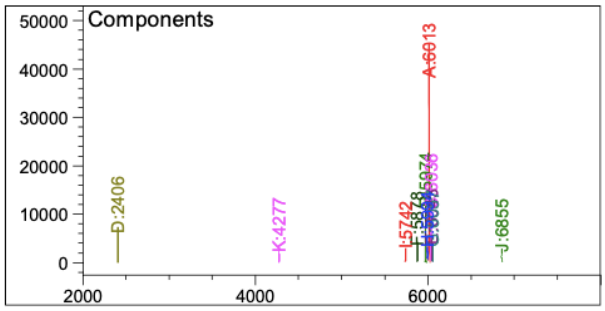

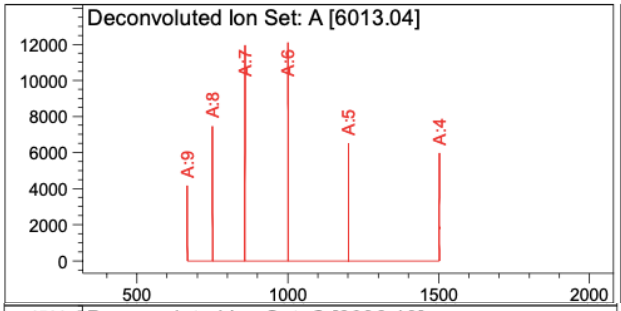

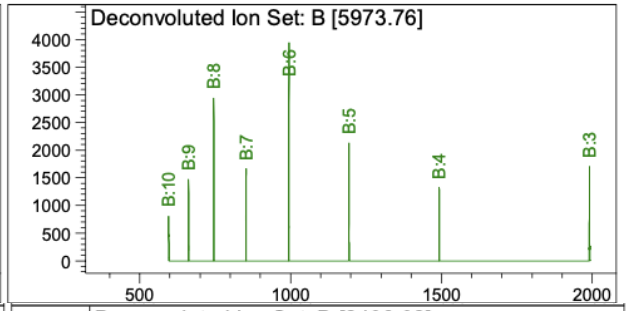

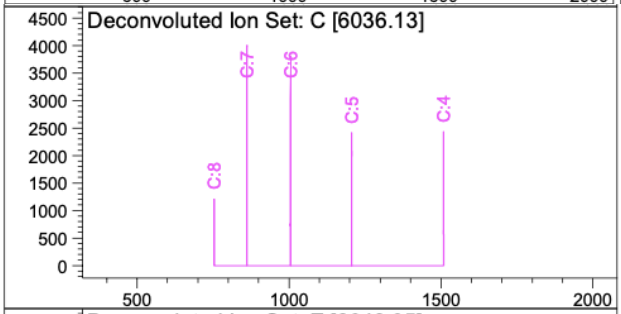

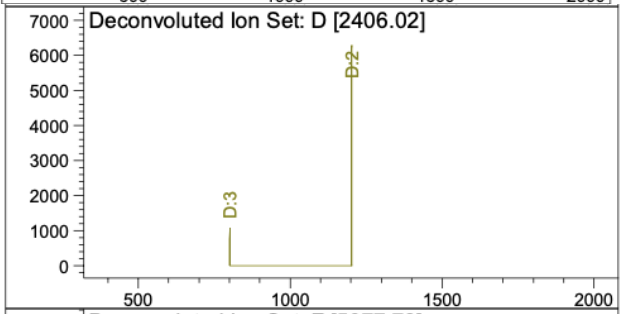

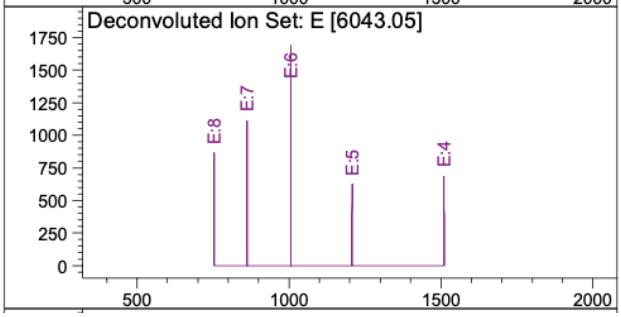

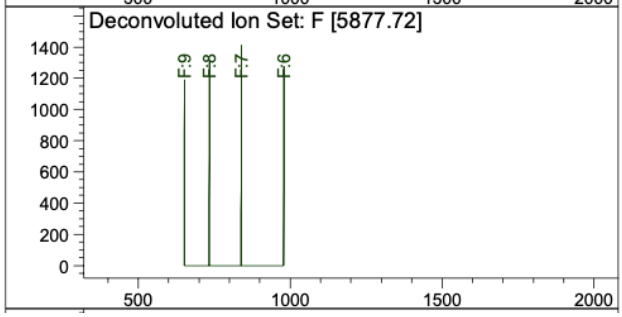

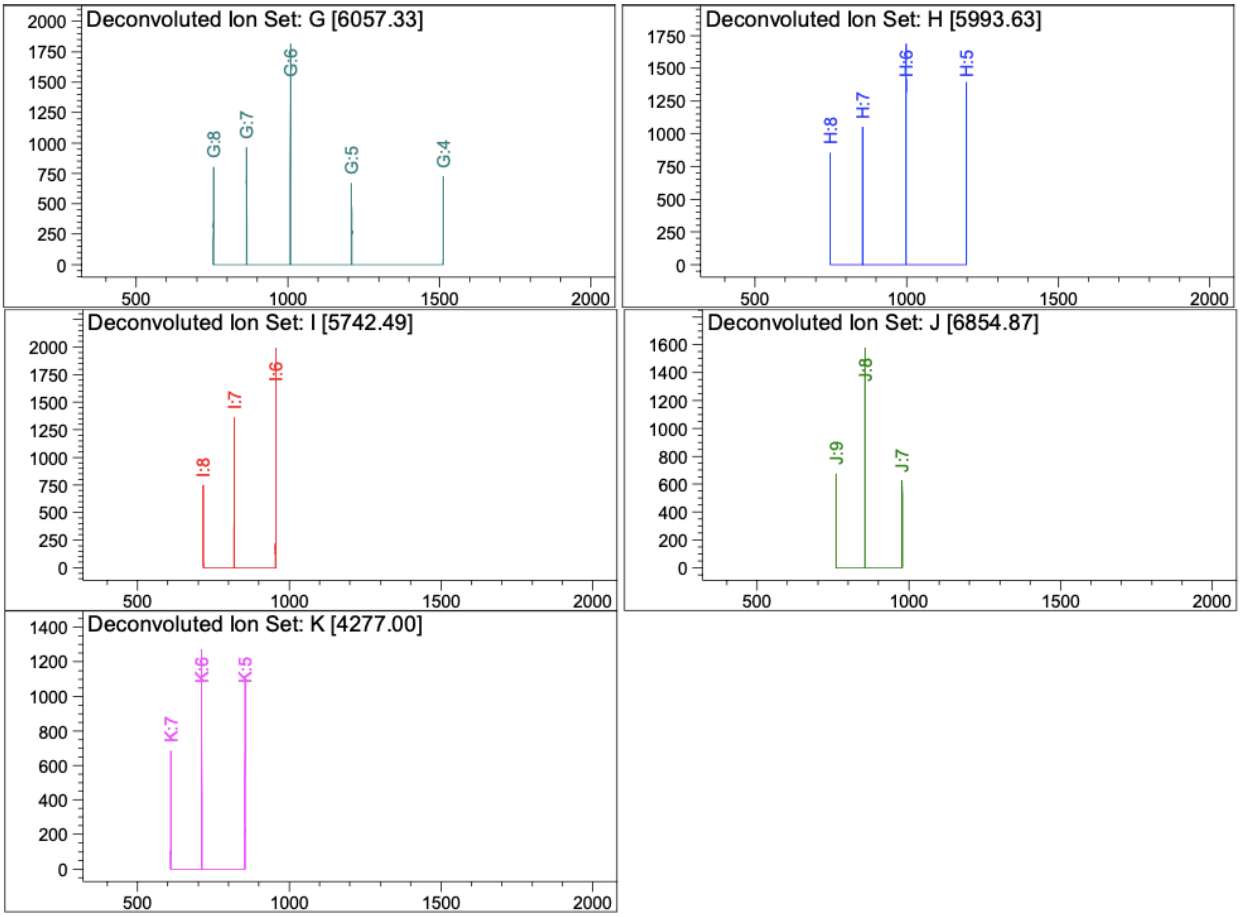

Component	Molecular Weight	Absolute Abundance	Relative Abundance
A	6013.04	45112	100.00
B	5973.76	13570	30.08
C	6036.13	13115	29.07
D	2406.02	7364	16.32
E	6043.05	4686	10.39
F	5877.72	4266	9.46
G	6057.33	3871	8.58
H	5993.63	3847	8.53
I	5742.49	3398	7.53
J	6854.87	2816	6.24
K	4277.00	2727	6.04

*** End of Report ***

Supplementary Data 16. Photooxidation of ssDNA-1G-3 by riboflavin with 5 min of exposure to blue light with an intensity of 3.54 mW/cm^2.

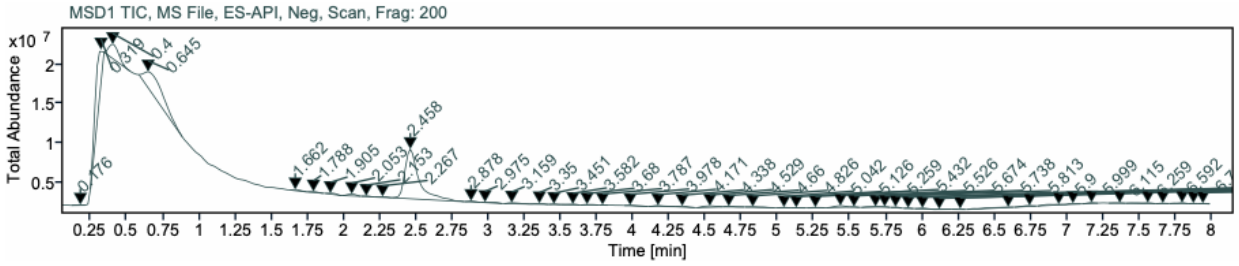

Deconvolution of Spectrum # 1 @ 2.408 - 2.522 min

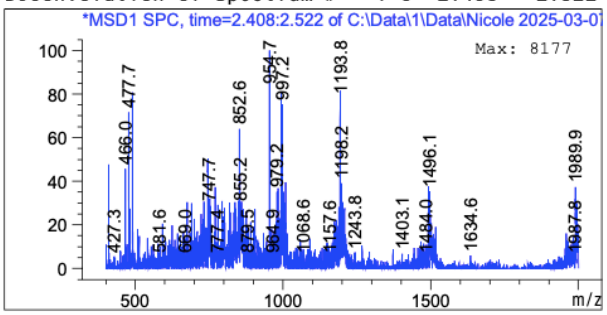

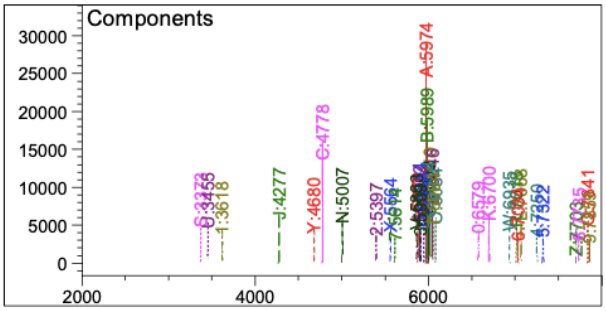

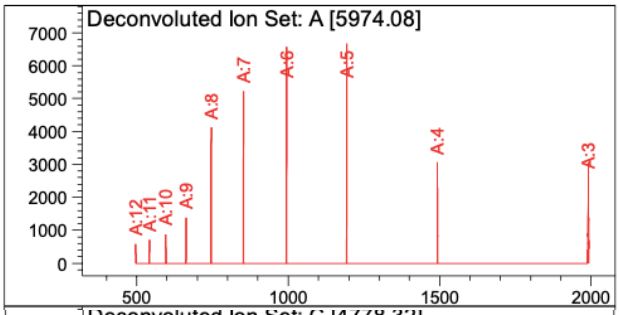

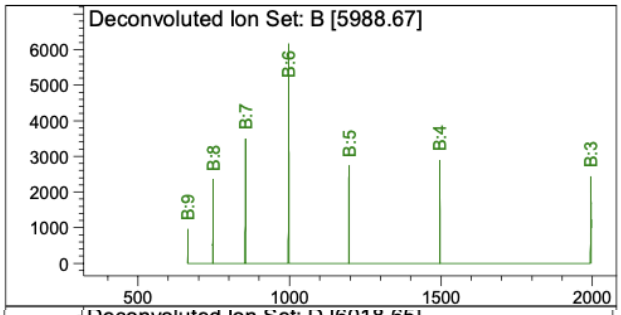

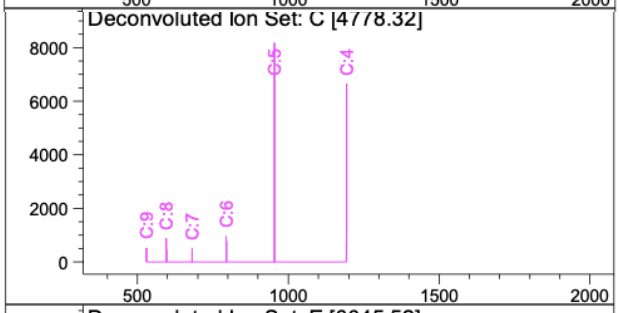

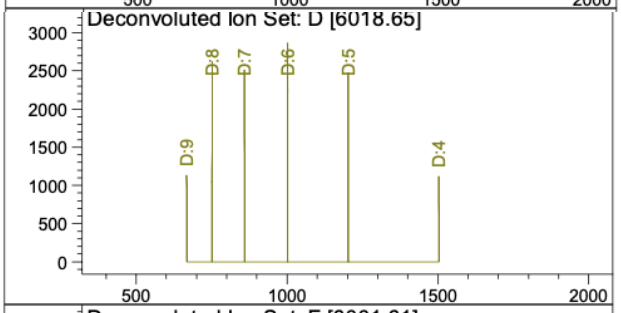

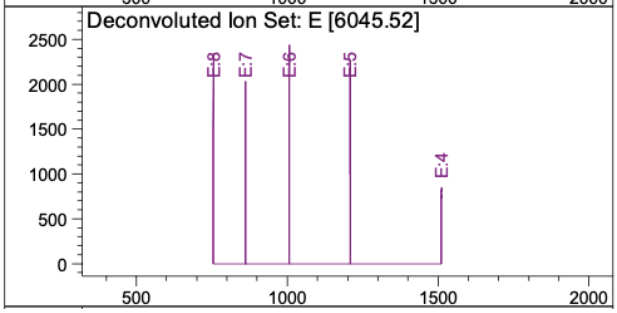

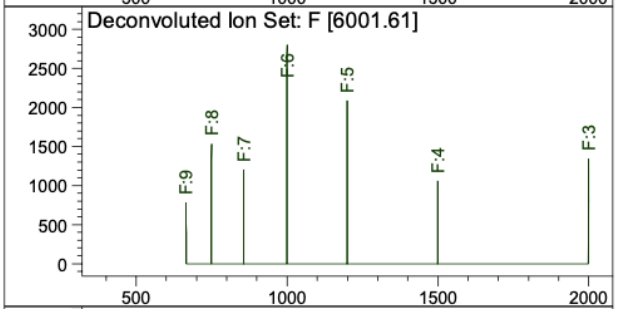

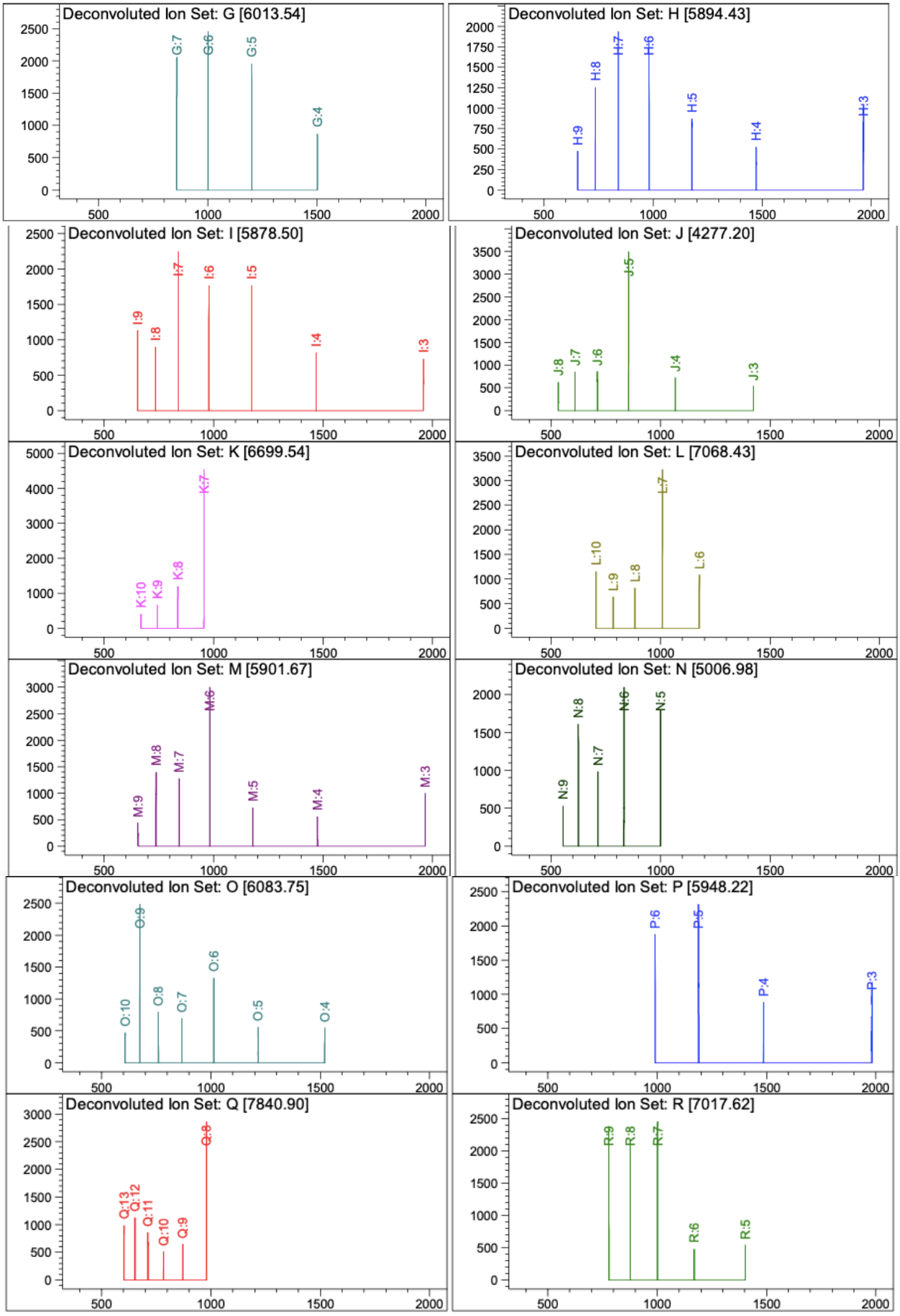
Deconvoluted Ion Set: G [6013.54]
G:7
G:6
G:5
G:4
Deconvoluted Ion Set: H [5894.43]
H:9
H:8
H:7
H:6
H:5
H:4
H:3
Deconvoluted Ion Set: I [5878.50]
I:9
I:8
I:7
I:6
I:5
I:4
I:3
Deconvoluted Ion Set: J [4277.20]
J:8
J:7
J:6
J:5
J:4
J:3
Deconvoluted Ion Set: K [6699.54]
K:10
K:9
K:8
K:7
Deconvoluted Ion Set: L [7068.43]
L:10
L:9
L:8
L:7
L:6
Deconvoluted Ion Set: M [5901.67]
M:9
M:8
M:7
M:6
M:5
M:4
M:3
Deconvoluted Ion Set: N [5006.98]
N:9
N:8
N:7
N:6
N:5
Deconvoluted Ion Set: O [6083.75]
O:10
O:9
O:8
O:7
O:6
O:5
O:4
Deconvoluted Ion Set: P [5948.22]
P:6
P:5
P:4
P:3
Deconvoluted Ion Set: Q [7840.90]
Q:13
Q:12
Q:11
Q:10
Q:9
Q:8
Deconvoluted Ion Set: R [7017.62]
R:9
R:8
R:7
R:6
R:5

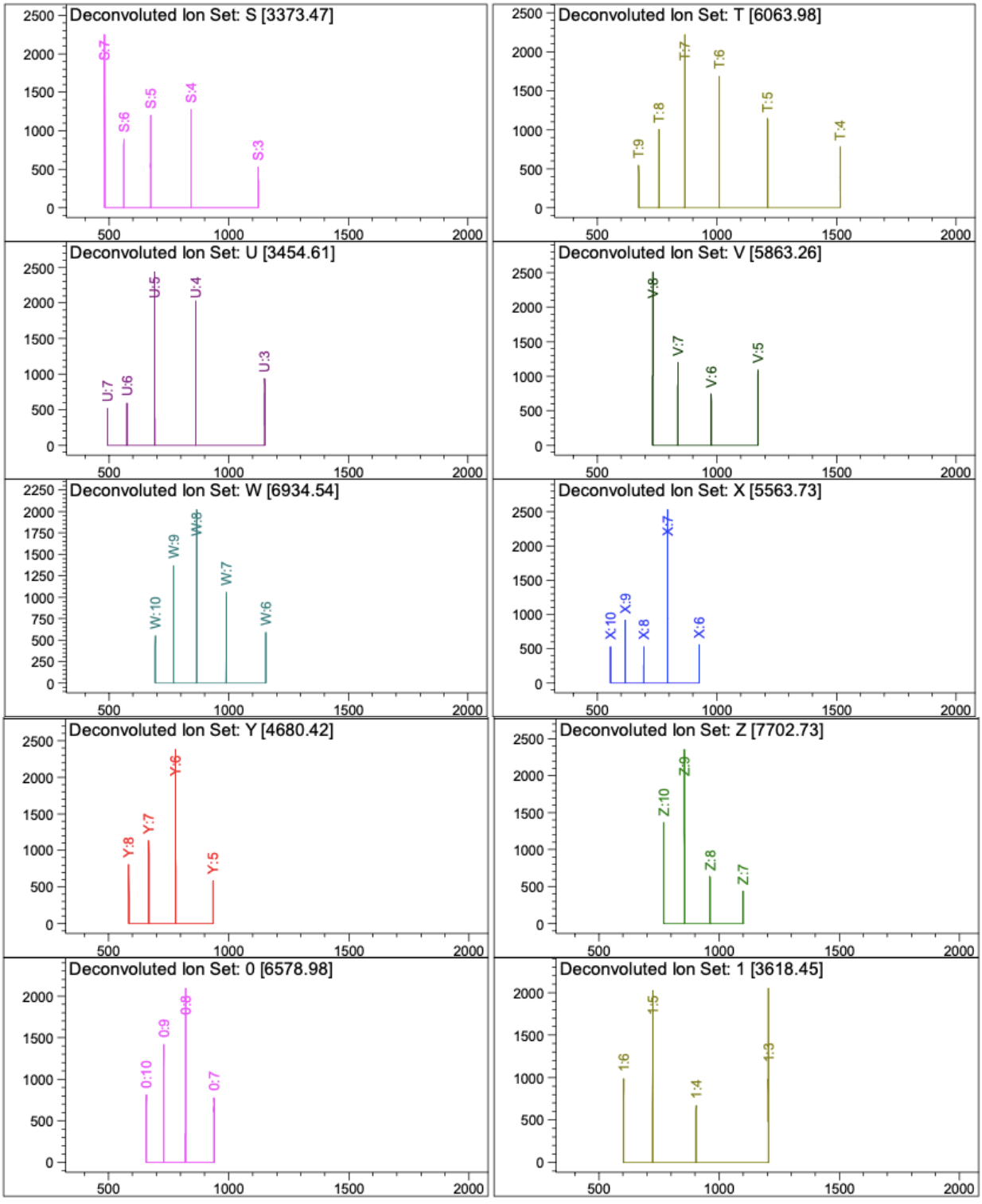
Deconvoluted Ion Set: S [3373.47]
S:7
S:6
S:5
S:4
S:3
Deconvoluted Ion Set: T [6063.98]
T:9
T:8
T:7
T:6
T:5
T:4
Deconvoluted Ion Set: U [3454.61]
U:7
U:6
U:5
U:4
U:3
Deconvoluted Ion Set: V [5863.26]
V:8
V:7
V:6
V:5
Deconvoluted Ion Set: W [6934.54]
W:10
W:9
W:8
W:7
W:6
Deconvoluted Ion Set: X [5563.73]
X:10
X:9
X:8
X:7
X:6
Deconvoluted Ion Set: Y [4680.42]
Y:8
Y:7
Y:6
Y:5
Deconvoluted Ion Set: Z [7702.73]
Z:10
Z:9
Z:8
Z:7
Deconvoluted Ion Set: 0 [6578.98]
0:10
0:9
0:8
0:7
Deconvoluted Ion Set: 1 [3618.45]
1:6
1:5
1:4
1:3

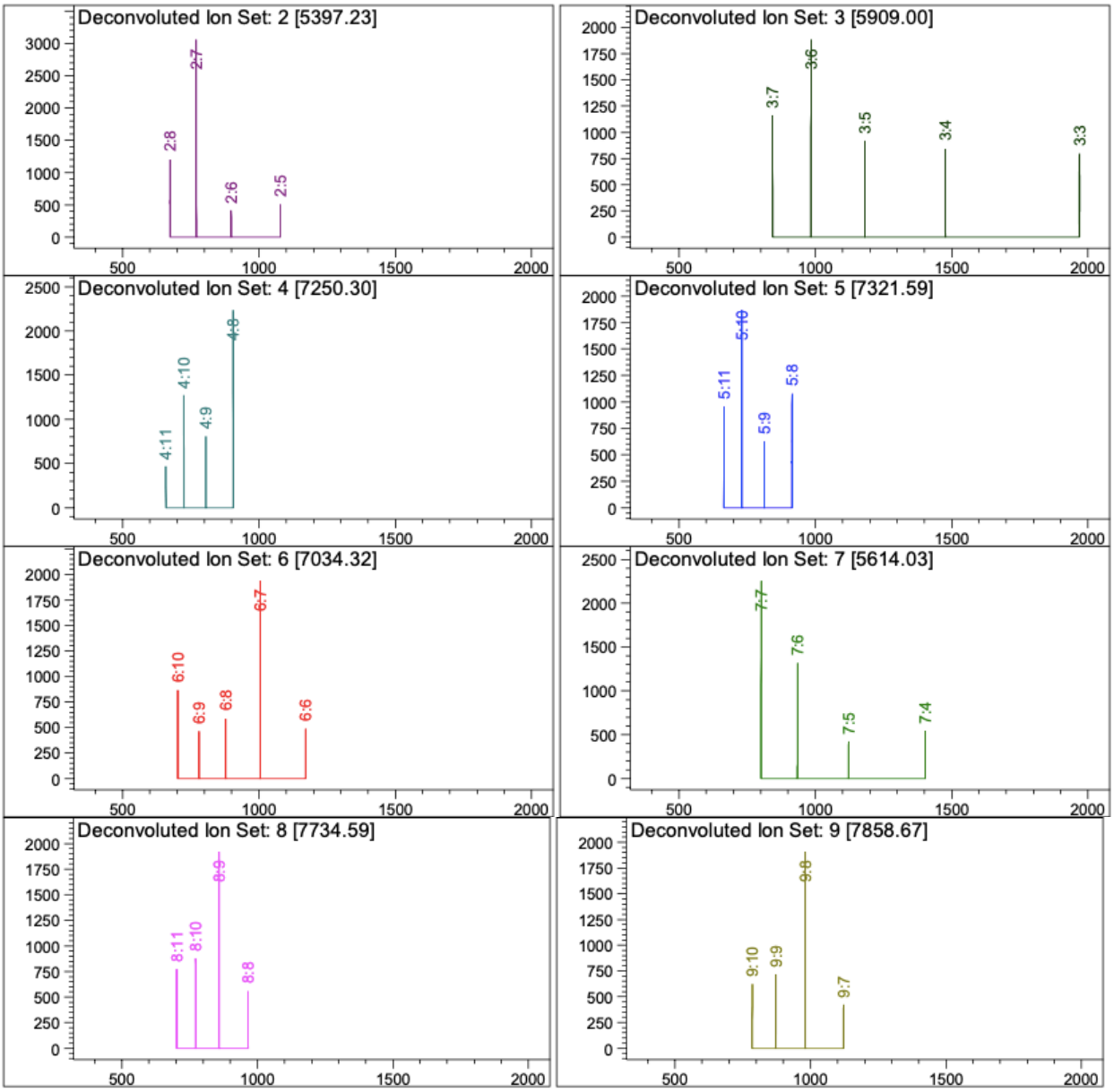

Component	Molecular Weight	Absolute Abundance	Relative Abundance
A	5974.08	28985	100.00
B	5988.67	18767	64.75
C	4778.32	15960	55.06
D	6018.65	9568	33.01
E	6045.52	9272	31.99
F	6001.61	7512	25.92
G	6013.54	6885	23.75
H	5894.43	6873	23.71
I	5878.50	6742	23.26
J	4277.20	6694	23.09
K	6699.54	6588	22.73
L	7068.43	6535	22.55
M	5901.67	6290	21.70

N	5006.98	6192	21.36
O	6083.75	5976	20.62
P	5948.22	5863	20.23
Q	7840.90	5691	19.63
R	7017.62	5657	19.52
S	3373.47	5628	19.42
T	6063.98	5616	19.38
U	3454.61	5521	19.05
V	5863.26	5306	18.31
W	6934.54	5035	17.37
X	5563.73	4809	16.59
Y	4680.42	4764	16.44
Z	7702.73	4601	15.87
0	6578.98	4525	15.61
1	3618.45	4492	15.50
2	5397.23	4345	14.99
3	5909.00	4238	14.62
4	7250.30	4102	14.15
5	7321.59	3944	13.61
6	7034.32	3586	12.37
7	5614.03	3464	11.95
8	7734.59	3457	11.93
9	7858.67	3093	10.67

*** End of Report ***

Supplementary Data 17. Photooxidation of ssDNA-1G-3 by riboflavin with 15 min of exposure to blue light with an intensity of 3.54 mW/cm^2.

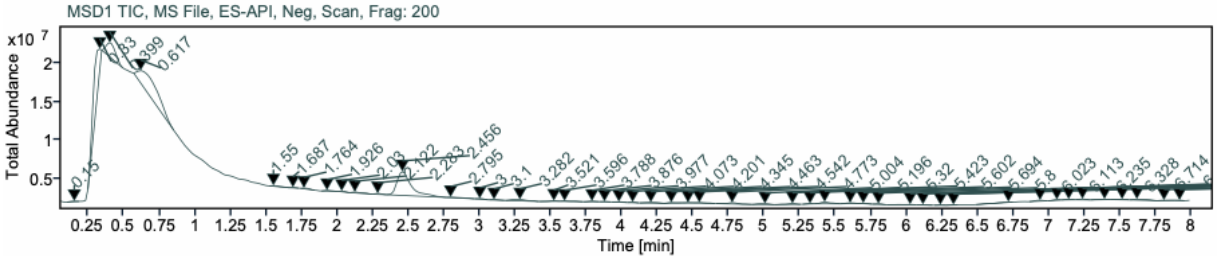

Deconvolution of Spectrum # 1 @ 2.409 - 2.506 min

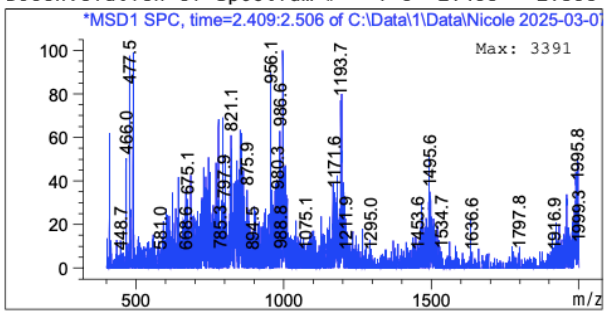

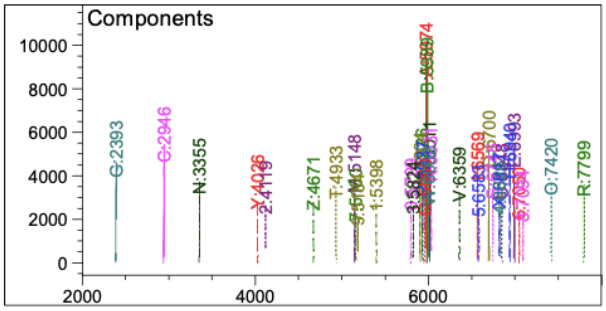

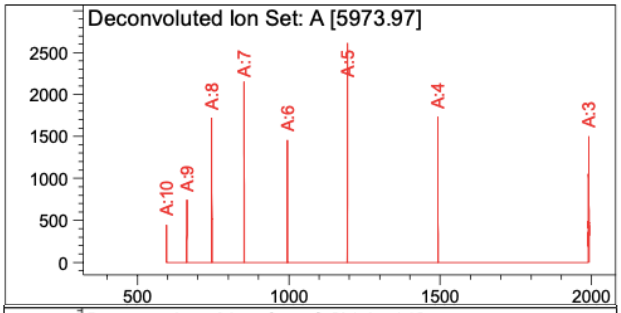

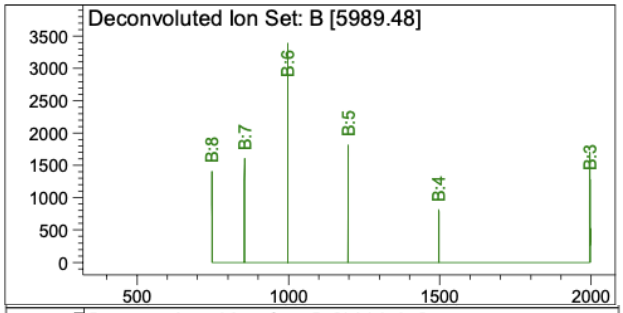

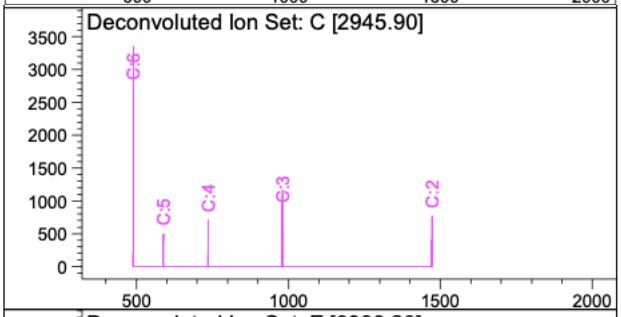

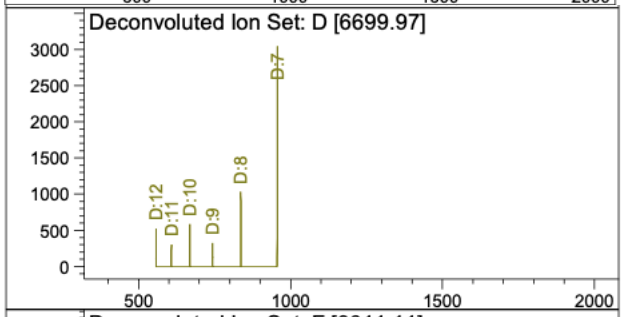

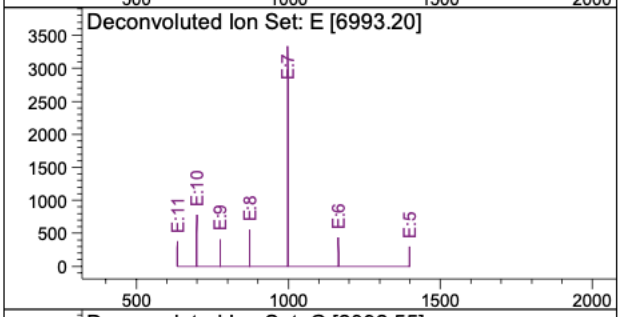

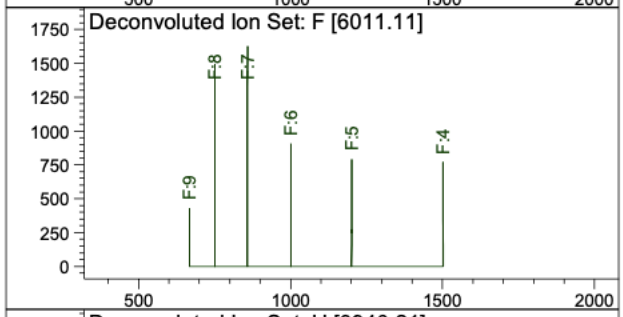

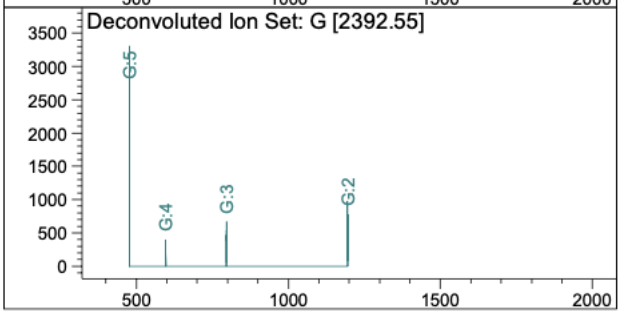

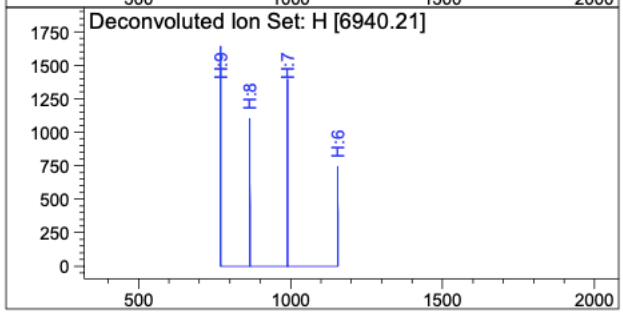

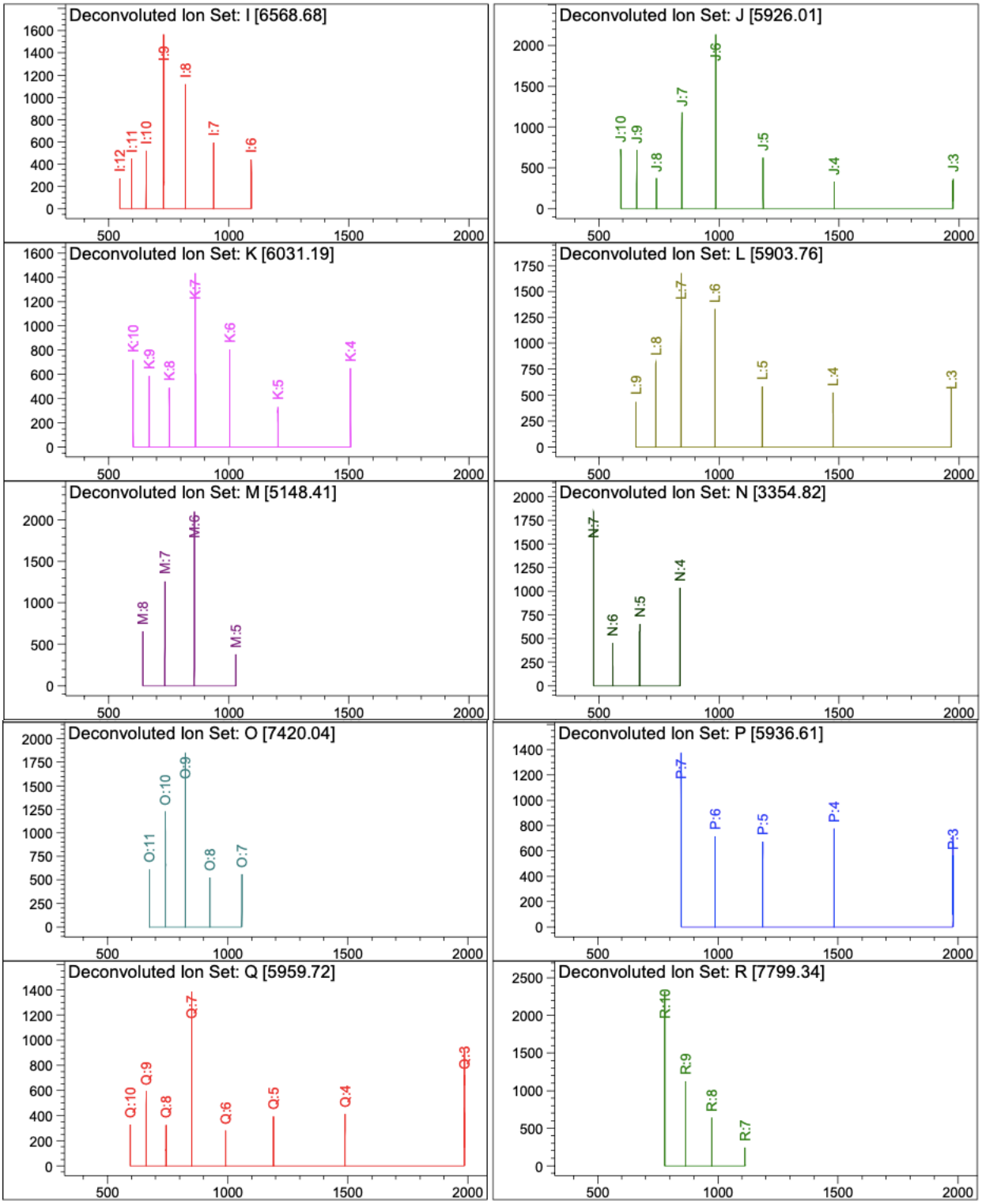
Deconvoluted Ion Set: I [6568.68]
I:12
I:11
I:10
I:9
I:8
I:7
I:6
Deconvoluted Ion Set: J [5926.01]
J:10
J:9
J:8
J:7
J:6
J:5
J:4
J:3
Deconvoluted Ion Set: K [6031.19]
K:10
K:9
K:8
K:7
K:6
K:5
K:4
Deconvoluted Ion Set: L [5903.76]
L:9
L:8
L:7
L:6
L:5
L:4
L:3
Deconvoluted Ion Set: M [5148.41]
M:8
M:7
M:6
M:5
Deconvoluted Ion Set: N [3354.82]
N:7
N:6
N:5
N:4
Deconvoluted Ion Set: O [7420.04]
O:11
O:10
O:9
O:8
O:7
Deconvoluted Ion Set: P [5936.61]
P:7
P:6
P:5
P:4
P:3
Deconvoluted Ion Set: Q [5959.72]
Q:10
Q:9
Q:8
Q:7
Q:6
Q:5
Q:4
Q:3
Deconvoluted Ion Set: R [7799.34]
R:10
R:9
R:8
R:7

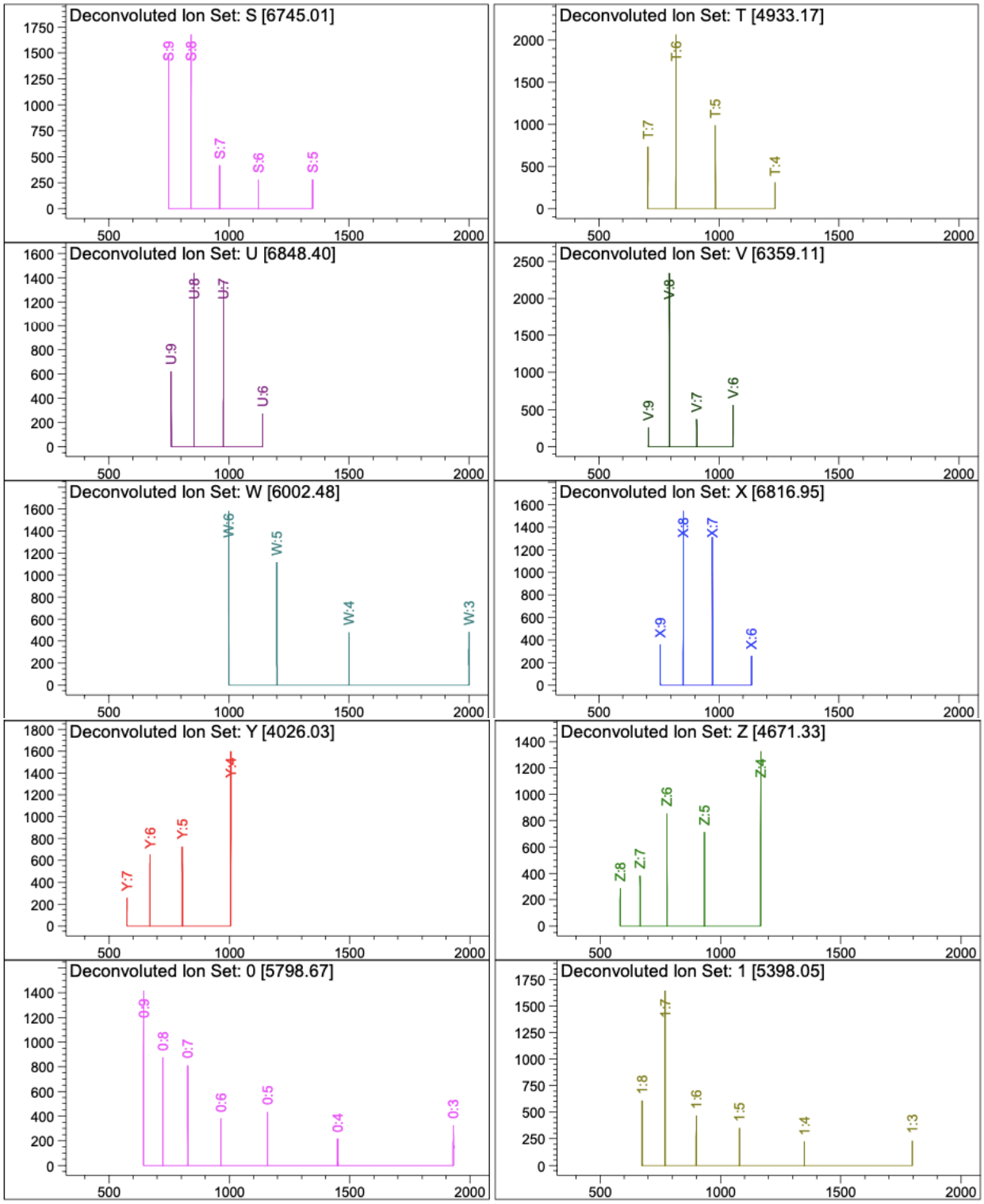
Deconvoluted Ion Set: S [6745.01]
S:9
S:8
S:7
S:6
S:5
Deconvoluted Ion Set: T [4933.17]
T:7
T:6
T:5
T:4
Deconvoluted Ion Set: U [6848.40]
U:9
U:8
U:7
U:6
Deconvoluted Ion Set: V [6359.11]
V:9
V:8
V:7
V:6
Deconvoluted Ion Set: W [6002.48]
W:6
W:5
W:4
W:3
Deconvoluted Ion Set: X [6816.95]
X:9
X:8
X:7
X:6
Deconvoluted Ion Set: Y [4026.03]
Y:7
Y:6
Y:5
Y:4
Deconvoluted Ion Set: Z [4671.33]
Z:8
Z:7
Z:6
Z:5
Z:4
Deconvoluted Ion Set: 0 [5798.67]
0:9
0:8
0:7
0:6
0:5
0:4
0:3
Deconvoluted Ion Set: 1 [5398.05]
1:8
1:7
1:6
1:5
1:4
1:3

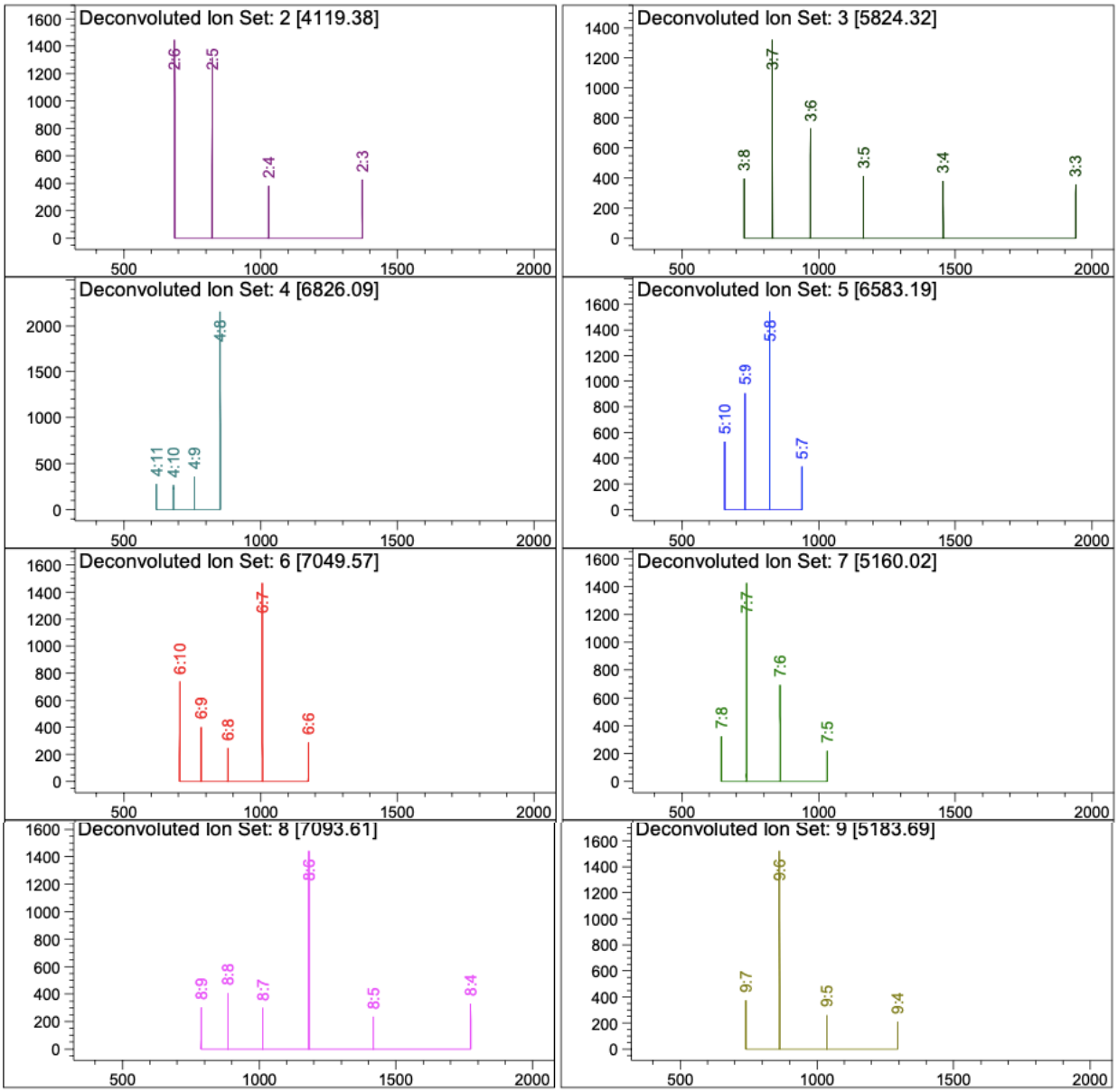

Component	Molecular Weight	Absolute Abundance	Relative Abundance
A	5973.97	10094	100.00
B	5989.48	9214	91.28
C	2945.90	5428	53.77
D	6699.97	5208	51.60
E	6993.20	5176	51.28
F	6011.11	4785	47.40
G	2392.55	4609	45.66
H	6940.21	4567	45.24
I	6568.68	4505	44.63
J	5926.01	4437	43.96
K	6031.19	4397	43.56
L	5903.76	4223	41.84
M	5148.41	3831	37.95

N	3354.82	3716	36.81
O	7420.04	3696	36.62
P	5936.61	3619	35.85
Q	5959.72	3587	35.54
R	7799.34	3576	35.43
S	6745.01	3479	34.47
T	4933.17	3459	34.27
U	6848.40	3456	34.24
V	6359.11	3331	33.00
W	6002.48	3105	30.76
X	6816.95	3013	29.85
Y	4026.03	2920	28.93
Z	4671.33	2878	28.51
0	5798.67	2827	28.01
1	5398.05	2752	27.26
2	4119.38	2676	26.51
3	5824.32	2657	26.32
4	6826.09	2627	26.03
5	6583.19	2490	24.67
6	7049.57	2342	23.20
7	5160.02	2254	22.33
8	7093.61	2211	21.90
9	5183.69	2030	20.11

*** End of Report ***

Supplementary Data 18. Photooxidation of ssDNA-1G-3 by riboflavin with 30 min of exposure to blue light with an intensity of 3.54 mW/cm^2.

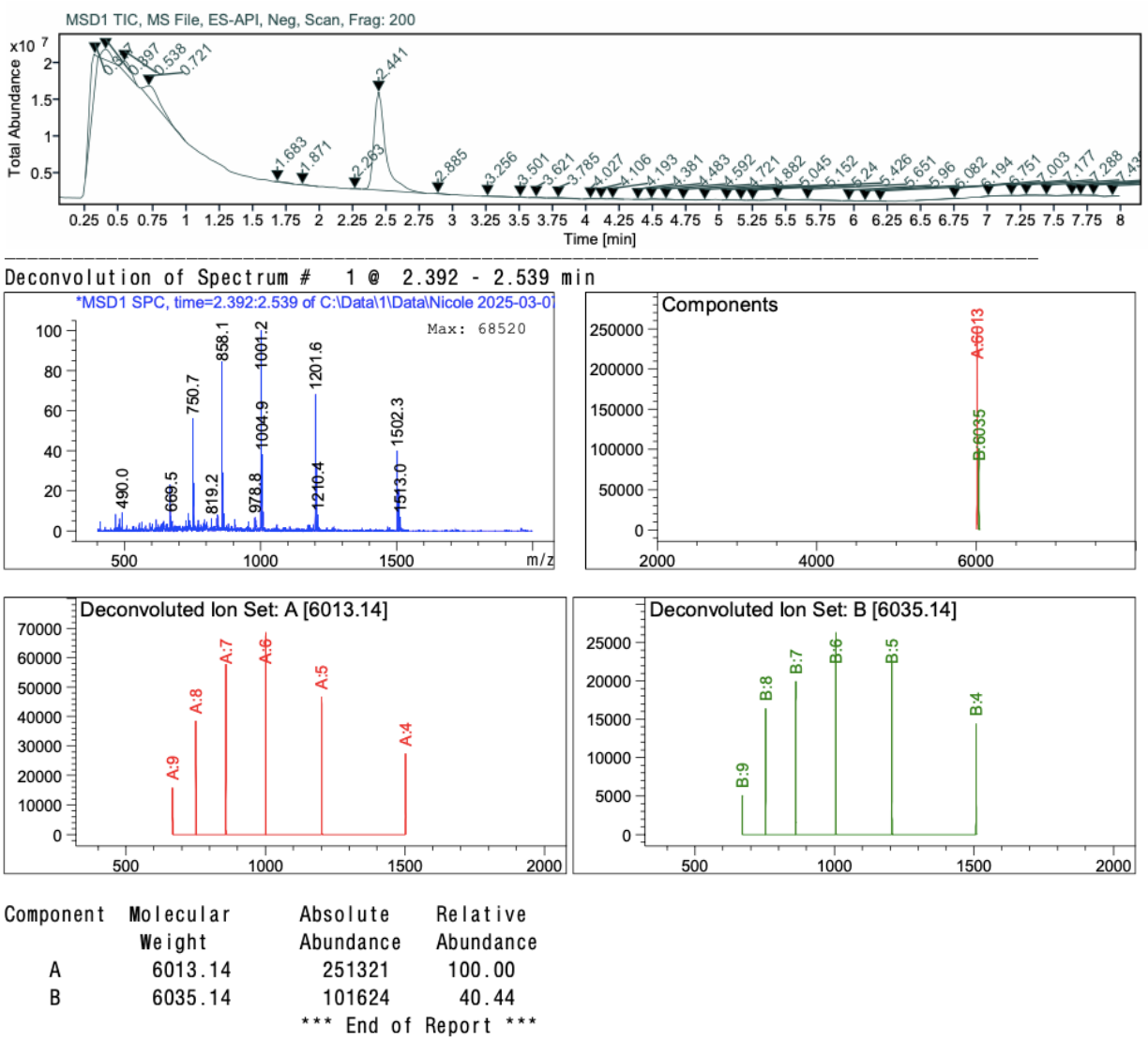

Component	Molecular Weight	Absolute Abundance	Relative Abundance
A	6013.14	251321	100.00
B	6035.14	101624	40.44

*** End of Report ***

Supplementary Data 19. Photooxidation of ssDNA-1G-3 by riboflavin with 0 min of exposure to blue light with an intensity of 1.27 mW/cm^2.

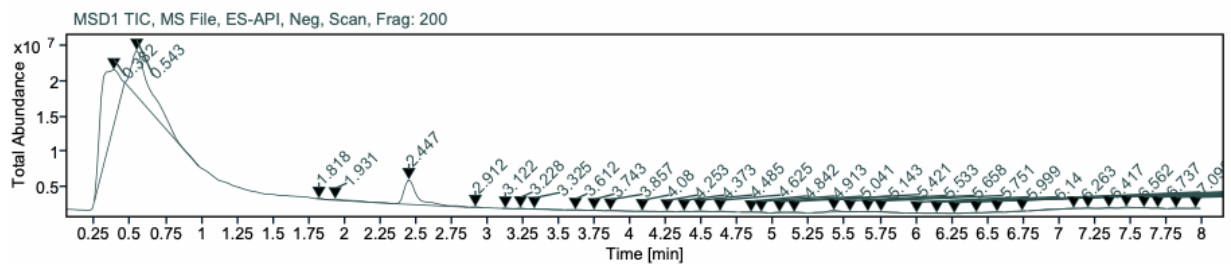

Deconvolution of Spectrum # 1 @ 2.376 - 2.620 min

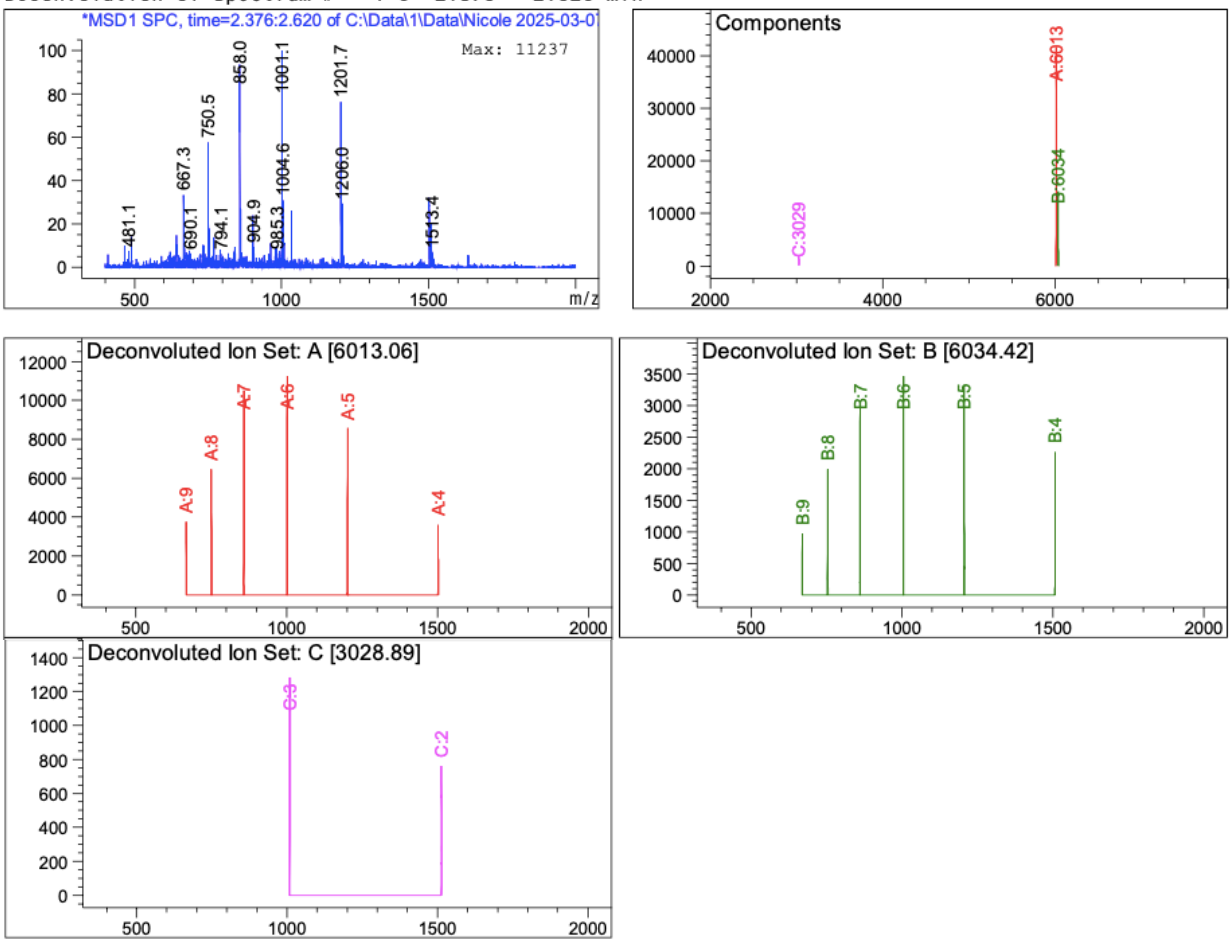

Component	Molecular Weight	Absolute Abundance	Relative Abundance
A	6013.06	41592	100.00
B	6034.42	14243	34.24
C	3028.89	1971	4.74

*** End of Report ***

Supplementary Data 20. Photooxidation of ssDNA-1G-3 by riboflavin with 2 min of exposure to blue light with an intensity of 1.27 mW/cm^2.

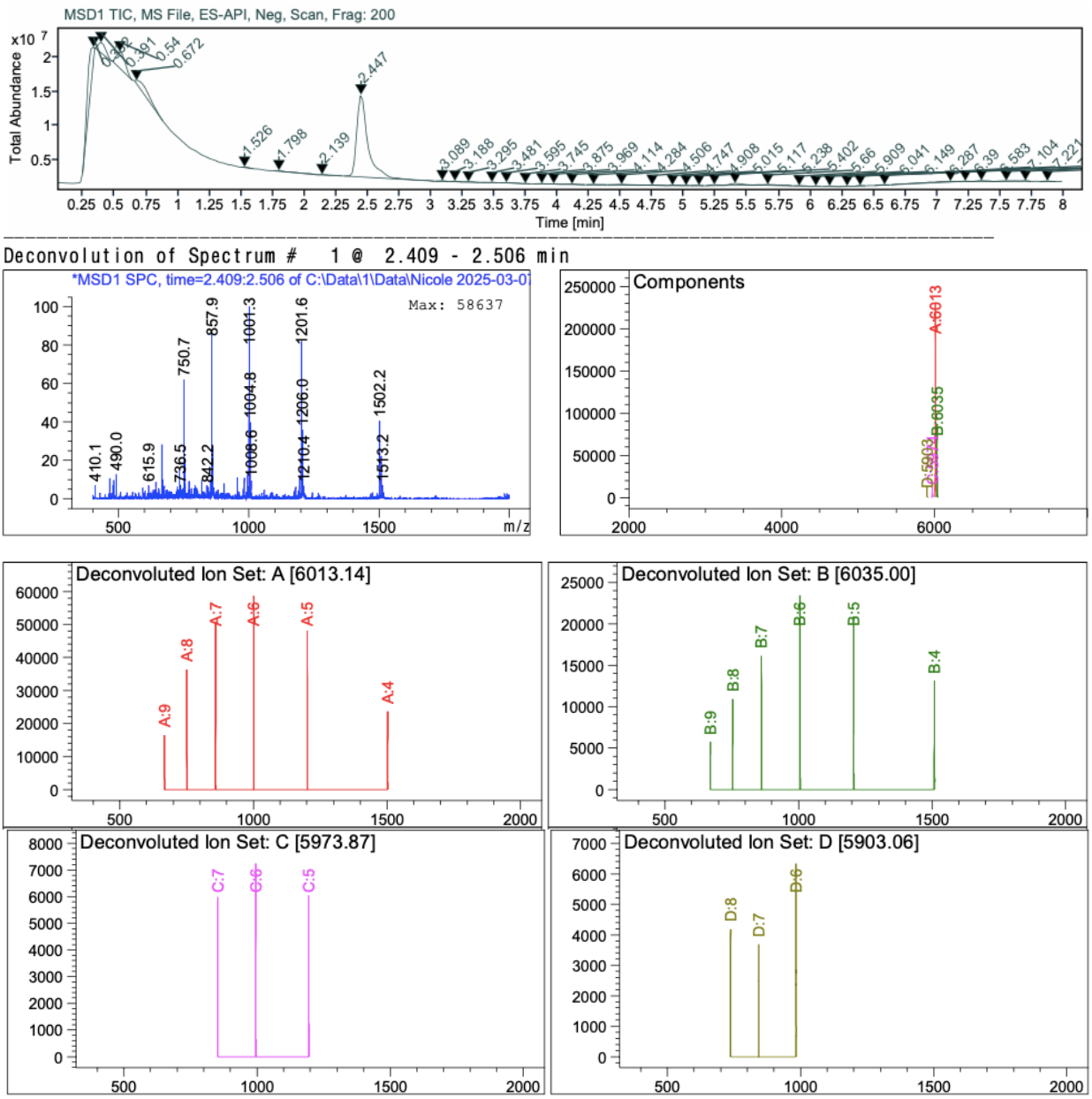

Component	Molecular Weight	Absolute Abundance	Relative Abundance
A	6013.14	229348	100.00
B	6035.00	87303	38.07
C	5973.87	17471	7.62
D	5903.06	13220	5.76

*** End of Report ***

Supplementary Data 21. Photooxidation of ssDNA-1G-3 by riboflavin with 5 min of exposure to blue light with an intensity of 1.27 mW/cm^2.

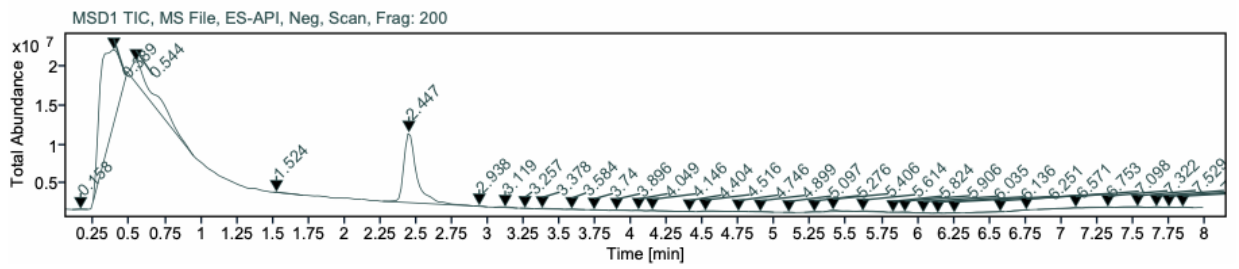

Deconvolution of Spectrum # 1 @ 2.392 - 2.555 min

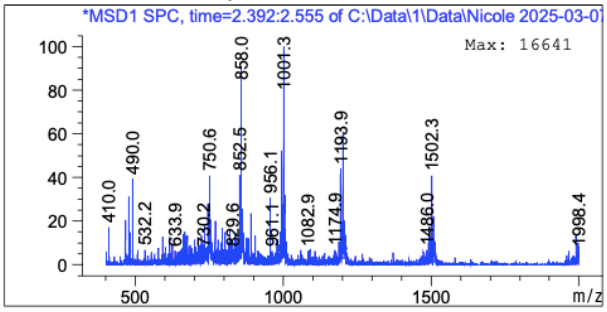

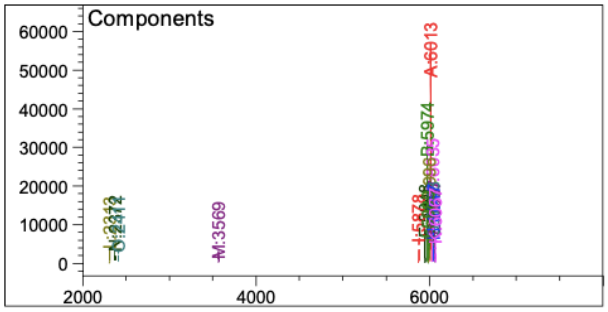

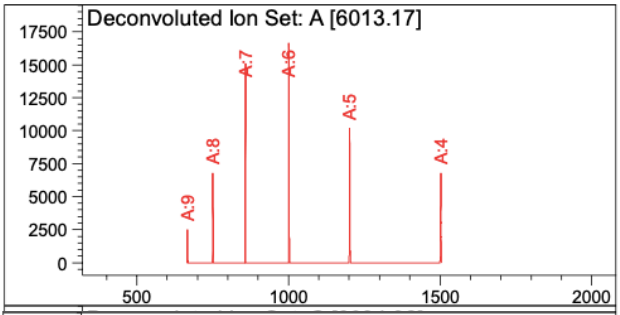

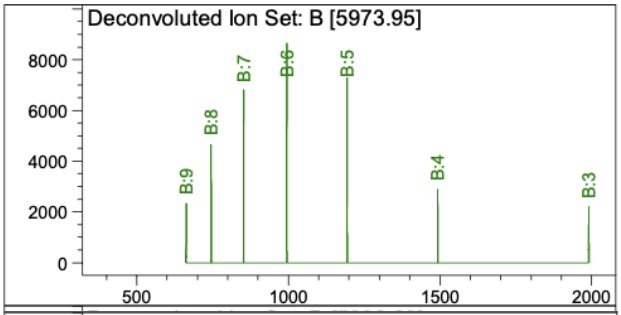

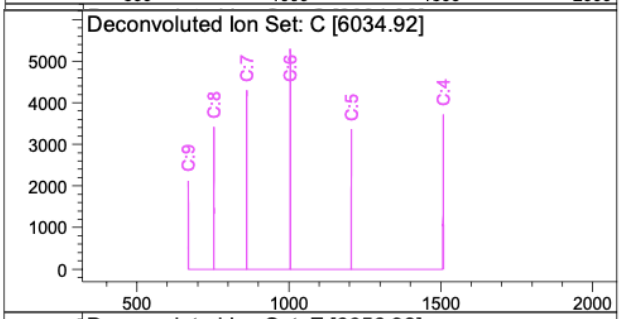

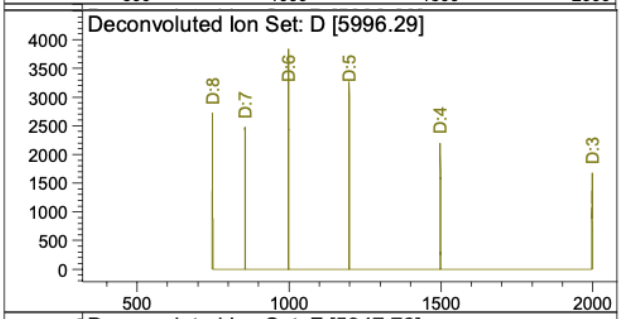

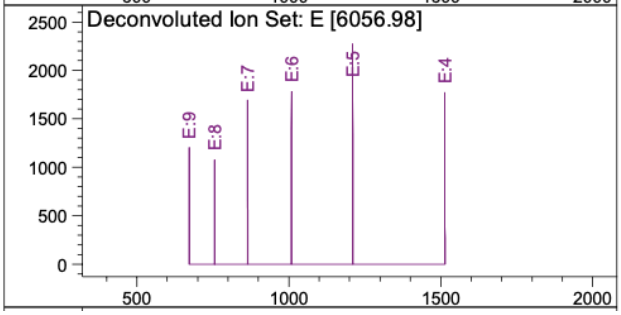

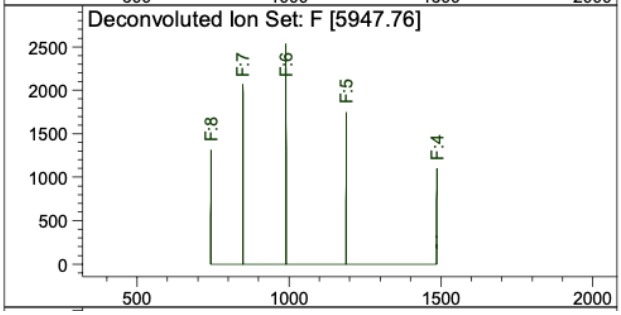

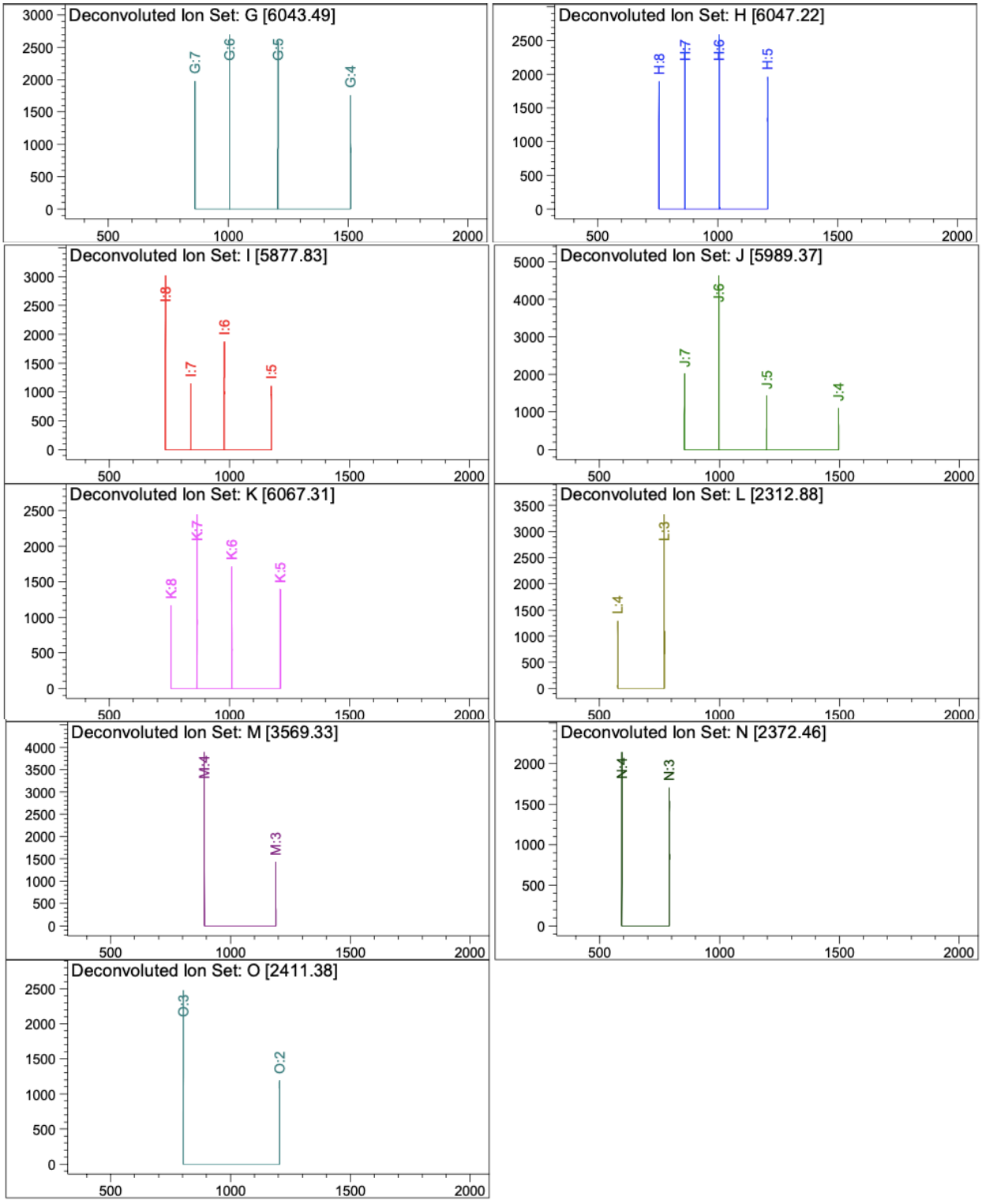
Deconvoluted Ion Set: G [6043.49]
G:7
G:6
G:5
G:4
Deconvoluted Ion Set: H [6047.22]
H:8
H:7
H:6
H:5
Deconvoluted Ion Set: I [5877.83]
I:8
I:7
I:6
I:5
Deconvoluted Ion Set: J [5989.37]
J:7
J:6
J:5
J:4
Deconvoluted Ion Set: K [6067.31]
K:8
K:7
K:6
K:5
Deconvoluted Ion Set: L [2312.88]
L:4
L:3
Deconvoluted Ion Set: M [3569.33]
M:4
M:3
Deconvoluted Ion Set: N [2372.46]
N:4
N:3
Deconvoluted Ion Set: O [2411.38]
O:3
O:2

Component	Molecular Weight	Absolute Abundance	Relative Abundance
A	6013.17	56888	100.00
B	5973.95	32616	57.33
C	6034.92	21015	36.94
D	5996.29	15256	26.82
E	6056.98	8852	15.56
F	5947.76	7996	14.06
G	6043.49	7531	13.24
H	6047.22	7222	12.70
I	5877.83	6462	11.36
J	5989.37	6325	11.12
K	6067.31	6206	10.91
L	2312.88	4384	7.71
M	3569.33	3890	6.84
N	2372.46	3649	6.41
O	2411.38	3387	5.95

*** End of Report ***

Supplementary Data 22. Photooxidation of ssDNA-1G-3 by riboflavin with 15 min of exposure to blue light with an intensity of 1.27 mW/cm^2.

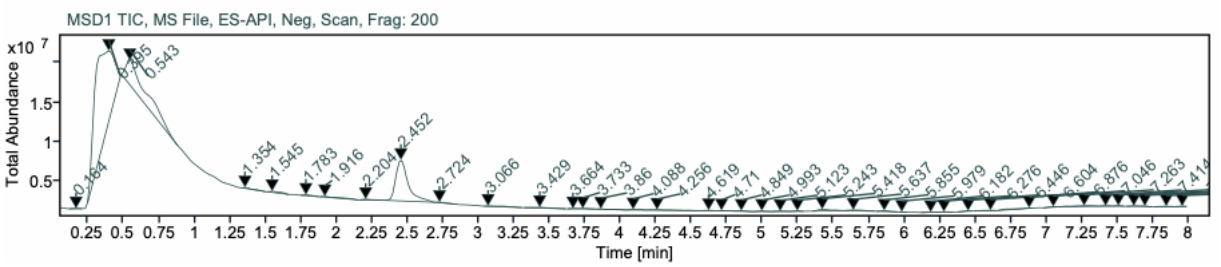

Deconvolution of Spectrum # 1 @ 2.409 - 2.506 min

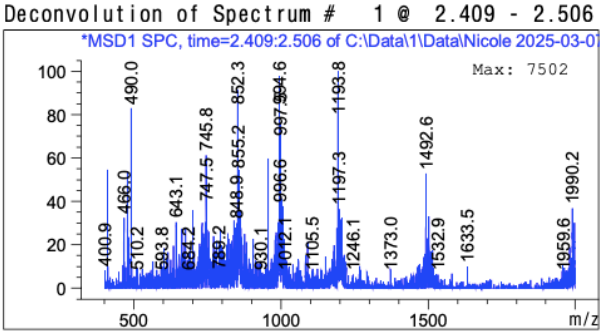

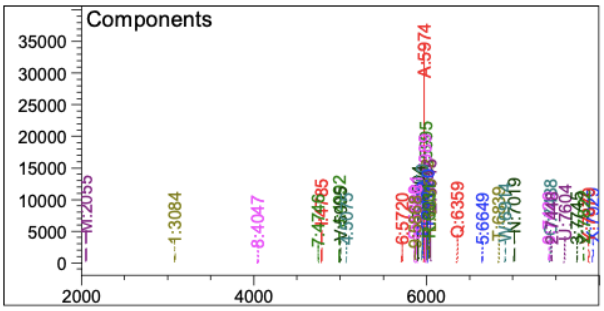

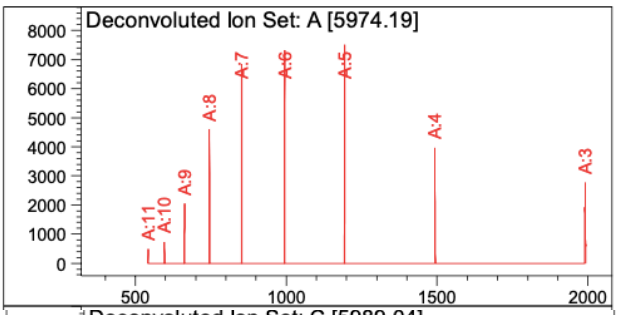

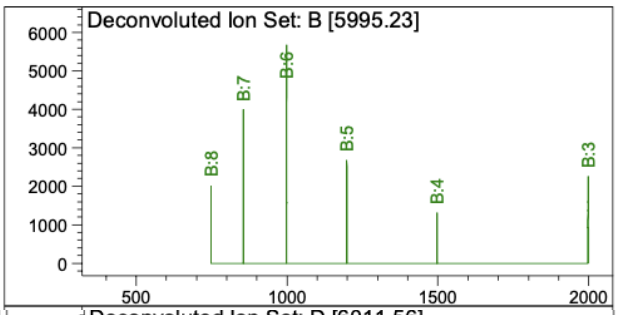

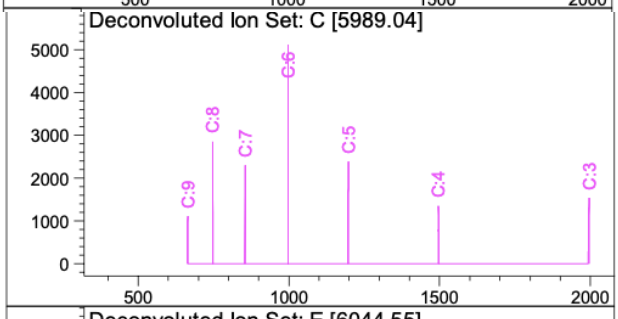

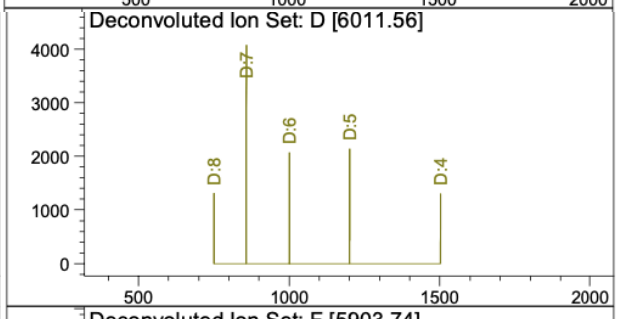

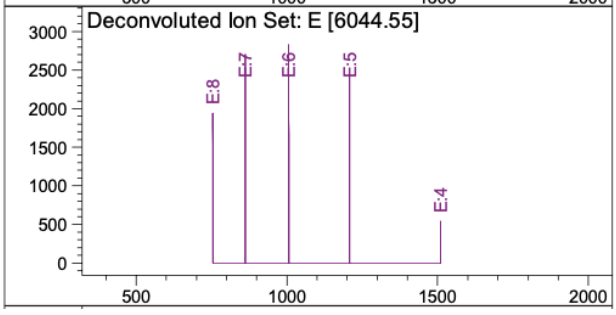

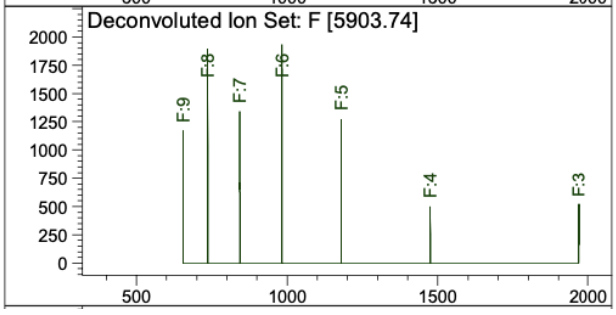

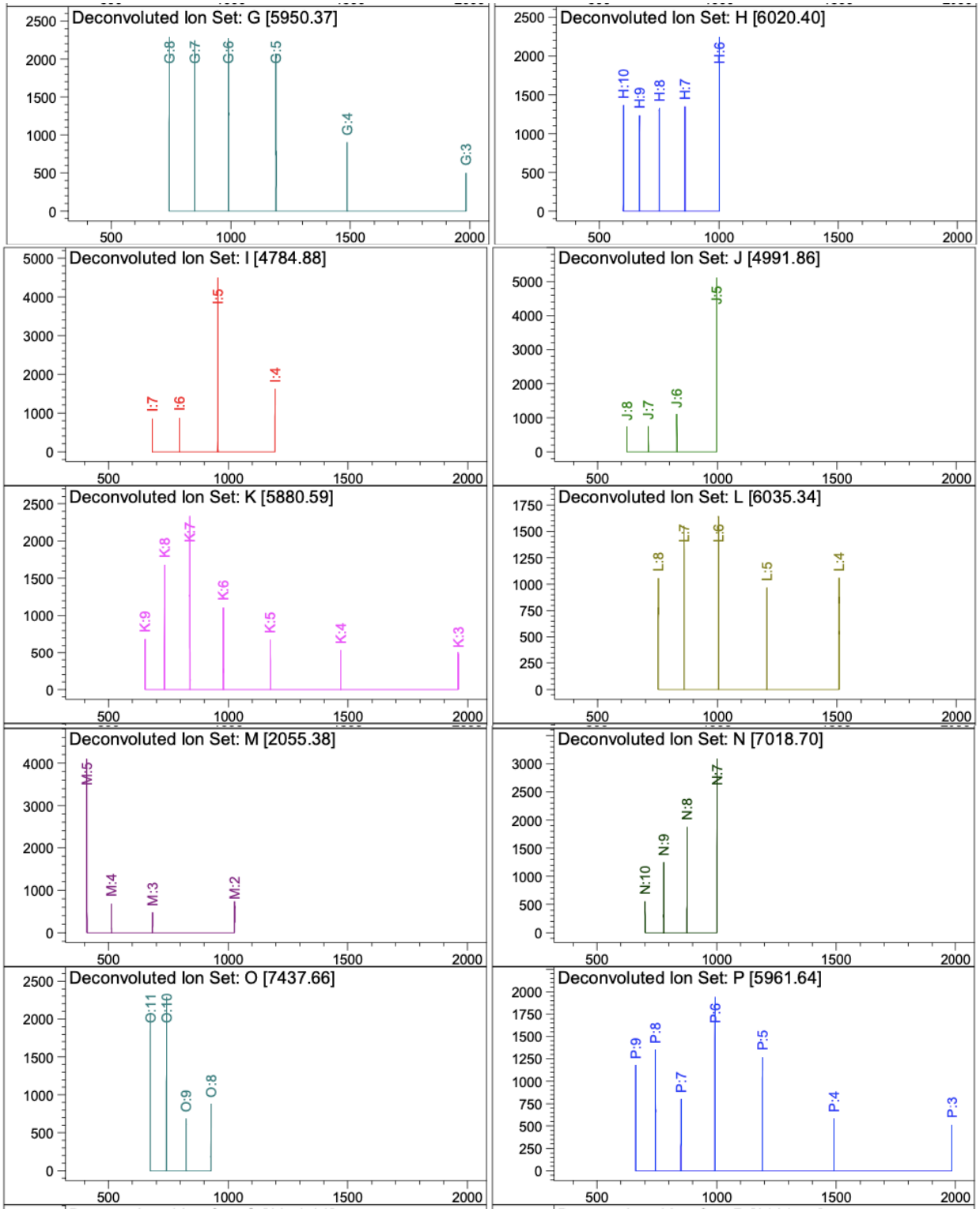
Deconvoluted Ion Set: G [5950.37]
G:8
G:7
G:6
G:5
G:4
G:3
Deconvoluted Ion Set: H [6020.40]
H:10
H:9
H:8
H:7
H:6
Deconvoluted Ion Set: I [4784.88]
I:7
I:6
I:5
I:4
Deconvoluted Ion Set: J [4991.86]
J:8
J:7
J:6
J:5
Deconvoluted Ion Set: K [5880.59]
K:9
K:8
K:7
K:6
K:5
K:4
K:3
Deconvoluted Ion Set: L [6035.34]
L:8
L:7
L:6
L:5
L:4
Deconvoluted Ion Set: M [2055.38]
M:5
M:4
M:3
M:2
Deconvoluted Ion Set: N [7018.70]
N:10
N:9
N:8
N:7
Deconvoluted Ion Set: O [7437.66]
O:11
O:10
O:9
O:8
Deconvoluted Ion Set: P [5961.64]
P:9
P:8
P:7
P:6
P:5
P:4
P:3

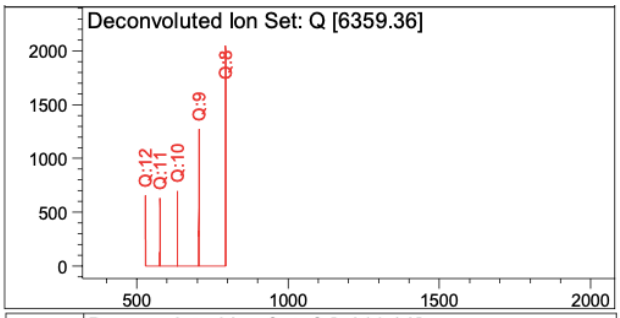
Deconvoluted Ion Set: Q [6359.36]
Q:12
Q:11
Q:10
Q:9
Q:8

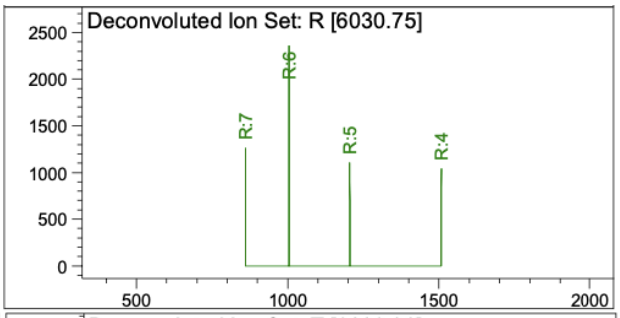
Deconvoluted Ion Set: R [6030.75]
R:7
R:6
R:5
R:4

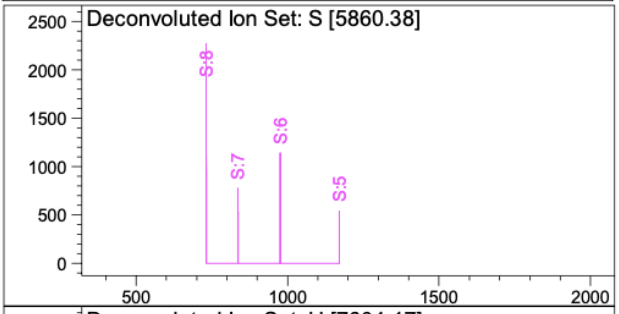
Deconvoluted Ion Set: S [5860.38]
S:8
S:7
S:6
S:5

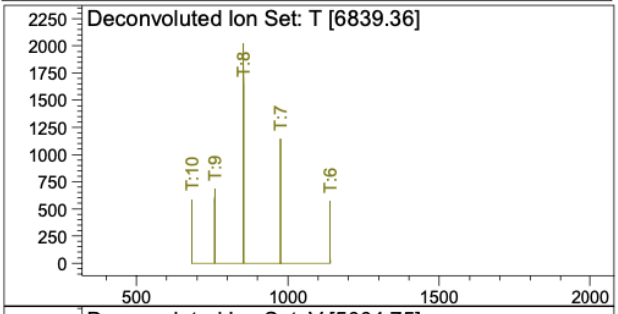
Deconvoluted Ion Set: T [6839.36]
T:10
T:9
T:8
T:7
T:6

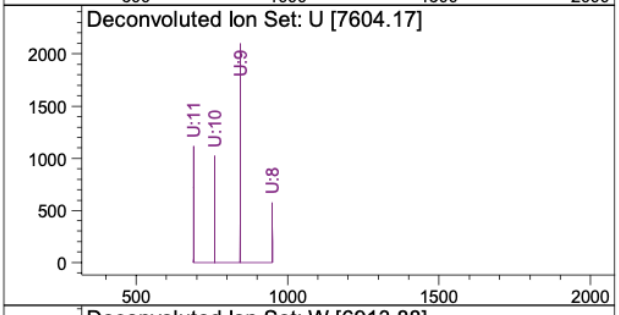
Deconvoluted Ion Set: U [7604.17]
U:11
U:10
U:9
U:8

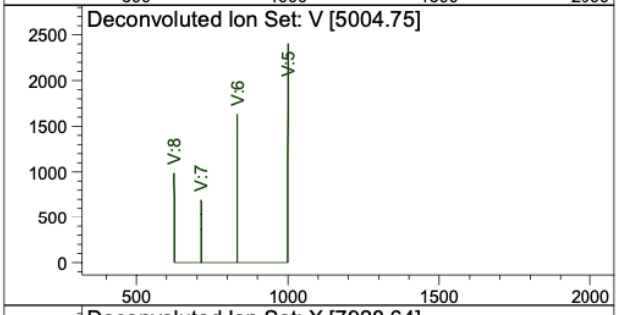
Deconvoluted Ion Set: V [5004.75]
V:8
V:7
V:6
V:5

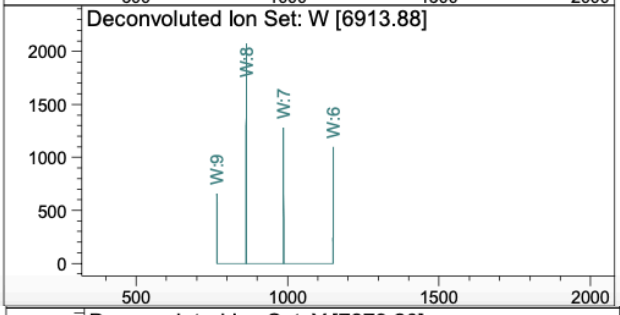
Deconvoluted Ion Set: W [6913.88]
W:9
W:8
W:7
W:6

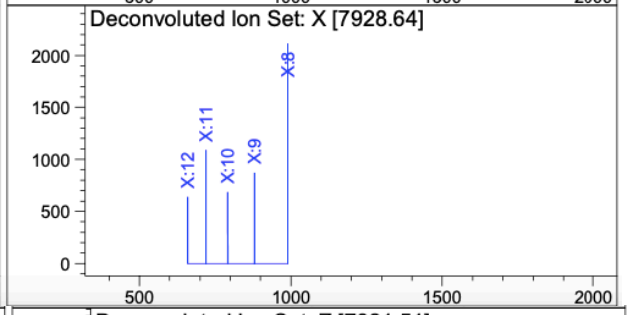
Deconvoluted Ion Set: X [7928.64]
X:12
X:11
X:10
X:9
X:8

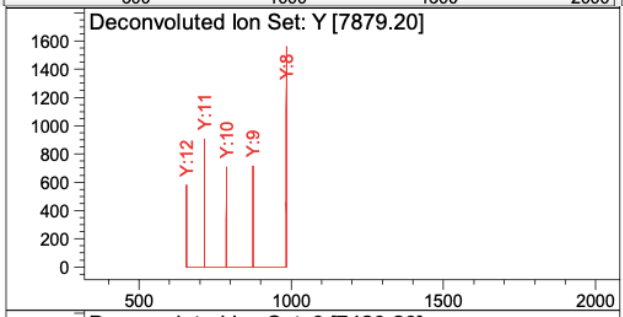
Deconvoluted Ion Set: Y [7879.20]
Y:12
Y:11
Y:10
Y:9
Y:8

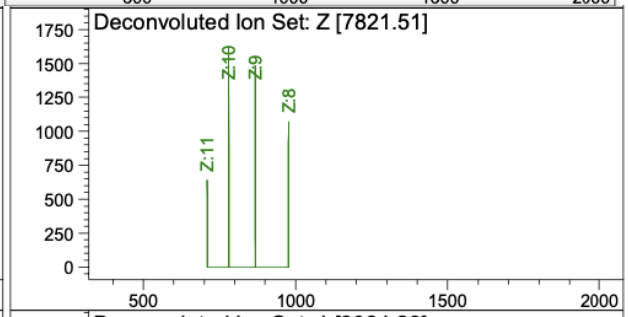
Deconvoluted Ion Set: Z [7821.51]
Z:11
Z:10
Z:9
Z:8

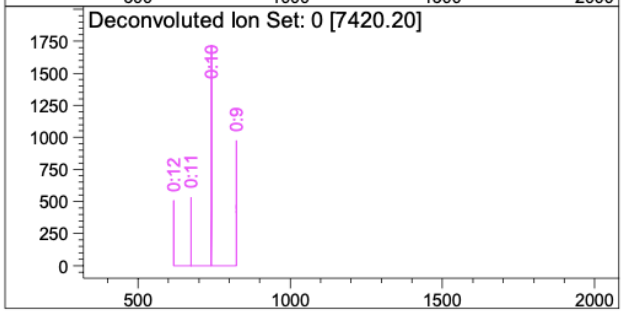
Deconvoluted Ion Set: 0 [7420.20]
0:12
0:11
0:10
0:9

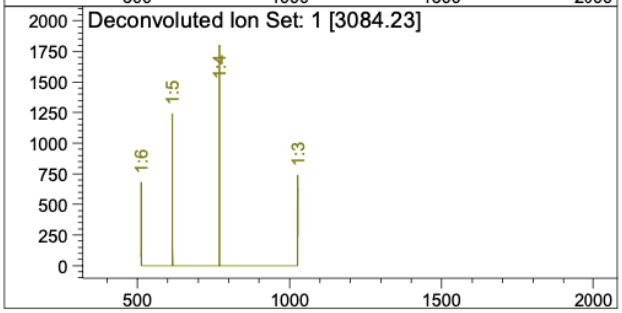
Deconvoluted Ion Set: 1 [3084.23]
1:6
1:5
1:4
1:3

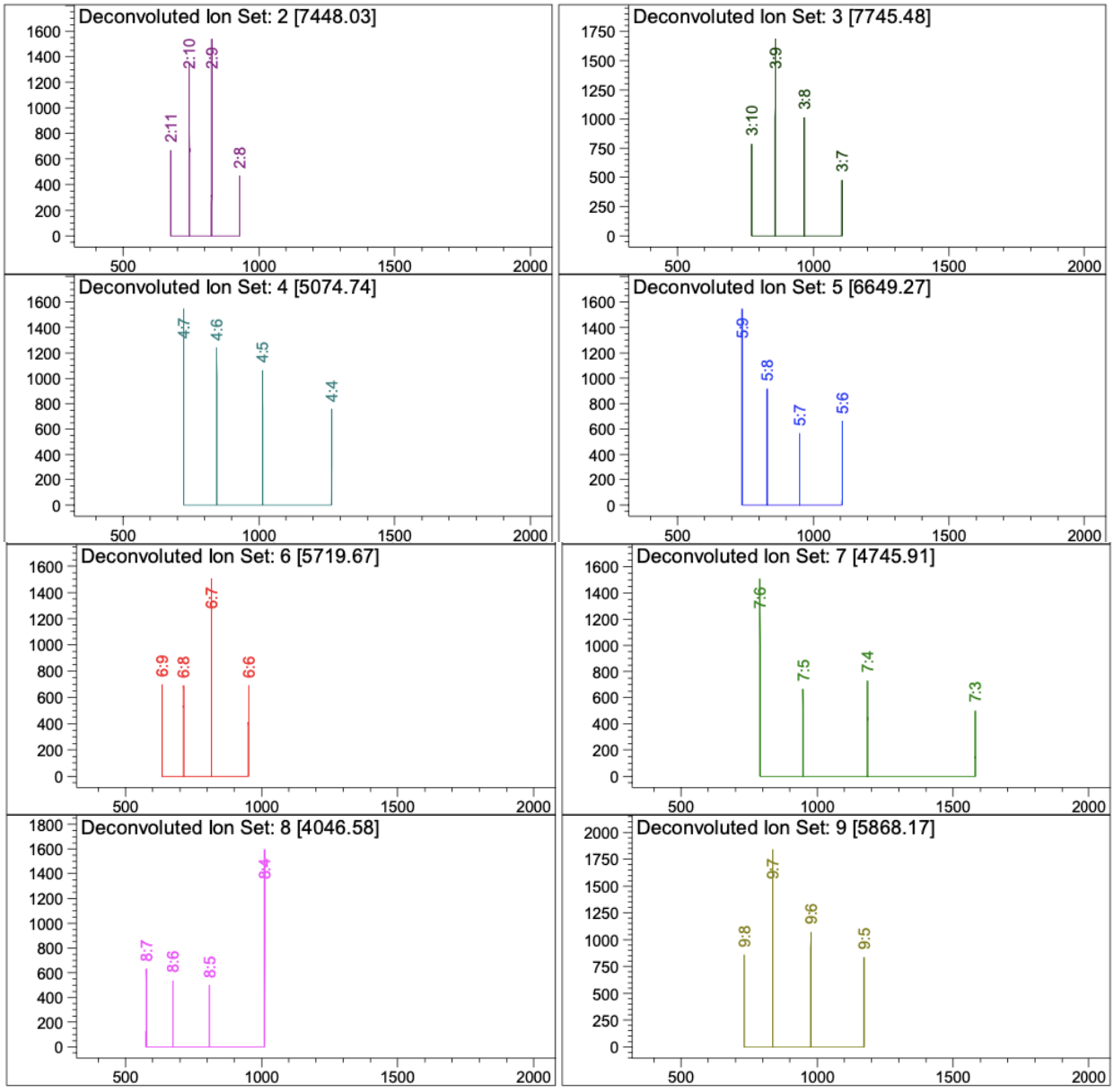
Deconvoluted Ion Set: 2 [7448.03]
2:11
2:10
2:9
2:8
Deconvoluted Ion Set: 3 [7745.48]
3:10
3:9
3:8
3:7
Deconvoluted Ion Set: 4 [5074.74]
4:7
4:6
4:5
4:4
Deconvoluted Ion Set: 5 [6649.27]
5:9
5:8
5:7
5:6
Deconvoluted Ion Set: 6 [5719.67]
6:9
6:8
6:7
6:6
Deconvoluted Ion Set: 7 [4745.91]
7:6
7:5
7:4
7:3
Deconvoluted Ion Set: 8 [4046.58]
8:7
8:6
8:5
8:4
Deconvoluted Ion Set: 9 [5868.17]
9:8
9:7
9:6
9:5

Component	Molecular Weight	Absolute Abundance	Relative Abundance
A	5974.19	34579	100.00
B	5995.23	16242	46.97
C	5989.04	13614	39.37
D	6011.56	9111	26.35
E	6044.55	9083	26.27
F	5903.74	8196	23.70
G	5950.37	7811	22.59
H	6020.40	7068	20.44
I	4784.88	6790	19.64
J	4991.86	6630	19.17
K	5880.59	6242	18.05
L	6035.34	5794	16.76
M	2055.38	5505	15.92
N	7018.70	5504	15.92
O	7437.66	5131	14.84
P	5961.64	5125	14.82
Q	6359.36	4615	13.35
R	6030.75	4582	13.25
S	5860.38	4375	12.65
T	6839.36	4259	12.32
U	7604.17	4211	12.18
V	5004.75	4013	11.61
W	6913.88	3915	11.32
X	7928.64	3873	11.20
Y	7879.20	3763	10.88
Z	7821.51	3691	10.67
0	7420.20	3578	10.35
1	3084.23	3576	10.34
2	7448.03	3524	10.19
3	7745.48	3426	9.91
4	5074.74	3371	9.75
5	6649.27	3353	9.70
6	5719.67	3339	9.66
7	4745.91	3005	8.69
8	4046.58	2862	8.28
9	5868.17	2711	7.84

*** End of Report ***

Supplementary Data 23. Photooxidation of ssDNA-1G-3 by riboflavin with 30 min of exposure to blue light with an intensity of 1.27 mW/cm^2.

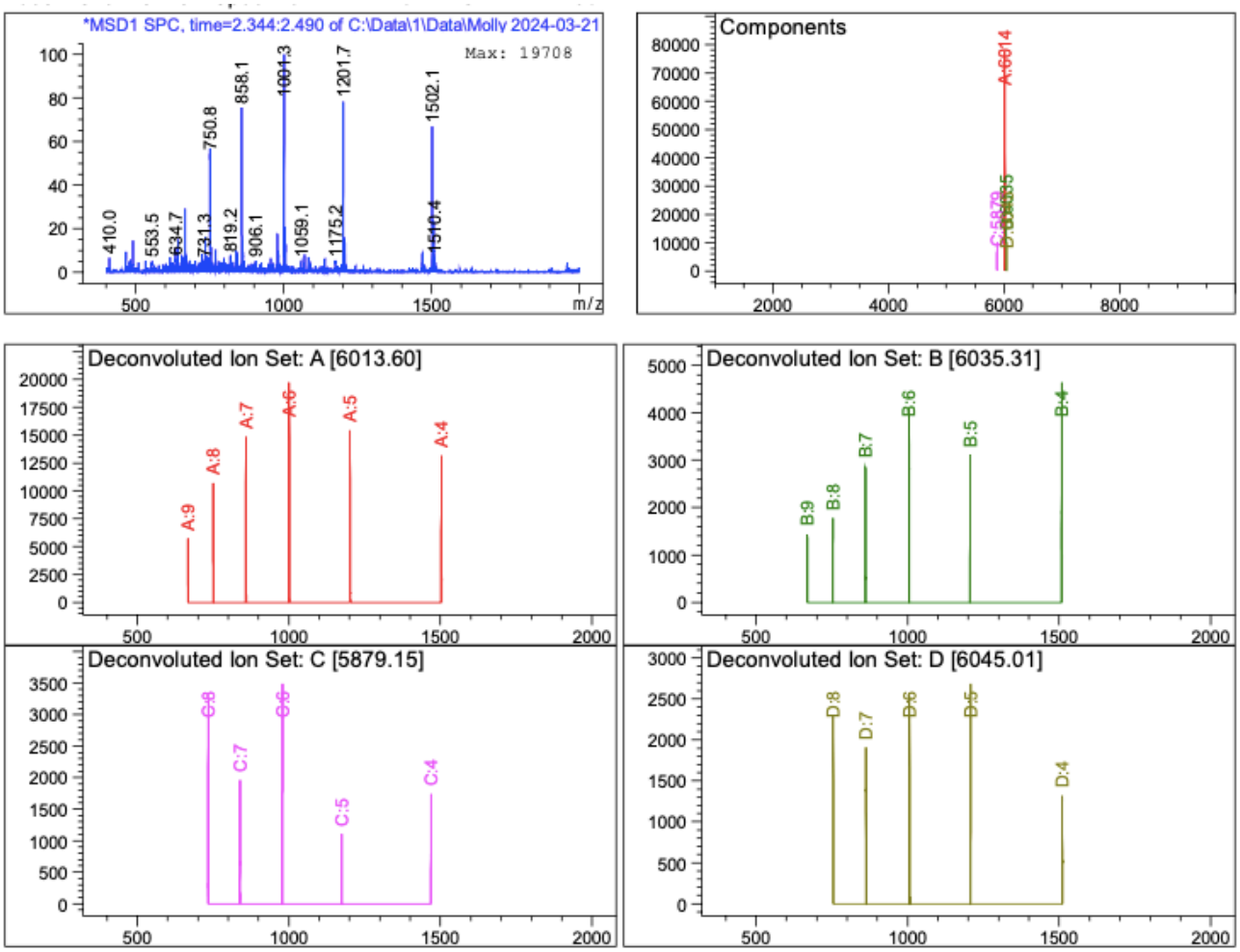

Component	Molecular Weight	Absolute Abundance	Relative Abundance
A	6013.60	77631	100.00
B	6035.31	17146	22.09
C	5879.15	10211	13.15
D	6045.01	9825	12.66

*** End of Report ***

Supplementary Data 24. Photooxidation of ssDNA-1G-2 by RB-heptylCOOH with 15 minutes of exposure to green light with an intensity of 14.3 mW/cm^2.

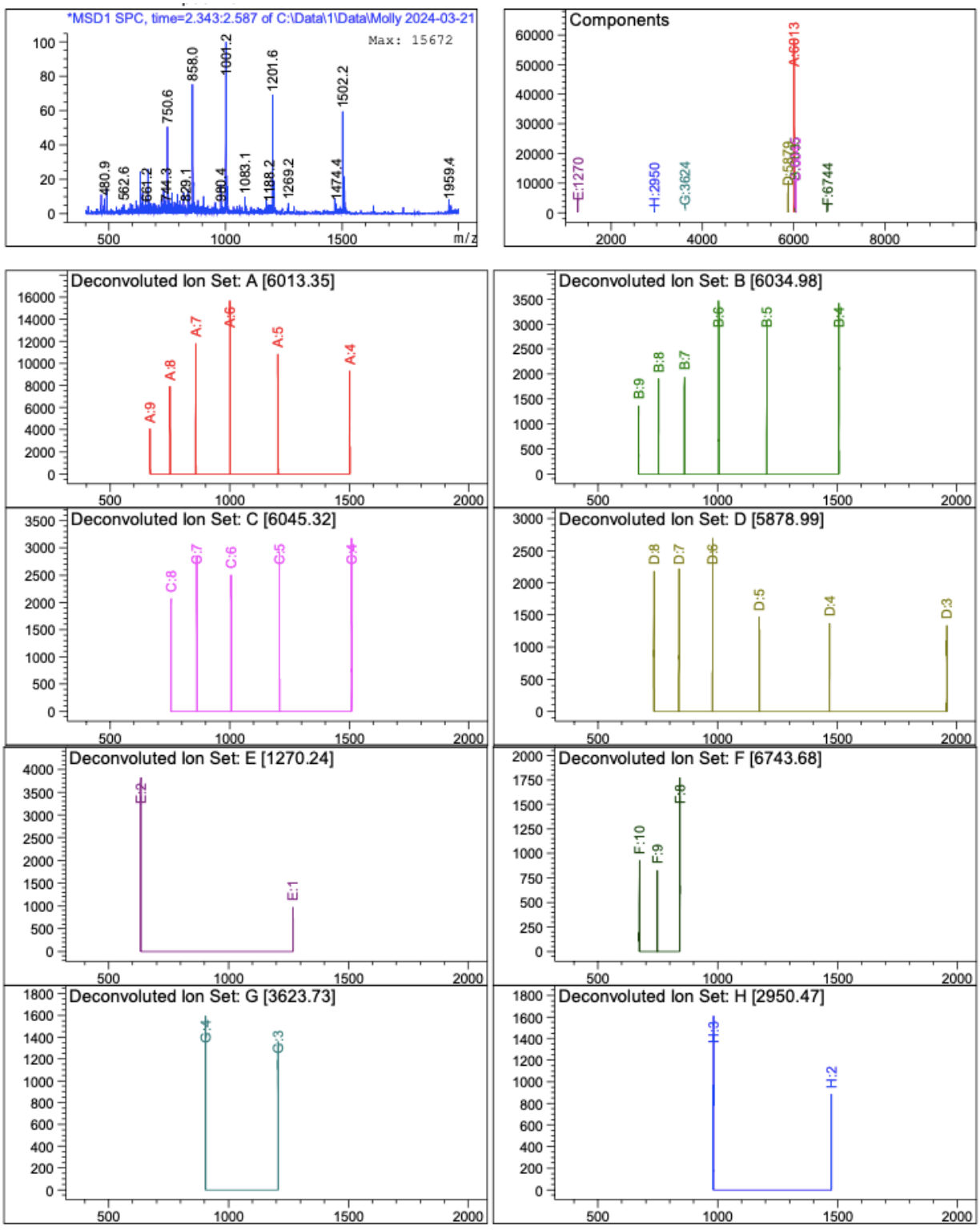
*MSD1 SPC, time=2.343:2.587 of C:\Data\1\Data\Molly 2024-03-21
Max: 15672
480.9
562.6
661.2
744.3
829.1
858.0
980.4
1001.2
1083.1
1188.2
1201.6
1269.2
1474.4
1502.2
1959.4
m/z
Components
E:1270
H:2950
G:3624
A:6013
D:5879
B:6035
F:6744
Deconvoluted Ion Set: A [6013.35]
A:9
A:8
A:7
A:6
A:5
A:4
Deconvoluted Ion Set: B [6034.98]
B:9
B:8
B:7
B:6
B:5
B:4
Deconvoluted Ion Set: C [6045.32]
C:8
C:7
C:6
C:5
C:4
Deconvoluted Ion Set: D [5878.99]
D:8
D:7
D:6
D:5
D:4
D:3
Deconvoluted Ion Set: E [1270.24]
E:2
E:1
Deconvoluted Ion Set: F [6743.68]
F:10
F:9
F:8
Deconvoluted Ion Set: G [3623.73]
G:4
G:3
Deconvoluted Ion Set: H [2950.47]
H:3
H:2

Component	Molecular Weight	Absolute Abundance	Relative Abundance
A	6013.35	58474	100.00
B	6034.98	13140	22.47
C	6045.32	12468	21.32
D	5878.99	10647	18.21
E	1270.24	4793	8.20
F	6743.68	2975	5.09
G	3623.73	2764	4.73
H	2950.47	2409	4.12

*** End of Report ***

Supplementary Data 25. Photooxidation of ssDNA-1G-2 by RB-heptylCOOH with 30 minutes of exposure to green light with an intensity of 14.3 mW/cm^2.

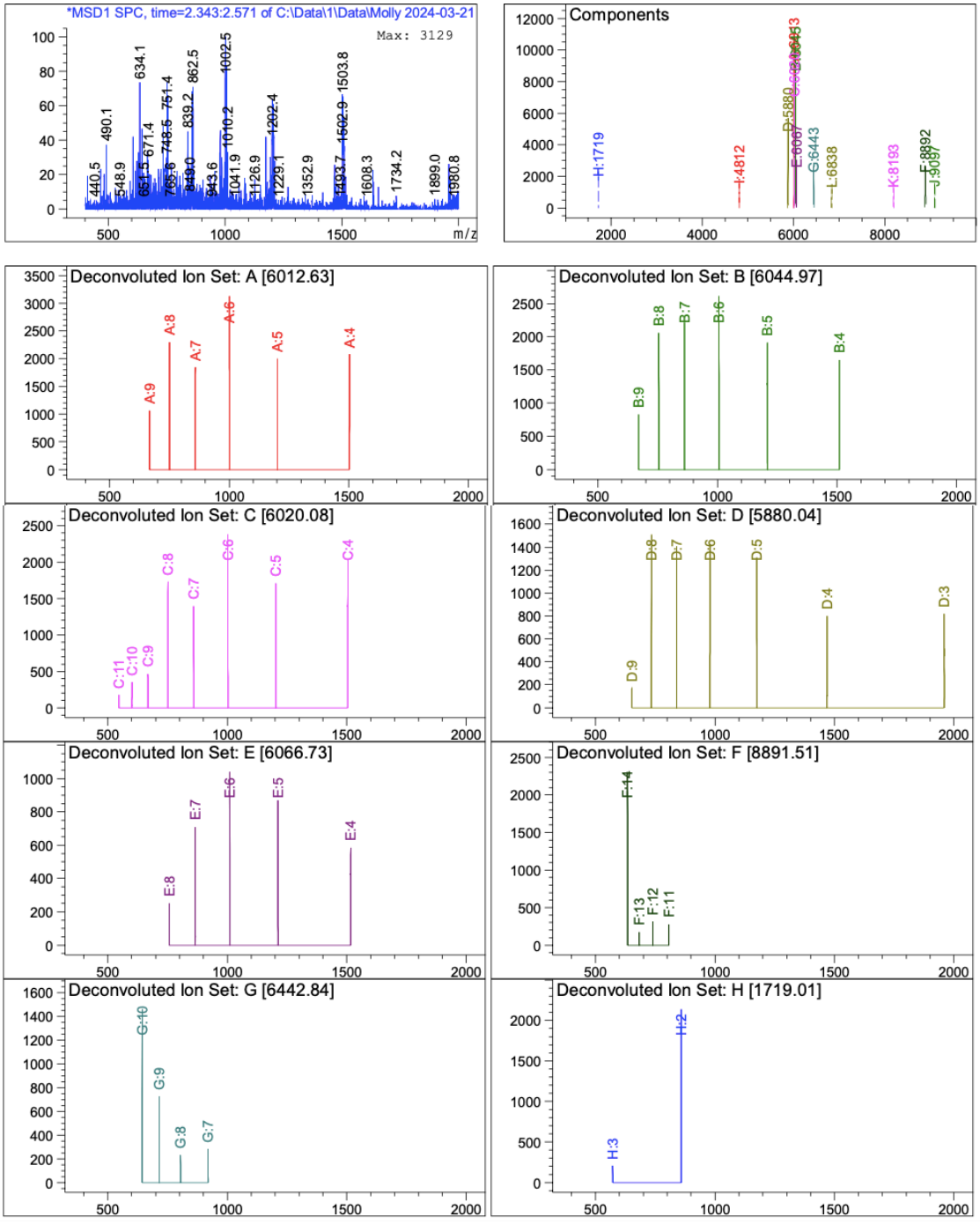
*MSD1 SPC, time=2.343:2.571 of C:\Data\1\Data\Molly 2024-03-21
Max: 3129
m/z
Components
H:1719
I:4812
D:5880
E:6067
G:6443
L:6838
K:8193
F:8892
J:9097
Deconvoluted Ion Set: A [6012.63]
A:9
A:8
A:7
A:6
A:5
A:4
Deconvoluted Ion Set: B [6044.97]
B:9
B:8
B:7
B:6
B:5
B:4
Deconvoluted Ion Set: C [6020.08]
C:11
C:10
C:9
C:8
C:7
C:6
C:5
C:4
Deconvoluted Ion Set: D [5880.04]
D:9
D:8
D:7
D:6
D:5
D:4
D:3
Deconvoluted Ion Set: E [6066.73]
E:8
E:7
E:6
E:5
E:4
Deconvoluted Ion Set: F [8891.51]
F:14
F:13
F:12
F:11
Deconvoluted Ion Set: G [6442.84]
G:10
G:9
G:8
G:7
Deconvoluted Ion Set: H [1719.01]
H:2
H:3

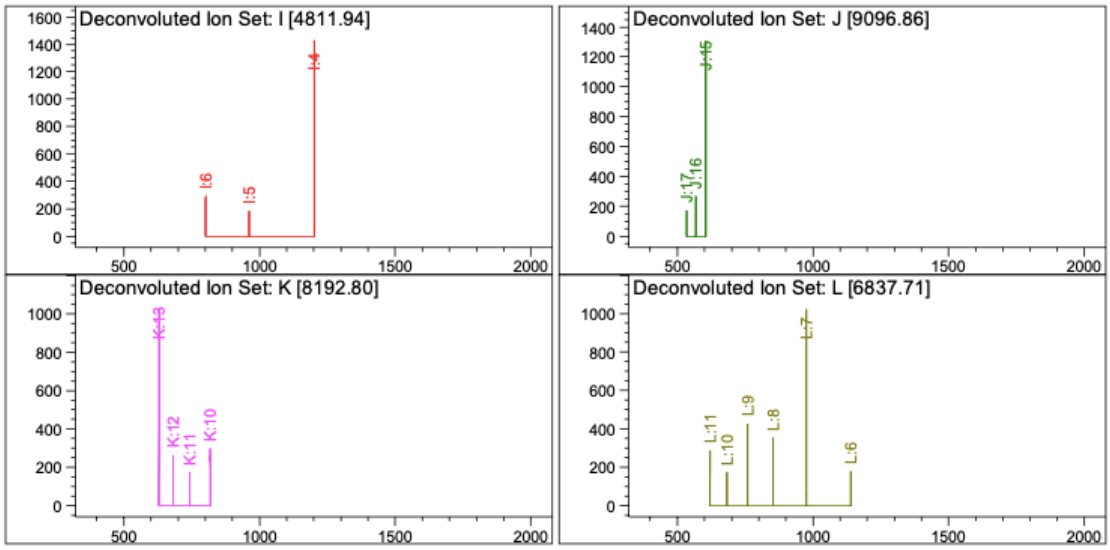

Component	Molecular Weight	Absolute Abundance	Relative Abundance
A	6012.63	10988	100.00
B	6044.97	10234	93.14
C	6020.08	8287	75.42
D	5880.04	5694	51.82
E	6066.73	3017	27.46
F	8891.51	2664	24.24
G	6442.84	2628	23.92
H	1719.01	2316	21.08
I	4811.94	1859	16.92
J	9096.86	1632	14.85
K	8192.80	1545	14.06
L	6837.71	1506	13.71

*** End of Report ***

Supplementary Data 26. Photooxidation of ssDNA-1G-2 by RB-heptylCOOH with 60 minutes of exposure to green light with an intensity of 14.3 mW/cm^2.

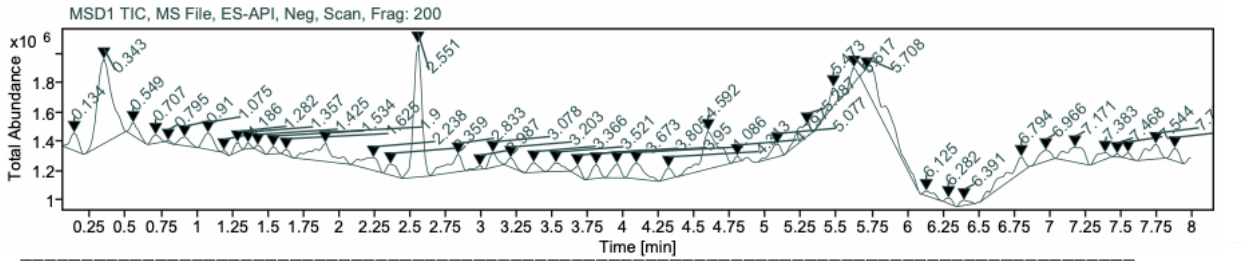

Deconvolution of Spectrum # 1 @ 2.523 - 2.588 min

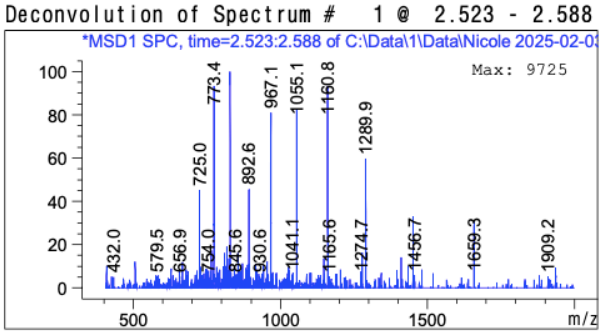

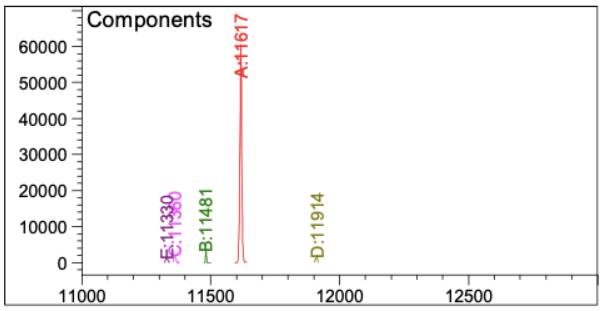

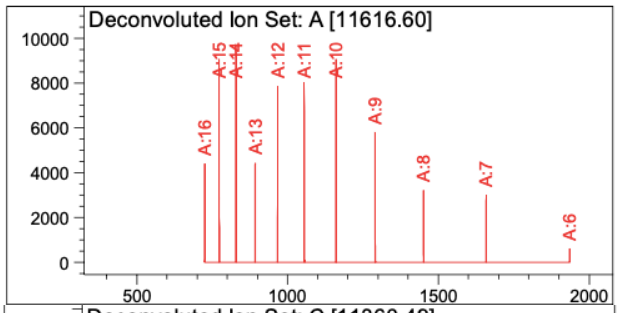

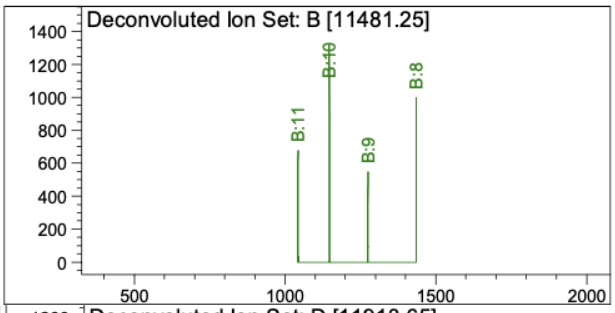

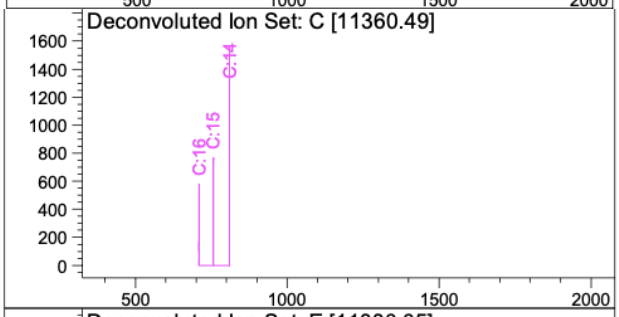

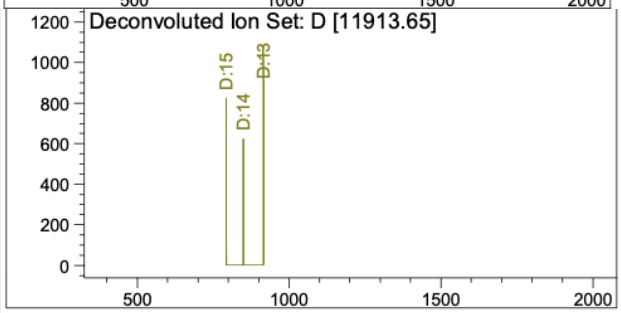

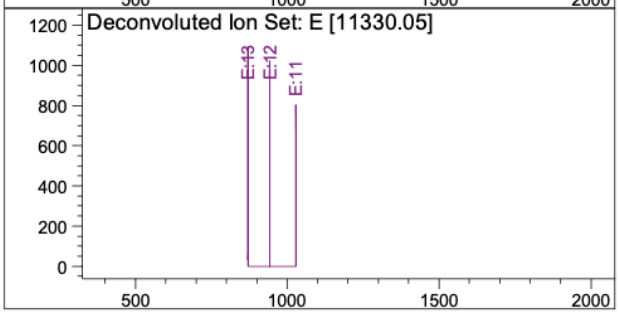

Component	Molecular Weight	Absolute Abundance	Relative Abundance
A	11616.60	60550	100.00
B	11481.25	3353	5.54
C	11360.49	2010	3.32
D	11913.65	1921	3.17
E	11330.05	1179	1.95

*** End of Report ***

Supplementary Data 27. Mass analysis of Bibb Lettuce DNA with no treatment.

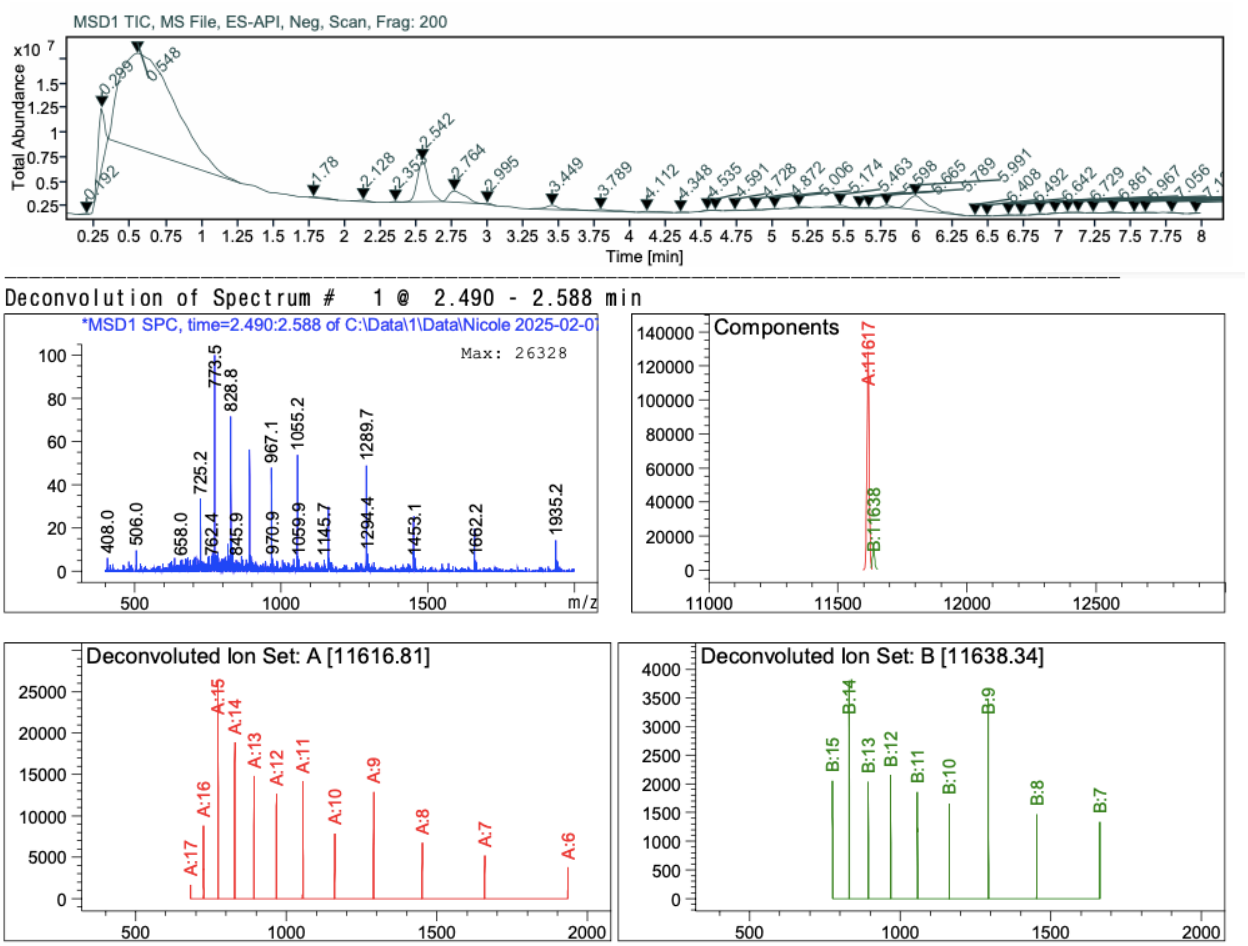

Component	Molecular Weight	Absolute Abundance	Relative Abundance
A	11616.81	128123	100.00
B	11638.34	12507	9.76

*** End of Report ***

Supplementary Data 28. Starting material from the RB-DFHBI-catalyzed photooxidation of Lettuce DNA with 1 h of white light.

Deconvolution of Spectrum # 1 @ 2.718 - 2.848 min

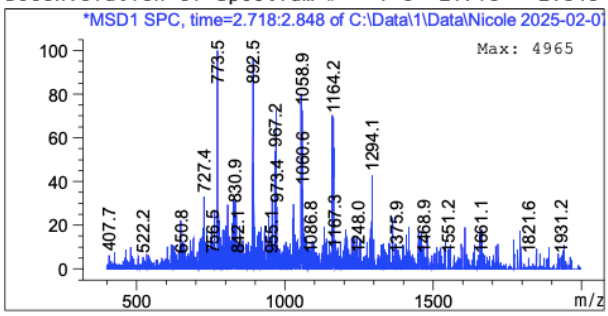

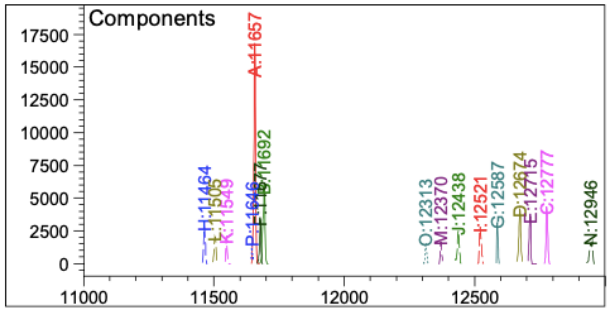

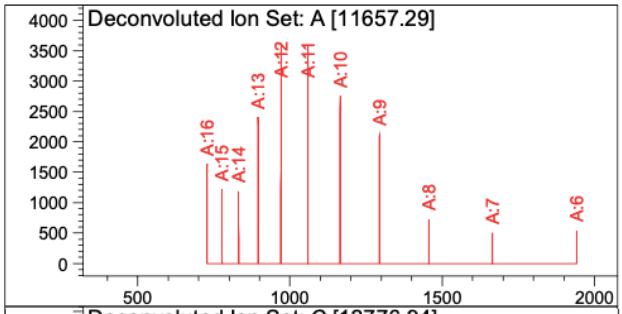

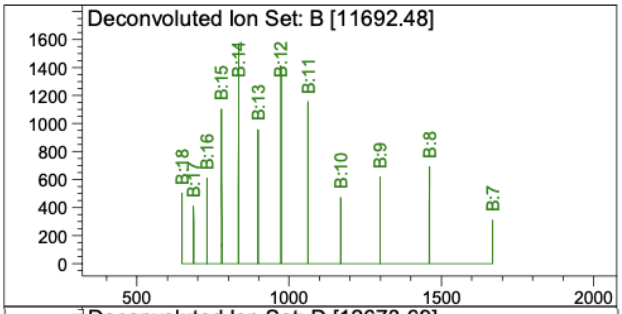

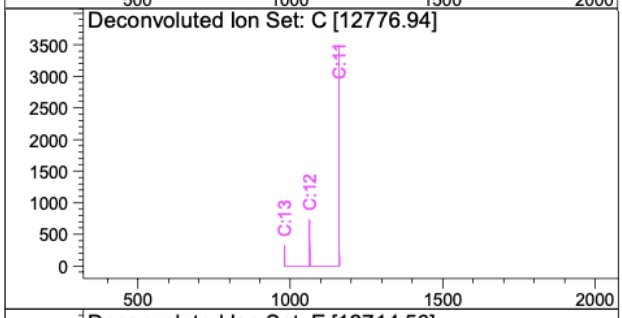

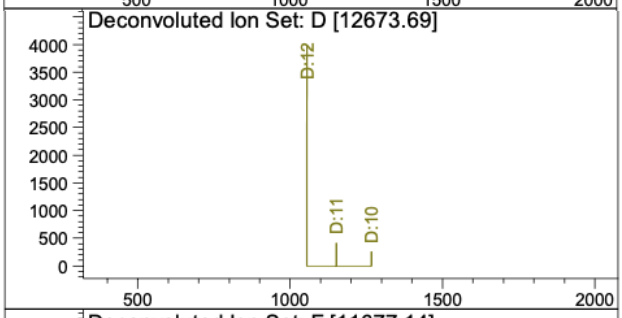

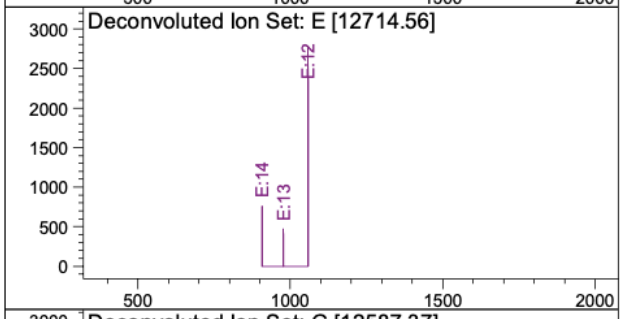

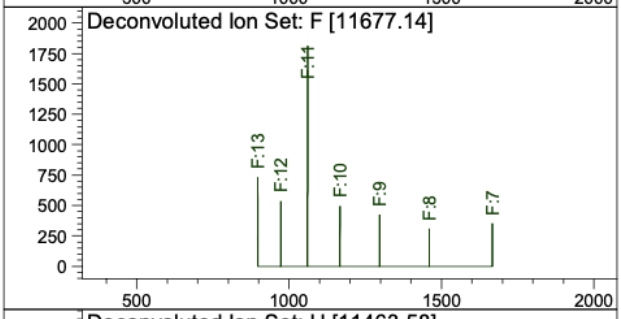

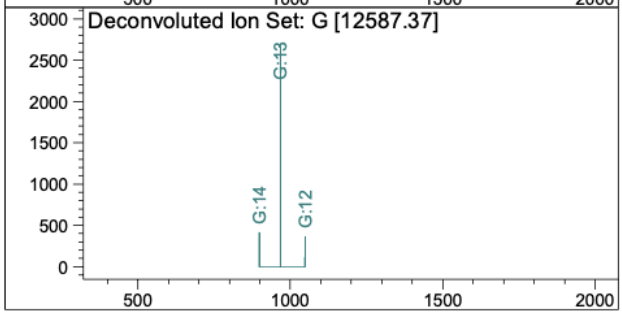

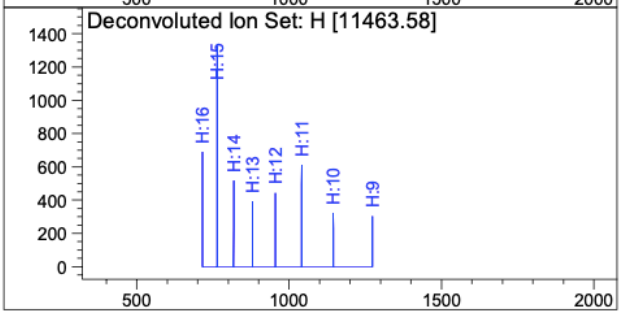

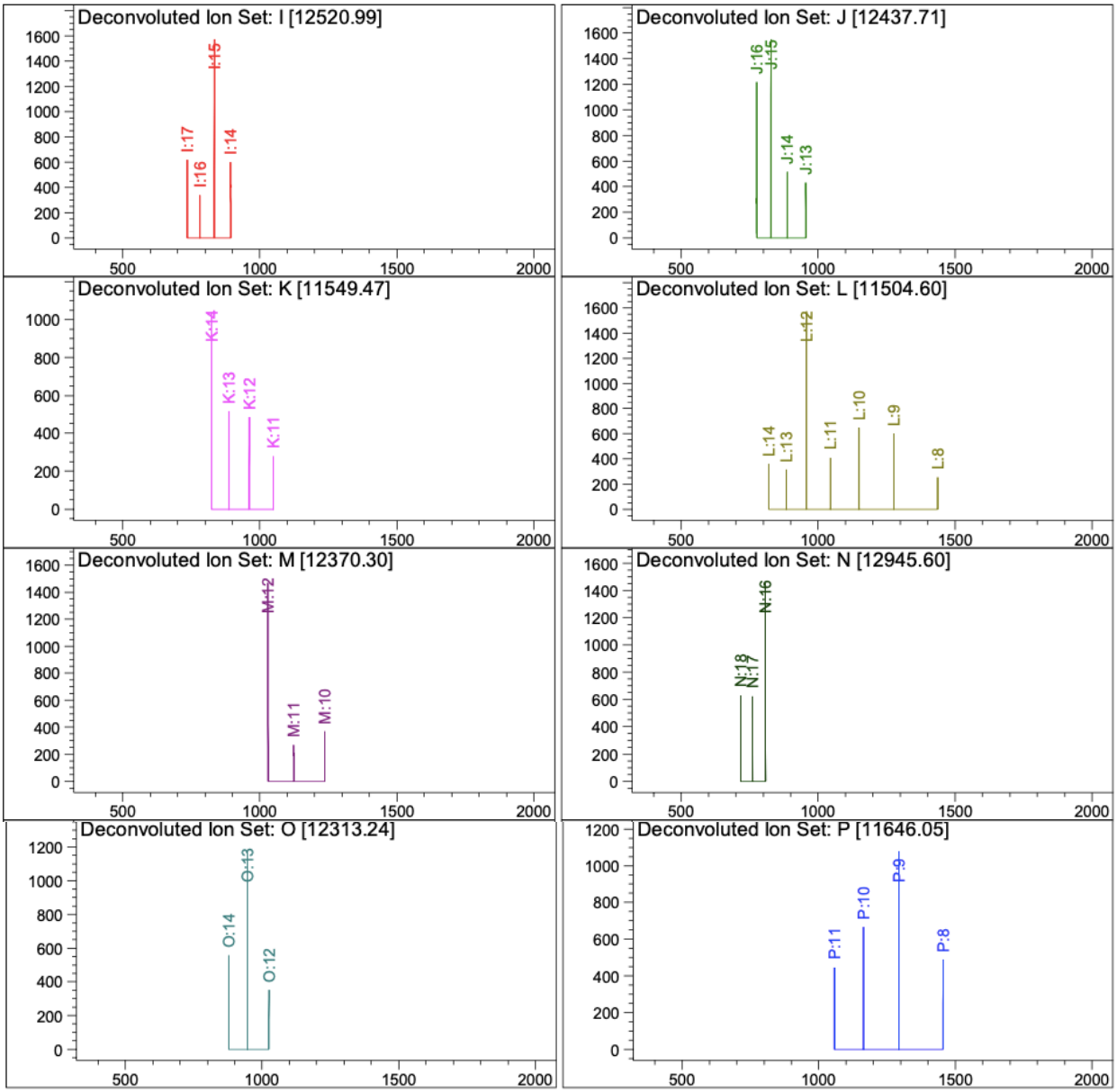

Component	Molecular Weight	Absolute Abundance	Relative Abundance
A	11657.29	16818	100.00
B	11692.48	6208	36.91
C	12776.94	4359	25.92
D	12673.69	4136	24.59
E	12714.56	3610	21.47
F	11677.14	3359	19.97
G	12587.37	3170	18.85
H	11463.58	2903	17.26
I	12520.99	2785	16.56
J	12437.71	2543	15.12
K	11549.47	2126	12.64
L	11504.60	2032	12.08
M	12370.30	1669	9.92

N	12945.60	1622	9.64
O	12313.24	1583	9.41
P	11646.05	1581	9.40

*** End of Report ***

Supplementary Data 29. Product analysis from the RB-DFHBI-catalyzed photooxidation of Lettuce DNA with 1 h of white light.

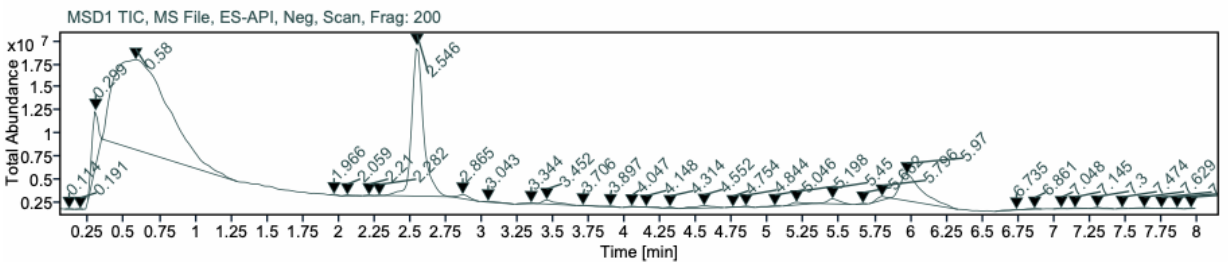

Deconvolution of Spectrum # 1 @ 2.490 - 2.604 min

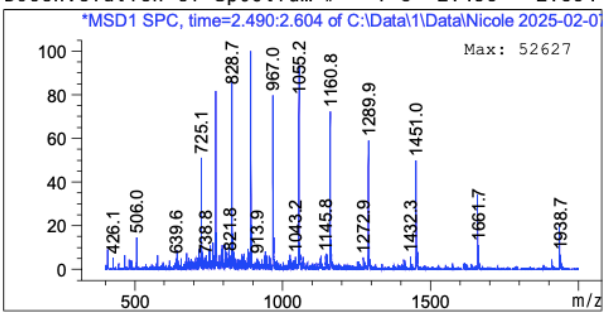

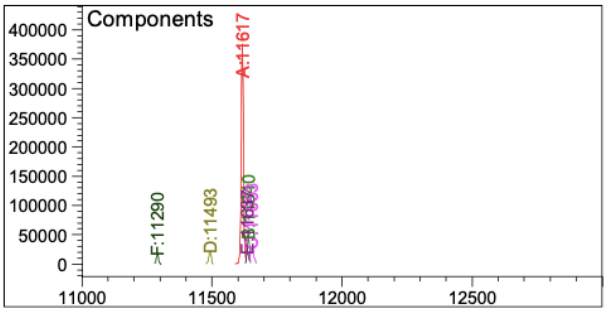

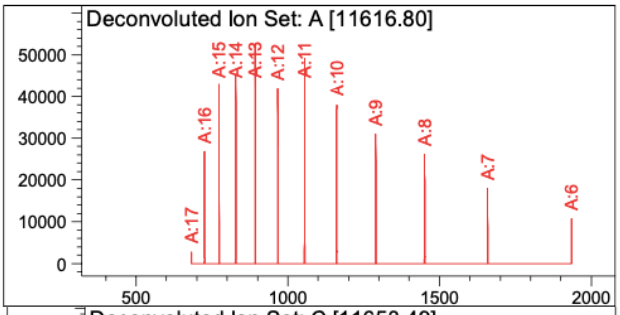

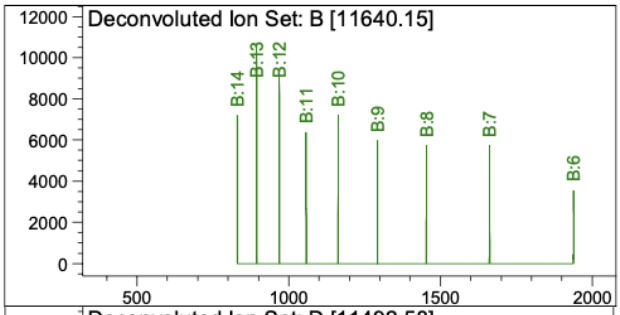

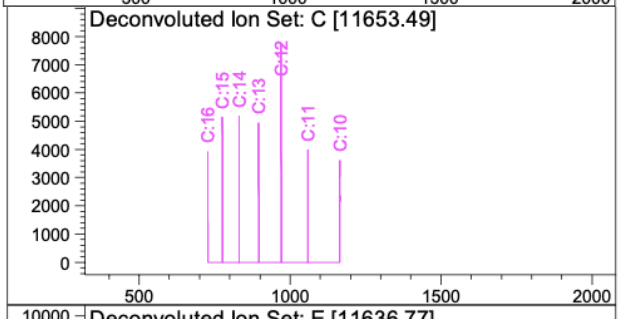

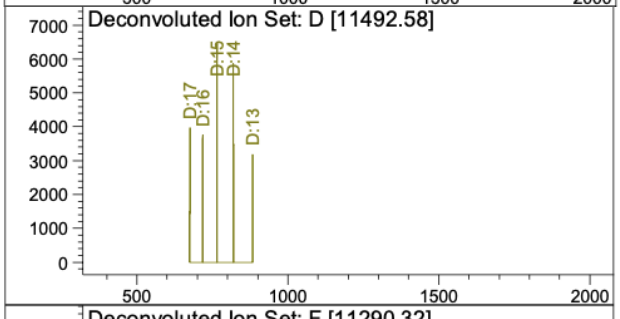

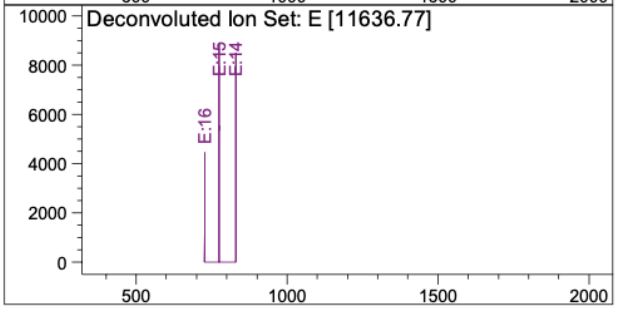

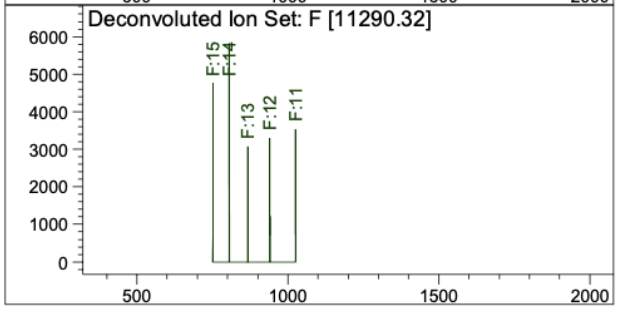

Component	Molecular Weight	Absolute Abundance	Relative Abundance
A	11616.80	375721	100.00
B	11640.15	49334	13.13
C	11653.49	30976	8.24
D	11492.58	21389	5.69
E	11636.77	19832	5.28
F	11290.32	16989	4.52

*** End of Report ***

Supplementary Data 30. Starting material and minor adducts from RB-DFHBI-catalyzed photooxidation of scrambled Lettuce DNA with 1 h of white light.

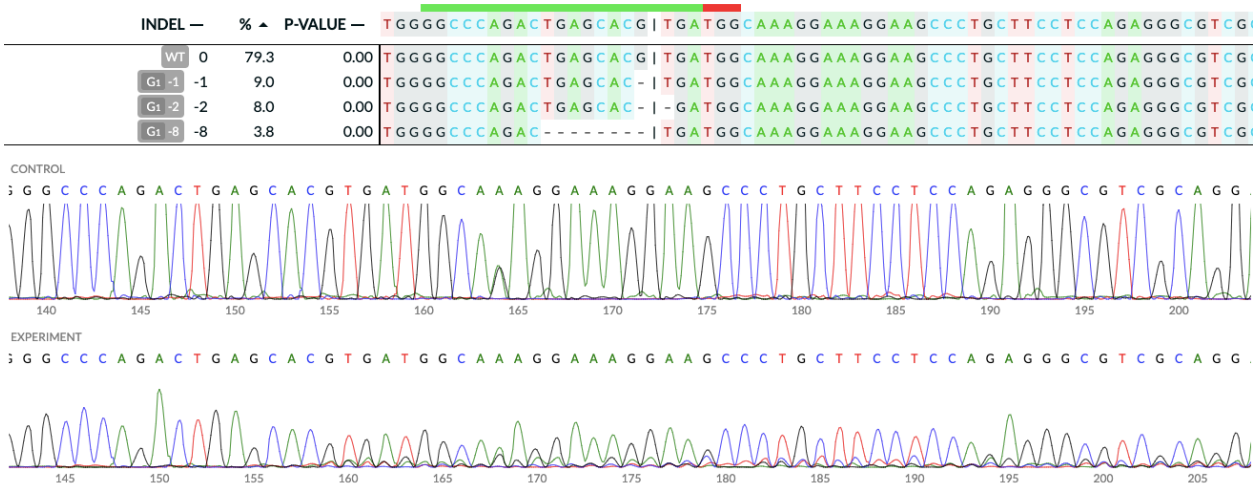

Supplementary Data 31. Cas9-induced indel formation for HEK3 control sgRNA.

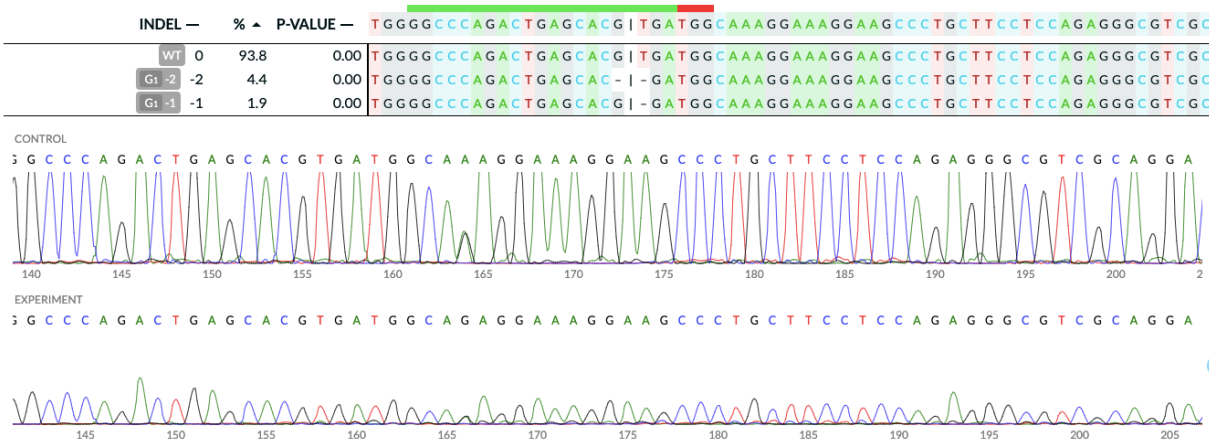

Supplementary Data 32. Cas9-induced indel formation against HEK3 with 5' X2B2-sgRNA.

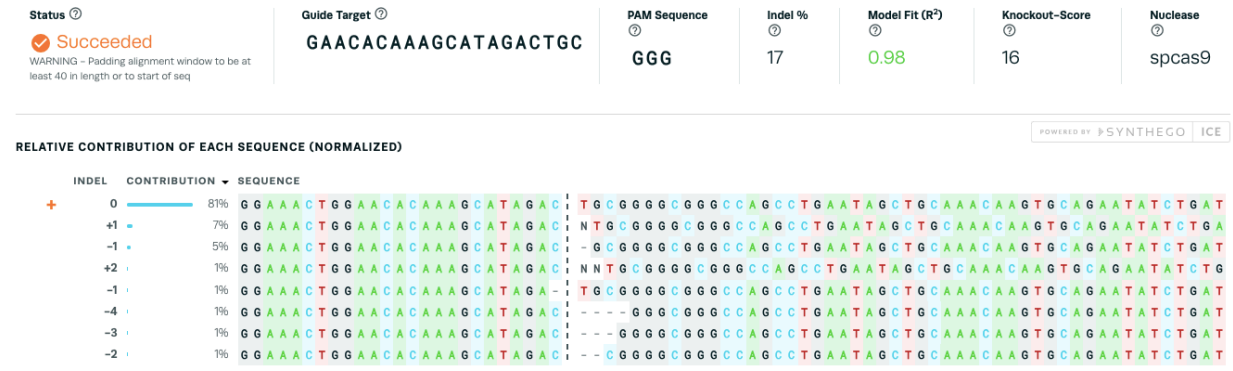

Supplementary Data 33. Cas9-induced indel formation for HEK2 control sgRNA.

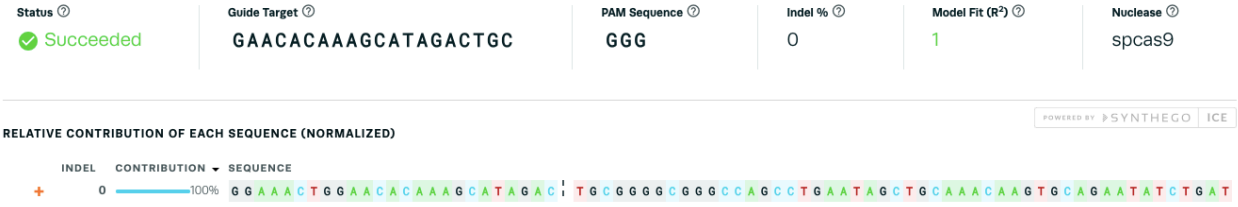

Supplementary Data 34. Cas9-induced indel formation against HEK2 with 5' X2B2 sgRNA.

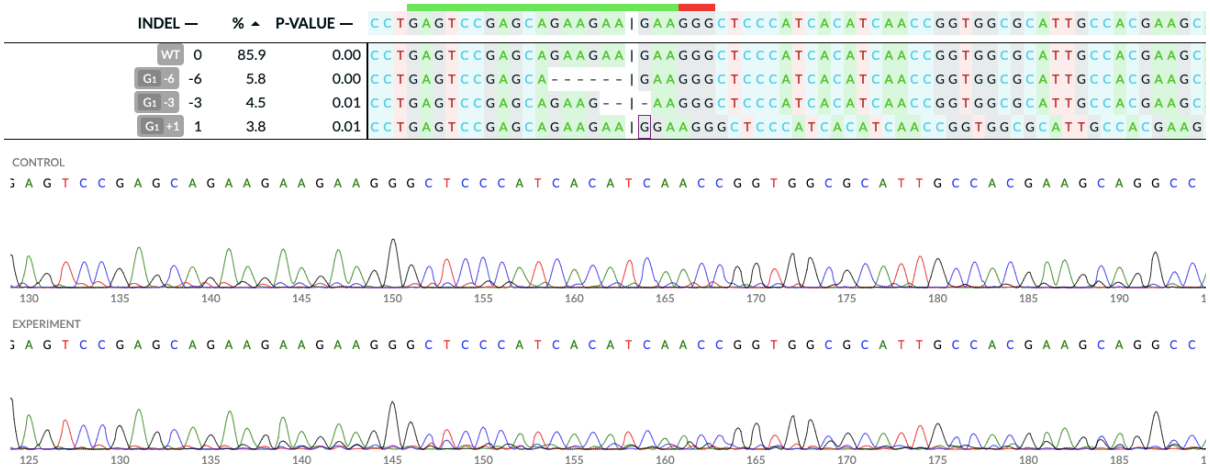

Supplementary Data 35. Cas9-induced indel formation for EMX1 control sgRNA.

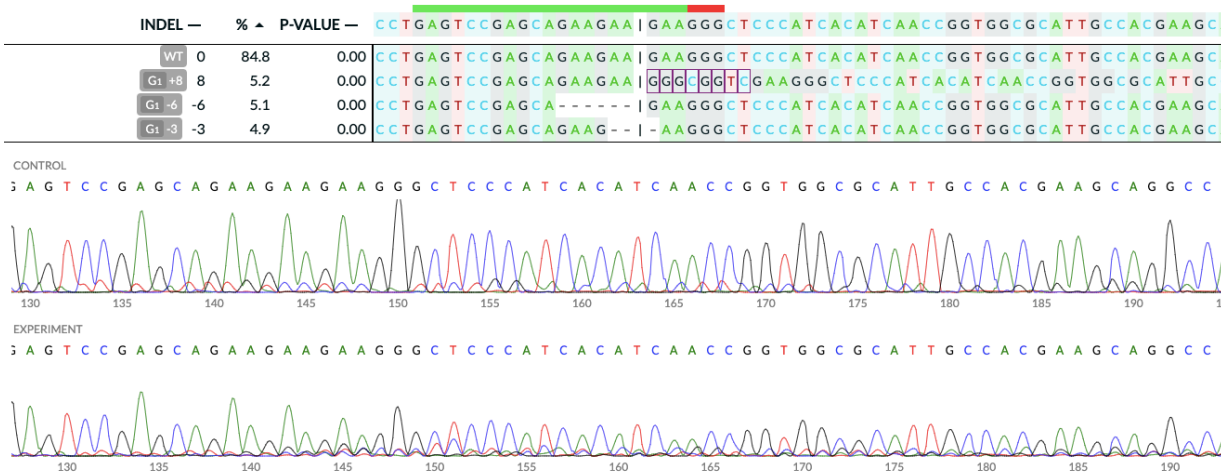

Supplementary Data 36. Cas9-induced indel formation against EMX1 with broccoli in the upper stem loop of sgRNA.

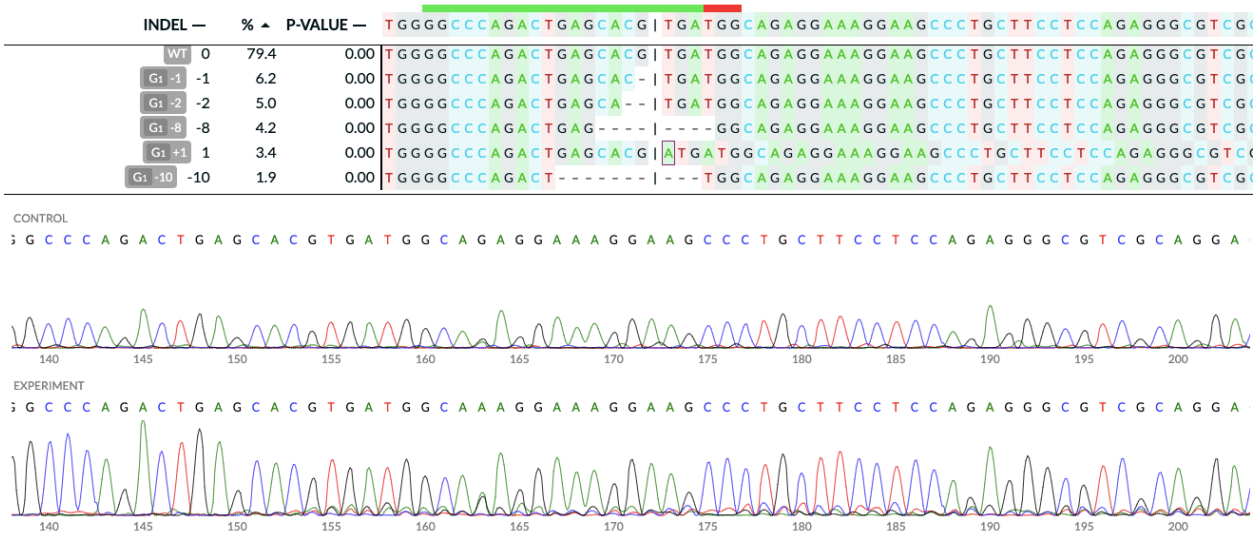

Supplementary Data 37. Cas9-induced indel formation against HEK3 with broccoli in the upper stem loop of sgRNA.

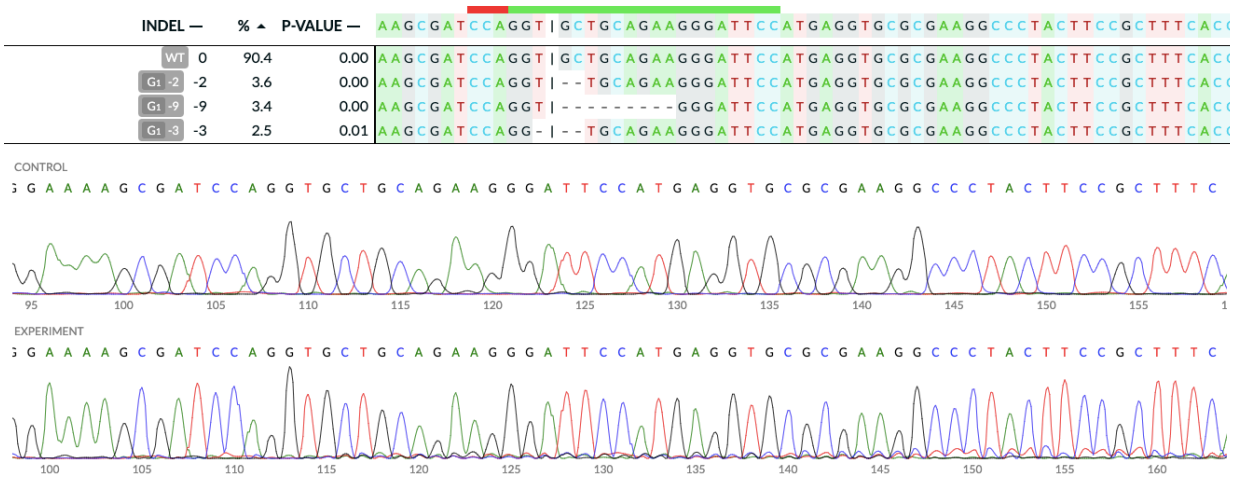

Supplementary Data 38. Cas9-induced indel formation for FANCF-A control sgRNA.

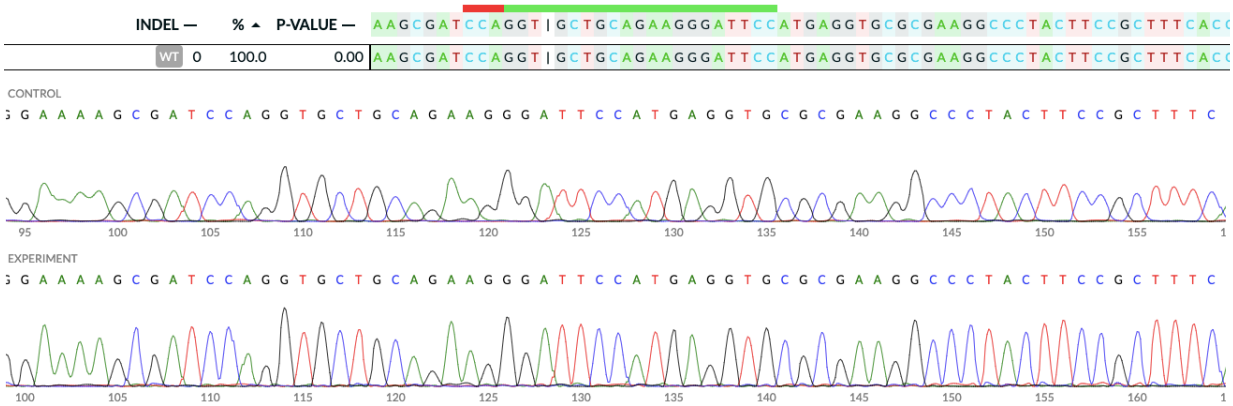

Supplementary Data 39. Cas9-induced indel formation against FANCF-A with X2B2 in the upper stem loop of sgRNA.

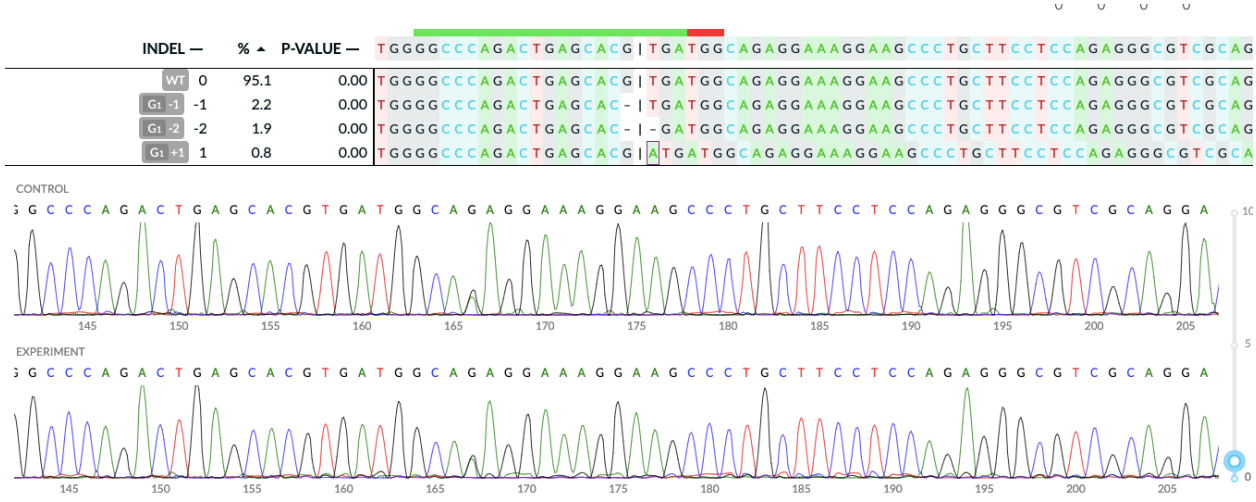

Supplementary Data 40. Cas9-induced indel formation against HEK3 with X2B2 in the upper stem loop of sgRNA.

References

(1) Ishino, Y.; Shinagawa, H.; Makino, K.; Amemura, M.; Nakata, A. Nucleotide Sequence of the Iap Gene, Responsible for Alkaline Phosphatase Isozyme Conversion in Escherichia Coli, and Identification of the Gene Product. *J. Bacteriol.* **1987**, *169* (12), 5429–5433.

(2) Wiedenheft, B.; Sternberg, S. H.; Doudna, J. A. RNA-Guided Genetic Silencing Systems in Bacteria and Archaea. *Nature* **2012**, *482* (7385), 331–338.

(3) Grissa, I.; Vergnaud, G.; Pourcel, C. CRISPRFinder: A Web Tool to Identify Clustered Regularly Interspaced Short Palindromic Repeats. *Nucleic Acids Res.* **2007**, *35*, 52–57.

(4) Koonin, E. V.; Makarova, K. S. Origins and Evolution of CRISPR-Cas Systems. *Philos. Trans. R. Soc. Lond. B. Biol. Sci.* **2019**, *374* (1772), 20180087.

(5) Makarova, K. S.; Haft, D. H.; Barrangou, R.; Brouns, S. J.; Charpentier, E.; Horvath, P.; Moineau, S.; Mojica, F. J.; Wolf, Y. I.; Yakunin, A. F.; van der Oost, J.; Koonin, E. V. Evolution and Classification of the CRISPR-Cas Systems. *Nat. Rev. Microbiol.* **2011**, *9* (6), 467–477.

(6) Nuñez, J. K.; Kranzusch, P. J.; Noeske, J.; Wright, A. V.; Davies, C. W.; Doudna, J. A. Cas1–Cas2 Complex Formation Mediates Spacer Acquisition during CRISPR–Cas Adaptive Immunity. *Nat. Struct. Mol. Biol.* **2014**, *21*, 528–534.

(7) Wang, J.; Li, J.; Zhao, H.; Sheng, G.; Wang, M.; Yin, M.; Wang, Y. Structural and Mechanistic Basis of PAM-Dependent Spacer Acquisition in CRISPR-Cas Systems. *Cell* **2015**, *163* (4), 840–853.

(8) Jansen, R.; Embden, J. D.; Gaastra, W.; Schouls, L. M. Identification of Genes That Are Associated with DNA Repeats in Prokaryotes. *Mol. Microbiol.* **2002**, *43* (6), 1565–1575.

(9) Tang, T. H.; Bachellerie, J. P.; Rozhdestvensky, T.; Bortolin, M. L.; Huber, H.; Drungowski, M.; Elge, T.; Brosius, J.; Hüttenhofer, A. Identification of 86 Candidates for Small Non-Messenger RNAs from the Archaeon Archaeoglobus Fulgidus. *Proc. Natl. Acad. Sci. U. S. A.* **2002**, *99* (11), 7536–7541.

(10) Deltcheva, E.; Chylinski, K.; Sharma, C. M.; Gonzales, K.; Chao, Y.; Pirzada, Z. A.; Eckert, M. R.; Vogel, J.; Charpentier, E. CRISPR RNA Maturation by Trans-Encoded Small RNA and Host Factor RNase III. *Nature* **2011**, *471*, 602–607.

(11) Marraffini, L. A.; Sontheimer, E. J. Self versus Non-Self Discrimination during CRISPR RNA-Directed Immunity. *Nature* **2010**, *463*, 568–571.

(12) Mojica, F. J.; Díez-Villaseñor, C.; García-Martínez, J.; Almendros, C. Short Motif Sequences Determine the Targets of the Prokaryotic CRISPR Defence System. *Microbiology* **2009**, *155* (3).

(13) Deveau, H.; Barrangou, R.; Garneau, J. E.; Labonté, J.; Fremaux, C.; Boyaval, P.; Romero, D. A.; Horvath, P.; Moineau, S. Phage Response to CRISPR-Encoded Resistance in Streptococcus Thermophilus. *J. Bacteriol.* **2008**, *190* (4).

(14) Jinek, M.; Chylinski, K.; Fonfara, I.; Hauer, M.; Doudna, J. A.; Charpentier, E. A Programmable Dual-RNA-Guided DNA Endonuclease in Adaptive Bacterial Immunity. *Science* **2012**, *337* (6096), 816–821.

(15) Nishimasu, H.; Ran, F. A.; Hsu, P. D.; Konermann, S.; Shehata, S. I.; Dohmae, N.; Ishitani, R.; Zhang, F.; Nureki, O. Crystal Structure of Cas9 in Complex with Guide RNA and Target DNA. *Cell* **2014**, *156* (5), 935–949.

(16) Jinek, M.; Jiang, F.; Taylor, D. W.; Sternberg, S. H.; Kaya, E.; Ma, E.; Anders, C.; Hauer, M.; Zhou, K.; Lin, S.; Kaplan, M.; Iavarone, A. T.; Charpentier, E.; Nogales, E.; Doudna, J.

A. Structures of Cas9 Endonucleases Reveal RNA-Mediated Conformational Activation. *Science* **2014**, *343* (6176), 1247997.
(17) Jiang, F.; Taylor, D. W.; Chen, J. S.; Kornfeld, J. E.; Zhou, K.; Thompson, A. J.; Nogales, E.; Doudna, J. A. Structures of a CRISPR-Cas9 R-Loop Complex Primed for DNA Cleavage. *Science* **2016**, *351* (6275), 867–871.
(18) Jiang, F.; Doudna, J. A. CRISPR–Cas9 Structures and Mechanisms. *Annu. Rev. Biophys.* **2017**, *46*, 505–529.
(19) Pattanayak, V.; Lin, S.; Guilinger, J. P.; Ma, E.; Doudna, J. A.; Liu, D. R. High-Throughput Profiling of off-Target DNA Cleavage Reveals RNA-Programmed Cas9 Nuclease Specificity. *Nat. Biotechnol.* **2013**, *31*, 839–843.
(20) Konermann, S.; Brigham, M. D.; Trevino, A. E.; Joung, J.; Abudayyeh, O. O.; Barcena, C.; Hsu, P. D.; Habib, N.; Gootenberg, J. S.; Nishimasu, H.; Nureki, O.; Zhang, F. Genome-Scale Transcriptional Activation by an Engineered CRISPR-Cas9 Complex. *Nature* **2015**, *517* (7536), 583–588.
(21) Zalatan, J. G.; Lee, M. E.; Almeida, R.; Gilbert, L. A.; Whitehead, E. H.; La Russa, M.; Tsai, J. C.; Weissman, J. S.; Dueber, J. E.; Qi, L. S.; Lim, W. A. Engineering Complex Synthetic Transcriptional Programs with CRISPR RNA Scaffolds. *Cell* **2015**, *160* (1), 339–350.
(22) Keefe, A. D.; Pai, S.; Ellington, A. Aptamers as Therapeutics. *Nat. Rev. Drug Discov.* **2010**, *9*, 537–550.
(23) Ma, H.; Tu, L.-C.; Naseri, A.; Huisman, M.; Zhang, S.; Grunwald, D.; Pederson, T. Multiplexed Labeling of Genomic Loci with dCas9 and Engineered sgRNAs Using CRISPRainbow. *Nat. Biotechnol.* **2016**, *34*, 528–530.
(24) Ma, H.; Tu, L.-C.; Naseri, A.; Chung, Y.-C.; Grunwald, D.; Zhang, S.; Pederson, T. CRISPR-Sirius: RNA Scaffolds for Signal Amplification in Genome Imaging. *Nat. Methods* **2018**, *15* (11), 928–931.
(25) Qin, P.; Parlak, M.; Kuscu, C.; Bandaria, J.; Mir, M.; Szlachta, K.; Singh, R.; Darzacq, X.; Yildiz, A.; Adli, M. Live Cell Imaging of Low- and Non-Repetitive Chromosome Loci Using CRISPR-Cas9. *Nat. Commun.* **2017**, *8* (14725).
(26) Gasiunas, G.; Barrangou, R.; Horvath, P.; Siksnys, V. Cas9–crRNA Ribonucleoprotein Complex Mediates Specific DNA Cleavage for Adaptive Immunity in Bacteria. *Proc. Natl. Acad. Sci.* **2012**, *109* (39), 2579–2586.
(27) Sander, J. D.; Joung, J. K. CRISPR–Cas Systems for Editing, Regulating and Targeting Genomes. *Nat. Biotechnol.* **2014**, *32*, 347–355.
(28) Carly Pflaum. FDA Approves First Gene Therapies to Treat Patients with Sickle Cell Disease. *U.S. Food & Drug Administration*. December 8, 2023.
(29) Wu, Y.; Zeng, J.; Roscoe, B. P.; Liu, P.; Yao, Q.; Lazzarotto, C. R.; Clement, K.; Cole, M. A.; Luk, K.; Baricordi, C.; Shen, A. H.; Ren, C.; Esrick, E. B.; Manis, J. P.; Dorfman, D. M.; Williams, D. A.; Biffi, A.; Brugnara, C.; Biasco, L.; Brendel, C.; Pinello, L.; Shengdar, Q. T.; Wolfe, S. A.; Bauer, D. Highly Efficient Therapeutic Gene Editing of Human Hematopoietic Stem Cells. *Nat. Med.* **2019**, *25* (5), 776–783.
(30) Liu, N.; Hargreaves, V. V.; Zhu, Q.; Kurland, J. V.; Hong, J.; Kim, W.; Sher, F.; Macias-Trevino, C.; Rogers, J. M.; Kurita, R.; Nakamura, Y.; Yuan, G. C.; Bauer, D. E.; Xu, J.; Bulyk, M. L.; Orkin, S. H. Direct Promoter Repression by BCL11A Controls the Fetal to Adult Hemoglobin Switch. *Cell* **2018**, *173* (2), 430–442.

(31) Shalem, O.; Sanjana, N. E.; Hartenian, E.; Shi, X.; Scott, D. A.; Mikkelson, T.; Heckl, D.; Ebert, B. L.; Root, D. E.; Doench, J. G.; Zhang, F. Genome-Scale CRISPR-Cas9 Knockout Screening in Human Cells. *Science* **2014**, *343* (6166), 84–87.
(32) Behan, F. M.; Iorio, F.; Picco, G.; Gonçalves, E.; Beaver, C. M.; Migliardi, G.; Santos, R.; Rao, Y.; Sassi, F.; Pinnelli, M.; Ansari, R.; Harper, S.; Jackson, D. J.; McRae, R.; Pooley, R.; Wilkinson, P.; van der Meer, D.; Dow, D.; Buser-Doepner, C.; Bertotti, A.; Trusolino, L.; Stronach, E. A.; Saez-Rodriguez, J.; Yusa, K.; Garnett, M. J. Prioritization of Cancer Therapeutic Targets Using CRISPR–Cas9 Screens. *Nature* **2019**, *568*, 511–516.
(33) Komor, A. C.; Kim, Y. B.; Packer, M. S.; Zuris, J. A.; Liu, D. R. Programmable Editing of a Target Base in Genomic DNA without Double-Stranded DNA Cleavage. *Nature* **2016**, *533* (7603), 420–424.
(34) Ciccia, A.; Elledge, S. J. The DNA Damage Response: Making It Safe to Play with Knives. *Mol. Cell* **2010**, *40* (2), 179–204.
(35) Fu, Y.; Foden, J. A.; Khayter, C.; Maeder, M. L.; Reyon, D.; Joung, J. K.; Sander, J. D. High-Frequency off-Target Mutagenesis Induced by CRISPR-Cas Nucleases in Human Cells. *Nat. Biotechnol.* **2013**, *31* (9), 822–826.
(36) Gaudelli, N. M.; Komor, A. C.; Rees, H. A.; Packer, M. S.; Badran, A. H.; Bryson, D. I.; Liu, D. R. Programmable Base Editing of A•T to G•C in Genomic DNA without DNA Cleavage. *Nature* **2017**, *551* (7681), 464–471.
(37) Pluciennik, A.; Dzantiev, L.; Iyer, R. R.; Constantin, N.; Kadyrov, F. A.; Modrich, P. PCNA Function in the Activation and Strand Direction of MutLα Endonuclease in Mismatch Repair. *Proc. Natl. Acad. Sci.* **2010**, *107* (37), 16066–16071.
(38) Mol, C. D.; Arvai, A. S.; Sanderson, R. J.; Slupphaug, G.; Kavli, B.; Krokan, H. E.; Mosbaugh, D. W.; Tainer, J. A. Crystal Structure of Human UraciI-DNA Glycosylase in Complex with a Protein Inhibitor: Protein Mimicry of DNA. *Cell* **1995**, *82*, 701–708.
(39) Wolf, J.; Gerber, A. P.; Keller, W. tadA, an Essential tRNA-Specific Adenosine Deaminase from Escherichia Coli. *EMBO J.* **2002**, *21* (14), 3841–3851.
(40) Chiesa, R.; Georgiadis, C.; Syed, F.; Zhan, H.; Etuk, A.; Gkazi, S. A.; Preece, R.; Ottaviano, G.; Braybrook, T.; Chu, J.; Kubat, A.; Adams, S.; Thomas, R.; Gilmour, K.; O'Connor, D.; Vora, A.; Qasim, W. Base-Edited CAR7 T Cells for Relapsed T-Cell Acute Lymphoblastic Leukemia. *N. Engl. J. Med.* **2023**, *389* (10), 899–910.
(41) Musunuru, K.; Chadwick, A. C.; Mizoguchi, T.; Garcia, S. P.; DeNizio, J. E.; Reiss, C. W.; Wang, K.; Iyer, S.; Dutta, C.; Clendaniel, V.; Amaonnye, M.; Beach, A.; Berth, K.; Biswas, S.; Braun, M. C.; Chen, H.-M.; Colace, T. V.; Ganey, J. D.; Gangopadhyay, S. A.; Garrity, R.; Kasiewicz, L. N.; Lavoie, J.; Madsen, J. A.; Matsumoto, Y.; Mazzola, A. M.; Nasrullah, Y. S.; Nneji, J.; Ren, H.; Sanjeev, A.; Shay, M.; Stahley, M. R.; Fan, S. H. Y.; Tam, Y. K.; Gaudelli, N. M.; Ciaramella, G.; Stolz, L. E.; Malyala, P.; Cheng, C. J.; Rajeev, K. G.; Rohde, E.; Bellinger, A. M.; Kathiresan, S. In Vivo CRISPR Base Editing of PCSK9 Durably Lowers Cholesterol in Primates. *Nature* **2021**, *593*, 429–434.
(42) Horie, T.; Ono, K. VERVE-101: A Promising CRISPR-Based Gene Editing Therapy That Reduces LDL-C and PCSK9 Levels in HeFH Patients. *Eur. Heart J. - Cardiovasc. Pharmacother.* **2024**, *10* (2), 89–90.
(43) Walton, R. T.; Christie, K. A.; Whittaker, M. N.; Kleinstiver, B. P. Unconstrained Genome Targeting with Near-PAMless Engineered CRISPR-Cas9 Variants. *Science* **2020**, *386* (6488), 290–296.

(44) Landrum, M. J.; Lee, J. M.; Benson, M.; Brown, G.; Chao, C.; Chitipiralla, S.; Gu, B.; Hart, J.; Hoffman, D.; Hoover, J.; Jang, W.; Katz, K.; Ovetsky, M.; Riley, G.; Sethi, A.; Tully, R.; Villamarin-Solomon, R.; Rubinstein, W.; Maglott, D. R. ClinVar: Public Archive of Interpretations of Clinically Relevant Variants. *Nucleic Acids Res.* **2016**, *44* (D1), D862–D868.
(45) Rees, H. A.; Liu, D. R. Base Editing: Precision Chemistry on the Genome and Transcriptome of Living Cells. *Nat. Rev. Genet.* **2018**, *19* (12), 770–788.
(46) Landrum, M. J.; Lee, J. M.; Riley, G. R.; Jang, W.; Rubinstein, W. S.; Church, D. M.; Maglott, D. R. ClinVar: Public Archive of Relationships among Sequence Variation and Human Phenotype. *Nucleic Acids Res.* **2014**, *42*, D980–D985.
(47) Tong, H.; Wang, H.; Wang, X.; Liu, N.; Li, G.; Wu, D.; Li, Y.; Jin, M.; Li, H.; Wei, Y.; Li, T.; Yuan, Y.; Shi, L.; Yao, X.; Zhou, Y.; Yang, H. Development of Deaminase-Free T-to-S Base Editor and C-to-G Base Editor by Engineered Human Uracil DNA Glycosylase. *Nat. Commun.* **2024**, *15* (4897).
(48) Tong, H.; Liu, N.; Wei, Y.; Zhou, Y.; Li, Y.; Wu, D.; Jin, M.; Cui, S.; Li, H.; Li, G.; Zhou, J.; Yuan, Y.; Zhang, H.; Shi, L.; Yao, X.; Yang, H. Programmable Deaminase-Free Base Editors for G-to-Y Conversion by Engineered Glycosylase. *Natl. Sci. Rev.* **2023**, *10* (8).
(49) Thompson, P. S.; Cortez, D. New Insights into Abasic Site Repair and Tolerance. *DNA Repair* **2020**, *90* (102866).
(50) Yamanaka, S.; Balestra, M. E.; Ferrell, L. D.; Fan, J.; Arnold, K. S.; Taylor, S.; Taylor, J. M.; Innerarity, T. L. Apolipoprotein B mRNA-Editing Protein Induces Hepatocellular Carcinoma and Dysplasia in Transgenic Animals. *Proc. Natl. Acad. Sci. U. S. A.* **1995**, *92* (18), 8483–8487.
(51) Burns, M. B.; Lackey, L.; Carpenter, M. A.; Rathore, A.; Land, A. M.; Leonard, B.; Refsland, E. W.; Kotandeniya, D.; Tretyakova, N.; Nikas, J. B.; Yee, D.; Temiz, N. A.; Donohue, D. E.; McDougle, R. M.; Brown, W. L.; Law, E. K.; Harris, R. S. APOBEC3B Is an Enzymatic Source of Mutation in Breast Cancer. *Nature* **2013**, *494* (7437), 366–370.
(52) Radany, E. H.; Dornfeld, K. J.; Sanderson, R. J.; Savage, M. K.; Majunder, A.; Seidman, M. M.; Mosbaugh, D. W. Increased Spontaneous Mutation Frequency in Human Cells Expressing the Phage PBS2-Encoded Inhibitor of Uracil-DNA Glycosylase. *Mutat. Res.* **2000**, *461* (1), 41–58.
(53) Romero, N. A.; Nicewicz, D. A. Organic Photoredox Catalysis. *Chem. Rev.* **2016**, *116* (17), 10075–10166.
(54) Kobayashi, K.; Tagawa, S. Direct Observation of Guanine Radical Cation Deprotonation in Duplex DNA Using Pulse Radiolysis. *J. Am. Chem. Soc.* **2003**, *125* (34), 10213–10218.
(55) Xie, H.; Yang, D.; Heller, A.; Gao, Z. Electrocatalytic Oxidation of Guanine, Guanosine, and Guanosine Monophosphate. *Biophys. J.* **2007**, *92* (8), 70–72.
(56) Fleming, A. M.; Xiao, S.; Chabot, M. B.; Burrows, C. J. Fluorophore-Mediated Photooxidation of the Guanine Heterocycle. *J. Phys. Org. Chem.* **2022**, *35* (11).
(57) Morikawa, M.; Kino, K.; Oyoshi, T.; Suzuki, M.; Kobayashi, T.; Miyazawa, H. Product Analysis of Photooxidation in Isolated Quadruplex DNA; 8-Oxo-7,8-Dihydroguanine and Its Oxidation Product at 3′-G Are Formed Instead of 2,5-Diamino-4H-Imidazol-4-One. *RSC Adv.* **2013**, *3* (48), 25694–25697.
(58) Baptista, M. S.; Cadet, J.; Di Mascio, P.; Ghogare, A. A.; Greer, A.; Hamblin, M. R.; Lorente, C.; Nunez, S. C.; Ribeiro, M. S.; Thomas, A. H.; Vignoni, M.; Yoshimura, T. M.

Type I and Type II Photosensitized Oxidation Reactions: Guidelines and Mechanistic Pathways. *Photochem. Photobiol.* **2017**, *93* (4), 912–919.
(59) Srivastava, V.; Singh, P. K.; Srivastava, A.; Singh, P. P. Synthetic Applications of Flavin Photocatalysis: A Review. *RSC Adv.* **2021**, *11*, 14251–14259.
(60) Di Mascio, P.; Martinez, G. R.; Miyamoto, S.; Ronsein, G. E.; Medeiros, M. H. G.; Cadet, J. Singlet Molecular Oxygen Reactions with Nucleic Acids, Lipids, and Proteins. *Chem. Rev.* **2019**, *119* (3), 2043–2086.
(61) Filonov, G. S.; Moon, J. D.; Svensen, N.; Jaffrey, S. R. Broccoli: Rapid Selection of an RNA Mimic of Green Fluorescent Protein by Fluorescence-Based Selection and Directed Evolution. *J. Am. Chem. Soc.* **2014**, *136* (46), 16299–16308.
(62) Nilaratanakul, V.; Hauer, D. A.; Griffin, D. E. Development of Encoded Broccoli RNA Aptamers for Live Cell Imaging of Alphavirus Genomic and Subgenomic RNAs. *Sci. Rep.* **2020**, *10* (1), 5233.
(63) Al Shanaa, O.; Rumyantsev, A.; Sambuk, E.; Padkina, M. In Vivo Production of RNA Aptamers and Nanoparticles: Problems and Prospects. *Molecules* **2021**, *26* (5), 1422.
(64) Passalacqua, L. F. M.; Banco, M. T.; Moon, J. D.; Li, X.; Jaffrey, S. R.; Ferré-D'Amaré, A. R. Intricate 3D Architecture of a DNA Mimic of GFP. *Nature* **2023**, *618* (7967), 1078–1084.
(65) Paige, J. S.; Wu, K. Y.; Jaffrey, S. R. RNA Mimics of Green Fluorescent Protein. *Science* **2011**, *333* (6042), 642–646.
(66) Mills, B.; Kiang, A.; Mohanan, S. M. P. C.; Bradley, M.; Klausen, M. Riboflavin-Vancomycin Conjugate Enables Simultaneous Antibiotic Photo-Release and Photodynamic Killing against Resistant Gram-Positive Pathogens. *J. Am. Chem. Soc. Au* **2023**, *3* (11), 3014–3023.
(67) Sugita, N.; Kawabata, K.; Sasaki, K.; Sakata, I.; Umemura, S. Synthesis of Amphiphilic Derivatives of Rose Bengal and Their Tumor Accumulation. *Bioconjug. Chem.* **2007**, *18* (3), 866–873.
(68) Samuelian, J. S.; Gremminger, T. J.; Song, Z.; Poudyal, R. R.; Li, J.; Zhou, Y.; Staller, S. A.; Carballo, J. A.; Roychowdhury-Saha, M.; Chen, S.; Burke, D. H.; Heng, X.; Baum, D. A. An RNA Aptamer That Shifts the Reduction Potential of Metabolic Cofactors. *Nat. Chem. Biol.* **2022**, *18*, 1263–1269.
(69) Kino, K.; Kawada, T.; Hirao-Suzuki, M.; Morikawa, M.; Miyazawa, H. Products of Oxidative Guanine Damage Form Base Pairs with Guanine. *Int. J. Mol. Sci.* **2020**, *21* (20), 7645.
(70) Alghamdi, R. A.; Exposito-Rodriguez, M.; Mullineaux, P. M.; Brooke, G. N.; Laissue, P. P. Assessing Phototoxicity in a Mammalian Cell Line: How Low Levels of Blue Light Affect Motility in PC3 Cells. *Front. Cell Dev. Biol.* **2021**, *9*.
(71) Kaur, J.; Singhal, S. Heterogeneous Photocatalytic Degradation of Rose Bengal: Effect of Operational Parameters. *Phys. B Condens. Matter* **2014**, *450*, 49–53.
(72) Demchenko, A. P. Photobleaching of Organic Fluorophores: Quantitative Characterization, Mechanisms, Protection. *Methods Appl. Fluoresc.* **2020**, *8* (2).
(73) Fouquerel, E.; Barnes, R. P.; Uttam, S.; Watkins, S. C.; Bruchez, M. P.; Opresko, P. L. Targeted and Persistent 8-Oxoguanine Base Damage at Telomeres Promotes Telomere Loss and Crisis. *Mol. Cell* **2019**, *75* (1), 117–130.
(74) Thosar, S. A.; Barnes, R. P.; Detwiler, A.; Bhargava, R.; Wondisford, A.; O'Sullivan, R. J.; Opresko, P. L. Oxidative Guanine Base Damage Plays a Dual Role in Regulating Productive ALT-Associated Homology-Directed Repair. *Cell Rep.* **2024**, *43* (1), 113656.

(75) Kim, Y.-S.; Rubio, V.; Qi, J.; Xia, R.; Shi, Z.-Z.; Peterson, L.; Tung, C.-H.; O'Neill, B. E. Cancer Treatment Using an Optically Inert Rose Bengal Derivative Combined with Pulsed Focused Ultrasound. *J. Controlled Release* **2011**, *156* (3), 315–322.
(76) Carreon, J. R.; Roberts, M. A.; Wittenhagen, L. M.; Kelley, S. O. Synthesis, Characterization, and Cellular Uptake of DNA-Binding Rose Bengal Peptidoconjugates. *Org. Lett.* **2005**, *7* (1), 99–102.
(77) Dhillon, S. K.; Porter, S. L.; Rizk, N.; Sheng, Y.; McKaig, T.; Burnett, K.; White, B.; Nesbitt, H.; Matin, R. N.; McHale, A. P.; Callan, B.; Callan, J. F. Rose Bengal–Amphiphilic Peptide Conjugate for Enhanced Photodynamic Therapy of Malignant Melanoma. *J. Med. Chem.* **2020**, *63* (3), 1328–1336.
(78) Sugita, N.; Kawabata, K.; Sasaki, K.; Sakata, I.; Umemura, S. Synthesis of Amphiphilic Derivatives of Rose Bengal and Their Tumor Accumulation. *Bioconjug. Chem.* **2007**, *18* (3), 866–873.
(79) Shemesh, Y.; Yavin, E. PNA–Rose Bengal Conjugates as Efficient DNA Photomodulators. *Bioconjug. Chem.* **2015**, *26* (9), 1916–1922.
(80) Adachi, M.; Murata, Y.; Nakamura, S. Spectral Similarity and Difference of Naphthalenetetracarboxylic Dianhydride, Perylenetetracarboxylic Dianhydride, and Their Derivatives. *J. Phys. Chem.* **1995**, *99* (39), 14240–14246.
(81) Rauf, M. A.; Graham, J. P.; Bukallah, S. B.; Al-Saedi, M. A. Solvatochromic Behavior on the Absorption and Fluorescence Spectra of Rose Bengal Dye in Various Solvents. *Spectrochim. Acta. A. Mol. Biomol. Spectrosc.* **2009**, *72* (1), 133–137.
(82) Dao, N. T.; Haselsberger, R.; Khuc, M. T.; Phan, A. T.; Voityuk, A. A.; Michel-Beyerle, M. Photophysics of DFHBI Bound to RNA Aptamer Baby Spinach. *Sci. Rep.* **2021**, *11* (7356).
(83) Gao, Y.; Li, Z.; Wang, C.; You, J.; Jin, B.; Mo, F.; Chen, J.; Zheng, Y.; Chen, H. Self-Assembled Chitosan/Rose Bengal Derivative Nanoparticles for Targeted Sonodynamic Therapy: Preparation and Tumor Accumulation. *RSC Adv.* **2015**, *5*, 17915–17923.
(84) Lovell, J. F.; Chen, J.; Jarvi, M. T.; Cao, W.-G.; Allen, A. D.; Liu, Y.; Tidwell, T. T.; Wilson, B. C.; Zheng, G. FRET Quenching of Photosensitizer Singlet Oxygen Generation. *J. Phys. Chem. B* **2009**, *113* (10), 3203–3211.
(85) Escudero, D. Revising Intramolecular Photoinduced Electron Transfer (PET) from First-Principles. *Acc. Chem. Res.* **2016**, *49* (9), 1816–1824.
(86) VarnBuhler, B. S.; Moon, J.; Dey, S. K.; Wu, J.; Jaffrey, S. R. Detection of SARS-CoV-2 RNA Using a DNA Aptamer Mimic of Green Fluorescent Protein. *ACS Chem. Biol.* **2022**, *17* (4), 840–853.
(87) Zhang, X.-F. The Effect of Phenyl Substitution on the Fluorescence Characteristics of Fluorescein Derivatives via Intramolecular Photoinduced Electron Transfer. *Photochem. Photobiol. Sci.* **2010**, No. 9, 1261–1268.
(88) Zhang, X.-F.; Zhang, I.; Liu, L. Photophysics of Halogenated Fluoresceins: Involvement of Both Intramolecular Electron Transfer and Heavy Atom Effect in the Deactivation of Excited States. *Photochem. Photobiol.* **2010**, *86* (3), 482–498.
(89) Mullally, G.; van Aelst, K.; Naqvi, M. M.; Diffin, F. M.; Karvelis, T.; Gasiunas, G.; Siksnys, V.; Szczelkun, M. D. 5′ Modifications to CRISPR–Cas9 gRNA Can Change the Dynamics and Size of R-Loops and Inhibit DNA Cleavage. *Nucleic Acids Res.* **2020**, *48* (12), 6811–6823.